

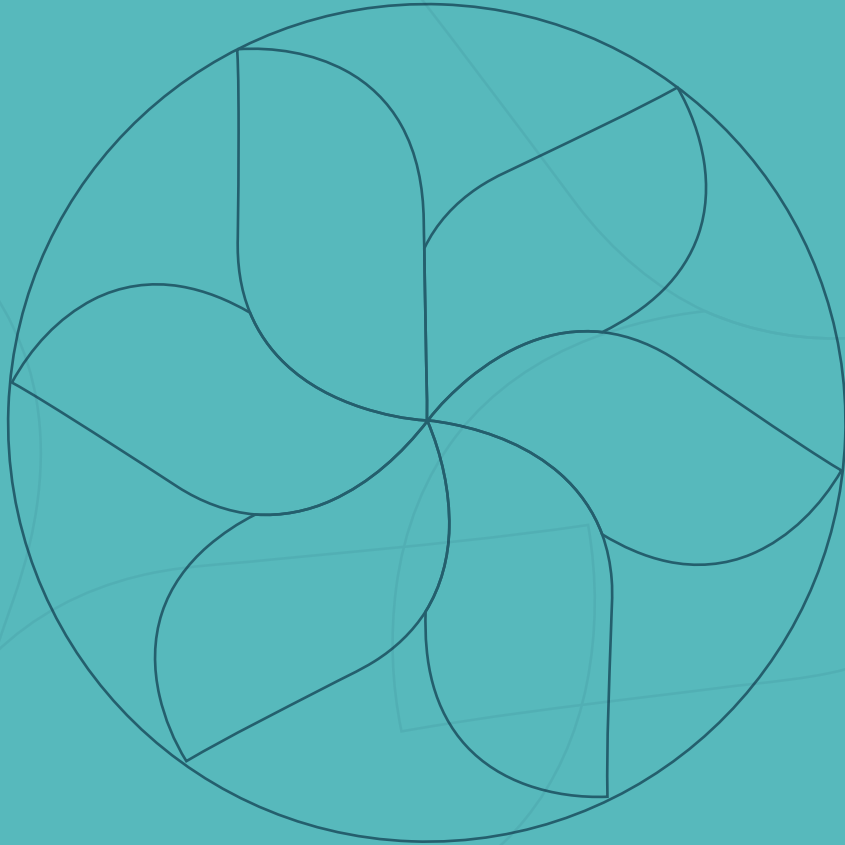


TÜRKİYE  
SCHOLARSHIPS  
BURSLARI

İSTANBUL  
BİLİMLER  
AKADEMİSİ

6. Uluslararası Öğrenci Bilimler  
Kongresi Bildiriler Kitabı - 2  
Fen, Mühendislik ve Sağlık Bilimleri

6<sup>th</sup> International Student Sciences  
Congress Proceedings Book-2  
Life, Engineering and Health Sciences



TÜRKİYE  
SCHOLARSHIPS  
BURSLARI



TÜRKİYE  
SCHOLARSHIPS  
BURSLARI

İSTANBUL  
BİLİMLER  
AKADEMİSİ

6. Uluslararası Öğrenci Bilimler  
Kongresi Bildiriler Kitabı - 2  
Fen, Mühendislik ve Sağlık Bilimleri

6<sup>th</sup> International Student Sciences  
Congress Proceedings Book-2  
Life, Engineering and Health Sciences

Cilt II  
Volume II

2021  
ANKARA  
Aralık/ December 9-12

2021

9-12  
Aralık/ December



# 6. ULUSLARARASI ÖĞRENCİ BİLİMLER KONGRESİ

## 6TH INTERNATIONAL STUDENT SCIENCES CONGRESS

-Fen, Mühendislik ve Sağlık Bilimleri-

-Life, Engineering and Health Sciences-

Cilt-2

Volume-2

9-12 Aralık/December 2021

Ankara





Kitabın Adı  
**6. ULUSLARARASI ÖĞRENCİ BİLİMLER KONGRESİ  
BİLDİRİLER KİTABI - 2**  
**Fen, Mühendislik ve Sağlık Bilimleri**

**6TH INTERNATIONAL STUDENT SCIENCES CONGRESS  
PROCEEDINGS BOOK - 2**  
**Life, Engineering and Health Sciences**

Editör  
**Dr. Enes Şahin**

Redaksiyon  
**Melek Kılıç**

Basım Tarihi  
**Aralık 2021**

Basım Yeri :  
**Saner Basım Hizmetleri San. Tic. Ltd. Şti.**  
Maltepe Mahallesi Litrosyolu Sokak 2. Matbaacılar Sitesi No: 2/4  
2BC3/4 - Zeytinburnu - İstanbul Tel: 0212 674 10 51-52-53  
(Sertifika No: 50633)  
İstanbul, 2021

ISBN : 978-605-65779-8-7 (Tk)  
978-605-65779-7-0 (2.c)

Yayıncı :  
**İstanbul Bilimler Akademisi Vakfı**

Mizanpaj : **Canan Aytaş**  
Kapak: **Mehmet Taha Ersöz**  
©Copyright 2021

Yazılı izin alınmadan çoğaltılamaz, yayınlanamaz, bilimsel çalışmalar dışında alıntı yapılamaz.

## **Düzenleyen Kurumlar / Organising Institutions**

Yurtdışı Türkler ve Akraba Topluluklar Başkanlığı (YTB) - İstanbul  
Bilimler Akademisi (İBA)

## **Onur Kurulu / Honory Board**

**Abdullah Eren**, Yurtdışı Türkler ve Akraba Topluluklar  
Başkanlığı (YTB) | **Gülfettin Çelik**, İstanbul Bilimler Akademisi (İBA)

## **Düzenleme Kurulu / Organising Committee**

**Abdüllatif Çeviker**, İstanbul Medeniyet Üniversitesi | **Ali Ramazan Tak**, İstanbul Bilimler Akademisi Vakfı (İdari Koordinatör) | **Berna Terzioğlu Bebitoğlu**, İstanbul Medeniyet Üniversitesi | **Cengiz İpek**, İstanbul Medeniyet Üniversitesi | **Faruk Bal**, İstanbul Medeniyet Üniversitesi | **Fırat Erdoğan**, İstanbul Medipol Üniversitesi | **Hamdi Genç**, İstanbul Medeniyet Üniversitesi | **İsmail Ermağan**, İstanbul Medeniyet Üniversitesi (Akademik Koordinatör) | **Kürşat Ayan**, İstanbul Medeniyet Üniversitesi | **Mehmet Emin Okur**, Marmara Üniversitesi | **Mehmet Küçükmehtetoğlu**, Gebze Teknik Üniversitesi | **Mehmet Lütfi Arslan**, İstanbul Bilimler Akademisi Vakfı

## **Bilim Kurulu / Scientific Committee**

### **Fen ve Mühendislik Bilimleri / Life and Engineering Sciences**

**Ahmet Altınay**, Aspilsan | **Cengiz İpek**, İstanbul Medeniyet Üniversitesi | **Cüneyt Bayılmış**, Sakarya Üniversitesi | **Cüneyt Fırat**, CTech | **Eylem Erdoğan**, İstanbul Medeniyet Üniversitesi | **Haluk Bayram**, İstanbul Medeniyet Üniversitesi | **Mehmet Küçükmehtetoğlu**, Gebze Teknik Üniversitesi | **Mustafa Ragıp Başbuğ**, İstinye Üniversitesi | **Süleyman Adak**, Mardin Artuklu Üniversitesi | **Vail Karakale**, İstanbul Medeniyet Üniversitesi | **Yasin Cengiz Çelik**, Aspilsan | **Yüksel Yurtay**, Sakarya Üniversitesi



## Sağlık Bilimleri / Health Sciences

**Bayram Toraman**, Karadeniz Teknik Üniversitesi | **Berna Terzioğlu Bebitoğlu**, İstanbul Medeniyet Üniversitesi | **Cengizhan Öztürk**, Boğaziçi Üniversitesi | **Elvan Yılmaz Akyüz**, Sağlık Bilimleri Üniversitesi | **Esra Sağlam**, Maltepe Üniversitesi | **Fahri Uçar**, Akdeniz Üniversitesi | **Gürkan Sert**, Marmara Üniversitesi | **Hasan Hüseyin Karadeli**, İstanbul Medeniyet Üniversitesi | **Havva Gonca Tamer**, İstanbul Medeniyet Üniversitesi | **Hürrem Bodur**, Sağlık Bilimleri Üniversitesi | **Işıl Maral**, İstanbul Medeniyet Üniversitesi | **Korhan Özkan**, İstanbul Medeniyet Üniversitesi | **Leyla Özer**, Acıbadem Üniversitesi | **Mehmet Sargın**, İstanbul Medeniyet Üniversitesi | **Mehmet Zafer Gören**, Marmara Üniversitesi | **Muhammed Fatih Önsüz**, Eskişehir Osmangazi Üniversitesi | **Mustafa Hayati Atala**, İstanbul Medeniyet Üniversitesi | **Mustafa Samastı**, İstanbul Medeniyet Üniversitesi | **Mustafa Ümit Uğurlu**, Marmara Üniversitesi | **Sabahat Aksaray**, Sağlık Bilimleri Üniversitesi | **Sadrettin Pençe**, İstanbul Medeniyet Üniversitesi

---

### İSTANBUL BİLİMLER AKADEMİSİ (İBA)

Adres: Büyükdere Cad. Raşit Rıza Sk. No:4, Ahmet Esin İşhanı, Kat:4,  
Mecidiyeköy/İstanbul Telefon: 0212 211 66 56 E-posta: bilgi@ibav.org

## İçindekiler / Contents

<b>Takdim</b> .....	8
<i>YTB</i>	

<b>Takdim</b> .....	9
<i>İBA</i>	

<b>Biyoloji Çalışmaları / Biology Studies</b> .....	11
---	----

<b>Epididymal Camel Spermatozoa Quality as Affected by Green Laser Irradiation During Incubation at 37°C</b> .....	13
<i>Ahmed Seioudy</i>	

<b>Production and Purification of Chromate Reductase from <i>Bacillus Paramycoides</i> S-9 for Biotransformation of Chromium (VI)</b> .....	31
<i>Kalsoom Kalsoom</i>	

<b>Beyaz Lahana ve Acı Otun Kayaşın Çimlenmesi ve Büyümesi Üzerindeki Allelopatik Etkisi</b> .....	69
<i>Muhammad Alsakran</i>	

<b>Enerji Çalışmaları / Energy Studies</b> .....	91
--	----

<b>Investigating the Effects of Reactant Gas Flow Geometrical Shape on The Performance of Solid Oxide Fuel Cell</b> .....	93
<i>Molla Asmare</i>	

**Co2 Emission Mitigation in A Natural Gas/Renewable Energy System  
And Impacts on the Carbon Budget.....113**

*Mujeeb Babatunde Adetayo*

**Energy and Exergy Analysis of a Trapezoidal Concentrated  
Photovoltaic-Thermoelectric System.....141**

*Aminu Yusuf*

**Biyodizel Üretimi için Yenilenebilir Kaynaklardan Katalizörlerin  
EldeEdilmesi.....159**

*Elnura Artykbaeva*

**Jeoloji Çalışmaları / Geology Studies.....175**

**Evaluation of the Associations Between Groundwater  
Fluctuations and Soil Salinity Using Landsat Imageries and  
Geostatistical Methods.....177**

*Behnam Khorrami*

**Rare Earth Elements in Indonesia: Preliminary Discussion on  
Regulation, Resources and Future Policy Paradigm.....199**

*Syamsul Hidayat*

**Mimarlık ve Mühendislik Çalışmaları / Architecture and  
Engineering Studies.....217**

**Kültür ve Politikanın Osmanlı Döneminden Günümüze Kadar Kuzey  
Kıbrıs Türk Cumhuriyeti Konutlarının Üzerinde Etkisi.....219**

*Ziba Sami*

**Blockchain Technology in the Education System.....245**

*Saadia Elgati*

**Climate Data Analysis: A Review of AI Methods in Drought Prediction and Evapotranspiration Estimation.....265**

*Yasser Zouzou*

**Deep Learning Model for Automated Diagnosis of Seizure Using EEG Signals.....283**

*Huda M. S. Algharib*

**Deep Camouflaged Object Segmentation.....303**

*Rabeb Hendaoui*

**Sağlık Bilimleri Çalışmaları / Health Sciences Studies.....321**

**Evaluation of Adverse Drug Reactions in Pediatric Patients at A Tertiary Care Hospital in Turkey: A Retrospective Approach.....323**

*Zakir Khan*

**N-heptil-D-galaktonamid ile Üç Boyutlu Olarak Kültüre Edilen Hipokampal Hücrelerde Epidermal Büyüme Faktörü'nün Önemi.....345**

*Aida Nurul Barokah*

**Medical Significance of Camel Urine: A Review.....365**

*Wasiu Ayodele Abibu, Sherifdeen Bamidele Onigbinde, Dahiru Salihu  
Abubakar, Abdullahi Tunde Aborode*

## Takdim (YTB)

“Uluslararası Öğrenci Bilimler Kongresi” 2015 yılından beri Türkiye Bursları’nın önemli bir parçasıdır. Denilebilir ki, dünyanın belli başlı tüm ülkelerinden gelen uluslararası öğrencilerin nitelikli üniversite eğitimi almak üzere yararlandıkları Türkiye Bursları’nın “çıktı”ları bu kongrede alınmaktadır. Vatandaşı oldukları ülkelerin yanı sıra dünyamızın sorunlarına da çözüm üretmeye aday olan Türkiye Bursluları, mezuniyetlerinden önce çeşitli meseleleri bilimsel bir zeminde tartışarak, hem bireysel kariyerlerine hem de genel akademik birikime katkı sunmaktadırlar.

Bu anlayış doğrultusunda bu yıl 6’ncısı düzenlenmiş ve 100 civarında bildiri sunulmuş olan Uluslararası Öğrenci Bilimler Kongresi, geçen yıllardan farklı olarak fen ve sağlık bilimleri alanlarını da kapsayacak şekilde genişletilmiştir. Böylece daha geniş bir kitleye hitap eden kongre, aynı zamanda disiplinlerarası bir özellik de sergilemiştir.

Türkiye, tüm insanlığın sorunlarının samimi olarak hissedildiği ve bunlara çözüm üretilmeye çalışıldığı evrensel bir ülkedir. Ülkemizin bu özelliğini bilim yoluyla güçlendiren Türkiye Bursları kapsamındaki Uluslararası Öğrenci Bilimler Kongresi, 6’ncı yılında da görüldüğü gibi, her seferinde yüze yakın ülkenin gençlerinin bir araya gelebildikleri ender ortamlardan olmakla birlikte, önümüzdeki yıllarda kapsamlı bir camia teşkil etmek üzere daha da zenginleştirilecektir.

Başta çalışmalarını bizlerle paylaşan ve bu kitabın bir bilgi rehberi hâline gelmesini sağlayan öğrencilerimize ve katkılarını esirgemeyen tüm kurum-kuruluşlarımıza içten teşekkürlerimi sunarım.

**Abdullah EREN**  
Yurtdışı Türkler ve Akraba  
Topluluklar Başkanı

## Takdim (İBA)

Türkiye'nin tarihi ve toplumsal yapısı, medeniyet ve kültür birikimi, bilgi ve düşünce ikliminden beslenen bir sivil toplum kuruluşu olan İstanbul Bilimler Akademisi (İBA), yurt içindeki öğrenciler ile yurt dışından gelen uluslararası öğrencilere yönelik projelerine devam ediyor.

Bu kapsamda İBA'nın uluslararası öğrencilere yönelik olarak Yurtdışı Türkler ve Akraba Topluluklar Başkanlığı ile ortak yürüttüğü 6. Uluslararası Öğrenci Bilimler Kongresi, başkent Ankara'da düzenlendi.

Dünyanın dört bir köşesinden ülkemize gelerek eğitimlerini sürdüren uluslararası öğrencilere, akademik ve entelektüel birikimlerini geliştirmeleri adına önemli bir fırsat sunan 6. Uluslararası Öğrenci Bilimler Kongresi'nde ülkemizde Sosyal Bilimler, Fen Bilimleri ve Sağlık Bilimleri alanında lisans ve lisansüstü düzeyde öğrenim gören uluslararası öğrenciler, müşterek çalışma alanlarından istifade ettiler, deneyimlerini paylaştılar ve çalışmalarını gerçekleştirdiler.

İki özel oturumla birlikte toplam yirmi üç farklı oturumun gerçekleştirildiği kongre boyunca, öğrenciler tarafından Edebiyat, Eğitim Bilimleri, Hukuk, İktisat, İşletme, Kamu Yönetimi, Mimarlık, Mühendislik, Siyaset Bilimi, Sosyoloji, Tarih, Tıp Bilimleri, Uluslararası İlişkiler ve daha pek çok farklı alanda 104 bildiri sunuldu.

Farklı ülkelerden gelerek farklı disiplinlerde eğitim gören öğrencilerin 6. Uluslararası Öğrenci Bilimler Kongresi vasıtasıyla ortaya koydukları eserler ile uluslararası toplumun çoğulcu bir gelecek kurma ihtiyacı ve arayışında olduğu bu dönemde Türkiye'nin kültürel diplomasi ve kültürlerarası etkileşim merkezli vizyonuna önemli bir destek sağlanmıştır.

Uluslararası öğrencilerin akademik, sosyal ve kültürel donanımlarını güçlendirmeye büyük önem veren İBA, 6. Uluslararası Öğrenci Bilimler Kongresi'nde sunulan bildirilerin muhtevisyatını oluşturduğu bu eser ile dünyanın pek çok farklı noktasından Türkiye'ye uzanan eğitim ve araştırma yolculuğunun bilimsel, zihinsel ve kültürel bir ürününü siz değerli okuyuculara sunmaktadır. Bu eser Orta Asya'dan Afrika'ya, Balkanlar'dan Ortadoğu'ya, oralardan Türkiye'ye uzanan ve geniş bir yelpazede şekillenen ilim yolculuğunun uluslararası bir çıktısı olarak görülebilir.

**Prof. Dr. Gülfettin ÇELİK**  
İstanbul Bilimler Akademisi Vakfı  
Yönetim Kurulu Başkanı



**BİYOLOJİ ÇALIŞMALARI**  
*BIOLOGY STUDIES*





# EPIDIDYMAL CAMEL SPERMATOZOA QUALITY AS AFFECTED BY GREEN LASER IRRADIATION DURING INCUBATION AT 37°C

Ahmed Seioudy<sup>1</sup>

---

## Abstract

A total number of forty testes from twenty Sudani camels (*Camelus dromedarius*) were used in the present study (>5-10 years old and 500-600 kg body weight). The experimental work was executed to define the effect of green laser irradiation with short-wavelength 532 nm and continuous wave from a diode laser light with a total output power of 3 mW on epididymal camel spermatozoa quality at different exposure times of 0 (control, non-irradiated), 2, 4, 6, 8, and 10 min. Following irradiation, the percentages of motile spermatozoa, viability, acrosomal damage and the enzymatic activity of AST, ALT and ALP enzymes were assessed of the epididymal camel spermatozoa during incubation at 37°C for 8 hours. Epididymal spermatozoa was diluted with lactose-yolk-citrate (LYC)

---

<sup>1</sup> PhD Student, Ege University, Faculty of Agriculture, Department of Animal Science, ORCID: 0000-0001-6627-0781

extender. The obtained results showed that the highest ( $P<0.05$ ) value of the percentage of motile spermatozoa was recorded with spermatozoa exposed to 6 min of laser irradiation and the lowest ( $P<0.05$ ) value was recorded with the control group. Otherwise, the highest ( $P<0.05$ ) value of the percentages of dead, acrosomal damage of spermatozoa and the enzymatic activity of AST, ALT and ALP enzymes were recorded with spermatozoa exposed to 10 min and the lowest ( $P<0.05$ ) value was recorded with 2 min. The advancement of incubation time at 37°C decreased ( $P<0.05$ ) the percentage of motile spermatozoa, while increased ( $P<0.05$ ) the percentages of dead, acrosomal damage of spermatozoa and the enzymatic activity of AST, ALT and ALP enzymes during incubation at 37°C for 8 hours. Consequently, enhancing the artificial insemination program can be achieved using the laser irradiation which is considered a cost-effective technique for improving semen quality. The profitable effects of laser irradiation on epididymal camel spermatozoa quality raised the motile spermatozoa, livability, acrosomal integrity which consider an indicator to improve mitochondrial function which extends the survival of spermatozoa.

**Keywords:** Camels, Epididymal Spermatozoa, Green Laser Irradiation, Incubation, Quality.

## 1. Introduction

The camel (*Camelus dromedarius*) is an important livestock species uniquely adapted to hot and arid environments. With increasing human population pressure and decline of food production in Africa there is an urgent need to develop previously marginal resources and optimize their utilization through appropriate livestock production systems of which camel production is certainly the most suitable one. However, plentiful and complicated natural restrictions can adversely affect the reproductive capacity of the one-humped camel (El-Hassanein et al., 2004).

Artificial insemination (AI) is considered as one of the most important and the fastest way in the modern technology for the application of genetic improvement through the breeding programmes of farm animals. The progress in AI, semen preservation and related techniques in camels has been slow in comparison to other animals due to the difficulty of semen collection, little information in semen characteristics, semen dilution and storage of semen. During preservation, several factors may be responsible of the possible decrease in fertilizing ability of semen during storage under different conditions (Anand, 1979). Therefore, it is necessary to evaluate other strategies which aim to improve sperm mitochondrial function.

The term laser stands for light amplification by stimulated emission of radiation. During the last two decades of the 20th Century, the effects of laser on biological tissues have been studied widely. It has been clearly revealed that laser irradiation, has declared biological effects. Irradiation of spermatozoa has been shown to improve sperm motility with a low intensity helium-neon (He-Ne) laser (Karu, 2012). The first application of laser to improve sperm function was shown in 1969 (Goldstein, 1969), which has been applied in various species like human (Lenzi et al., 1989), mouse (Cohen et al., 1998), sheep (Zan-Bar et al., 2005), dog (CorralBaqués et al., 2009), and rabbit (Iaffaldano et al., 2010) spermatozoa. Thus, the current study aimed to define the effect of green laser irradiation with short-wavelength 532 nm, 3 mW with different exposure times of 0, 2, 4, 6, 8, and 10 min on the epididymal camel spermatozoa quality during incubation at 37°C for 8 hours.

## **2. Materials and Methods**

The current study was carried out at Embryo Transfer Laboratory, Artificial Insemination and Embryo Transfer Department, Animal Reproduction Research Institute, Giza, Egypt, in cooperation with the Laser Atomic Spectroscopy Laboratory, Department of Laser Applications in Measurements, Photochemistry and Agriculture, National Institute of Laser Enhanced Sciences, Cairo University, Giza, Egypt.

### **2.1. Experimental animals**

A total number of twenty clinically healthy Sudani camels (*Camelus dromedarius*) with a total number of forty testes aged from >5 to 10 years or more with live body weights of 500-600 kg were used in the present work and provided from automated El-Bassatein slaughterhouse, Cairo, Egypt.

### **2.2. Epididymal spermatozoa collection**

#### ***Transportation of the samples:***

The genitalia (epididymides connected to the testes) were removed from the carcass and transported in a thermos flask including sterile physiological saline (0.9%) with 100 µg/ml streptomycin at 25°C according to the method described by Goto et al. (1989) through 2-3 hours after slaughtering.

#### ***Sperm recovery:***

Forty testes were fully cleaned then the blood was wiped off by puncturing the superficial blood vessels of the cauda. By using a sterile scalpel and forceps, the epididymis was sectioned into three respective parts, caput, corpus, and cauda in three sterile Petri dishes of 100 mm diameter containing saline solution.

### **2.3. Semen Extension**

Epididymal camel spermatozoa were collected, pooled, and evaluated for each camel and then diluted with lactose-yolk-citrate dilution (2.9 g sodium citrate dihydrate, 0.04 g citric acid anhydrous, 1.25 g lactose and 10 ml egg-yolk, per 100 ml distilled water, 500 I.U/ml penicillin and

500 µg streptomycin sulphate were also added to the extender) according to Musa et al. (1992).

#### **2.4. Incubation of Semen at 37°C**

Semen was divided into 6 groups, a control group (non-irradiated group) and 5 groups of irradiated semen with green laser irradiation for (2, 4, 6, 8, and 10 min). All groups were stored by incubation at 37°C for up to 8 hours. Motile, dead and acrosomal damage (%) of spermatozoa exposed to different exposure times of laser irradiation (0, 2, 4, 6, 8, and 10 min) were recorded following incubation. Moreover, enzymatic activity (AST, ALT and ALP enzymes) were also determined during incubation at 37°C for up to 8 hours.

#### **2.5. Semen evaluation**

##### ***Epididymal Sperm Motility (%):***

Motile spermatozoa (%) were detected as an oscillatory movement of the flagellum due to the highly viscous nature of camel semen according to Tibary and Anouassi (1997).

##### ***Dead Spermatozoa (%):***

The eosin/nigrosin staining procedure was carried out by dissolving 1.67 gm eosin and 10 gm nigrosin in distilled water up to 100 ml according to Hackett and Macpherson (1965).

##### ***Acrosomal Damage of Spermatozoa (%):***

The percentage of acrosomal damage was assessed according to Watson (1975). Spermatozoa were stained with 2% of trypan blue (T-0887 Sigma) for assessment of sperm viability then for 40 min with a 10% solution of Giemsa (Merck, Darmstadt, Germany) in distilled water prepared immediately before use.

#### **2.6. Enzymatic activity of AST, ALT and ALP enzymes (U/10<sup>6</sup> spermatozoa):**

Extended semen samples were centrifuged at 600g for 15 minutes. The supernatant fluid (diluted seminal plasma) was collected then kept

at -20°C until analysis of AST, ALT and ALP enzymes. All enzymatic activities of AST, ALT and ALP in the seminal plasma were adjusted according to sperm cell concentration (U/10<sup>6</sup> spermatozoa) according to Reitman and Frankle (1957). The activities of AST, ALT and ALP enzymes were determined colourimetrically using QCA kit, Amposta, Spain.

## 2.7. Laser specifications and irradiation parameters

Green laser ( $\lambda=532$  nm) from a Diode Pumped Solid State (DPSS) laser [LSR-PS-II] with an output power of 3 mW was used for irradiation of spermatozoa with different exposure times (0, 2, 4, 6, 8, and 10 min). Parameters of green laser irradiation were shown in Table (1) as follows: 532 nm wavelength and average power output 3 mW. The irradiance of 3 mW/cm<sup>2</sup> was calculated according to Calderhead (1990) using the following equation:

$$\text{Irradiance} = \frac{\text{Power output (mW)}}{\text{Application surface (cm}^2\text{)}}$$

**Table 1.** Laser fluency and corresponding exposure times

Fluency (J/cm <sup>2</sup> )	Power output (mW)	Exposure time (min)	Wavelength (nm), (Colour)
0.38	3	0, 2, 4, 6, 8, and 10	532 (Green)

## 2.8. Statistical analysis

Two-way ANOVA was used to analyze data statistically, using the procedure of General Linear Model (GLM) of SAS (SAS, 2000). Duncan's Multiple Range Test (Duncan, 1955) was used to detect significant differences among means. Percentage values were transformed into arc-sin values before being statistically analyzed. The statistical model used in the experimental work was as follows:

$$Y_{ijk} = \mu + L_i + I_j + (L_i \times I_j) + e_{ijk}$$

Where,

$Y_{ijk}$  = the observed value of the dependent variable determined from a sample taken of spermatozoa.

$\mu$  = the overall mean.

$L_i$  = the fixed effect of laser irradiation durations (min),  $i = 0, 2, 4, 6, 8$ , and  $10$ .

$I_j$  = the fixed effect of incubation time (hours),  $j = 0, 1, 2, 4, 6$ , and  $8$ .

$L_i \times I_j$  = the interaction between laser irradiation durations (min) and incubation time (hours).

$e_{ijk}$  = the residual error.

### 3. Results and Discussion

#### 3.1. Sperm Motility (%)

Table 2 revealed that the effect of green laser irradiation (532 nm, 3 mW) for 6 min ( $P < 0.05$ ) increased the percentage of motile spermatozoa of the dromedary camel during incubation at 37°C than the control group. These results were in agreement with Nicolae et al. (2015) who found that exposure to helium neon (He-Ne) laser irradiation led to enhanced ram sperm motility, viability, mitochondrial function and hypo-osmotic swelling response at dose of 6.12 J/cm<sup>2</sup> comparing to the dose of 3.96 J/cm<sup>2</sup> which reduced the quality of seminal attributes than the control sample. Similarly, Iaffaldano et al. (2016) found that irradiated frozen-thawed ram semen by He-Ne laser irradiation with fluencies ranged from 3.96 to 9 J/cm<sup>2</sup> resulted in a significant increase in sperm motility and viability at 6.12 J/cm<sup>2</sup>. It could be attributed to the interaction between the mitochondria and laser irradiation which in turn enhance semen quality (Lone et al., 2018), in which higher levels of cytochrome C oxidase activity (COX) and adenosine-5-triphosphate (ATP) were observed in irradiated spermatozoa comparing to non-irradiated spermatozoa and a positive correlation between COX activity and ATP levels was observed; also COX activity and ATP levels were positively correlated with sperm motility.

The present study showed the prolongation of incubation time at 37°C for 8 hours decreased ( $P < 0.05$ ) the percentage of sperm motility at



all exposure times of laser irradiation and the control group (Table 2). These findings may be due to the high metabolic activity of spermatozoa which leads to a toxic effect on the sperm by increasing the production of lactic acid. A similar trend was observed by Abd El-Salaam et al. (2012) who found that the percentage of sperm motility of camel spermatozoa was significantly ( $P<0.01$ ) decreased with advancement of incubation time at  $37^{\circ}\text{C}$  for up to 12 hours. Furthermore, the current study revealed that the interaction effect between incubation time at  $37^{\circ}\text{C}$  for 8 hours and green laser irradiation on motile spermatozoa was insignificant.

### 3.2. Dead Spermatozoa (%)

The dead spermatozoa (%) during incubation at  $37^{\circ}\text{C}$  was higher ( $P<0.05$ ) of spermatozoa exposed to 10 min of laser irradiation than other exposure times and the control group (Table 3). Comparing to the control group (57.96%), the dead spermatozoa (%) decreased ( $P<0.05$ ) with spermatozoa exposed to 2, 4, and 6 min of laser irradiation with an average value of 47.41, 49.07, and 54.44%, respectively. A similar trend was reported by Iaffaldano et al. (2010 & 2016), who found that the viable spermatozoa (%) was higher ( $P<0.05$ ) at 24 hours of storage with 6.12 and  $9.0\text{ J/cm}^2$  than the control in rabbit semen. Similarly, Nicolae et al. (2015) reported that the percentage of viable spermatozoa in ram semen was significantly ( $P<0.05$ ) increased for both of control and irradiated spermatozoa with a dose of  $6.12\text{ J/cm}^2$  than those irradiated with a dose of  $3.96\text{ J/cm}^2$ .

The present study showed that the prolongation of incubation time at  $37^{\circ}\text{C}$  for 8 hours increased ( $P<0.05$ ) the dead spermatozoa (%) of the dromedary camels at all exposure times of laser irradiation and the control group (Table 3). A similar trend was observed by Abd El-Salaam et al. (2012) in the camel spermatozoa, in which the advancement of incubation time at  $37^{\circ}\text{C}$  for up to 12 hours increased significantly ( $P<0.05$ ) the percentage of dead spermatozoa. The interaction effect between incubation time and green laser irradiation on dead spermatozoa was insignificant.

### 3.3. Acrosomal Damage of Spermatozoa (%)

The percentage of acrosomal damage was significantly ( $P<0.05$ ) higher of spermatozoa exposed to 10 min of laser irradiation than other exposure times and the control group (Table 4). In respect to the control group (25.76%), acrosomal damage (%) decreased significantly ( $P<0.05$ ) with spermatozoa exposed to 2 and 4 min of laser irradiation with an average value of 23.22 and 24.07%, respectively. Similar trends were observed by Yeste et al. (2016) who reported that there was no change in acrosomal integrity and viability in liquid stored boar semen, while an increase in sperm motility was observed in which there was a higher reduction in semen quality parameters in non-exposed spermatozoa than irradiated spermatozoa after incubation for 90 min at 37°C.

The present study showed that the prolongation of incubation time at 37°C for 8 hours increased ( $P<0.05$ ) the acrosomal damage (%) at all exposure times of laser irradiation and the control group (Table 4). The current results agreed with Abd El-Salaam et al. (2012) in the camel spermatozoa, in which the advancement of incubation time at 37°C for up to 12 hours increased significantly ( $P<0.05$ ) the percentage of dead spermatozoa. The interaction effect between incubation time at 37°C for 8 hours and green laser irradiation on acrosomal damage of spermatozoa was insignificant.

### 3.4. Enzymatic Activity of AST, ALT and ALP Enzymes (U/10<sup>6</sup> Spermatozoa):

The activity of AST and ALT enzymes as affected by laser irradiation was significantly ( $P<0.05$ ) higher of spermatozoa exposed to 10 min of laser irradiation than the other irradiated spermatozoa and the control group (Tables 5 & 6), respectively while the activity of ALP enzyme was significantly ( $P<0.05$ ) higher of spermatozoa exposed to 8 and 10 min of laser irradiation than the other irradiated spermatozoa and the control group (Table 7). The increase in leakage of the intracellular AST, ALT and ALP enzymes during long exposure times of laser irradiation may reflect the breakdown of the cellular sperm membrane.

The present study showed that the advancement of incubation time at 37°C for 8 hours increased ( $P<0.05$ ) the leakage of AST, ALT and ALP enzymes into the extracellular medium at all exposure times of laser irra-

diation and the control group (Tables 5, 6 & 7), respectively. The current results agreed with Abd El-Salaam et al. (2012) in the camel spermatozoa, in which the advancement of incubation time at 37°C for up to 12 hours increased significantly ( $P<0.05$ ) the amount of AST, ALT and ALP enzymes released into the extracellular medium of the male dromedary camel semen. The interaction effect between incubation time at 37°C for 8 hours and green laser irradiation on AST, ALT and ALP enzymes activity of spermatozoa was insignificant.

#### **4. Conclusion**

In conclusion, laser in the field of semen biology may be regarded as an easy, time saving, less costly, effective and more sensitive technique which can be used for enhancing the artificial insemination program of the dromedary camel due to the beneficial effects of laser on semen quality which included the increase in sperm motility, livability and acrosomal integrity which consider an indicator to improve mitochondrial function which in turn lead to enhanced sperm survival.

It could be recommended for collection and short-term storage of the epididymal spermatozoa of the dromedary camels at 37°C for artificial insemination by being exposed to 6 min of green laser irradiation with short-wavelength (532 nm, 3 mW) to reinforce the fertilizing ability of she-camel, especially in the desert regions where liquid nitrogen may not be available for freezing of semen for a long time.

## REFERENCES

- Abd El-Salaam, A.M., Absy, G.M., Gabr, Sh.A., & Zeidan, A.E.B. (2012). Viability, enzymatic activity and penetrating ability of spermatozoa into she-camel cervical mucous as affected by different extenders. *J. Camel Pract. Res.*, 18(2), 1-9.
- Anand, S. R. (1979). Buffalo sperm metabolism. An assessment of motility, live spermcounts and leakage of acrosomal enzymes from buffalo spermatozoa during dilution and preservation. In: Buffalo Reprod. Artif. Insemin. Proc. Seminar FAO/SIAD/Govit. of India. N.D.R.I., (pp. 284-291). Karnal, India.
- Calderhead, R. G. (1990). On the correct reporting of parameters and consistent use of terminology in reporting clinical and experimental LLLT procedures. *Laser Therapy*, 3, 2-7.
- Cohen, N., Lubart, R., Rubinstein, S., & Breitbart, H. (1998). Light irradiation of mouse spermatozoa: Stimulation of in vitro fertilization and calcium signals. *J. Photochem. Photobiol. B*, 68, 407-413.
- Corral-Baque's, M.I., Rivera, M.M., Rigau, T., Rodriguez-Gil, J.E., & Rigau, J. (2009). The effect of low-level laser irradiation on dog spermatozoa motility is dependent on laser output power. *Lasers Med. Sci.*, 24 (5) 703-713.
- Duncan, D. B. (1955). Multiple range and multiple F-test. *Biometrics*, 11, 1-42.
- El-Hassanein, E. E., El-Bahrawy, K.A., Fateh El-Bab, A.Z., & Zeitoun, M.M. (2004). Sexual behavior and semen physical traits of desert male camels in rut. *J. Egypt. Vet. Med. Assoc.*, 64, 305-321.
- Goldstein, S. F. (1969). Irradiation of sperm tails by laser microbeam. *J. Exp. Biol.*, 51: 431-441.
- Goto, K., Kajihara, Y., Koba, M., Kosaka, S., Nakamishi, Y., & Ogawa, K. (1989). *In-vitro* fertilization and development of *in-vitro* matured bovine follicular oocytes. *J. Anim. Sci.*, 76, 2181-2185.
- Hackett, A.J., & Macpherson, J.W. (1965). Some staining procedures for spermatozoa. *Canadian Vet. J.*, 6, 55-62.
- Iaffaldano, N., Paventi, G., Pizzuto, R., Dilorio, M., Bailey, J.L., & Manchisi, A. (2016). Helium-neon laser irradiation of cryopreserved ram sperm enhances cytochrome C oxidase activity and ATP levels improving semen quality. *Theriogenology*, 86, 778- 784.

Iaffaldano, N., Rosato, M.P., Paventi, G., Pizzuto, R., Gambacorta, M., & Manchisi, A. (2010). The irradiation of rabbit sperm cells with He-Ne laser prevents their in vitro liquid storage dependent damage. *Anim. Reprod. Sci.*, 119, 123-129.

Karu, T. I. (2012). Lasers in infertility treatment: Irradiation of oocytes and spermatozoa. *Photomed. Laser Surg.*, 30, 239-241.

Lenzi, A., Claroni, F., Gandini, L., Lombardo, F., Barbieri, C., & Lino, A. (1989). Laser radiation and motility patterns of human sperm. *Syst. Biol. Reprod. Med.*, 23, 229-234.

Lone, S. A., Mohanty, T.K., Kumaresan, A., & Bhakat, M. (2018). Laser irradiation effects and its possible mechanisms of action on spermatozoa functions in domestic animals. *Asian Pacific J. Reprod.*, 6(3), 97-103.

Musa, B., Sieme, H., Merkt, H., & Hego, B.E.D. (1992). Artificial insemination in dromedary camels. Proc. 1<sup>st</sup> Intern. Camel Conf. (pp. 179-182). UK, Newmarket.

Nicolae, D., Stela, Z., Hortanse, A.A., Irina, T., Iaffaldano, N., Paventi, G., & Dragomir, C. (2015). Study on the effects of exposure to different doses of energy generated by a He-Ne laser on the quality of frozen-thawed semen of ram. *Rom Biotech. Lett. M*, 20(3), 10381-10387.

Reitman, S., & Frankle, M. (1957). A colorimetric method for determination of serum oxaloacetic and glutamic pyruvic transaminase. *Anim. Clin. Pathol. J.*, 16, 28-56.

SAS (2000). SAS User's Guide. Statistical Analysis System Institute Inc., Cary, NC.

Tibary, A., & Anouassi, A. (1997). Male breeding soundness examination. *Theriogenology in camelidae*, 1st Edition, Published by Ministry of Agriculture and Information, UAE., 79-114.

Watson, P. F. (1975). Use of a giemsa stain to detect changes in acrosomes of frozen ram spermatozoa. *Vet. Rec.*, 97, 12-15.

Yeste, M., Codony, F., Estrada, E., Lleonart, M., Balasch, S., & Peña, A. (2016). Specific LED-based red light photo-stimulation procedures improve overall sperm function and reproductive performance of boar ejaculates. *Sci. Rep.* Mar 6(1), 22569.

Zan-Bar, T., Bartoov, B., Segal, R., Yehuda, R., Lavi, R., & Lubart, R. (2005). Influence of visible light and ultraviolet irradiation on motility and fertility of mammalian and fish sperm. *Photomed. Laser Surg.*, 23, 549-555.

**Table 2.** Mean percentage of motile epididymal camel spermatozoa, with different exposure times (min) of green laser irradiation during incubation at 37°C for up to 8 hours

Incubation time (hours)	Laser exposure times (min)						Mean
	Control	2	4	6	8	10	
0	50.56±1.55	52.22±1.21	58.89±2.16	70.56±1.00	69.44±1.30	63.89±1.39	60.93 <sup>a</sup> ±1.21
1	40.00±1.44	46.11±1.11	51.67±1.44	65.56±0.56	63.89±0.73	58.33±0.17	54.26 <sup>b</sup> ±1.34
2	34.44±1.30	40.56±1.30	45.56±1.55	56.67±1.86	55.00±1.67	52.22±1.21	47.41 <sup>c</sup> ±1.25
4	30.00±0.83	34.44±1.00	41.67±1.44	53.33±1.17	51.11±1.11	46.11±1.11	42.78 <sup>d</sup> ±1.24
6	25.00±1.17	33.33±1.17	37.78±0.87	46.67±1.17	44.44±1.30	40.00±0.83	37.87 <sup>e</sup> ±1.07
8	21.11±0.73	30.00±0.00	33.33±1.17	41.67±0.83	38.89±1.11	33.89±1.39	33.15 <sup>f</sup> ±0.98
Overall mean	33.52 <sup>f</sup> ±1.42	39.44 <sup>e</sup> ±1.14	44.81 <sup>d</sup> ±1.31	55.74 <sup>a</sup> ±1.45	53.79 <sup>b</sup> ±1.52	49.07 <sup>c</sup> ±1.48	46.06

<sup>A-F</sup> Values with different superscripts within a column are significantly different (P<0.05).

<sup>a-f</sup> Values with different superscripts within a row are significantly different (P<0.05).

**Table 3.** Mean percentage of dead epididymal camel spermatozoa, with different exposure times (min) of green laser irradiation during incubation at 37°C for up to 8 hours

Incubation time (hours)	Laser exposure times (min)						Mean
	Control	2	4	6	8	10	
0	36.67±1.67	28.89±2.00	30.56±2.27	34.44±1.94	36.67±2.04	43.33±1.86	35.09 <sup>f</sup> ±1.00
1	46.67±1.67	36.11±1.39	37.22±1.68	42.78±1.68	45.00±1.86	50.56±1.94	43.06 <sup>f</sup> ±0.96
2	54.44±1.30	43.89±2.00	46.67±2.35	52.22±1.68	55.56±1.94	61.67±1.86	52.41 <sup>b</sup> ±1.08
4	62.22±1.68	48.89±2.00	52.78±1.68	58.33±1.67	61.67±1.67	67.78±1.21	58.61 <sup>c</sup> ±1.07
6	70.00±1.67	58.89±2.00	58.89±2.00	66.11±1.39	67.78±1.46	72.22±1.68	65.65 <sup>d</sup> ±0.97
8	77.78±1.46	67.78±1.46	68.33±1.17	72.78±1.88	77.78±1.46	78.89±1.11	73.89 <sup>a</sup> ±0.84
Overall mean	57.96 <sup>b</sup> ±1.99	47.41 <sup>a</sup> ±1.94	49.07 <sup>d</sup> ±1.89	54.44 <sup>c</sup> ±1.92	57.41 <sup>b</sup> ±2.00	62.41 <sup>a</sup> ±1.80	54.78

<sup>A-E</sup> Values with different superscripts within a column are significantly different (P<0.05).

<sup>a-d</sup> Values with different superscripts within a row are significantly different (P<0.05).

**Table 4.** Mean percentage of acrosomal damage of epididymal camel spermatozoa, with different exposure times (min) of green laser irradiation during incubation at 37°C for up to 8 hours

Incubation time (hours)	Laser exposure times (min)					Mean
	Control	2	4	6	8	10
0	20.22±0.57	18.56±0.50	18.78±0.57	20.11±0.58	20.44±0.60	22.33±0.75
1	22.22±0.57	19.78±0.55	20.33±0.65	21.44±0.66	22.11±0.72	24.11±0.67
2	24.11±0.63	21.67±0.73	22.44±0.73	23.44±0.63	24.00±0.75	26.33±0.82
4	26.78±0.64	24.22±0.74	25.11±0.58	26.11±0.81	26.89±0.63	29.33±0.85
6	29.22±0.64	26.44±0.47	27.11±0.69	28.56±0.58	28.89±0.67	31.78±0.87
8	32.00±0.85	28.67±0.68	30.67±1.30	31.22±0.89	32.11±0.87	34.11±0.92
Overall mean	25.76 <sup>b</sup> ±0.61	23.22 <sup>d</sup> ±0.55	24.07 <sup>c</sup> ±0.64	25.15 <sup>b</sup> ±0.60	25.74 <sup>b</sup> ±0.62	28.00 <sup>a</sup> ±0.65
						25.32

<sup>A-F</sup> Values with different superscripts within a column are significantly different (P<0.05).

<sup>a-d</sup> Values with different superscripts within a row are significantly different (P<0.05).



**Table 5.** Activity of aspartate-aminotransferase enzyme (U/10<sup>6</sup> spermatozoa) of epididymal camel spermatozoa, with different exposure times (min) of green laser irradiation during incubation at 37°C for up to 8 hours

Incubation time (hours)	Laser exposure times (min)					Mean
	Control	2	4	6	8	10
0	42.56 <sup>a</sup> ±1.51	42.56±1.51	43.56±1.57	43.89±1.52	44.78±1.49	47.56±1.53
1	46.22±1.53	45.78±1.62	46.44±1.61	47.11±1.73	47.67±1.65	50.67±1.64
2	50.11±1.70	50.00±1.74	50.89±1.76	51.56±1.65	51.89±1.81	54.89±1.83
4	54.56±1.74	54.33±1.67	55.11±1.64	55.44±1.82	56.33±1.72	59.67±1.72
6	59.78±1.87	59.56±1.84	59.89±1.83	60.89±1.81	61.22±1.86	64.22±2.03
8	64.56±1.72	64.11±5.08	64.78±1.67	65.78±1.71	66.11±1.68	69.67±1.72
Overall mean	52.96 <sup>b</sup> ±1.23	52.72 <sup>b</sup> ±1.22	53.44 <sup>b</sup> ±1.21	54.11 <sup>b</sup> ±1.23	54.67 <sup>b</sup> ±1.22	57.78 <sup>a</sup> ±1.25
						54.28

<sup>A-F</sup> Values with different superscripts within a column are significantly different (P<0.05).

<sup>a-c</sup> Values with different superscripts within a row are significantly different (P<0.05).

**Table 6.** Activity of alkaline phosphatase enzyme (U/10<sup>6</sup> spermatozoa) of epididymal camel spermatozoa, with different exposure times (min) of green laser irradiation, during incubation at 37°C for up to 8 hours

Incubation time (hours)	Laser exposure times (min)						Mean
	Control	2	4	6	8	10	
0	21.44±0.94	21.22±0.94	21.89±0.97	23.00±1.05	24.00±1.00	27.33±1.01	23.15 <sup>f</sup> ±0.48
1	24.67±0.93	24.22±1.06	25.00±1.09	25.56±1.06	26.44±1.14	29.67±1.31	25.93 <sup>f</sup> ±0.49
2	27.33±0.95	27.11±1.02	27.56±1.04	28.00±1.03	28.67±1.09	31.89±1.12	28.43 <sup>d</sup> ±0.46
4	30.78±1.17	30.78±1.17	31.56±1.17	32.33±1.15	33.00±1.17	36.22±1.15	32.44 <sup>c</sup> ±0.52
6	34.33±1.25	34.22±1.28	35.44±1.33	35.67±1.36	36.22±1.36	39.44±1.37	35.89 <sup>a</sup> ±0.56
8	37.67±1.17	37.67±1.17	38.11±1.34	38.67±1.20	39.22±1.16	42.44±1.30	38.96 <sup>a</sup> ±0.53
Overall mean	29.37±0.86	29.20±0.88	29.93 <sup>bc</sup> ±0.90	30.54 <sup>bc</sup> ±0.88	31.25 <sup>b</sup> ±0.86	34.50 <sup>a</sup> ±0.87	30.79

<sup>A-F</sup> Values with different superscripts within a column are significantly different ( $P<0.05$ ).

<sup>a-c</sup> Values with different superscripts within a row are significantly different ( $P<0.05$ ).



# PRODUCTION AND PURIFICATION OF CHROMATE REDUCTASE FROM BACILLUS PARAMYCOIDES S-9 FOR BIOTRANSFORMATION OF CHROMIUM (VI)

*Kalsoom Kalsoom*<sup>1</sup>

---

## Abstract

A chromium (Cr) resistant bacterium designated as strain S-9 was isolated from industrial sludge. Strain S-9 was identified via 16S rRNA sequencing and showed 99% similarity with *Bacillus paramycoides*. *Bacillus* sp. strain S-9 was found resistant to chromium as indicated by its significant growth upto 1400 mg/L of  $K_2Cr_2O_7$  at mesophilic temperature. The enzyme chromate reductase activity was found during the experiment that causes reduction of Cr into non-toxic state. The physicochemical variables influencing chromate reductase production were identified by statistical tools, Plackette Burman Design (PBD) and Central Composite Design (CCD). The chromate reductase was purified through size exclusion column chromatography from strain S-9, exhibited specific

---

<sup>1</sup> PhD Student, Karadeniz Technical University, Faculty of Science, Biology, ORCID: 0000-0002-2633-6018

activity of 1416.549 U/mg, 59.5% yield, and 6.6-fold increase in purity under optimum physicochemical conditions. The maximum activity chromate reductase was observed at temperature 40°C and pH 7.0. The  $K_m$  and  $V_{max}$  value of bacterium were 1.36  $\mu$ M and 909.09  $\mu$ M respectively, using  $K_2Cr_2O_7$  as a substrate. The activity of chromate reductase was strongly inhibited by Hg, SDS, and CTAB. *Bacillus* sp. strain S-9 reduced 69% of chromium at concentration upto 100 mg/L after 96 hrs. Furthermore, effluent containing 100 mg/L of  $K_2Cr_2O_7$  was treated with 1-10% of both crude and purified chromate reductase. The crude and purified chromate reductase (10% v/v) showed maximum reduction of 75% and 87% after 120 hours, respectively. The results in this study indicates that this strain could effectively be utilized for remediation of metals polluted sites.

**Keywords:** Bioreduction, Chromate Reductase, Industrial Effluent, *Bacillus Paramycoides*.

## 1. Introduction

Heavy metals are toxic environmental pollutants and are present as natural constituents of the earth's surface. Heavy metal ions have densities greater than  $5\text{gm/cm}^3$  and they are five times denser than water which is highly lethal at very low concentrations. Metals such as Chromium(Cr), mercury (Hg), cadmium (Cd), thallium (TI), lead (Pb), and arsenic (As) are major environmental pollutants (Vardhan et al., 2019). Heavy metals have both significant and detrimental impact on the life of human, plants, aquatic creature, and microorganisms depend on concentration of heavy metals. High HM concentration uptake by the plants and subsequent accumulation of HM in human tissue followed by the biomagnification via the food chain, pose a threat to both human health and the environment (Asati et al., 2016).

Chromium is a firm, steel-gray metal present in the form of chromite ore in the earth's mantle. It mainly belongs to the transition elements and is the first member of group VI of periodic table. It occurs in different oxidation states (from  $\text{Cr}^{+2}$  to  $\text{Cr}^{+6}$ ) and hexavalent form of the chromium are the most stable. Naturally in trace amounts they present in the environmental components like water, air, and soil (Coetzee et al., 2020). The uptake of hexavalent chromium by eukaryotic and prokaryotic become more accessible than trivalent chromium because of its high solubility and mobility. Chromium is considered an essential micronutrient in human beings' and animals' diets because it show a major role in metabolism of proteins, sugar, and lipids. The oxidation state of Chromium decides its level of toxicity, e.g.,  $\text{Cr}^{+6}$  is more destructive than  $\text{Cr}^{+3}$  and cause adverse health effects on animals and humans like ulcers, diarrhea, kidney dysfunction, irritation of skin, eye, and carcinoma of lungs (Qian et al., 2017). The toxicity of chromium in eukaryotes and prokaryotes is linked to its fast diffusion of chromium through the bacterial membrane and produce free radicals through reduction of chromium. These free radicals cause alteration of DNA and other lethal effects (Jobby et al., 2018). Heavy metals have been eliminated using a variety of conventional physicochemical methods from contaminated sites but, these approaches are incompetent as a result of high energy and power supplies, produce unwanted by-products, and unsuccessful

to eradicate all-metal pollution (Singh & Prasad, 2015). Whereas biological treatments of chromium using native and non-hazardous bacteria is considered a fast, cost-effective, economical, chemical-free, and energy-efficient technique. Among microbes, bacteria are most effective in transforming toxic hexavalent chromium into non-toxic form of chromium. more economical, inexpensive, and ecofriendly due to their cost (Trellu et al., 2016). As Microorganisms can live in heavy metal contaminated soil due to their ubiquitous existence and can convert heavy metals into non-toxic forms (Verma & Kuila, 2019). The use of enzymes extracted from the microbial cell is more valuable than using the whole microbe. Microbial biotransformation produces lethal side products that are harmful to the environment while enzymatic biotransformation is safe to the environment because no lethal products are formed (Jobby et al., 2018). Previous studies reported only batch Chromate reduction but chromate reduction through enzymes are still unclear. Furthermore less valuable information are available on purified chromate reductase characterization and its applications for treatment of chromium contamination. To develop an effective enzymatic reduction process for chromium contamination, it is important to not only focus on new bacterial strains but also on enzymatic machinery, parameters optimization for obtaining high yield of enzyme. To address these shortcomings, we design this study to not only optimize fermentation conditions that are influencing bioreduction and enzyme production but also to provide an effective bioremediation strategy that can be employed for cleanin of heavy metals polluted environments. In our study chromium resistant strain S-9 was isolated from chromium contaminated industrial sludge and studied for maximum chromium resistance. This strain S-9 was then further utilized for bioreduction experiments with whole bacterial cell and for chromate reductase production.

## **2. Material and Methods**

### **2.1 Materials**

1,5 diphenylcarbazide (DPC) Potassium di chromate ( $K_2Cr_2O_7$ ), NADH, phosphoric acid were obtained from Sigma Aldrich.

## 2.2 Sample Collection and Strains Isolation

Sludge sample was collected from industrial zone in sterile bottle which are highly polluted and contain considerable amount of heavy metals like chromium, lead, mercury, etc for isolation of metal resistant bacteria, sludge was ten-fold diluted ranging from  $10^{-1}$  to  $10^{-10}$ . 100µl of the sample was shifted to nutrient agar plates amended with 200 mg/L of potassium dichromate ( $K_2Cr_2O_7$ ) and incubated at 37°C for 24 hrs. A bacteria designated as S-9 was selected in total 35 bacterial strains on the basis of maximum resistance to ( $K_2Cr_2O_7$ ). The selected strain S-9 was store at 4°C for further analysis.

## 2.3 Screening for Chromium (Cr) Resistance

Bacterial strain S-9 was analyzed for maximum chromium resistance through both broth and plate assay. Strain S9 was inoculated separately to both nutrient agar and broth amended with chromium concentration ranging from 50mg/L to 1500mg/L and incubated at 35°C for 24 hrs.

## 2.4 Characterization of Isolate

### *Macroscopic, Microscopic and Biochemical Examination*

Colony morphology of bacterial strain S-9 was determined on nutrient agar plate and various feature were observed such as shape, size, opacity, and texture etc. Bacterial strain S-9 was stained gram stained and examined microscopically (Olympus Optical, CX21FS, Japan) for cell microscopic morphology. For biochemical characteristics various tests were performed i.e. catalase, oxidase, MacConkey agar, triple iron sugar, urease, simmon citrate and indole test.

### *Molecular Analysis*

For molecular identification of Strain S-9, DNA extraction kit was used as per manufacturer's instructions (Eco-Pure-Genomi, Product Code # E1075). Concentration and purity of genomic DNA was determined using Nano Drop (Thermo Scientific, 2000). The 16S rRNA region of genomic DNA was amplified using universal primers Forward (AT-



TCTAGAGTTTGATCATGGCTCA) and reverse complement primers (TACACACCGCCCGTCACACGGTACCAT). The PCR mixture contained 1  $\mu$ L of each primer of 10 mM, 10  $\mu$ L of Go-Taq buffer, (3  $\mu$ L of  $MgCl_2$  (25 Mm), 1  $\mu$ L of dNTPs (10mM), 0.5  $\mu$ L of Taq polymerase, 1  $\mu$ L of DNA template and 32.5  $\mu$ L of deionized water making total volume of reaction 50  $\mu$ L. The PCR conditions were; denaturation temperature and time 95°C for 3 min followed annealing temperature 55°C for 1 min, extension temperature for 36 cycles 72°C for 1hr and 40sec and one cycle of final elongation at 72°C for 7 min. PCR product amplification was confirmed by using a 1% agarose gel containing ethidium bromide, and analyzed using a Bio-Rad Gel Doc imaging system. The 16S rRNA sequence of our strain was checked for similarity using the ezbiocloud program (<https://www.ezbiocloud.net/>) and all sequences showing similarity > 95% were downloaded. All downloaded and selected sequences were aligned by using BioEdit.exe 7.2 Software, then the Neighbor-Joining phylogenetic tree was assembled based upon MEGA-X software (Kumar et al., 2018).

### 2.5 Batch Bioreduction of Toxic Chromium (VI) By Whole Cell

Batch bioreduction experiment was performed under optimized condition at pH 7.0 and temperature 35°C. Bioreduction was performed by varying Cr(VI) concentration (0–400 mg/L) and contact time (24 hrs–120 hrs), the abiotic control flask containing Cr(VI) without inoculums was also maintained. The Cr(VI) reduction was analyzed by 1,5 diphenylcarbazide method (Fulladosa et al., 2006), after 24, 48, and 72 hours 1mL of sample from bacterial cultures were taken. The supernatant was collected after centrifugation at 14000rpm, 4°C for 5 min. Cr(VI) in the media was estimated using the supernatant. Reaction mixture containing, 10mL distilled water in test tubes, 400 $\mu$ L supernatant, 1mL DPC (0.25g DPC in 100mL acetone), and one drop of phosphoric acid in test tubes. Incubate for 10 min to develop color and then absorbance was determined spectrophotometry at 540nm using spectrophotometer (Agilent Technologies, G6860A, Malaysia). Reduction activity was determined using the  $K_2Cr_2O_7$  as a standard curve.

## 2.6 Chromate Reductase Quantitative Assay

The chromate reductase was assayed through quantitative assay with minor modifications (Thatoi et al., 2014). A reaction mixture containing 0.2mL (0.2mM), potassium dichromate ( $K_2Cr_2O_7$ ) substrate, 0.2 mL of 0.2M-buffer, pH (7.2), NADH solution 0.2mL of 0.2mM, 0.4mL solution of cell free supernatant, a total volume of 1mL was incubated for 30 min at 30°C. After incubation of 30 min. Reaction mixture was kept in water bath for 30 min at 37°C. The reaction was stopped by adding 0.5 mL of TCA (20%). Finally, 2mL of 0.5%(W/V) of DPC in acetone were supplemented. For blank, instead of enzyme solution, distilled water is added. The absorbance of hexavalent chromium was determined at the wavelength of 540nm. The amount of enzyme that will release 1  $\mu$ mol/mL of chromate per min is stated as enzyme unit. For the determination of protein content in the crude sample, Lowry's (1951) method was used, bovine serum albumins (10–100 $\mu$ g) was used as standard. Chromate reductase specific activity is calculated as U/mg. Chromate specific activity was measured by the following formula:

Specific Activity = Unit per mL of enzyme activity/ mg per mL of total protein.

## 2.7 Standardization of Chromate Reductase Assay Conditions

The enzyme production media contain different components g/L,  $KH_2PO_4$ , 3;  $Na_2HPO_4$ , 6;  $CaCl_2$ , 0.1;  $MgSO_4 \cdot H_2O$ , 0.1; NaCl, 0.5; sucrose, 10.05; Luria broth (LB), 20 and Cr(IV), 100mg/L. 24 hrs fresh bacterial culture S-9 was inoculated and incubate for 48 hrs at 37°C. After incubation, cell free supernatant was use for enzyme assay. Optimization of temperature and pH were determined by performing enzyme assay at different temperatures 20°C to 50°C and pH (3.0 to 9.0). the incubation time was determined by incubated reaction mixture for 10 min to 60 min, Enzyme solution (100  $\mu$ L 500  $\mu$ L) and substrate (100  $\mu$ L to 500  $\mu$ L) concentration was optimized at already optimum condition.

## 2.8 Optimization of Physical Parameters for Chromate Reductase Production

The growth condition of bacterial strain S9 for maximum production of chromate reductase was optimized via the method of submerged

fermentation. Optimum temperature and pH of chromate reductase of strain S-9 was achieved by incubating enzyme reaction solution at different temperature values ranging from 20°C-45°C and pH values ranging from 5-9 for 1 hour. Similarly, the effect of incubation time and inoculum size on production chromate reductase was calculated by growing bacterial strain S-9 at different intervals of time (24 to 96 hours) and at different sizes of inoculum (0.1-3%) respectively. The specific activity was calculated by performing chromate assay and protein quantification at 24 hrs intervals upto the maximum of 96 hrs.

## 2.9 Optimization of Media Constituents for Chromate Reductase Production

### *The Plackett-Burman Design (PBD)*

The PBD was used to figure out the most important parameters influencing enzyme production. Different constituents of the production medium were optimized by using Plackett-Burman. Mostly, Design Expert 7 software (Stat-Ease Inc.) was used to plan experiments. Bacterial inoculum was prepared from 24 hrs fresh culture and incubated in production media. The composition of production media for maximum enzyme, 11 factors were analyzed ( $\text{Na}_2\text{HPO}_4$ , yeast extract,  $\text{MgSO}_4 \cdot 7\text{H}_2\text{O}$ ,  $\text{KH}_2\text{PO}_4$ ,  $\text{CaCl}_2$ ,  $\text{NaCl}$ , sucrose,  $\text{K}_2\text{Cr}_2\text{O}_7$ ,  $\text{Na}_2\text{HPO}_4$ ,  $\text{K}_2\text{HPO}_4$ , and  $(\text{NH}_4)_2\text{SO}_4$ ). For mathematical modeling, first order polynomial model was used described below.

$$Y = \beta_0 + \sum \beta_i X_i$$

In this equation Y is representing specific activity of enzyme in term of predicted response where  $\beta_0$ ,  $\beta_i$  and  $X_i$  represent the intercept of the model, the level of self-regulating variable and linear coefficient respectively. At two different stages, the effect of these different factors was observed; -1 for the low concentration and +1 for the maximum concentration. Design Expert 7 software was used to run 15 sets with various concentrations of compounds. All the 15 sets of selected strains were run at 37°C through submerged fermentation at 150rpm. Crude and specific chromate reductase activity were calculated after 72 hours by performing enzyme assay and protein quantification. By analyzing the responses,

important factors were observed. Factors having a p-value of <0.05 for the production of chromate reductase were regarded as important and further optimized by another design named central composite design.

### *Central Composite Design (CCD)*

The important factors provided by Plackett-Burman were further optimized by CCD, having both positive as well as the negative effect on the production of the Chromate Reductase from strain S-9. The optimum reading of factors, their significant effect, and their interaction with one another to positively affect the production was determined for enzyme production. Four varying factors ( $\text{KH}_2\text{PO}_4$ ,  $\text{K}_2\text{Cr}_2\text{O}_7$ , Sucrose, and  $\text{MgSO}_4 \cdot 7\text{H}_2\text{O}$ ) obtained from using PBD were further checked for their effect and analyzed in runs at two different levels. Specific activity of the enzyme was evaluated using second order polynomial equation and multiple regressions were used for fitting data. Effects of the significant independent factors i.e. Linear, quadratic and mutual interactions over dependent variable enzyme specific activity (U/mg) were evaluated. The given quadratic polynomial equation is representing mathematical connection between in need of variable and the significant independent variable;

$$Y = \beta_0 + \sum_{i=1}^5 \beta_i X_i + \sum_{i=1}^5 \beta_i X_i^2 + \sum_{i < j=2}^5 \beta_{ij} X_i X_j$$

In this equation Y;  $X_i$ ,  $\beta_0$ ,  $\beta_i$ ,  $\beta_{ij}$ ,  $\beta_{ii}$  are representing the specific activity; significant independent variables, linear regression coefficients, quadratic regression coefficients, interactive regression coefficients and a constant term respectively. The model suitability was assessed using ANOVA.

## **2.10 Bulk Production of Chromate Reductase Under Optimized Culture Conditions**

500ml of production media Ph (7.0) and 1% of fresh inoculum size of *Bacillus paramycoides* strain S-9 was inoculated and incubate for 72 hrs in a shaker incubator at 150rpm and temperature 37°C The composition of enzyme production media is [g/L;  $\text{KH}_2\text{PO}_4$ , 1;  $\text{Na}_2\text{HPO}_4$ , 4;  $\text{NaH}_2\text{PO}_4$ , 3;  $\text{CaCl}_2$ , 0.1; NaCl, 0.6;  $\text{MgSO}_4 \cdot 7\text{H}_2\text{O}$ , 5; Sucrose, 15;  $\text{K}_2\text{Cr}_2\text{O}_7$ , 0.002;  $\text{K}_2\text{H}$

$\text{PO}_4^{3-}$ ; Yeast extract 8 and  $(\text{NH}_4)_2\text{SO}_4$  2.5]. The supernatant was collected after centrifugation and protein quantification and enzyme assay was performed.

## **2.11 Purification of chromium reductase**

### ***Ammonium Sulfate Precipitation***

All steps of purification were analyzed at 4°C. Cell free supernatant was obtained by centrifugation of production media. Ammonium sulfate was added slowly by continuous stirring at 4°C to the supernatant to get 80% saturated solution using EnCor Biotechnology Inc calculator. The saturated solution was kept for 12 hrs at 4°C. The precipitated solution was centrifuged at 10,000Xg for 10 min and resulted pellet was dissolved in potassium phosphate buffer having pH 7.2. Ammonium sulfate was removed followed by dialysis. The partially purified enzyme was stored at -20°C.

### ***Purification by Gel Filtration Chromatography***

Gel permeation chromatography was used for the separation of proteins (Determann, 2012). The column was filled with Sephadex G-100 gel up to a length of 21cm in phosphate buffer pH (7.2). For degassing, sonicate buffer and gel solution for fifteen minutes. The column was then filled with gel with great care taken to avoid the formation of bubbles, up to a length of 27cm, of which 21cm was made of gel while the rest was phosphate buffer. The flow rate of the column was maintained to collect 3ml in 15 min. Approximately 4ml of the crude enzyme was loaded into the Sephadex column. For a smooth and continuous flow rate of the sample in the column, potassium phosphate buffer was added. Total 30 fractions were collected and analyze for total protein at 280nm. The enzyme assay was performed for all fractions. Fractions with high chromate reductase activity were collected and kept at 4°C for further analysis.

### ***Molecular Weight Determination***

Purified chromium reductase molecular size was determined by (SDS-PAGE). 10% gel was used in SDS-PAGE to run the sample. Coomassie brilliant blue R-250 dye was used to stain gel.

## 2.12 Characterization of purified chromium reductase

### *Effect of Temperature and Ph on Chromium Reductase Activity and Stability*

The effect of temperature on purified chromate reductase enzyme was measured from 30°C to 60°C for 30 minutes. The thermal stability of enzyme from bacterial strains was calculated by incubating it at varying temperatures from 30°C to 60°C in the absence of (potassium dichromate) substrate for 120 minutes. The effect of pH on purified enzyme activity and stability was measured at different pH values (pH 3.0 –pH 9.0) by using different buffers i.e. 100mM acetate buffer (pH 3.0- 5.0), phosphate buffer for (pH 6.0 – 8.0), and Glycine NaOH buffer (pH 9.0 – 11.0). The activity was analyzed in terms of relative activity using standard enzyme assay.

### *Metal Ions Effect on the Activity of Enzyme*

The effect of metals on purified chromium reductase was determined metals ions were used at concentration of 2mM and 10Mm. Metals ions were used in the form of the following salts ;( barium sulfate, calcium chloride, copper sulfate, magnesium sulfate, calcium sulfate, zinc sulfate, copper chloride, potassium chloride, sodium chloride, mercury sulfate, ferrous sulfate, nickel chloride, potassium sulfate, cobalt chloride, urea, nickel sulfate, and sodium sulfate). The effect of metals was determined in terms of relative activity.

### *Surfactants Effect on The Activity of the Enzyme*

The purified chromate reductase enzyme was examined in the presence of different surfactants to determine its relative activity. Surfactants with concentration 0.5% and 1% were used. These surfactants include Tween 80, Tween 20, SDS, CTAB, Triton X-100, and Polyethylene Glycol (PEG). Determine the effect of surfactants in terms of relative activity.

### *Organic Solvents Effect on The Activity of the Enzyme*

The effect of organic solvent on purified chromate reductase activity was carried out by calculating activity in the presence of different organic solvents. Organic solvents with a concentration of 15% were used. The organic solvents include methanol, acetonitrile, acetone, propanol, butanol, ethanol, formaldehyde, glycerol, and ethyl acetate. After that, determine the effect of different organic solvents in terms of relative activity.

### ***Determination of Kinetic Parameters***

Chromate reductase from chromium resistant bacteria strain S-9 was determined at 40°C, pH 7.2 in a reaction mixture with various concentrations of chromate (0.1mM to 1mM). The  $V_{max}$  and  $K_m$  of kinetic constant were determined by plotting the results on the Lineweaver-Burk software program.

### **2.13 Bioreduction of Toxic Form of Chromium by Purified Chromate Reductase**

Effluent was prepared by adding 500 mg/L of potassium dichromate to sterile distilled water and then treated with varying concentration of crude and purified enzymes in term of percentage (1-10 v/v). The samples were incubated at 35°C for 72 hours and concentration of remaining chromium was analyzed using Di-Phenyl Carbazide method after every 24 h.

### **2.14 Statistical analyses**

All experiments were carried out in triplicates, statistical analysis were determined by mean of Plackett Burman and Central Composite Design. Both software used for optimization of nutritional factors and acceptability of models were determined by ANOVA.

## **3. Results**

### ***Screening of Chromium and Bacterial Isolates in Sludge Sample***

#### **3.1 Isolation of Chromium Resistant Bacteria**

Sludge samples were collected industrial waste and metal was recorded by mean atomic absorption spectroscopy (AA-7000, Shimadzu, Japan). The total chromium concentration was found 2648.644 mg/Kg. Initially total 38 bacterial strains were isolated by selective enrichment and bacterial strain designated S-9 was selected for further analysis based on maximum resistant to  $K_2Cr_2O_7$  at 35°C.

### 3.2 Screening for Chromium Resistance

All 38 bacterial strains were screened for Cr resistance using agar plate and broth, bacterial strain S-9 was found resistant to high concentration of chromium (1500 mg/L) on agar plate, while exhibited maximum chromium resistance upto 1400 mg/L in broth (Fig3.1).

### 3.3 Characterization of Bacterial Strain

#### *Macroscopic, Microscopic and Biochemical Examination*

Colony morphology of strain S-9 on nutrient agar showed medium size, flat white color colony with rough edges at 35°C. Microscopy was performed and bacterial strain S-9 was found gram positive rod shaped. Biochemical examination of bacterial strain S-9 showed negative result for MacConkey, Urease, Indole, TSI and Simmon citrate test, and positive result for Catalase and Oxidase test.

#### *Molecular Identification*

16S rRNA sequencing was analyzed by comparing the nucleotide sequences present in NCBI databases using search blast analysis. The 16S rRNA gene sequence analysis of strain S-9 showed close homology to *Bacillus paramycoides*. The S-9 was identified as *Bacillus paramycoides* obtained the nucleotide sequence from NCBI database (Figure 3.2).

### 3.4 Batch Bioreduction of Toxic Chromium (VI)

Cr (VI) bioreduction by bacterial strain S-9 was determined at varying initial concentrations ranging from 50 to 400 mg/l using  $K_2Cr_2O_7$  as a source of chromium. The bacterial strain S-9 was showed potential to successfully reduce chromium rapidly. In figure 3 showed (Fig 3.3). Rapid bioreduction of chromium with concentration of 50 mg/L after 48 hrs of incubation with chromate reduction rate 1mg/L in hour. With increase in initial concentration chromium 100, 200, 300 and 400 mg/L complete bioreduction was achieved after 72, 96 and 120 hours respectively. The experiment results clearly showing the potential ability of bacterial strain S-9 in bioreduction.



### 3.5 Qualitative Assay and Its Standardization for Chromate Reductase

Bacterial strains S-9 was screened for chromium reductase activity. Strain S-9 was grown on defined medium (g/L:  $\text{KH}_2\text{PO}_4$ , 3.0;  $\text{CaCl}_2$ , 0.1;  $\text{Na}_2\text{HPO}_4$ , 6;  $\text{NaCl}$ , 0.5; Sucrose, 10.5;  $\text{MgSO}_4 \cdot 7\text{H}_2\text{O}$ , 0.1; and  $\text{K}_2\text{Cr}_2\text{O}_7$ , 0.01) for screening of chromate reductase. Strain S-9 showed 190.43 U/mg chromate reductase activity at 540 nm after 72 hrs at 35°C. Chromate reductase assay was determined using the optimized assay condition carried out. The reaction mixture for S9 chromium reductase contained enzyme concentration 400  $\mu\text{L}$ , substrate concentration 200  $\mu\text{L}$  at 35°C and pH 7.0 and incubation time period of 50 min.

### 3.6 Physical Parameters for Chromate Reductase Production

The effect of various physical factor for maximum chromium reductase was optimized and activity was determined in the term of specific activity U/mg. Maximum specific activity (224.5 U/mg) was achieved at 35°C, pH 7.0 after 72 hrs of incubation with inoculum size 2%.

### 3.7 Optimization of Nutritional Factorschromate Reductase Production by Plackett-Burman and Central Composite Design

#### *Plackett-Burman Design*

The factors optimized through Plackett-Burman design showed significant effect on production and yield of chromium reductase. Total 11 factors were used in 15 different experimental run. The significant factors on production of chromium reductase was achieved by placket burman. Maximum specific activity (305.386 U/mg) was achieved in run number 08 and minimum activity observed was (60.162 U/mg) in run number 3 (Table 3.1). Furthermore, Pareto chart obtained from Placket-Burman explain the effect of each individual factor toward chromate reductase production (Fig 3.4). Total of 11 factor only 05 factors were found to have significant effect on chromate reductase production including B;  $\text{KH}_2\text{PO}_4$ , G;  $\text{K}_2\text{Cr}_2\text{O}_7$ , F; Sucrose, C;  $\text{MgSO}_4 \cdot 7\text{H}_2\text{O}$  and K; Yeast extract and the apparent by the values of "Prob > F" of each factor showed in table 3.2. The

chromium activity was highly augmented by  $\text{KH}_2\text{PO}_4$  as indicated by largest coefficient followed by  $\text{K}_2\text{Cr}_2\text{O}_7$ , Sucrose and  $\text{MgSO}_4 \cdot 7\text{H}_2\text{O}$ .  $\text{KH}_2\text{PO}_4$  and  $\text{K}_2\text{Cr}_2\text{O}_7$  had negative influence while Sucrose and  $\text{MgSO}_4 \cdot 7\text{H}_2\text{O}$  had significant augment on enzyme production. The chromate reductase yield was enhanced by decreasing  $\text{KH}_2\text{PO}_4$  and  $\text{K}_2\text{Cr}_2\text{O}_7$  concentration and increasing Sucrose and  $\text{MgSO}_4 \cdot 7\text{H}_2\text{O}$  in production media.

The model equation for chromium reductase specific activity U/mg can be written as:

$$\text{Specific activity: (R)} = (+196.15) + (-7.32 \text{ A}) + (-39.30\text{B}) + (30.20\text{C}) + (5.32\text{D}) + (-13.48\text{E}) + (31.49\text{F}) + (-34.30\text{G}) + (7.26\text{H}) + (-5.29\text{J}) + (-22.06\text{K})$$

The Model was found to be significant by implies F-value of 12.11. In the model, 3.20% chance that a "F-Value" this large could occurred because of noise. The significant factore in the model were observed by the "Prob > F" value lower than 0.0500. while in some circumstance B, C, F, G, K value in the model were observed. Values in the model showed higher than 0.1000 are not signidicant terms in model. If the insignificant terms in model are many (not including those mandatory to maintenance hierarchy), model reduction may improve your model. The "Curvature F-value" of 48.70 suggests in the model significant curvature (as calculated by alteration between the normal of the center points and factorial points of the average) in the design space. In the model, 0.60% chance that a "F-Value of Curvature " this large could occurred because of noise.

### ***Central Composite Design (CCD)***

For further optimization, two-level CCD was used on the significant factors achieved from Placket-Burman Design that have a positive effect on chromate reductase production. For strain S-9, the CCD was performed on four factors obtained from Placket-Burman design and the effect of these factors study in 30 runs at two levels in 30 runs (Table 3.3). The suitability of the model was assessed using ANOVA showed in table 3.4. For strain S-9, among the quadratic terms and linear, only interactive term AB and AC were significant model terms, whereas A represent  $\text{KH}_2\text{PO}_4$  and B represent  $\text{K}_2\text{Cr}_2\text{O}_7$  while, C represent sucrose. Response surface plot (AB) shows that increase in  $\text{K}_2\text{Cr}_2\text{O}_7$  and decrease in  $\text{KH}_2\text{PO}_4$  enhanced enzyme activity (Fig 3.5). Same in response plot (AC) shows

the highest Chromate reductase activity was recorded by decreasing both the  $\text{KH}_2\text{PO}_4$  and sucrose (Fig 3.6). Second polynomial equation was obtained after multiple regression analysis data. Final Equation in Terms of Coded Factors:

$$\text{Specific activity} = +512.56 - 25.86A - 22.90B - 39.80C + 6.36D - 57.57AB + 41.05AC + 11.34AD - 7.66BC - 3.85 BD - 27.91CD - 6.47A^2 - 104.05B^2 - 61.15C^2 - 29.41D^2$$

The Model was found to be significant by implies F-value of 6.84. In the model, 0.01% chance that a "F-Value" this large could occurred because of noise. The significant factore in the model were observed by the "Prob > F" value lower than 0.0500. while in some circumstance C, AB, AC,  $B^2$ ,  $C^2$  value in the model were observed. Values in the model showed higher than 0.1000 are not signidicant terms in model. If the insignificant terms in model are many (not including those mandatory to maintenance hierarchy), model reduction may improve your model.

### **3.8 Bulk Production of Chromate Reductase Under Optimized Culture Conditions**

After optimization of all physicochemical conditions 1000 mL of bulk production medium (pH 7.0) was inoculated with bacterial strain S-9 and incubated at 35°C in shaking incubator 150 rpm for 72 h. After incubation culture was was harvested by centrifuged at 10,000 rpm/ 10 minutes at 4°C and cell free supernatant was collected and observed for chromium reductase activity and then processed for purification.

### **3.9 Chromate Reductase Purification from Bacterial Strain S-9**

The collected cell free supernatant was treated with ammonium sulphate on stirrer and crude chromate reductase was precipitated with 60% of ammonium sulphate. The chromate reductase was purified by gel filtration column chromatography using (sephadex G-100). The fractions that contained highest activity were pooled and the molecular size of chromium reductase was observed approximately, 70 kDa (Fig 3.7). During various purification step specific activity, purification fold and yield were calculated showed in table 3.5.

### 3.10 Characterization of Purified Chromate Reductase

#### *Effect of Temperature and Ph on The Activity and Stability*

The purified chromium reductase showed maximum activity at 40°C (Fig 3.8). The enzyme retained 100% stability between 30°C to 40°C for 120 min while, retained more than 60% stability at 45°C for 120 min (Fig 3.9). The purified chromium reductase showed highest activity at pH 7.0 (3.10). The enzyme retained 100% stability at pH 7.0 for 120 min for 120 min. while, retained more than 80% stability between pH 5.0 to 8.0 for 120 min (Fig 3.11).

#### *Effect of Metal Ions and Surfactants on The Activity of Enzyme*

The effect of different metals on purified chromium reductase from strain S-9 was analyzed at a concentration of 2 mM and 10 mM. Metals that have shown a positive effect on activity of chromate reductase at a concentration of 10 mM are  $\text{CaSO}_4$ ,  $\text{BaSO}_4$ ,  $\text{FeSO}_4$ ,  $\text{ZnSO}_4$ ,  $\text{NaCl}$ ,  $\text{K}_2\text{SO}_4$ ,  $\text{KCl}$ , and  $\text{MgSO}_4$  and increase 20% of the activity. A strong inhibitory effect was observed for  $\text{HgCl}_2$  at both concentrations 2 mM and 10 mM and retained approximately 20% of the activity (Table 3.6). Different surfactants at 0.50% and 1.0% concentration were used to analyze their effect on the activity of the purified enzyme of S-9 strain. SDS and CTAB completely inhibited enzyme activity of strains S-9 at both concentrations (0.50 and 1.0%), while in the occurrence of Tween 20, enzyme of strain S-9 retained 100% activity at both concentration 0.50% and 1.0%. Comparatively, Triton X 100, Tween 80, and PEG, potentially enhanced chromate reductase activity at both concentrations (0.5% and 1.0%) and retained more than 120% activity (Table 3.7).

#### *Effect of Organic Solvent and Determination of Kinetic Parameters*

Different organic solvent (15%) ultimate concentration was used to determine the effect on the activity of the purified enzyme for 120 mins. Acetonitrile, formaldehyde, ethanol and butanol reduced enzyme activity with increase time. Glycerol, methanol, propanol, and acetone increase enzyme activity with increase time and retained more than 120% for 120 min. (Table 3.9).

The Michaelis Menten constant ( $K_m$ ) and rate of reaction ( $V_{max}$ ) values of purified chromium reductase for strain S-9 were calculated by

Lineweaver and Burk's) plot. Strain S9 chromate reductase were incubated with varying concentrations 1  $\mu\text{M}$  to 10  $\mu\text{M}$  of substrate (potassium dichromate). The  $K_m$  and  $V_{max}$  of purified enzyme were found to be 1.3636  $\mu\text{M}$  and 909.09  $\mu\text{M}$  (Fig 12).

### **3.11 Application of Chromate Reductase in Bio-reduction of Toxic Chromium (VI)**

Deionized water containing 100mg/L of chromium was treated with 1%, 5%, and 10% of both crude enzyme and purified enzyme. Crude enzyme of S-9 showed 20%, 45%, and 75% chromate reduction at 120 hours with 1%, 5%, and 10% (v/v) enzyme. Purified chromate reductase of S-9 showed 42%, 64%, and 87% chromate reduction at 120 hours with 1%, 5%, and 10% (v/v) enzyme (Fig 3.13).

## **4. Discussion**

Widespread industrialization and their activities have harmful effect on environment because it leads high concentration of lead and chromium in the environment, which effect terrestrial and marine life by accumulation of chromium in soil, water and atmosphere and produce serious damages. The chromium enhancement in the environment and ultimately damage human health through the food chain. In this study sludge samples were collected from metal contaminated industrial zone. Elemental analysis of sludge samples were performed and high concentration of different metals were observed, chromium was found in very high concentration 2648.644 mg/L, which is above US-EPA standard values. Total chromium load in industrial effluents were found varying from 0.005 to 1423.05 mg/L (Hossan et al., 2020). The order of abundance of the metals in rivers and sea coastal side were as;  $\text{Ni} > \text{Mn} > \text{Zn} > \text{Fe} > \text{Cu} > \text{Cd} > \text{Pb} > \text{Hg} > \text{As}$ . (Yousaf et al., 2021). This previous information adds an advantage to our sampling site for isolation of bacterial strains from one of biggest industrial area. In our study total of 38 bacterial strains were isolated through selective enrichment on nutrient agar plates containing 100 mg/L of  $\text{K}_2\text{Cr}_2\text{O}_7$  and bacterial strain designated as S-9 selected based upon on highest resistant to chromium. Based on 16S

rRNA sequencing analysis, bacterial strain S-9 showed 99% of the similarity to *Bacillus Paramycoides* (MAOI01000012). Bacterial strain S-9 was screened for Cr resistance on both nutrient broth and agar, was found resistant to high concentration of chromium 1400 mg/L and 15 mg/L on nutrient agar plate. In similar study bacterial strain found higher resistant of 1000 µg/ml on gar plate and 450 µg/ml in nutrient broth which is much lower concentration in comparison to our results. Significant difference in tolerance of strain on nutrient agar and broth occur due to the formation of complex between nutrient agar and  $K_2Cr_2O_7$  which will not expose bacteria to maximum concentrations of metal while as in broth media bacteria are directly exposed to the metal (Sanjay 2021). Rapid bioreduction of bacterial strain S-9 was observed with chromium concentration of upto 50 mg/L with 48 hours of incubation with chromate reduction rate 1 mg/L in hour. With increase in initial concentration chromium 100, 200, 300 and 400 mg/L complete bioreduction was achieved after 72, 96 and 120 hours respectively. Our result showed high significant bioreduction of chromium with short incubation in comparison to the study in which Chromium (VI) with initial concentration 150µg/ml was reduced upto 80% after 120 hours by *Pseudomonas sp.* MAI4 (Wani et al., 2019). Strain S-9 significantly reduced toxic Cr (VI), thus confirming its potential as a Bio-reductor for industrial waste treatment. The intracellular mechanisms by which toxic Cr(VI) is convert to the nontoxic Cr(III) is of rehabilitated interests; however, the exact pathways of reduction still remain unclear. For bulk production and use of chromate reductase enzyme in bioreduction of chromium we optimized different condition and Strain S-9 showed highest activity at temperature 35°C, PH 7.0, incubation time 72 hours and inoculum size 1%. Nutritional parameters were improved through PB and CCD. The factors optimized through Plackett-Burman showed significant effect on production and yield of chromium reductase. Maximum specific activity 305.386 U/mg was achieved and lowest activity observed was 60.162 U/mg. For further enhancing yield of chromate reductase, two-level CCD was used on the significant factors achieved from Plackett-Burman Design that have a positive effect on chromate reductase production and increase production yield up to 545.993 U/mg. Mala et al., 2015in obtained an preliminary chromate reductase activity of 212.84 U/mg pro-

tein at 48 h in a low-cost defined medium amended with 0.25 mM chromate and increase upto 312.99 U/mg at 48 h by addition of inducer (Mala, 2015), which showed that we have significantly increase the enzyme yield by using Plackett-Burman and CCD then previously used optimization methods. Very few studies are available on use statistical design for optimization of chromate reductase production and bioreduction of Cr(VI). Plackett-Burman design, an efficient technique for medium component optimization (Pulimi et al., 2012; Mabrouk et al., 2013; Mabrouk et al., 2014). The enhanced production of chromate reductase and determined certain physicochemical characteristics from bacterial strain S-9 isolated from industrial sludge, which has been found to be highly suitable for bioreduction of chromium. The S-9 chromate reductase was purified 6.6 fold, with an overall yield of 59% to homogeneity from the crude extract by ammonium sulfate fractionation and gel filtration column chromatography. The fractions with maximum activity were pooled and the molecular size of enzyme was found to be 25 kDa. chromate reductase enzyme obtained from novel *Ochrobactrum* sp. strain Cr-B4 partially purified and characterized and molecular mass was found to be 31.53 kDa, with a specific activity 14.26 U/mg (Hora and Shetty, 2015). We further characterize Chromate reductase and the optimum temperature for strain S9 reductase turned out to be 40°C where maximum activity was 80 U/ml and the optimum pH was observed 7.2. The maximum enzyme stability of strain S-9 was achieved at 40°C and retained 100% of the stability for 120 min. More than 90% of the stability was achieved at temperature 30°C and 35°C for 120 minutes. Moreover, Strain S-9 chromate reductase were stable at pH 7.0 and retained more than 90% of activity for 120 minutes, 80% of the stability was retained at pH 6.0. Exposure to pH 10.0, chromate reductase of S-9 retained 5% and 8% stability for 120 minutes. The effect of different metals on strain S-9 was analyzed at a concentration of 2 mM and 10 mM. Metals that have shown a positive effect on activity of chromate reductase at a concentration of 10 mM are  $\text{CaSO}_4$ ,  $\text{BaSO}_4$ ,  $\text{FeSO}_4$ ,  $\text{ZnSO}_4$ ,  $\text{NaCl}$ ,  $\text{K}_2\text{SO}_4$ ,  $\text{KCl}$ , and  $\text{MgSO}_4$ . A strong inhibitory effect was observed for  $\text{HgCl}_2$  at both concentrations. The enzyme was activated by metal ions in the order of  $\text{Cu}^{2+} > \text{Mg}^{2+} > \text{Mn}^{2+} > \text{K}^{+} > \text{Ni}^{2+}$ , while  $\text{Cd}^{2+}$ ,  $\text{Zn}^{2+}$  and  $\text{Cu}^{2+}$  inhibited chromate reductase activity in *Rhodopseudomonas palustris* KU003 (Merugu et al., 2013). Enzyme activity obtained in our

study arisen due to the need for the enzyme to utilize the metal ions as cofactors and/or by increasing the bioavailability of the enzyme (Garbisu et al., 1997). Different surfactants at 0.50% and 1.0% concentration were used to analyze their effect on the activity of the purified enzyme of S-9 strain. SDS and CTAB completely inhibited enzyme activity of strains S-9 at both concentrations (0.50 and 1.0%), while in the occurrence of Tween 20, enzyme of strain S-9 retained 100% activity at both concentrations 0.50% and 1.0%. Comparatively, Triton X 100, Tween 80, and PEG, potentially enhanced chromate reductase activity at both concentrations (0.5% and 1.0%). Different organic solvent (15%) ultimate concentration was used to determine the effect on the activity of the purified enzyme for 120 mins. Acetonitrile and butanol reduced enzyme activity with increase time. Chromate reductase retained 100% activity in the presence of glycerol, methanol, formaldehyde, and acetone for 120 mins. Our results are significant since most waste waters contain in addition to Cr, several other metal ions, surfactants and organic solvents due to industrial consumption. An increase in chromate reductase activity in presence of metal ions is beneficial for effective bioremediation of polluted wastewaters. The  $K_m$  and  $V_{max}$  of Strain S-9 was 1.3636  $\mu\text{M}$  and 909.09  $\mu\text{M}/\text{min}/\text{mg}$  respectively. The enzyme exhibited favourable  $V_{max}$  and  $K_m$  values indicating a high feasibility of the reaction system with  $\text{K}_2\text{Cr}_2\text{O}_7$  as its substrate (Mala 2015; Hora and Shetty, 2015). Similarly, The  $K_m$  values for NADPH and NADH were determined to be 47.5 and 17.2  $\mu\text{mol}$ , and the  $V_{max}$  values 322.2 and 130.7  $\mu\text{mol Cr(VI) min}^{-1}\text{mg}^{-1}$  protein, respectively (Bae et al., 2005). The enzyme followed Michaelis-Menten kinetics with  $K_m$  of 4.64  $\mu\text{M}$  and a  $V_{max}$  of 104.29  $\mu\text{M}/\text{min}/\text{mg}$  (Hora and Shetty, 2015). Effluent containing 100mg/L of chromium was treated with 1%, 5%, and 10% of both crude enzyme and purified enzyme. Crude enzyme of S9 showed 20%, 45%, and 75% chromate reduction at 120 hours with 1%, 5%, and 10% (v/v) enzyme. Purified chromate reductase of S-9 showed 42%, 64%, and 87% chromate reduction at 120 hours with 1%, 5%, and 10% (v/v) enzyme. Similar result of chromate reduction was obtained using the crude enzyme by treatment in tannery effluent. Hence, an efficient enzyme-mediated chromate reduction process has been developed for bioremediation of Cr which can further be investigated for pilot-scale operations (Mala et al., 2015).



## **5. Conclusion**

The survival of microorganisms in extremely harsh condition in presence of increasing concentration of chromium makes it a suitable candidate for establishment of bioremediation strategies. Strain S-9 showed significant reduction of chromium in tested sample. Furthermore, the enhanced bulk production of enzyme chromate reductase with maximum specific activity has been achieved in a very low cost defined medium formulation using  $K_2Cr_2O_7$  as the chromate source, the use of crude and purified enzyme can also serve as potential candidate for bioremediation of Cr from industrial wastewaters.

## REFERENCES

- Asati, A., Pichhode, M., & Nikhil, K. (2016). Effect of heavy metals on plants: an overview. *International Journal of Application or Innovation in Engineering & Management*, 5(3), 56-66.
- Bae, W. C., Lee, H. K., Choe, Y. C., Jahng, D. J., Lee, S. H., Kim, S. J. & Jeong, B. C. (2005). Purification and characterization of NADPH-dependent Cr (VI) reductase from *Escherichia coli* ATCC 33456. *J Microbiol*, 43(1), 21-27.
- Coetzee, J. J., Bansal, N., & Chirwa, E. M. (2020). Chromium in environment, its toxic effect from chromite-mining and ferrochrome industries, and its possible bioremediation. *Exposure and health*, 12(1), 51-62.
- Determann, H. (2012). *Gel Chromatography Gel Filtration · Gel Permeation · Molecular Sieves: A Laboratory Handbook*: Springer Science & Business Media.
- Fulladosa, E., Desjardin, V., Murat, J.-C., Gourdon, R., & Villaescusa, I. J. C. (2006). Cr (VI) reduction into Cr (III) as a mechanism to explain the low sensitivity of *Vibrio fischeri* bioassay to detect chromium pollution. 65(4), 644-650.
- Garbisu C, Alkorta I, Llama MJ, Serra JL. (1998). Aerobic chromate reduction by *Bacillus subtilis*. *Biodegradation*, 9, 133-41.
- Hora, A., & Shetty, V. K. (2015). Partial purification and characterization of chromate reductase of a novel *Ochrobactrum* sp. strain Cr-B4. *Preparative Biochemistry and Biotechnology*, 45(8), 769-784.
- Hossan, S., Hossain, S., Islam, M. R., Kabir, M. H., Ali, S., Islam, M. S. & Mahmud, Z. H. (2020). Bioremediation of Hexavalent Chromium by Chromium Resistant Bacteria Reduces Phytotoxicity. *International journal of environmental research and public health*, 17(17), 6013.
- Jobby, R., Jha, P., Yadav, A. K., & Desai, N. (2018). Biosorption and biotransformation of hexavalent chromium [Cr (VI)]: a comprehensive review. *Chemosphere*, 207, 255-266.
- Kumar S, Stecher G, Li M, Knyaz C, Tamura K. 2018. MEGA X: Molecular Evolutionary Genetics Analysis across computing platforms. *Mol Biol Evol* 35(6), 1547-1549.
- Lowry, O. H., Rosebrough, N. J., Lewis, A. F., & Randall, J. R. (1951). Protein measurement with the folin phenol reagent. *Journal of Biological Chemistry*, 193, 265-275.
- Mabrouk MEM, ElAhwany AMD, Beliah MMB, Sabry SA. (2013). Xanthan production by a novel mutant strain of *Xanthomonas campestris*: Application of statistical design for optimization of process parameters. *Life Sci J.*, 10, 1660-1667.

Mabrouk, M. E., Arayes, M. A., & Sabry, S. A. (2014). Hexavalent chromium reduction by chromate-resistant haloalkaliphilic *Halomonas* sp. M-Cr newly isolated from tannery effluent. *Biotechnology & Biotechnological Equipment*, 28(4), 659-667.

Mala, J. G. S., Sujatha, D., & Rose, C. (2015). Inducible chromate reductase exhibiting extracellular activity in *Bacillus methylotrophicus* for chromium bioremediation. *Microbiological research*, 170, 235-241.

Merugu R, Rajyalaxmi K, Girisham S, Reddy SM. (2013). Chromate reduction by purple nonsulfur phototrophic bacterium *Rhodospseudomonas palustris* KU003 isolated from tannery effluent. *Int J Environ Bioener*, 6, 187-92.

Pulimi M, Subika J, Jastin S, Natarajan C, Amitava M. (2012). Enhancing the hexavalent chromium bioremediation potential of *Acinetobacter junii* VITSUK-MW2 using statistical design experiments. *J Microbiol Biotechnol*, 22, 1767-1775.

Qian, J., Zhou, J., Wang, L., Wei, L., Li, Q., Wang, D., & Wang, Q. (2017). Direct Cr (VI) bio-reduction with organics as electron donor by anaerobic sludge. *Chemical Engineering Journal*, 309, 330-338.

Sanjay, M. S., Sudarsanam, D., Raj, G. A., & Baskar, K. (2020). Isolation and identification of chromium reducing bacteria from tannery effluent. *Journal of King Saud University-Science*, 32(1), 265-271.

Singh, A., & Prasad, S. (2015). Remediation of heavy metal contaminated ecosystem: an overview on technology advancement. *International Journal of Environmental Science and Technology*, 12(1), 353-366.

Thatoi, H., Das, S., Mishra, J., Rath, B. P., & Das, N. J. J. o. E. M. (2014). Bacterial chromate reductase, a potential enzyme for bioremediation of hexavalent chromium: a review. 146, 383-399.

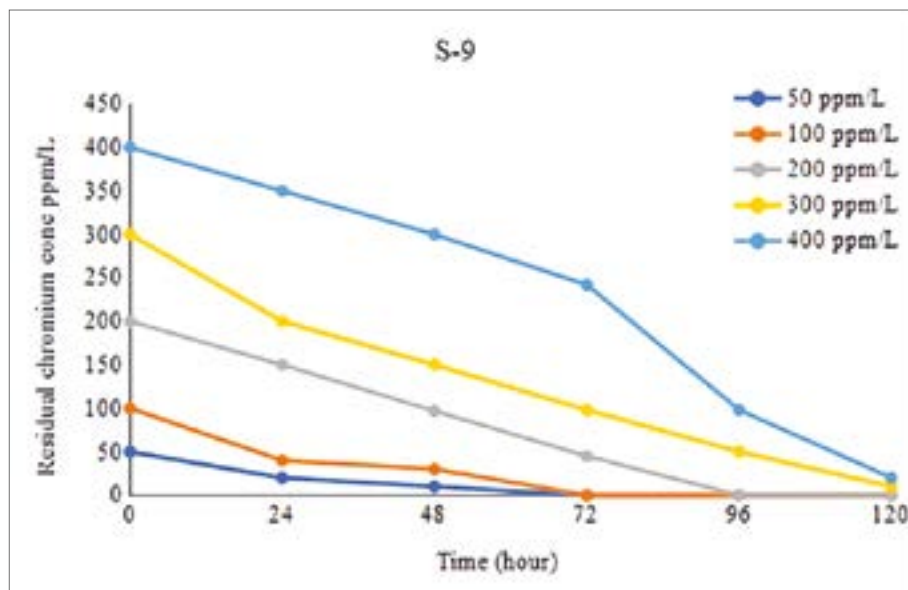
Trellu, C., Mousset, E., Pechaud, Y., Huguenot, D., van Hullebusch, E. D., Esposito, G., & Oturan, M. A. (2016). Removal of hydrophobic organic pollutants from soil washing/flushing solutions: a critical review. *Journal of hazardous materials*, 306, 149-174.

Verma, S., & Kuila, A. (2019). Bioremediation of heavy metals by microbial process. *Environmental Technology & Innovation*, 14, 100369.

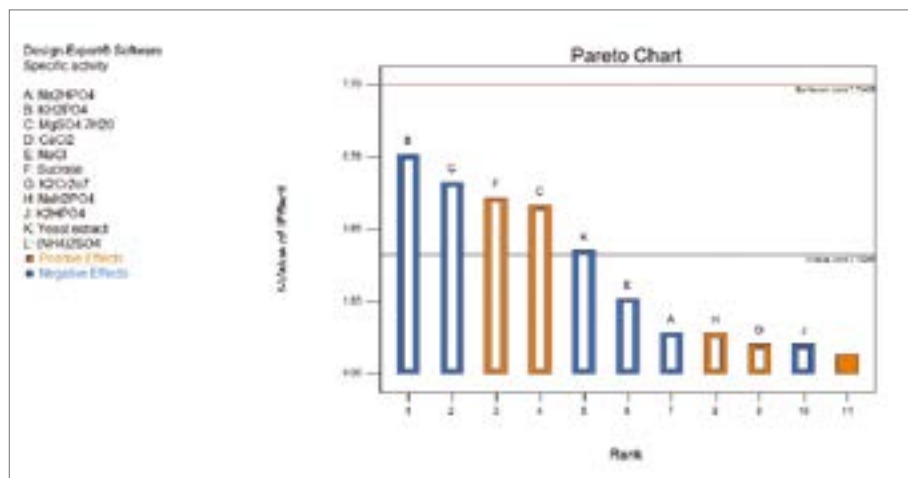
Wani, P. A., Wahid, S., Khan, M. S. A., Rafi, N., & Wahid, N. (2019). Investigation of the role of chromium reductase for Cr (VI) reduction by *Pseudomonas* species isolated from Cr (VI) contaminated effluent. *Biotechnology Research and Innovation*, 3(1), 38-46.

Yousif, R., CHOUDHARY, M. I., AHMED, S., & AHMED, Q. (2021). Bioaccumulation of heavy metals in fish and other aquatic organisms from Karachi Coast, Pakistan. *Nusantara Bioscience*, 13(1).





**Fig 3.3:** Bioreduction of Cr (VI) with varying initial concentration 50-400 mg/L by bacterial strain S-9.



**Fig. 3.4:** Pareto chart showing the effect of different factors generated by Plackett-Burman design on the rate of enzyme production.

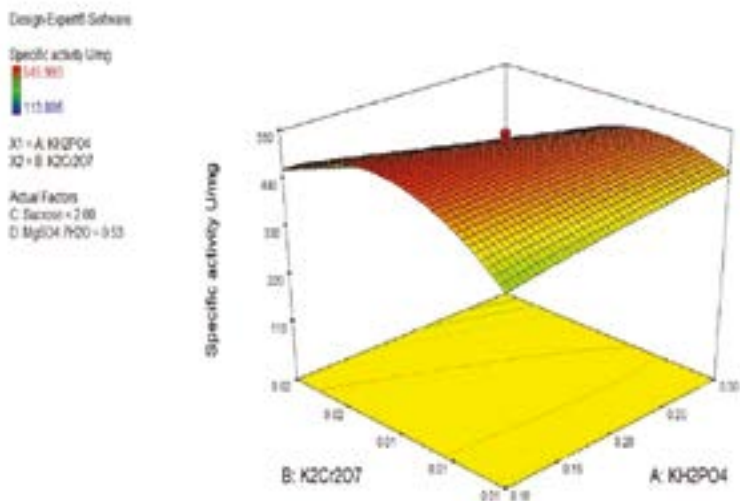


Fig 3.5 Response surface plots showing the combined effects of A; KH<sub>2</sub>PO<sub>4</sub> B; K<sub>2</sub>Cr<sub>2</sub>O<sub>7</sub>.

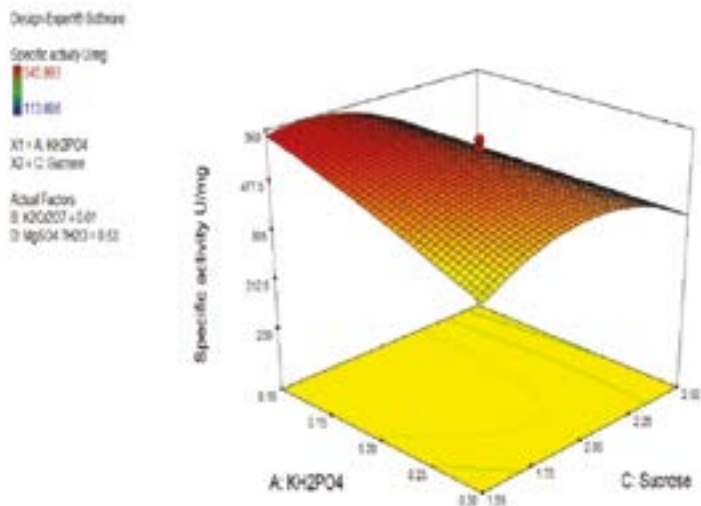
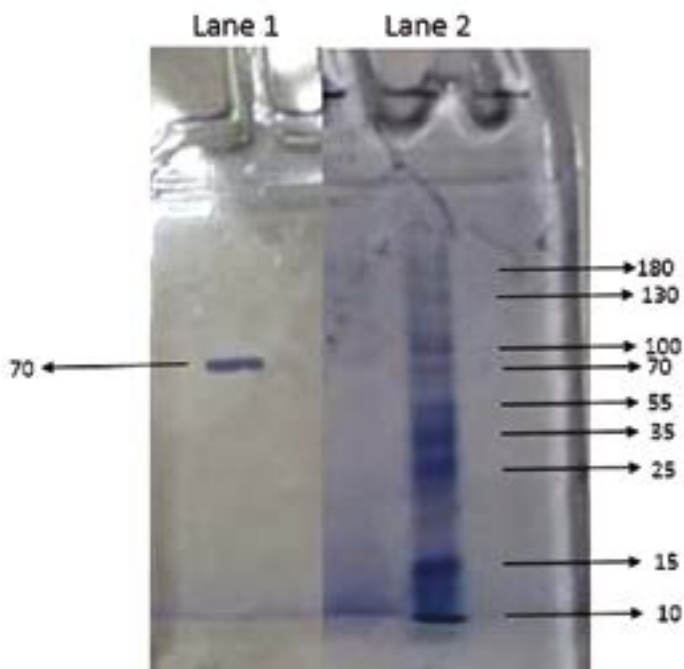
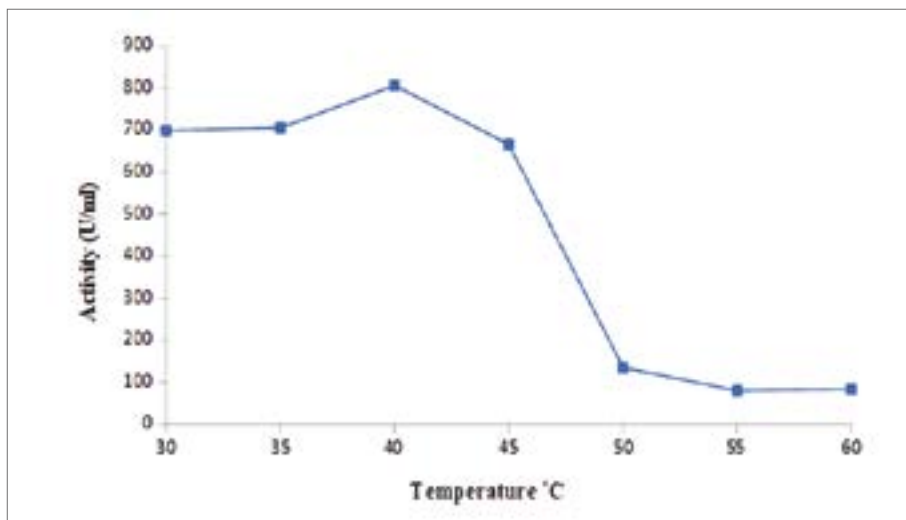


Fig 3.6: Response surface plots showing the combined effects of A, KH<sub>2</sub>PO<sub>4</sub>; B, Sucrose.



**Fig. 3.7:** Estimation of molecular weight of chromate reductase by SDS-PAGE, Lane 2: Prism Ultra Protein Ladder of molecular size 10-180 kDa, lane 1: purified enzyme.



**Fig. 3.8:** Effect of temperature on the specific activity of chromate reductase from strain S9.

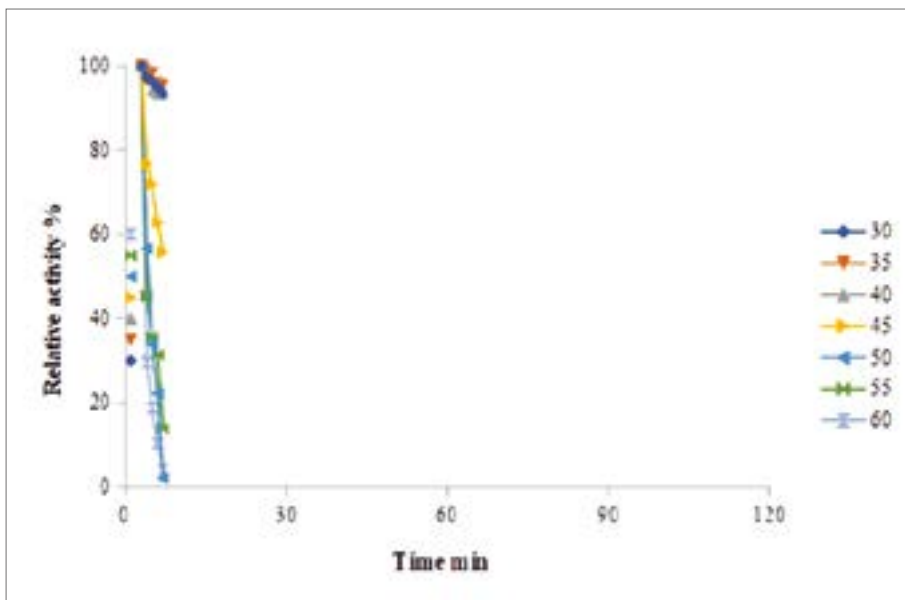


Fig. 3.9: Temperature stability of chromate reductase from strain S-9.

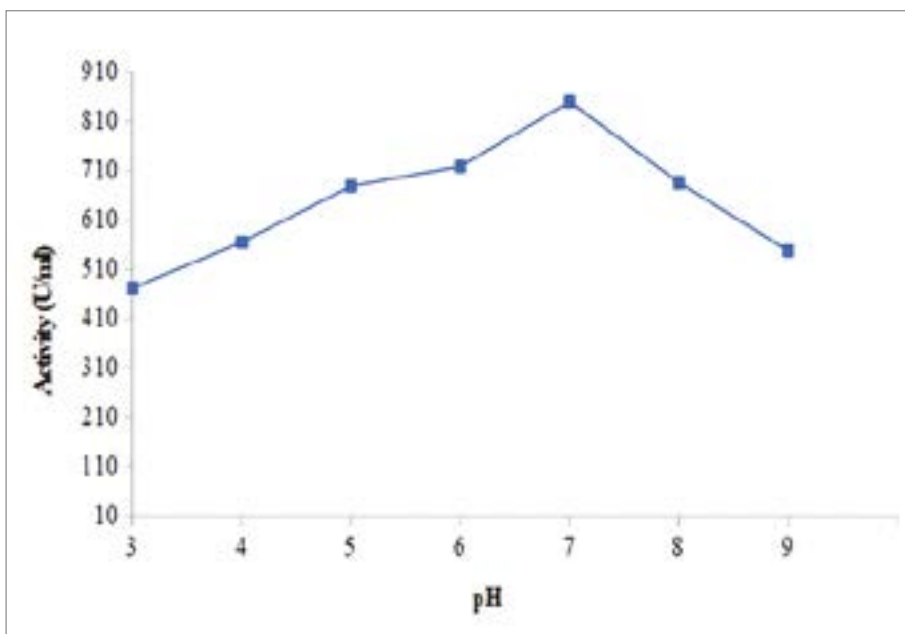


Fig 3.10: Effect of pH on the activity of Chromate Reductase from strain S-9.



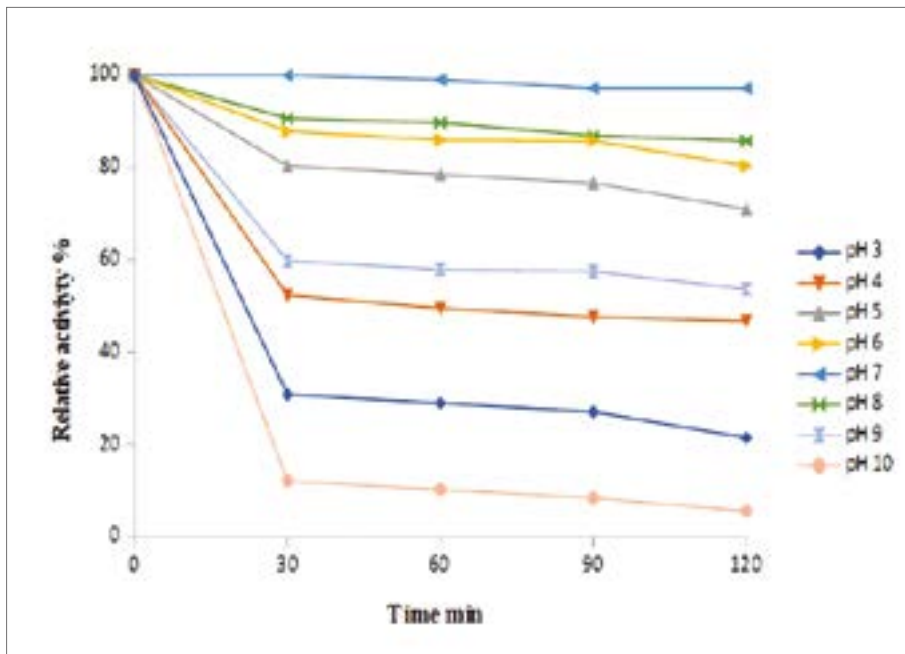


Fig 3.11: pH stability profile of S-9 chromate reductase.

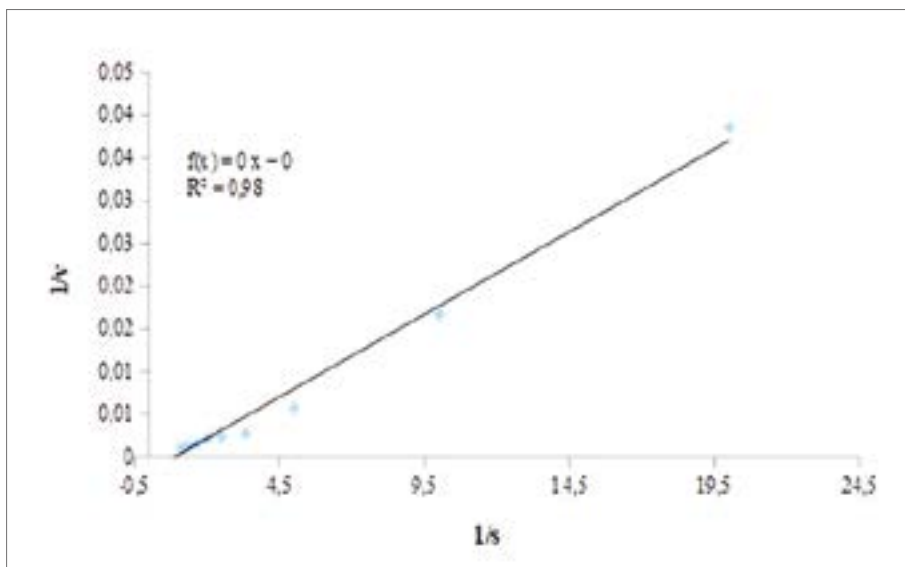
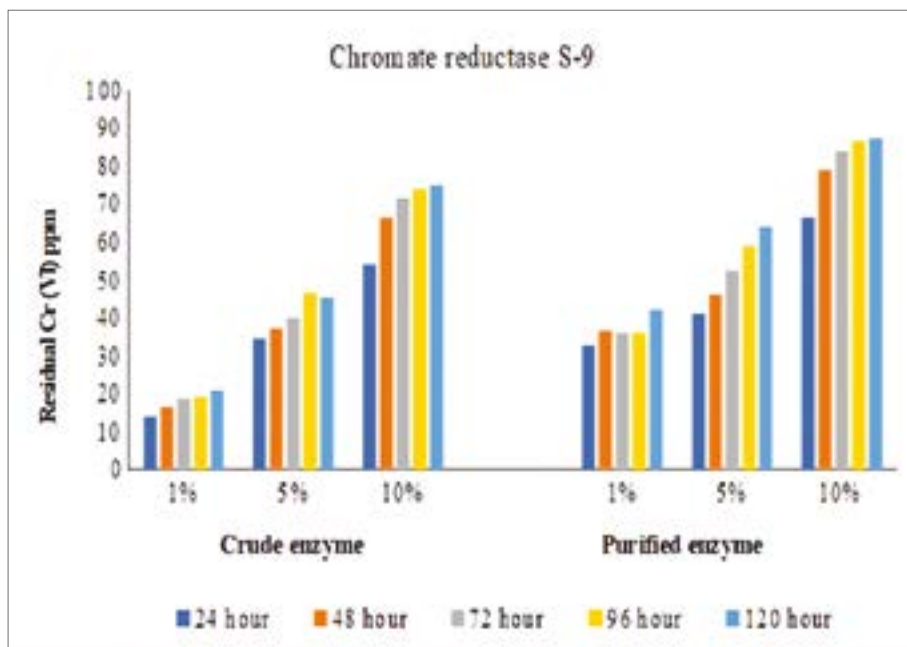


Fig 3.12: Kinetics analysis of chromate reductase from Strain S-9.



**Fig 3.13:** Enzymatic Cr(VI) reduction with crude and purified chromate reductase from strain S-9.

## List of Tables

**Table 3.1.** Placket Burman design of factors with specific enzyme activity (U/ mg) of Strain S-9 as a response.

Run No	Factor A $\text{Na}_2\text{HPO}_4$ %	Factor B $\text{KH}_2\text{PO}_4$	Factor C Mg- $\text{SO}_4 \cdot 7\text{H}_2\text{O}$ %	Factor D CaCl <sub>2</sub> %	Factor E NaCl %	Factor F sucrose %	Factor G $\text{K}_2\text{Cr}_2\text{O}_7$ %	Factor H $\text{NaH}_2\text{PO}_4$ %	Factor I $\text{K}_2\text{HPO}_4$ %	Factor J Yeast extract %	Factor $\text{K}(\text{NH}_4)\text{SO}_4$ %	Response 1 specific activity U/ mg
1	0.4	0.1	0.01	0.01	0.02	0.5	0.01	0.1	0.3	0.3	0.3	240.07
2	0.4	0.5	0	0.04	0.02	0.5	0.01	0.3	0.3	1.3	0.5	210.01
3	0.6	0.3	0.03	0.03	0.04	1	0.02	0.2	0.4	1.05	0.4	60.162
4	0.8	0.5	0.04	0.01	0.002	0.5	0.03	0.1	0.5	1.3	0.3	83.93
5	0.8	0.1	0.04	0.04	0.06	0.5	0.01	0.1	0.5	0.8	0.5	266.04
6	0.4	0.1	0.04	0.01	0.06	1.5	0.01	0.3	0.5	1.3	0.3	296.32
7	0.4	0.5	0.04	0.01	0.08	1.5	0.03	0.1	0.3	0.8	0.5	196.39
8	0.8	0.1	0.04	0.04	0.02	1.5	0.03	0.3	0.3	0.8	0.3	305.33
9	0.8	0.5	0.01	0.01	0.02	1.5	0.01	0.3	0.5	0.8	0.5	220.85
10	0.4	0.5	0.01	0.04	0.08	0.5	0.03	0.3	0.5	0.8	0.3	80.495
11	0.4	0.1	0.01	0.04	0.02	1.5	0.03	0.1	0.5	1.3	0.5	197.49
12	0.6	0.5	0.03	0.03	0.04	1	0.02	0.2	0.4	1.05	0.4	106.88
13	0.6	0.3	0.03	0.03	0.04	1	0.02	0.2	0.4	1.05	0.4	105.09
14	0.8	0.5	0.01	0.04	0.06	1.5	0.01	0.1	0.3	1.3	0.3	149.39
15	0.8	0.1	0.01	0.01	0.06	0.5	0.03	0.3	0.3	1.3	0.5	107.35

**Table 3.2** ANOVA of strain S-9 for Placket-Burman Design.

Source	Sum of square	Df	Mean square	F value	p-value probe> F
Model	65474.78	10	6547.48	12.11	0.0320
A- $\text{Na}_2\text{HPO}_4$	642.69	1	642.69	1.19	0.3553
B- $\text{KH}_2\text{PO}_4$	18533.99	1	18533.99	34.28	0.0099
C- $\text{MgSO}_4 \cdot 7\text{H}_2\text{O}$	10946.10	1	10946.10	20.25	0.0205
D- $\text{CaCl}_2$	339.99	1	339.99	0.63	0.4857
E- $\text{NaCl}$	2180.55	1	2180.55	4.03	0.1382
F-sucrose	11902.13	1	11902.13	22.01	0.0183
G- $\text{K}_2\text{Cr}_2\text{O}_7$	14121.19	1	14121.19	26.12	0.0145
H- $\text{NaH}_2\text{PO}_4$	632.16	1	632.16	1.17	0.3587
$\text{K}_2\text{HPO}_4$	335.51	1	335.51	0.62	0.4884
Yeast Extract	5840.46	1	5840.46	10.80	0.0462

**Table 3.3** CCD for S-9 significant factors with specific enzyme activity (U/mg) as a response.

S.No	Factor 1 KH <sub>2</sub> PO <sub>4</sub> %	Factor 2K <sub>2</sub> Cr <sub>2</sub> O <sub>7</sub> %	Factor 3 sucrose	Factor 4 MgSO <sub>4</sub> . 7H <sub>2</sub> O 7H <sub>2</sub> O	Response Specific Activity
1	0.10	0.01	2.00	0.53	545.993
2	0.20	0.01	2.00	0.53	543.614
3	0.20	0.02	1.00	0.06	355.134
4	0.20	0.01	1.50	0.41	484.383
5	0.20	0.01	2.00	0.53	232.155
6	0.20	0.01	2.50	0.53	545.156
7	0.20	0.01	2.00	0.53	530.135
8	0.20	0.01	2.00	0.53	350.879
9	0.30	0.01	2.00	1.00	379.947
10	0.40	0.01	1.50	0.53	483.266
11	0.10	0.02	2.50	1.00	173.723
12	0.20	0.03	2.00	0.53	130.879
13	0.20	0.01	2.00	0.53	401.259
14	0.20	0.01	2.00	1.47	483.983
15	0.20	0.00	2.00	0.53	117.755
16	0.30	0.01	1.50	0.06	334.172
17	0.10	0.01	2.50	1.00	203.872
18	0.20	0.01	2.00	0.53	542.752
19	0.10	0.02	2.50	0.06	337.551
20	0.10	0.01	1.50	0.06	411.373
21	0.30	0.02	2.50	0.06	216.033
22	0.30	0.02	1.50	1.00	205.913
23	0.10	0.02	1.50	1.00	533.00
24	0.30	0.01	2.50	0.06	317.88
25	0.30	0.01	2.50	1.00	406.358
26	0.10	0.01	1.50	1.00	352.019
27	0.30	0.02	2.50	1.00	113.006
28	0.20	0.01	2.00	0.53	528.449
29	0.30	0.02	1.50	0.06	156.981
30	0.10	0.01	2.50	0.06	259.353

**Table 3.4** ANNOVA for central composite design.

Source	Sum of square	Df	Mean square	F value	p-value probe> F
Model	5.523E+005	14	39452.65	8.64	0.0001
A-KH <sub>2</sub> PO <sub>4</sub>	16051.11	1	16051.11	3.52	0.0804
B- K <sub>2</sub> Cr <sub>2</sub> O <sub>7</sub>	12581.36	1	12581.36	2.76	0.1177
C- sucrose	38024.40	1	38024.40	8.33	0.0113
D-MgSO <sub>4</sub> .7H <sub>2</sub> O	696.53	1	696.53	0.15	0.7016
AB	53025.59	1	53025.59	11.61	0.0039
AC	26958.97	1	26958.97	5.90	0.0281
AD	2058.29	1	2058.29	0.45	0.5122
BC	938.56	1	938.56	0.21	0.6568
BD	237.10	1	237.10	0.052	0.8228
CD	12463.30	1	12463.30	2.73	0.1193

**Table 3.5** Purification steps of chromate reductase from strain S-9.

Protein purification steps	Activity U/ml	Protein mg/ml	SA U/mg	Yield (%)	Purification fold
Crude extract	432.9	2.02	214.0	100	1
Precipitation	797.3	1.54	516.7	92.0	2.4
Sephadax-G100	1171.5	0.82	1416	59.5	6.6

**Table 3.6** Effect of metals on the activity of chromate reductase from Strain S-9.

Metals	10 mM Relative Activity	2 mM Relative Activity
Control	100	100
BaSO <sub>4</sub>	120.5	117.8082
CaCl <sub>2</sub>	124.65	127.39
CuSO <sub>4</sub>	135.61	132.87
MgSO <sub>4</sub>	116.43	113.69
CaSO <sub>4</sub>	100	98.63
ZnSO <sub>4</sub>	123.28	127.39
CuCl <sub>2</sub>	127.39	120.54
KCl	86.30	100
NaCl	102.73	106.84
HgSO <sub>4</sub>	13.69	15.06
FeSO <sub>4</sub>	83.56	86.30
NiSO <sub>4</sub>	124.65	110.95
K <sub>2</sub> SO <sub>4</sub>	134.24	127.39
CoCl <sub>2</sub>	30.13	39.72
Urea	113.69	100
Na <sub>2</sub> SO <sub>4</sub>	135.	120.54

**Table 3.7** Effect of Surfactant on the activity of chromate reductase from S-9 strain.

Surfactants	Residual Activity (%)	Residual Activity (%)
	0.5%	1.0%
Control	100	100
Tween 80	118.18	129.54
Tween 20	140.90	145.45
SDS	18.18	20.45
CTAB	25	22.27
Triton X-100	88.63	81.81
PEG	102.27	111.36

**Table 3.8** Effect of organic solvents on the activity of chromate reductase from S-9 strain.

Organic Solvents		Minutes		
	30 min	60 min	90 min	120 min
Control	100	100	100	100
Ethanol	91.89	92.64	79.80	73.56
Methanol	124.56	128.80	129.42	127.80
Acetonitrile	65.33	62.71	59.60	53.86
Acetone	134.53	135.78	132.7	136.90
Ethyl Acetate	106.60	109.47	103.99	102.24
Propanol	117.83	125.93	127.18	127.68
Butanol	79.80	74.81	72.31	61.09
Formaldehyde	96.88	87.53	87.53	77.68
Glycerol	114.96	115.08	123.06	136.28





# BEYAZ LAHANA VE ACI OTUN KANYAŞIN ÇİMLENMESİ VE BÜYÜMESİ ÜZERİNDEKİ ALLELOPATİK ETKİSİ

*Muhammad Alsakran<sup>1</sup>*

---

## Özet

Yabancı otlar, tarımsal ürünlerin miktar ve kalitesinde büyük kayıplara neden olmaktadır. Kanyaş (*Sorghum halepense* (L.) Pers), çiftçilere büyük ekonomik kayıplara sebep olup mücadelesi zor olan en tehlikeli yabancı otlardan biridir. Allelopati, yabancı ot mücadelesinde güvenli ve sıklıkla etkili bir biyolojik mücadele yöntemidir. Lahanagiller, allelokimyasal maddelerin içerdiği nedeniyle yabancı otlara karşı olumsuz etkiye sahip olduğu birkaç çalışmada tespit edilmiştir. Aynı zamanda acı ot (*Dittrichia graveolens* L. Greuter) allelopatik potansiyel olduğunu belirlenmiştir. Bu çalışmada hem beyaz lahana hem de acı otun allelopatik bitki olarak kullanılmasıyla kanyaş biyogöstergesi üzerine etkilerinin incelenmesi amaçlandı. Allelopatik bitkiler ayrı ayrı ve her ikisinin karışımı

---

<sup>1</sup> Doktora Öğrencisi, Kahramanmaraş Sütçü İmam Üniversitesi, Ziraat Fakültesi, Bitki Koruma, ORCID: 0000-0001-6672-7016

olarak kullanılmıştır. Kullanılan konsantrasyonlar 2, 5 ve %7 ek olarak kontrol uygulamalar (%0) belirlenmiştir. Bu deneme, saksılar kullanılarak sera koşullarında gerçekleştirilmiş ve bir ay sürmüştür. kanyaşın çimlenme oranı, çimlenme indeksi, bitki boyu, yaş ve kuru ağırlığı hesaplanmıştır. Bu denemenin sonuçları, kullanılan allelopatik bitkilerin, kanyaşın çimlenmesi ve büyümesi üzerine farklı etkilere sahip olduğunu göstermiştir. Beyaz lahana, kanyaş üzerine acı ottan daha fazla etkiye sahipken, beyaz lahana ve acı ot karışımının her ikisinden ayrı ayrı de daha etkili olduğu tespit edilmiştir. Kanyaş mücadelesinde en iyi sonuçlar, yüksek konsantrasyonlardaki bitki özlerinden elde edilmiştir. Acı ot %2 konsantrasyonda olduğu gibi, düşük konsantrasyonlar ya zayıf ya da uyarıcı olarak tespit edilmiştir. Beyaz lahana ve acı ot, özellikle artan konsantrasyon durumunda, kanyaş mücadelesinde yeterli allelopatik etkilere sahip olabilir.

**Anahtar Kelimeler:** Biyolojik Mücadele, Allelopatik, Kanyaş, Beyaz Lahan, Acı Ot.

## 1. Giriş

Dünya nüfusunda büyük artışla birlikte gıda ihtiyacı da artmaktadır. Ancak tarımsal ürünlerin üretimindeki artış birçok biyolojik faktör tarafından engellenmekte ve bu faktörlerin başında yabancı otlar gelmektedir (Ustuner, AL Sakran ve Almhemed, 2020).

Yabancı otlar, kültür bitkilerinde böcek, fungus, bakteri ve virüslerden daha çok zararlı oldukları bildirilmiştir (Gharde, Singh, Dubey ve Gupta, 2018). Yabancı otlar, özellikle rizom, stolon ve yumru köke sahip; kanyaş (*S. halepense*) ve *Cyperus rotundus* gibi mücadelesi oldukça zor dolayısıyla bu türler için birden fazla mücadele yöntemi uygulanması gerekmektedir (Uludag, Gozcu, Rusen, Guvercin ve Demir, 2007; Barros ve ark., 2016)

Kanyaş (*Sorghum halepense* (L.) Pers.) monokotil poaceae familyasına ait, çok yıllık bir yabancı ottur (Grace, Smith, Grace, Collins ve Stohlgren, 2001). Kanyaş, 50 farklı kültür bitkisinde zarar yapar. Dünya genelinde milyonlarca hektar üzerinde istila etmiş durumdadır. Kanyaş, Türkiye’de yerli bitki olarak sayılır ve çevre koşullarının bu türün yayılmasında önemli bir etken olduğu bildirilmiştir (Peerzada ve ark., 2017). Kanyaş, tohum ve rizomlardan yetişebilir (Ceskeski, AL-Khatib ve Dahlberg, 2017). Ancak tohum çimlenme oranı düşük olup %3,3’e kadar ulaşabilir. Dormansiye neden olan tohum kabuğunu kaldırmadaki etkinliğine göre bu oranı biyotik ve abiyotik çevre koşullarının etkisiyle artabilir (AL Sakran, Almhemed, Dal ve Ustuner, 2020). Kanyaş, ekonomik açıdan önem taşıyan tarım ürünlerinde %57-88 oranında verim kaybına neden olur (Peerzada ve ark., 2017). Soya fasulyesi, mısır, pamuk, domates, patlıcan ve biber gibi ekonomik açıdan önemli bitkilerde önemli verim kayıplarına neden olmaktadır (Uremis, Uludag ve Sangun, 2009). Kanyaşın yüksek yoğunlukta rekabeti, pamuk %70, mısır %88-100, şeker kamışı %69 ve soya fasulyesinde %59-88 oranında verim kaybına neden olduğu belirlenmiştir (Barroso ve ark., 2016). McWhorter (1993) tarafından yapılan bir çalışmaya göre, kanyaşın, ABD’de yılda milyonlarca dolarlık tarımsal gelir kaybına neden olduğu bildirilmiştir.

Türkiye’nin birçok ilinde kanyaş bulunması, orta veya çok yüksek yoğunluklar ile sapatanmıştır. Kahramanmaraş ili pamuk ekim alanlarında yoğunluğu 2.65 bitki/m<sup>2</sup> olarak belirlenmiştir (Tursun, Tursun ve

Kaçan, 2004). Diyarbakır ili ise 4.06 bitki/m<sup>2</sup> yoğunluk ve rastlanma sıklığı %58 olarak belirlenmiştir (Özaslan ve Kendal, 2014). Marmara bölgesi kanyaş yoğunluğunun; 13.40 ve 30.12 m<sup>-2</sup> arasında, rastlanma sıklığının ise %34.20 ve 100 arasında değiştiği belirlenmiştir (Yazlık, 2014). Isparta ili domates ekim alanlarında tespit edilen önemli yabancı ot türlerden kanyaş olup rastlama sıklığı %25.32, kaplama alanı %1.256 ve Yoğunluk 1.865 bitki/m<sup>2</sup> olarak belirlenmiştir (Arslan, 2011). Manisa ili domates fideliklerinde kanyaş en yoğun bulunan yabancı otlar türlerden olduğu belirlenmiştir (Tepe ve Nemli, 1992).

Yabancı ot zararını azaltmak için bugünlerde kullanılan birincil yöntem herbisitlerdir. Ancak bu herbisitler insan sağlığını, çevreye tehdit ettiği ve çoğu defa etkili olmadığı gibi nedenlerle yabancı otlar mücadelede güvenli ve etkili bir alternatif yöntem bulunması çok önemli hale gelmektedir. Bu yöntemlerden biyolojik mücadele en önemli olup etkili ve güvenilir olması nedeniyle dünyada dikkat çekmiştir (Ustuner ve ark., 2020).

Yabancı ot alanında allelopati en çok kullanılan biyolojik mücadele yöntemi olarak tanımlanmıştır. Allelopati, bir bitki tarafından oluşturulan ve salgılanan bazı kimyasal maddelerin, başka bir bitkiyi olumlu ya da olumsuz yönde etkilemesidir (Güncan, 2013).

Birkaç araştırmacı, allelopatik bitkilerden elde edilen sulu ekstraktların biyoherbisitler olarak kullanılabileceğini belirtmiştir (Khan ve Khan, 2012; Khan, Marwat, Hassan, Khan ve Ullah, 2012; Miri ve Armin, 2013).

Brassica cinsi allelopatik potansiyele sahip olduğu için yabancı otlar mücadelesinde kullanılabilir. *Brassica* spp.'nin yabancı otlara toksik etkisine sahip olduğu ve herbisite alternatif olabileceği bulunmuştur (Jafarieh-yazdi ve Javidfar, 2011; Jabran, 2017).

Kural ve Özkan (2020), beyaz lahananın allelopatik etkisini yabancı otlar *Amaranthus retroflexus* L., *Chenopodium album* L. ve *Solanum nigrum* L., kültür bitkiler *Zea mays* L., *Beta vulgaris* L., üzeri petri kaplarında incelemiştir. *A. retroflexus*, *C. album*, *S. nigrum*, *Z. mays* ve *B. vulgaris* tohumlarına uygulanan %50 konsantrasyonda beyaz lahana, su ekstraktında sırasıyla %95, %93, %34, %86 ve %94 oranında çimlenmeyi önlemiştir. Beyaz lahana ekstraktlarının %3'ünün hem *Cuscuta approximata* Bab. hem de *Medicago sativa* L. çimlenmesine etkili olduğu görülmüştür (Özkan, 2014).

Beyaz lahanada bazı glucosinolates (GSL), sinigrin (7.8 mikromol/g)

ve glukobrassisin (0.9 mikromol/g) belirlenmiştir (Kushad ve ark., 1999). Brassicaceae'den bir bitki, türleri ve büyüme koşullarına bağlı olarak yaklaşık 20 farklı GSL sentezleyebilir (Bangarwa, Norsworthy, Mattice ve Gbur, 2011; Shah ve ark., 2016). Analiz edilen beyaz lahana çeşitlerinin kimyasal olarak farklı toplam 12 GLS tespit edilmiştir (Wermter, Rohn ve Hanschen, 2020).

Beyaz lahana, 100 g yaş ağırlık başına ortalama 148 mg'lık bir ortalama toplam değerle en yüksek GSL seviyesini içerdiği görülmektedir (Possenti, Baima, Raffo, Durazzo, Giusti ve Natella, 2016). GSL'ler, toksik olmamasına rağmen mirosinazlar (tiyoglukosidazlar) tarafından katalize edilen hidroliz biyolojik olarak aktif ürünlerin oluşumuna yol açmaktadır (Rask, Andreasson, Ekblom, Eriksson, Pontoppidan ve Meijer 2000). GSL, Brassicaceae bitkilerinin kofullarında bulunur, enzimler ise bitkinin başka bölüm ya da başka hücre içinde bulunabilir. Bu enzimler, glikoz-sülfür bağının bölünmesinden sorumludur ve biyosidal isothiocyanate (ITC) üretimine yol açar (Jafariehyazdi ve Javidfar, 2011; Jabran, 2017). Beyaz lahanadan salınan en belirgin GLS hidroliz ürünleri arasında ITC'ler 3- (metilsülfinil) propil ITC, 4- (metilsülfinil) butil ITC ve 3-butenil ITC izomerleri tespit edilmiştir (Wermter ve ark., 2020).

Dittrichia, Asteraceae familyasına ait bir cinistir. Yaklaşık 100 tür içerir ve Akdeniz bölgesinde geniş bir yayılım göstermektedir (Seca, Grigore, Pinto ve Silva, 2014). Acı ot (*D. graveolens*) (Eş anlamlısı: *Inula graveolens* (L.) Desf), kötü bir kokusu olan yıllık aromatik bir bitkidir. Hazirandan Ağustos ayına kadar çiçek açar. Yol kenarlarında ve kırsal alanlarda yetişen nitrofilik bir türdür. Farklı coğrafi bölgelerden acı ot ile ilgili birçok çalışma rapor edilmiş ve önemli farmakolojik etkileri ortaya konmuştur. Türkiye, Irak, Ürdün ve Tunus'tan alınan acı ot etanolik ve metanolik ekstraktları, allelopatik, antifungal, antioksidan, antiproliferatif, sitotoksik ve antibakteriyel aktiviteler göstermiştir (Topçu ve ark., 1993; Abu-Dahab ve Afifi, 2007; Al-Fartosy, 2011; Omezzine, Ladhari, Rinez ve Haouala, 2011).

Birkaç çalışma, acı otunun potansiyel biyolojik herbisit olarak etki yapan birkaç allelokimyasal maddeler içerdiğini göstermiştir (Omezzine ve ark., 2011; Anžlovar, 2020). Acı otun sulu ekstraktları, buğday (*Triticum aestivum* L.) ve adi kanarya otu (*Ambrosia artemisiifolia* L.) tohumlarının çimlenme oranını önemli ölçüde azaltmıştır (Grašič, Anžlovar ve Krajsek

2016). Acı otun etanolik ekstraktı, *P. oleracea* fidelerinin kök uzunluğunun gelişimini %99 oranında azaltmıştır (Abu Irmaileh, Al-Aboudi, Abu Zarga, Awwadi ve Haddad 2015). Acı ot, 2,3,11 $\beta$ ,13-tetrahidroaromatikin ve ilisik asit gibi biyolojik olarak aktif allelokimyasallar içerir. Biyolojik olarak yönlendirilmiş bitki özlerinin fraksiyonlanması, 2,3,11 $\beta$ ,13-tetrahidroaromatikin ve ilisik asidin izolasyonu ile sonuçlanmıştır. Her iki bileşik de seçici fitotoksik aktivite göstermiştir. Arpa, yulaf, darı, kanarya otu ve mercimeklerin kök uzunluğu önemli ölçüde azalırken, brokoli kökü, tere ve turp benzer şekilde ilisik asit tarafından azaltılmıştır (Abu Irmaileh ve ark., 2015).

Bu araştırmanın amacı beyaz lahana, acı ot ve karışımının farklı konsantrasyonlarda kanyasın biyogöstergesi üzerine allelopatik etkisini değerlendirmektir.

## 2. Materyal ve Yöntem

### 2.1. Materyal

Deneme Kahramanmaraş Sütçü İmam Üniversitesi Ziraat Fakültesi'ne ait serada 2020 yılında gerçekleştirilmiştir. Denemede plastik saksı kullanılarak tarladan toprak elde edildikten sonra saksılara 1: 1: 1 oranında toprak, kum ve torfindan oluşan toprak eklenmiştir. Saksılar % 10 konsantrasyonda formaldehyde ile sterilmiştir (şekil 1). Kanyas tohumun dormansiye kırmak için mekanik yöntemi ile kabukları kaldırılmıştır (AL Sakran ve ark., 2020).



Şekil 1. Denemede kullanılan saksıların hazırlanması.

Rizomlar 1cm uzunluğunda ve 1 göz içirdiği kısımlara kesilmiştir. Kanyaş tohum ve rizomları NaOCl %1'de 30 dk bırakılıp sonra kurutulmuş 20 tane tohum veya 10 rizom ekim zamanında saksılara ekilmiştir. Alleopatik bitkiler beyaz lahana Yellow sarmalick çeşidi tarlalardan ve acı ot KSÜ arazisinden (Şekil 2) toplanarak 25°C gölgede kurutulmuş ve daha sonra öğütülmüştür. Konsantrasyonları %2, 5 ve 7 olarak denemede uygulamadan bir gün önce suda bırakılıp 24 saat sonra filtre kâğıdı ile süzölmüştür. Önceden öğütöldüğü alleopatik bitkilerin numunelerden %2 konsantrasyon hazırlanmak için 20 g tartırılıp 1L suya eklenmiştir. Kontrol uygulamalara sadece su eklenmiştir.



Şekil 2. Denemede kullanılan allelopatik bitkiler.

## 2.2. Yöntem

Deneme deseni bölünmüş bölünmüş parseller tesadüfi planına göre dört tekerrür ile kanyaşın tohumu ve rizomu ana parseller, ön bitki türleri, beyaz lahana, acı ot ve karışım alt parseller ve konsantrasyonlar (0, 2, 5 ve 7 gr\100ml) altın altı parseller olmuştur.

Deneme desene göre saksılar, çözeltilerin konsantrasyonlarından 300 ml ve kontrol uygulamalara ise 300 ml su ile sulanmıştır. Daha sonra denemeye gerektiği kadar su eklenmiştir. Sera koşulları maksimum sı-



caklık ortalaması 33°C, minimum sıcaklık ortalaması 18°C ve nispi nem ortalaması %70 olarak bulunmuştur.

Bundan sonra deneme haftalık 3 gün kontrol edilip çimlenen tohum ve rizom sayısı kaydedilmiştir.

Çimlenme oranı hesaplamak için formül (1) kullanılmıştır.

$$\text{ÇO} = (\text{çimlenen tohum sayısı} / \text{toplam tohum sayısı}) \times 100 \quad (1)$$

Çimlenme inhibasyon oranı, kontrol uygulamalarda çimlenme oranına göre yüzde olarak formül (2) ile hesaplanmıştır.

$$\text{Çimlenme inhibasyon oranı} = 1 - (\text{uygulamada çimlenen tohum veya rizom sayısı} / \text{kontrolde çimlenen tohum veya rizom sayısı}) \times 100 \quad (2)$$

Çimlenme indeksi, günde çimlenen tohum veya rizom sayısını göstermek için formül (3) kullanılmıştır.

$$\text{Çimlenme İndeksi} = S_i / G_i + \dots + S_s / G_s \quad (3)$$

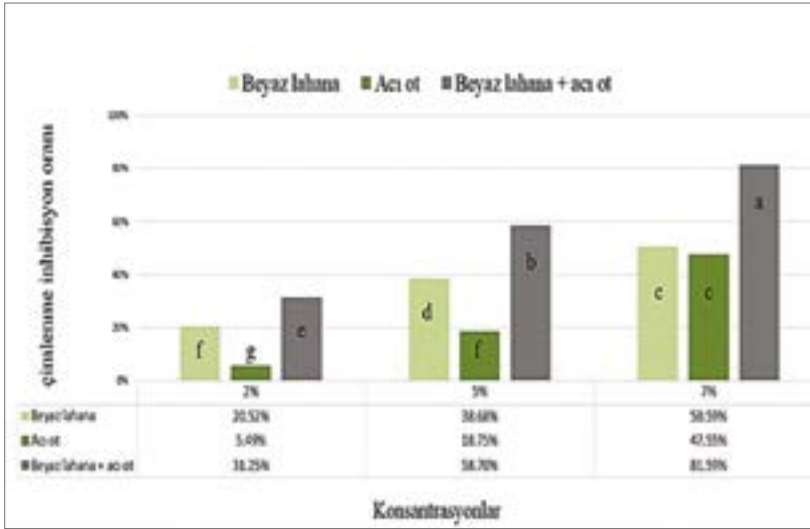
$S_i$ ,  $D_i$ 'de çimlenen tohum sayısı (ilk sayımın günleri) ve  $S_s$ ,  $G_s$ 'de çimlenen tohumların sayısı (son sayımın günleri).

Deneme 30 gün sürülmüş sonra kanyanın boyunu ölçmüştür. Kanyanın toprak yüzeyin seviyesinden kesilip kanyanın ağırlığı tartılmıştır. Kuru ağırlığı hesaplamak için kesilen kanyanın oda koşullarında 25±2°C'de 3 hafta bırakılmıştır.

Denemede bütün veriler, SPSS programı kullanılarak 0.05 olasılık düzeyinde Duncan testi ile analiz edilmiştir.

### 3. Bulgular

Yabancı otlarla mücadelede çimlenme inhibasyon oranı, kullanılan aktif maddelerin değerlendirilmesinde en önemli göstergelerden biridir. Bu çalışmada çimlenme inhibasyon oranı, kontrol uygulamalarında çimlenme oranına göre yüzdesi olarak hesaplanmıştır. Şekil 1'de görüldüğü gibi, kanyanın tohum çimlenmesinin en yüksek inhibasyon oranı beyaz lahana + acı ot karışımında gözlemlenmiştir (Şekil 3). Aynı zamanda allelopatik bitkilerin konsantrasyon artışı ile çimlenme inhibasyon oranının arttığı tespit edilmiştir.



Şekil 3. Allelopatik bitkilerin etkisiyle kanyaş tohumları çimlenme inhibasyon oranı.

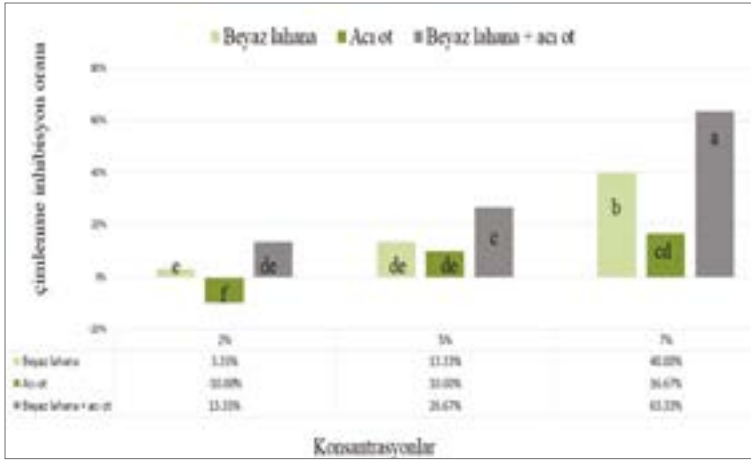
Aynı harf(ler)in takip ettiği değerler 0.05 olasılık düzeyinde birbirinden önemli fark yoktur.

En yüksek çimlenme inhibasyon oranı %81,59, 58.70 ve 50.59 ile beyaz lahana + acı ot %7 ve %5 konsantrasyonu ve beyaz lahana %7 konsantrasyon uygulamalarında sırası ile hesaplandı. Ayrıca acı otun %2 ve 5 konsantrasyonda en düşük etkiye sahip olduğu bulunmuştur (Şekil 3).

Bu denemenin sonuçları, allelopatik bitkilerin farklı konsantrasyon ile kanyaş rizomların çimlenmesinde inhibasyon oranını bazen etkilemiş bazen ise etkili olmamıştır. Beyaz lahana %2, %5 ve acı ot %5, %7 konsantrasyonları kanyaş rizomların çimlenmesinde inhibasyon oranına istatistiksel olarak fazla etkilememesine rağmen, beyaz lahana ve acı ot karışımı için %5 ve %7 konsantrasyonlarda ayrıca beyaz lahana %7 konsantrasyonda kanyaş rizomların çimlenmesini inhibasyon oranında istatistiksel olarak önemli etkileri olduğu gözlemlenmiştir (Şekil 4).

Aynı harf(ler)in takip ettiği değerler 0.05 olasılık düzeyinde birbirinden önemli fark yoktur.

En yüksek çimlenme inhibasyon oranı %63,33 ile karışımın %7 konsantrasyonda uygulanılmasında görülürken, en düşük çimlenme inhibasyon oranı %3.33 ile beyaz lahanada %2 konsantrasyonda gözlemlenmiştir (Şekil 4).



**Şekil 4.** Allelopatik bitkilerin etkisiyle kanyaş rizomları çimlenme inhibisyon oranı.

Acı otun %2 konsantrasyon uygulamasında, kontrol uygulamalarına göre kanyaş rizomlarının çimlenme oranında bir artış gözlemlenmiştir. Bu nedenle bu uygulamanın sonucu negatif bir değer göstermekte, yani acı otun %2 konsantrasyonda kanyaş rizomlarının çimlenmesinde uyarıcı bir etkiye sahip olduğu belirlenmiştir.

Bu denemede kullanılan allelopatik bitkiler, kanyaş tohumlarının çimlenme indeksinde farklı etkilere sahip olduğu bulunmuştur. Beyaz lahananın çimlenme indeksinin farklı konsantrasyonlarda acı otuna göre daha fazla etkili olduğu görülmüştür. Sonuçta, kanyaş tohumlarının çimlenme indeksinin kontrolünde en yüksek olduğunu ve ardından acı otun %2 konsantrasyonda olduğunu göstermiştir (Çizelge 1).

**Çizelge 1.** Allelopatik bitki ekstraktlarının kanyaş tohumlarının çimlenme indeksi üzerine etkisi (çimlenen tohum/gün).

Allelopaty bitkiler	Konsantrasyonlar			
	Kontrol (%0)	%2	%5	%7
Beyaz lahanası	3.57±0.63 <sup>h</sup>	1.71±0.33 <sup>ef</sup>	1.07±0.42 <sup>cd</sup>	0.87±0.19 <sup>bc</sup>
Acı ot		2.66±0.71 <sup>g</sup>	1.87±0.38 <sup>f</sup>	1.35±0.36 <sup>de</sup>
Beyaz lahanası + acı ot		1.50±0.61 <sup>ef</sup>	0.65±0.31 <sup>ab</sup>	0.35±0.27 <sup>a</sup>

Aynı harf(ler)in takip ettiği değerler 0.05 olasılık düzeyinde birbirinden önemli farklı değildir.

Aynı zamanda en düşük çimlenme indeks oranı %7 ve 5 konsantrasyon ile beyaz lahana + acı ot uygulamalarında 0.35 ve 0.65 çimlenen tohum/gün sırayla gözlemlenmiştir. Çizelge (1), allelopatik bitkilerin farklı konsantrasyon ile kanyaş tohumunun çimlenme endeksine etkisini göstermektedir (Çizelge 1).

Kanyaş rizomlarının çimlenme indeks oranı, tohumları gibi allelopatik bitkilerin konsantrasyonlarından etkilenmemiştir. Kontrol uygulamalarından sonra en yüksek kanyaş rizomların çimlenme ideks oranı acı ot uygulamalarında bulunup allelopatik bitkiler için konsantrasyon artışı ile çimlenme ideks oranı artışı tespit edilmiştir (Çizelge 2).

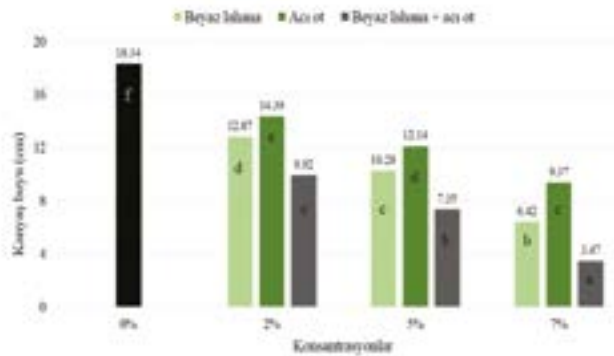
**Çizelge 2.** Allelopatik bitki ekstraktlarının kanyaş rizomlarının çimlenme indeksi üzerine etkisi.

Allelopaty bitkiler	Konsantrasyonlar			
	Kontrol (%0)	%2	%5	%7
Beyaz lahana	2.59±0.73 <sup>f</sup>	1.61±0.51 <sup>cd</sup>	1.27±0.48 <sup>abc</sup>	1.15±0.33 <sup>ab</sup>
Acı ot		2.21±0.61 <sup>e</sup>	1.75±0.67 <sup>d</sup>	1.22±0.41 <sup>abc</sup>
Beyaz lahana + acı ot		1.49±0.33 <sup>bcd</sup>	1.01±0.29 <sup>a</sup>	0.88±0.25 <sup>a</sup>

Aynı harf(ler)in takip ettiği değerler 0.05 olasılık düzeyinde birbirinden önemli fark yoktur.

Beyaz lahana + acı ot %7 konsantrasyonu uygulanmasında kanyaş rizomların çimlenme ideks oranı 0.88 çimlenen rizomlar sayısı/gün ile en düşük bulunmuştur. Çizelge (2), kanyaş rizomlarının çimlenme indeksi-ne allelopatik bitkilerin konsantrasyonları arasındaki önemli farklılıkları göstermektedir.

Farklı konsantrasyonlara sahip olan allelopatik bitkiler, kontrol uygulamalara kıyasla tohumdan çimlenen kanyaşın bitki boyunda önemli farklılıklara sebep olmuştur. Tohumdan çimlenen kanyaşın bitki boyu kontrol uygulamalarında 18,34 cm iken, acı ot %2 ve %5 konsantrasyonlar uygulamalarında 14.39 ve 12.14 cm olarak görülmüştür. Bu bitki boyunun, beyaz lahana ve acı ot karışımı %7 konsantrasyon uygulamasında 3.47 cm'a kadar düştüğü gözlemlenmiştir (şekil 5).

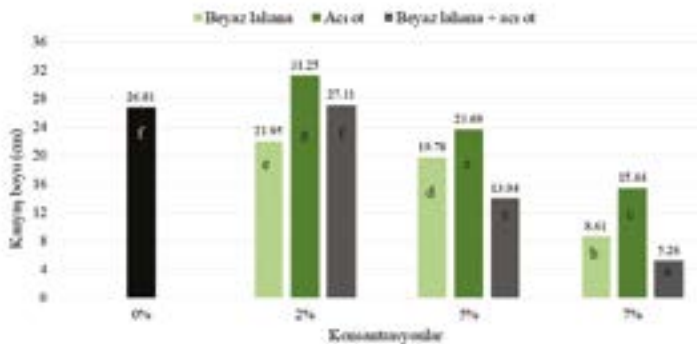


**Şekil 5.** Farklı konsantrasyonlarda allelopatik bitkilerin tohumdan çimlenen kanyaşın bitki boyuna etkisi.

Aynı harf(ler)in takip ettiği değerler 0.05 olasılık düzeyinde birbirinden önemli fark yoktur.

Tohumdan çimlenen kanyaşın bitki boyuna en etkili olan karışım, sırası ile beyaz lahana ve acı ot olarak tespit edilmiştir.

Rizomdan çimlenen kanyaşın bitki boyu ise 31.25 ile 5.26 cm arasında değişmiştir. Rizomdan çimlenen kanyaşın bitki boyu, karışımın etkisiyle %7 konsantrasyonda kontrol uygulamalarına (26,81 cm) kıyasla 5.26 cm'ye düşmüştür. Bununla birlikte, kanyaşın bitki boyuda, %2 konsantrasyonda karışım uygulamaları ile kontrol uygulamaları arasında önemli fark görülmemiştir (Şekil 6).



**Şekil 6.** Farklı konsantrasyonlarda allelopatik bitkilerin rizomdan çimlenen kanyaşın bitki boyuna etkisi.

Aynı harf(ler)in takip ettiği değerler 0.05 olasılık düzeyinde birbirinden önemli fark yoktur.

Beyaz lahana %7 konsantrasyon uygulamasında kanyaşın bitki boyu 8,61 cm olarak hesaplanmıştır. Rizomların çimlenmesini inhibasyonda olduğu gibi, %2 acı ot konsantrasyonu kanyaş büyümesini uyarmıştır. Böylece bu uygulamada kanyaşın bitki boyu 31.25 cm'ye yükseldi ve kontrol uygulamalarını aştığı görülmüştür.

Tohumdan çimlenen kanyaş yaş ve kuru biyokütle uygulamalarına göre farklı bulunmuştur. Kanyaşın yaş ve kuru ağırlığı önemli fark açısından 7 grupta yer almıştır. En düşük yaş ve kuru ağırlığı karışım uygulamalarda %7 ve %5 konsantrasyonlarda ve beyaz lahana %7 konsantrasyonu uygulamasında gözlemlenmiştir. Bu uygulamalarda yaş ağırlığı 0.015 ve 0.073 g arasında olup kontrol uygulamalarda 0.42 g tespit edilmiştir (Çizelge 3).

**Çizelge 3.** Farklı uygulamaların etkisinin altında tohumdan çimlenen kanyaşın yaş ve kuru ağırlığı.

Allelopatik bitkiler	Yaş ağırlığı				Kuru ağırlığı			
	Konsantrasyonlar							
	%0	%2	%5	%7	%0	%2	%5	%7
Beyaz lahana	0.42 <sup>g</sup>	0.234 <sup>e</sup>	0.145 <sup>d</sup>	0.073 <sup>b</sup>	0.091 <sup>g</sup>	0.049 <sup>e</sup>	0.030 <sup>d</sup>	0.014 <sup>b</sup>
Acı ot		0.312 <sup>f</sup>	0.227 <sup>e</sup>	0.113 <sup>c</sup>		0.067 <sup>f</sup>	0.048 <sup>e</sup>	0.023 <sup>c</sup>
Beyaz lahana + acı ot		0.154 <sup>d</sup>	0.068 <sup>b</sup>	0.015 <sup>a</sup>		0.030 <sup>d</sup>	0.013 <sup>b</sup>	0.003 <sup>a</sup>

Aynı harf(ler)in takip ettiği değerler 0.05 olasılık düzeyinde birbirinden önemli fark yoktur.

Tohumdan çimlenen kanyaşın kuru ağırlığı uygulamaları arasında önemli fark açısından yaş ağırlığına benzerlik görülmüştür. Kuru ağırlığı kontrol uygulamalarında 0.091 g'dan 0.003 g'a beyaz lahana ve acı ot karışımının %7 konsantrasyon uygulaması arasında değişmiştir (Çizelge 3).

Uygulamaların rizomlardan çimlenen kanyaşın yaş ve kuru ağırlığına etkisinin sonuçları, önemli ölçüde farklı olan 7 grubun açısından tohumdan çimlenen kaynaşa benzermiştir. Ayrıca hem yaş hem de kuru ağırlık üzerine en fazla etkiye sahip uygulamalar açısından benzerlik

varmıştır (Çizelge 3 ve Çizelge 4). Ancak uygulamaların etkisi tohumdan çimlenen kanyaş yaş ve kuru ağırlığı üzere rizomdan çimlenen kanyaş yaş ve kuru ağırlığına göre daha etkili olarak tespit edilmiştir.

**Çizelge 4.** Farklı uygulamaların etkisinin altında rizomdan çimlenen kanyaş yaş ve kuru ağırlığı.

Allelopatik bitkiler	Yaş ağırlığı				Kuru ağırlığı			
	Konsantrasyonlar							
	%0	%2	%5	%7	%0	%2	%5	%7
Beyaz lahana	4.43 <sup>g</sup>	3.18 <sup>f</sup>	2.48 <sup>e</sup>	0.72 <sup>b</sup>	0.97 <sup>g</sup>	0.67 <sup>f</sup>	0.50 <sup>e</sup>	0.13 <sup>b</sup>
Acı ot		5.07 <sup>h</sup>	3.17 <sup>f</sup>	1.93 <sup>d</sup>		1.12 <sup>h</sup>	0.63 <sup>f</sup>	0.37 <sup>d</sup>
Beyaz lahana + acı ot		3.56 <sup>f</sup>	1.37 <sup>c</sup>	0.25 <sup>a</sup>		0.75 <sup>f</sup>	0.27 <sup>c</sup>	0.05 <sup>a</sup>

Aynı harf(ler)in takip ettiği değerler 0.05 olasılık düzeyinde birbirinden önemli fark yoktur.

Rizomdan çimlenen kanyaş yaş ağırlığı 4.43 g kontrol uygulamalarında ve 0.25 g beyaz lahana ve acı ot karışımının %7 konsantrasyonda uygulamasında arasında değişmiştir. Aynı zamanda %2 konsantrasyon acı ot uygulamasında yaş ve kuru ağırlığı kontrol uygulamalarından daha yüksek bulunmuştur.

#### 4. Tartışma

Bu araştırmanın sonuçları, allelopatik bitkilerin, kanyaş kaynağının tohumlardan veya rizomlardan olup olmadığına bakılmaksızın, kanyaş çimlenmesi ve büyümesi üzerine bir etkisi olduğunu göstermiştir. Genel olarak, allelopatik bitkilerin etkisi tohumlar üzerine rizomlardan daha fazla bulunmuştur. Allelokimyasalların çimlenme üzerine etkisi, hedef bitkinin büyümesi ve gelişmesinden daha büyük olabilmektedir (AL Sakran, Almhedmed, Ustuner ve Dal, 2021).

Sonuçlar ayrıca beyaz lahananın acı otundan daha büyük bir etkiye sahip olduğunu göstermiştir. Aynı zamanda allelopatik bitkiler karıştırıldığında etki sinerjik olduğu tespit edilmiştir. Karışımından elde edilen sonuçlar, allelopatik bitkilerden her biri ayrı ayrı daha üstün olduğu gözlemlenmiştir. Ayrıca allelopatik bitkilerin sulu ekstraktlarının, kanyaşın çeşitli çimlenme ve büyüme göstergeleri üzerine etkisinin, konsantras-

yonların artmasıyla arttığı bulunmuştur. AL Sakran ve ark. (2021) göre allelopatik bitkilerin sulu ekstraktının konsantrasyonunun genel olarak arttırılması, büyüme inhibasyonunda bir artışa yol açar.

Çimlenmenin inhibasyonu, ister çıkış öncesi herbisitler isterse potansiyel allelopatik etkilere sahip olan bitki ekstraktları olsun, aktif maddeleri değerlendirmek için en önemli göstergelerden biridir. Karışım ekstraktı %7 konsantrasyonda kanyaş tohumu çimlenmesini %81,59 oranında engellemiştir. Ancak rizomlarda bu oran %63,33'e düşmüştür. Yani bu ekstraktın etkisi rizomlar üzerine daha az etkilere sahip olduğu belirlenmiştir. Beyaz lahana ekstraktlarının %3'ünün *C. approximata* ve *M. sativa* çimlenmesi üzerine etkili olduğunu göstermiştir (Özkan, 2014). Düşük konsantrasyonların ayrıca kanyaş tohumlarının ve rizomlarının çimlenmesini engellemede zayıf etkileri olmuştur. Anžlovar (2020), sulu ekstraktın artan konsantrasyonuna bağlı olarak tohumların çimlenme oranının azaldığı belirlenmiştir.

Kontrole kıyasla acı otun %2 konsantrasyonda rizom çimlenmesi üzerinde %10 uyarıcı bir etkiye sahip olduğu tespit edilmiştir. Bu nedenle potansiyel allelopatik bitkilerin farklı konsantrasyonlarının incelenmesi, inhibitör ve uyarıcı konsantrasyonlarının bilinmesi için büyük önem taşımaktadır. Güncan'ın (2013) açıkladığı gibi, allelopatik maddelerin etkisi bitki büyümesinin bir uyarıcısı olabilmektedir. Acı ot 10 g/l'de konsantrasyonun kök özütü, marul, turp ve üzerlik fidelerinin büyümesini teşvik etmiş, ancak devedikeni için zararlı olduğu bulunmuştur (Omezzine ve ark., 2011).

Çimlenme indeksi, bir günde çimlenen tohum sayısını gösterir ve bu indeksin daha düşük bir değeri, yabancı ot popülasyonunun büyümesinde ve gelişmesinde bir gecikme olduğunu gösterir. Bu, kültür bitkisinin yabancı otlarların rekabete girmeden önce büyümesini ve gelişmesini sağlar. Bu denemede, kullanılan allelopatik bitkilerin farklı konsantrasyonlarının etkisi altında çimlenme indeksinin değeri kontrol uygulamalarında olduğundan daha düşük olduğu görülmüştür. Bununla birlikte, tohum ve rizom durumunda, kanyaşın çimlenme indeksini düşürmede en etkili olan karışımın ve beyaz lahananın yüksek konsantrasyonları olmuştur. Kural ve Özkan'a (2020), göre *A. retroflexus*, *C. album* ve *B. vulgaris* tohumlarına uygulanan %50 konsantrasyonda beyaz



lahana, su ekstraktında sırasıyla %95, %93 ve %94 oranında çimlenmeyi önlemiştir. Omezzine ve ark. (2011), acı otun %4 konsantrasyonunda sulu ekstraktların *L. sativa*, *R. sativus*, *P. harmala* ve *S. marianum* 'nun çimlenme indeksi ve büyümesi üzerine etkili olamadığı tespit etmiştir.

Genel olarak tohum uygulamalarında kanyaş bitki boyunun rizomlardakinden daha kısa olduğu gözlemlenmiş, burada kontrol uygulamalarında bitki boyu sırasıyla 18,34 ve 26,81 cm hesaplanmıştır. Tohumlardan çimlenen kanyaş boyu %7 konsantrasyonda karışım, beyaz lahana ve acı ot uygulamalarında sırasıyla 3.47, 6.42 ve 9.37 cm'ye düşmüştür. Kanyaş, denemenin başlangıcından 30 gün sonra bu boya ulaşmıştır. Bu, kullanılan ekstraktların, kanyaşın büyümesini, kültür bitkisinin büyümesini ve gelişmesini sağlayacak şekilde yavaşlattığı ve böylece rekabetin kültür bitkisi lehine olduğu anlamına gelmektedir. Rizomlar söz konusu olduğunda, beyaz lahana ve karışımın sadece %7 konsantrasyonu bu etkiyi sağlayabilir. Acı otun sürgün ve çiçek sulu ekstraktlarının toprakta uygulanması fide boyunu azaltmıştır (Omezzine ve ark., 2011).

Topraktan emilen su ve besin maddelerinin miktarındaki rekabet ve fotosentez olayından elde edilen organik madde üretiminde gereken ışık rekabeti yabancı otun yaş ve kuru ağırlığını göstermiştir. Allelopatik bitkilerin yüksek konsantrasyonları, kontrol uygulamalarına kıyasla kanyaşın yaş ve kuru ağırlığını önemli ölçüde azaltmıştır. Bu uygulamalarda kanyaşın zayıf olduğu ve kültür bitkisi ile rekabet edemediği kaydedilmiştir. Ancak kullanılan allelopatik bitkilerin etkisinin kültür bitkileri üzerine ne kadar etki yapacağı belirlenmelidir. Beyaz lahanadan en belirgin GLS hidroliz ürünleri arasında ITC'ler 3- (metilsülfinil) propil ITC, 4- (metilsülfinil) butil ITC ve 3-butenil ITC salgılamaktadır (Wermter ve ark., 2020). Acı ot ise 2,3,11 $\beta$ ,13-tetrahidroaromatikin ve ilisik asit sentezler (Abu Irmaileh ve ark., 2015). Bu denemenin sonuçlara göre bu iki bitkiden salgılanan allelokimyasal maddeler birbirine sinerjik olabilmektedir.

## 5. Sonuç

Bu denemenin sonuçları, kullanılan allelopatik bitki ekstraktlarının kanyaşla mücadelede etkili olabileceğini göstermiştir. Acı ot, beyaz lahana ve karışım ile karşılaştırıldığında kanyaş üzerine zayıf bir etkiye sahip olmasına rağmen, yüksek konsantrasyonlarının kanyaşın büyüme ve gelişme göstergeleri üzerine önemli etkilere sahip olduğu gözlemlenmiştir. Ayrıca acı otun beyaz lahana ile karıştırılması, bu bitkilerin her birinin ayrı ayrı ekstraktlarının etkisini aşan sonuçlar vermiştir. Acı ot %2 konsantrasyonu, kanyaş büyümesinin bazı göstergeleri üzerinde uyarıcı bir etkiye sahip olduğu ve daha yüksek konsantrasyon, kanyaş olumsuz etkilemiştir. Bu denemede kullanılan en yüksek konsantrasyonun %7 olduğu belirlenmiştir. Fakat %10 ve %20 daha yüksek konsantrasyonlar, özellikle rizomlar olmak üzere kanyaş üzerine daha büyük bir etkiye sahip olabilir. Bu nedenle, daha yüksek konsantrasyonların test edilmesi ve bu denemelerin tarla koşullarında uygulanması önerilmektedir. Ayrıca bu bitkilerde bulunan aktif maddelerin bitkinin farklı kısımlarındaki konsantrasyonlarının belirlenmesi allelopatik etkisinin de doğrulanması gerekmektedir.

## KAYNAKÇA

Abu Irmaileh, B. E., Al-Aboudi A. M., Abu Zarga M. H., Awwadi F., & Haddad S. F. (2015). Selective phytotoxic activity of 2,3,11 $\beta$ ,13- tetrahydroaromaticin and ilicic acid isolated from *Inula graveolens*. *Natural Product Research*, 29(10), 893-8.

Abu-Dahab, R. & Afifi, F. (2007). Antiproliferative activity of selected medicinal plants of Jordan against a breast adenocarcinoma cell line (MCF7). *Scientia Pharmaceutica*, 75, 121-136.

AL Sakran, M., Almhemed K., Ustuner T., & Dal S. (2021). Effect of aqueous extract of *Sorghum halepense* (L.) Pers. on germination and growth of some weed species. *International Journal of Science and Research*, 11(1), 404-408.

AL Sakran, M., Almhemed, K., Dal, S., & Ustuner, T. (2020). Test the effect of some methods of breaking the dormancy on the germination and growth of johnson grass seed (*Sorghum halepense* (L.) Pers.). *International Journal of Innovative Science and Research Technology*, 4, 557-561.

Al-Fartosy, A. J. (2011). Antioxidant properties of methanolic extract from *Inula graveolens* L. *Turkish Journal of Agriculture and Forestry*, 35, 591-596.

Anžlovar, S. (2020). Stinkwort (*Dittrichia graveolens*) organic extracts as potential biofungicides for *Fusarium poae*. *Acta Biol. Slovenica*, 63(2), 19-29.

Arslan, Z. F. (2011). *Domates üretiminde sorun olan yabancı otlara karşı organik tarıma uygun bazı mücadele yöntemlerinin araştırılması*, (Doktora Tezi). Çukurova Üniversitesi, Adana. Erişim adresi: <https://tez.yok.gov.tr/Ulusal-TezMerkezi/>

Bangarwa, S. K., Norsworthy, J. K., Mattice, J. D., & Gbur, E. E. (2011). Glucosinolate and isothiocyanate production from brassicaceae cover crops in a plasticulture production System. *Weed Science*, 59, 247-254.

Barroso J., Maxwell B. D., Dorado J., Andújar D., Martín C. S., & Quintanilla C. F. (2016). Response of *Sorghum halepense* demographic processes to plant density and rimsulfuron dose in maize. *Weed Research*. 56(4), 304-312.

Ceseski, A., AL-Khatib, K., & Dahlberg, J. A. (2017). Biology and management of johnsongrass (*Sorghum halepense*). Erişim adresi: <https://anrcatalog.ucanr.edu/pdf/8569.pdf>

Gharde, Y., Singh, P. K., Dubey, R. P., & Gupta, P. K. (2018). Assessment of yield and economic losses in agriculture due to weeds in India. *Agricultural and Biological Sciences*, 107, 12-18.

Grace, J. B., Smith, M. D., Grace, S. L., Collins, S. L., & Stohlgren, T. J. (2001). Interactions between fire and invasive plants in temperate grasslands of north America. In *Proceedings of the invasive species workshop: the role of fire in the control and spread of invasive species. Fire conference*, 40-65.

Grašič, M., Anzlovar, S., & Krajsek, S. S. (2016). The impact of aqueous extracts of stinkwort (*Dittrichia graveolens*) and false yellowhead (*D. viscosa*) on germination of selected plant species. *Phyton; Annales Rei Botanicae*, 56(2), 293-301.

Günçan A. (2013). *Yabancı otlar ve mücadele prensipleri*. Konya.

Jabran, K. (2017). Brassicaceae Allelopathy for Weed Control. In: *Manipulation of Allelopathic Crops for Weed Control*, Springer, Cham, 21-27.

Jafariehyazdi, E., & Javidfar, F. (2011). Comparison of allelopathic effects of some brassica species in two growth stages on germination and growth of sunflower. *Plant Soil and Environment*, 57(2), 52-56.

Khan, A., Marwat, K. B., Hassan, G., Khan, R., & Ullah, Z. (2012). Suppressive capability of herbicides and plant extracts against chickpea weeds. *The Journal of Animal and Plant Sciences*, 22, 67-69.

Khan, R., & Khan, M. A. (2012). Weed control efficiency of bioherbicides and their impact on grain yield of wheat (*Triticum aestivum* L.). *European Journal of Applied Sciences*, 4, 216-219.

Kural, L., & Özkan, Y. R. (2020). Allelopathic potential of white cabbage on some plants. *Plant, Soil and Environment*, 66(11), 559-563.

Kushad, M. M., Brown, A. F., Kurilich, A. C., Juvik, J. A., Klein, B. P., Wallig, M. A., & Jeffery, E. H. (1999). Variation of glucosinolates in vegetable crops of Brassica oleracea. *Agricultural and Food Chemistry*, 47(4), 1541-1548.

McWhorter, C. G. (1993). A 16 year survey on levels of johnsongrass (*Sorghum halepense*) in Arkansas, Louisiana, Mississippi. *Weed Sciences*, 41, 669-677.

Miri, H. R., & Armin, M. (2013). The use of plant water extracts in order to reduce herbicide application in wheat. *European Journal of Experimental Biology*, 3, 155-164.

Omezzine, F., Ladhari, A., Rinez, A., & Haouala, R. (2011). Allelopathic potential of *Inula graveolens* on crops and weeds. *Allelopathy Journal*, 28(1), 63-76.

Özaslan, C., & Kendal, E. (2014). Lice Domatesi üretim alanlarındaki yabancı otların belirlenmesi. *Iğdır Univ. J. Inst. Sci. & Tech*, 4(3), 29-34.

Özkan, Y. R. (2014). *Küçük tohumlu yonca küskütü (Cuscuta approximata Bab.)'nün çimlenme fizyolojisi ve çıkış özellikleri ile bazı bitkilerin küçük tohumlu yonca küskütüne ve yonca (Medicago sativa L.)'ya allelopatik etkilerinin belirlenmesi.* (Doktora Tezi). Yuzuncu Yıl University, Van. Erişim adresi: <https://tez.yok.gov.tr/UlusalTezMerkezi/>

Peerzada, A. M., Ali, H. H., Hanif, Z., Bajwa, A. A., Kebaso, L., Frimpong, D. & Chauhan, B. S. (2017). Eco-biology, impact, and management of *Sorghum halepense* (L.) Pers. *Biological Invasions*, 1-19.

Possenti, M., Baima, S., Raffo, A., Durazzo, A., Giusti, A. M., & Natella, F. (2016). Glucosinolates in Food. *Glucosinolates. Ref. Ser. Phytochem*, 87-132.

Rask, L., Andreasson, E., Ekbom, B., Eriksson, S., Pontoppidan, B., & Meijer, J. (2000). Myrosinase: gene family evolution and herbivore defense in Brassicaceae. *Plant Molecular Biology*, 42, 93-113.

Seca, A. M. L., Grigore, A., Pinto, D. C. G. A., & Silva, A. M. S. (2014). The genus *Inula* and their metabolites: from ethnopharmacological to medicinal uses. *The Journal of Ethnopharmacology*, 154, 286-310.

Shah, N. A., Iqbal, J., Ullah, A., Yang, G., Yousaf, M., Fahad, S. & Wu, Y. (2016). Allelopathic potential of oil seed crops in production of crops: a review. *Environmental Science and Pollution Research*, 23(15), 54-67.

Tepe, I. & Nemli, Y. (1992). *Domates fideliklerinde sorun olan yabancı otlar ve kimyasal mücadeleleri üzerinde araştırmalar.* (Doktora Tezi). Ege Üniversitesi, İzmir.

Topçu, G., Öksüz, S., Shieh, H., Cordell, G.A., Pezzuto, J.M., & Bozok Johansson, C. (1993). Cytotoxic and antibacterial sesquiterpenes from *Inula graveolens*. *Phytochemistry*, 33, 407-410.

Tursun, N., Tursun, A. Ö. ve Kaçan, K. (2004). Kahramanmaraş ili ve ilçelerinde pamuk ekim alanlarında sorun olan yabancı otların belirlenmesi. *KSÜ Fen ve Mühendislik Dergisi*, 7(1), 92-95.

Uludag A., Gozcu D., Rusen M., Guvercin R. S., & Demir A. (2007). The

effect of johnsongrass (*Sorghum halepense* L. Pers.) densities on cotton yield. *Pakistan Journal of Biological Sciences*, 10,523-525.

Uremis, I., Uludag, A. M., & Sangun, A. (2009). Allelopathic potentials of residues of 6 brassica species on johnsongrass [*Sorghum halepense* (L.) Pers.]. *African Journal of Biotechnology*, 8, 3497-3501.

Ustuner, T., AL Sakran, M., & Almhemed, K. (2020). Effect of herbicides on living organisms in the ecosystem and available alternative control methods, *International Journal of Scientific and Research Publications*, 10(8), 633-641.

Wermter, N. S., Rohn, S., & Hanschen, F. S. (2020). Seasonal variation of glucosinolate hydrolysis products in commercial white and red cabbages (*Brassica oleracea* var. *capitata*). *Foods*, 9(11), 16-82.

Yazlık, A. (2014). *Kanyaş (Sorghum halepense (L.) Pers.)'ın Marmara Bölgesindeki yaygınlığı, yoğunluğu, biyolojisi ve alternative mücadele olan aklarının belirlenmesi*. (Doktora Tezi). Mustafa Kemal Üniversitesi, Hatay. Erişim adresi: [https:// tez.yok.gov.tr/UlusalTezMerkezi/](https://tez.yok.gov.tr/UlusalTezMerkezi/)



**ENERJİ ÇALIŞMALARI**  
*ENERGY STUDIES*





# INVESTIGATING THE EFFECTS OF REACTANT GAS FLOW GEOMETRICAL SHAPE ON THE PERFORMANCE OF SOLID OXIDE FUEL CELL

*Molla Asmare<sup>1</sup>*

---

## Abstract

Solid oxide fuel cell supplied with renewable fuels will be a panacea for the current challenges we are faced to meet the global energy demand and alleviate the climate changes stemmed from extensively usage of carbon-rich fuels. Accordingly, this numerical investigation has been examined the geometrical shape effects of reactant gas ducts and the thickness of electrodes on solid oxide fuel cell performance. The finding of this work disclosed that semicircular gas flow duct has outstanding performance following the rectangular, trapezoidal and triangular geometrical shapes. The additional remarkable results of this work are that the reactant gas flow channel shape and the thickness of cathode have substantial effects on airflow than fuel flow under identical electrolyte

---

<sup>1</sup> Gazi University, Faculty of Engineering, Department of Energy Systems Engineering, ORCID: 0000-0003-0119-388X

thickness. The finding also disclosed that a peak power density has been achieved when the thickness of anode gets thicker up to a certain limit then after it is sharply decreasing. On the contrary, the performance of the model is increasing as the thickness of the air electrode is increasing.

**Keywords:** Geometrical Shape, Gas Flow Channel, Electrode Thickness, Solid Oxide Fuel Cell.

## 1. Introduction

Energy is one of the pivotal preconditions to attain sustainable economic development and enhancing the life quality of human beings. A few decades ago, speedy industrializations, growth of inhabitants, and swift urbanizations have huge pressure on carbons-rich fuels, which is finite. Consequently, fossil fuel consumption is rapidly snowballing which leads to rapid fossil fuel reserve depletion. Moreover, they are the principal source of greenhouse gases leading to a harmful impact on the surroundings. For these reasons, finding an alternative green and clean renewable basis energy, advancing their efficiency, and diminishing the obliteration of the environment is unquestionable responsibility for a researcher.

Today, the most decisive challenges we are fronting are clean energy making and battling climate changes. In line with this, hydrogen has abundant merits for stationary, mobile, and transportation applications. According to different studies, more than 23% of the global CO<sub>2</sub> emissions are released from vehicles running with fossil fuels (Lan, Irvine, & Tao, 2012). On the Contrary, utilizing fuel cells driven with hydrogen to power electric vehicles is carbon-free and zero pollutant emissions at the final consumer. This can be owing to the last exhaust of hydrogen fuel is merely water.

Solid oxide fuel cells are one types of electrochemical device that transforms the fuel's chemical energy into electricity without intermediate products by combining numerous fuels (gaseous or gasified, liquid) with an oxidant mainly air (Kakaç, Pramuanjaroenkij, & Zhou, 2007; Wojcik, Middleton, Damopoulos, Van Herle, & Van, 2003) They are the most efficient electrochemical devices yet invented and developed (Ke An, 2003; Ricardo De la Torre García, 2011; S. C. Singhal, 2002; Su, Zhang, Gao, Periasamy, & Kong, 2016) that worked at higher temperatures mainly from 500 to 1000°C (Atkinson et al., 2004; Etemadi, Ghorbani, Masoumpour, & Dadkhah, 2016; Mench, 2008; Walther & Ahn, 2011) Besides, they are also distinguished as a ceramic oxide electrolyte with better fuel adaptability and essay scalability (Jiang, Fang, Khan, & Dougal, 2006; Su, Gao, Zhang, Kong, & Chen, 2015). It also provide high-quality waste heat that can be recovered through cogeneration (S.C

Singhal, 2000) with zero or minimal pollutants even using carbon-rich fuels. SOFCs are quiet solid-state devices that have vibration-free operation with minimal NO<sub>x</sub> and SO<sub>x</sub> emissions compared with traditional energy conversion technologies(S. C. Singhal, 2002). For these reasons, they are obtained a critical attention of various scholars and governments.

Further, because of having high operating temperatures, some hydrocarbon fuels like natural gas can be reformed within the cell stack. As a result, they are eliminating the need of expensive external reformer(Ke An, 2003; Ricardo De la Torre García, 2011; S. C. Singhal, 2002; Subhash C. Singhal & Kendall, 2003). Besides, SOFCs can be integrated with conventional heat engines like gas turbines to reuse the waste heat from exhausted gases(Ke An, 2003; Xiurong Fang & Cell, 2018). According to Singhal (S.C Singhal, 2000) and Chan et al., (Chan, Khor, & Xia, 2001), the efficiencies of hybrid SOFC-gas or steam turbine power systems are estimated to 70%. However, the recent studies indicate that the efficiency of SOFCs combined with gas turbines is above 90 % with zero GHGs (Choudhury, Chandra, & Arora, 2013; Siddiqui & Dincer, 2018; S. C. Singhal, 2002; Su et al., 2016). This is because the exhaust product is only water when the fuel cells run with hydrogen or carbon free fuel.

Nowadays, different design of SOFC is available in the open literature(Fang, Zhu, & Lin, 2018; Ilbas, Kumuk, Alemu, & Arslan, 2020; Minh, 2004; Molla & Ilbas, 2020; Yu, Liu, Zheng, & Ding, 2016). Yet, the planar design is obtained a remarkable attention because of having supreme power. Connected with this, aplenty of numerical and experimental studies are available on planar SOFC (P-SOFC) feed with different fuels(Molla & Ilbas, 2020)the most decisive challenges we are fronting are perfectly clean energy making for equitable and sustainable modern energy access, and battling the emerging alteration of the climate. This is because, carbon-rich fuels are the fundamental supply of utilized energy for strengthening human society, and it will be sustained in the near future. In connection with this, electrochemical technologies are an emerging and domineering tool for efficiently transforming the existing scarce fossil fuels and renewable energy sources into electric power with a trivial environmental impact. Com-

pared with conventional power generation technologies, SOFC that operate at high temperature is emerging as a frontrunner to convert the fuels chemical energy into electric power and permits the deployment of varieties of fuels with negligible ecological destructions. According to this critical review, direct ammonia is obtained as a primary possible choice and price-effective green fuel for T-SOFCs. This is because T-SOFCs have higher volumetric power density, mechanically stable, and high thermal shocking resistance. Also, there is no sealing issue problem which is the chronic issues of the planar one. As a result, the toxicity of ammonia to use as a fuel is minimized if there may be a leakage during operation. It is portable and manageable that can be work everywhere when there is energy demand. Besides, manufacturing, onboard hydrogen deposition, and transportation infrastructure connected snags of hydrogen will be solved using ammonia. Ammonia is a low-priced carbon-neutral source of energy and has more stored volumetric energy compared with hydrogen. Yet, to utilize direct  $\text{NH}_3$  as a means of hydrogen carrier and an alternative green fuel in T-SOFCs practically determining the optimum operating temperatures, reactant flow.”,”author”:[{”dropping-particle”：“”,”family”：“Molla”,”given”：“Asmare”,”non-dropping-particle”：“”,”parse-names”：false,”suffix”：“”},{”dropping-particle”：“”,”family”：“Ilbas”,”given”：“Mustafa”,”non-dropping-particle”：“”,”parse-names”：false,”suffix”：“”}],”container-title”：“International Journal of Energy Technology”,”id”：“ITEM-1”,”issue”：“June”,”issued”：[{”date-parts”：[[”2020”]]}],”page”：“70-91”,”title”：“Direct ammonia fueled solid oxide fuel cells: A comprehensive review on challenges, opportunities and future outlooks”,”type”：“article-journal”,”volume”：“2”},”uris”：[”http://www.mendeley.com/documents/?uuid=5c1a9b5b-55d1-499b-a27d-23c53677545e”]],”mendeley”：{”formattedCitation”：“(Molla & Ilbas, 2020. It is know that the current density is strongly a temperature dependent function. This is because the electrochemical reaction is faster at higher operating temperatures. The convective and diffusive heat, mass, and species transport are also a function of duct geometrical shape because of its influence on the flow regime. Yet, the effects of fuel and airflow duct shape are not studied. And also, the effects of PEN have been studied yet not sufficient. Thus, the influence of semicircular, triangular,

trapezoidal and rectangular geometrical shape of reactant gas flow conduits has been investigated on the performance of the model. The numerical simulation has been performed at constant area of gas flow duct and active PEN. As well, the performance of the cell has been examined using different thickness of electrodes at the same electrolyte thickness. However, at the beginning, the model has been simulated and analyzed under similar thickness of PEN then after their thicknesses have been changed. Thus, the central goal of this study is investigating the influence of different geometrical orientation of reactant gas flow ducts and electrode thickness on the performance of hydrogen fuelled P-SOFC. As the knowledge of the author, this model is novel and will be used as a cornerstone to understand the influence of duct shapes on cell performances.

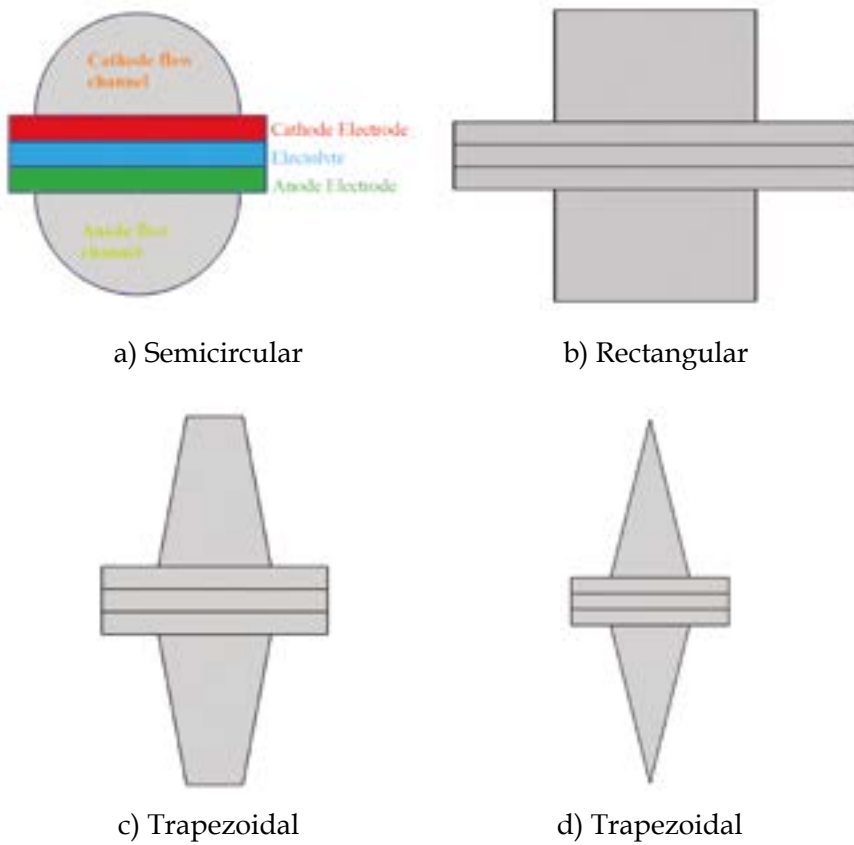
## 2. Numerical Investigation of Solid Oxide Fuel Cell

Mathematical Simulation is fundamental to investigate the performance of SOFC that are used for clean energy generation in the future. This is because numerical simulation is a viable means to assure the practicability of SOFC before experimental work. Also, experimental work requires much cost and time. Not only that, it is difficult to analysis what is going inside the cell using experimental study. Thus, in this numerical study, a finite element based commercial COMSOL Multiphysics software 5.5 has been used for 3D hydrogen feed SOFC model development and numerical simulation analyses. The rectangular geometrical dimensions have been adopted from [www.comsol.com](http://www.comsol.com) (Multiphysics & Software, n.d.). That comprises of electrolyte, fuel, and air electrodes coupled with their gas flow ducts as illustrated in Table 1. Yet, the semicircular, triangular and trapezoidal dimensions of gas flow channels are developed using constant area of gas flow channel and PEN thickness. For all geometrical structures, a co-flow of reactant gases has been used. Fig.1 and Fig.2 shows the cross-sectional view and the geometrical structure of the developed model coupled with its mesh respectively. The basic operating and fitting parameters are displayed in Table 2.

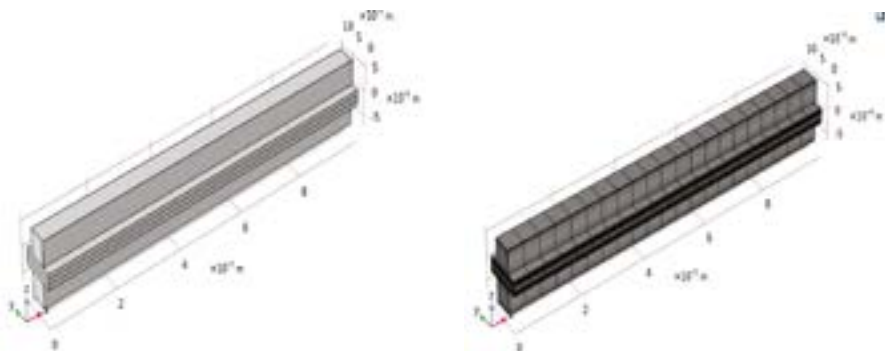
<b>Table1:</b> Geometrical Dimensions.	
<b>Dimensions</b>	<b>Size</b>
Anode thickness( $H_{gdea}$ )	0.1[mm]
Electrolyte thickness ( $H_{ely}$ )	0.1[mm]
Cathode thickness( $H_{gdec}$ )	0.1[mm]
Gas flow channel height	0.5[mm]
Gas flow channel width	0.5[mm]
Rib width	0.5[mm]
Flow channel length	10[mm]

<b>Table 2:</b> Input Variable and Operating Conditions.	
<b>Parameters</b>	<b>Value</b>
Inlet Temperature	1073K
Initial cell polarization ( $V_{LL\ pol}$ )	0.05V
Exchange current density, anode	0.1 [A/m <sup>2</sup> ]
Exchange current density, cathode	0.01 [A/m <sup>2</sup> ]
Specific surface area, anode	1e9[1/m]
Specific surface area, cathode	1e9[1/m]
Anode Equilibrium voltage ( $\Phi_{an}^0$ )	0V
Cathode Equilibrium voltage ( $\Phi_{cat}^0$ )	1V
Cell voltage( $V_{cell}$ )	$\Phi_{cat} - \Phi_{an} - V_p$
Reference diffusivity( $K_d$ )	3.16e-8[m <sup>2</sup> /s]
Porosity	0.4
Electrolyte conductivity	5[S/m]
Solid effective conductivity, anode	1000[S/m]
Solid effective conductivity, cathode	1000[S/m]
Inlet weight fraction, H <sub>2</sub> at anode	0.4
Inlet weight fraction, H <sub>2</sub> O at cathode	0.37
Inlet weight fraction, O2 at cathode	0.15





**Figure 1:** A Cross-Sectional View of SOFC Model with Different Reactant Gas Channel Ducts.



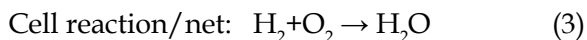
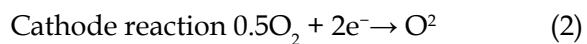
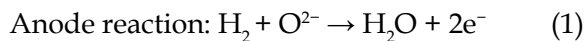
**Figure 2:** Schematic Drawing of Solid Oxide Fuel Cell.

## 2.1. Assumptions and Boundary Conductions Used for Model development

The main assumptions were applied in this numerical study is that the distribution of temperature is isothermal, the velocities of the fluid and the partial pressures are averagely uniform, and the viscosity of the fluid in each subsystem is the same. As well, during fuel and air flow via the systems, the density of the gas is constant, chemical reactions does not occur in both conduits and operated at steady state. Boundary conditions are also formulated to solve different coupled partial differential equations. Accordingly, some of the working circumstances were considered is nonslip conditions, which means the velocity of boundary and fluid are identical, the boundary layers for gas flow are negligible, uniform potential at the electrode or gas channel interface and the flux is zero at the end of electrodes and electrolyte.

## 2.2. Electrochemical Modelling

An electrochemical reaction is an oxidation-reduction reaction of a fuel and oxidant mainly air take apart in a fuel cell. It constituted a source terms coupled with transport equations of charge transfer, energy, mass and momentum. In this modelling, moist hydrogen and air is feed into the anode and cathode electrode respectively. Accordingly, the anticipated oxidation-reduction electrochemical reaction of hydrogen fuelled SOFC using  $O^{2-}$  transfer is expressed as follows.



The electrochemical performance of a fuel cell is investigated as a function of polarization and power density plot to identify the effect of embedded current collector. The ideal voltage is determined at standard conditions yet fuel cell is always running above it. The voltage variation is more perceptible in cells that run at elevated temperatures. Alongside,

current is not flowing outside of the cell unless connected to an external load. As a result, the operating voltage is equal to the open circuit voltage ( $V_{OC}$ ). Nernst voltage ( $E_{Nernst}$ ) is same to equilibrium voltage at the air electrode that has been estimated by the following formulas (Cheddie, 2013).

$$E_{Nernst} = 1.253 - \frac{T}{4079} + \frac{RT}{nF} \ln \left[ \frac{P_{H_2} [P_{O_2}]^{0.5}}{P_{H_2O}} \right] \quad (4)$$

Here,  $P_{H_2}$ ,  $P_{H_2O}$ , and  $P_{O_2}$  are the partial pressure of hydrogen, water vapor and oxygen at the anode and cathode-electrolyte interface, respectively.

Further, the cell voltage ( $V_{cell}$ ) is plummeting because of internal charge transfer, conduction, and diffusion losses. As a result,  $V_{cell}$  is always lower than Nernst voltage as shown in equation (5). These losses are independently characterized as activation, concentration and ohmic polarization. They are prevailing factors that determine the  $V_{cell}$  and collectively considered as voltage losses ( $V_{oss}$ ). Consequently,  $V_{cell}$  can be expressed as:

$$V_{cell} = E_{Nernst} - V_{loss} \quad (5)$$

And

$$V_{loss} = \eta_{ohmic} + \eta_{act} + \eta_{con} \quad (6)$$

Where,  $\eta_{act}$ ,  $\eta_{ohm}$ , and  $\eta_{con}$  are the activation, ohmic, and concentration polarization at anode and cathode electrodes respectively.

Besides, for this numerical study, Maxwell-Stefan diffusion and convection mode is also applied for mass and species balance in gas channels and porous electrodes regarding the substantial difference between molecular weight of species. This is because the transport of mass is primarily motivated by diffusion and convection. As well, Brinkman equation is used for momentum balance through the porous media to solve the pressure and velocity field. Ohm's law is also used to determine the transfer of charge between ionic and electronic conductors and conductive phases. Accordingly, the rudimentary governing equations for charge carriers, species, momentum, energy, and mass conservation

are summarized in Table 3. The molecular diffusion of gases is also determined using Fuller's correlation where M is the molecular weight in kg/kmol,  $v$  is the special Fuller's diffusion volume as expressed below;

$$D_{ij} = \frac{k T^{1.75}}{P \left[ \frac{2 M_i M_j}{M_i + M_j} \right]^{1/4} \left[ v_i^{1/3} + v_j^{1/3} \right]^2} \quad (7)$$

**Table 3:** Governing Equation.

Charge conservation equations	$\nabla \cdot i_{io} = \Phi_{io} \quad i_{io} = -\delta_{io} \cdot \nabla \cdot \Phi_{io}$ $\nabla \cdot i_{el} = \Phi_{el} \quad i_{el} = -\delta_{el} \cdot \nabla \cdot \Phi_{el}$
Bulter-Volmer equation	$i = i_{0,j}$
Continuity Equation	$\frac{\partial(\epsilon_{eff} \rho)}{\partial t} + \frac{\partial(\epsilon_{eff} \rho u_i)}{\partial x_i} = S_n$
Momentum Equation	$\frac{\partial(\rho_{eff} u_i)}{\partial t} + \frac{\partial(\rho_{eff} u_j u_i)}{\partial x_j} = -\frac{\partial P}{\partial x_i} + \frac{\partial}{\partial x_j} \left( \mu_{eff} \left( \frac{\partial u_i}{\partial x_j} + \frac{\partial u_j}{\partial x_i} \right) \right) + S_d$
Energy equation	$\frac{\partial(\rho C_p T)}{\partial t} + u_i \frac{\partial(\rho C_p T)}{\partial x_i} = \frac{\partial}{\partial x_j} \left( k_{eff} \left( \frac{\partial T}{\partial x_j} + \frac{\partial T}{\partial x_i} \right) \right) + S_T$
Chemical species	$\frac{\partial(\rho C^k)}{\partial t} + \frac{\partial}{\partial x_i} (\rho u_i C^k) = \frac{\partial}{\partial x_i} \left[ \rho D_{eff}^k \left( \frac{\partial C^k}{\partial x_j} + \frac{\partial C^k}{\partial x_i} \right) \right]$

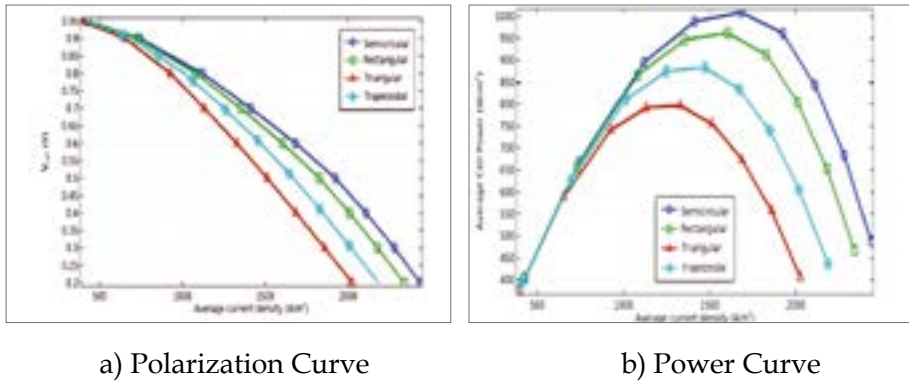
Likewise, during the electrochemical reaction, the rate of hydrogen and oxygen consumption and production of water as a byproduct of the reaction is given as follows.

$$r_{H_2} = \frac{-i}{2F}, r_{O_2} = \frac{-i}{4F}, r_{H_2O} = \frac{i}{2F}$$

### 3. Results and Discussions

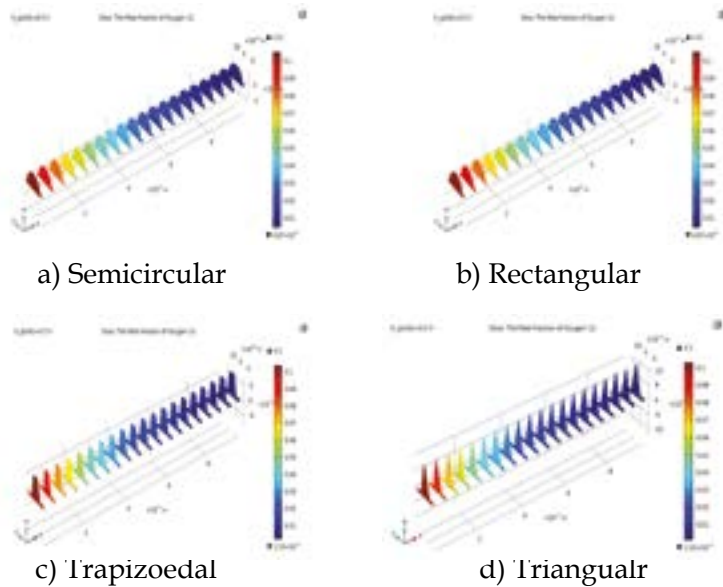
Today, the performance of the fuel cell has been tried using different fuels (hydrocarbons, hydrogen, natural gas, biogas, methanol, ethanol, etc.) Among them, hydrogen is a perfect fuel choice from energy density and environmental outlooks to resolve the global warming glitches due to fossil fuel combustion. Yet, the storage and distribution system of hydrogen needs further research, which is out of the scope of this work. Accordingly, in this numerical work, a 3D hydrogen fuelled P-SOFC model has been developed and its performance has been evaluated using different shape of reactant gas flow channels under similar operating conditions and active area. In addition to this, a parametric sweep analysis has been studied to examine the effects of electrodes thickness under similar electrolyte thickness. A number of runs were conducted at cell voltage ranged from 0.95V to 0.2V in step down of 0.05V through parametric mode to generate a complete polarization curve as a function of voltage and current density. A parametric nonlinear stationary with direct linear system solver (MUMPS) has been used to linearize the PDEs at convergence relative tolerance of 0.001.

In this numerical modelling, the fuel cell ducts are changed from rectangular to semicircular, triangular and trapezoidal geometrical designs under similar working conditions and active area. Among them, a semicircular gas flow duct outperforms succeeding rectangular, trapezoidal and triangular as displayed in Fig3. As well, the effect of duct shape is more influential at the cathode electrodes. Accordingly, the finding of this work is revealed that the geometrical structure of reactant gas flow duct has played frolicked contribution on fuel cell performance. The polarization curve determines the fuel cell performance that indicates the electrochemical efficiency at any operating current. The maximum voltage output is achieved at open circuit when there is no current flow. As can be seen in the figure, the voltage output decreases when the current surges due to different potential lose. The figure also illustrates that a maximum power density of 1008.91, 961.32, 882.51, and 796.3W/m<sup>2</sup> is noted at a cell voltage of 0.5V when the reactant gas channel is modeled in semicircular, rectangular, trapezoidal and, triangular duct shapes, respectively.



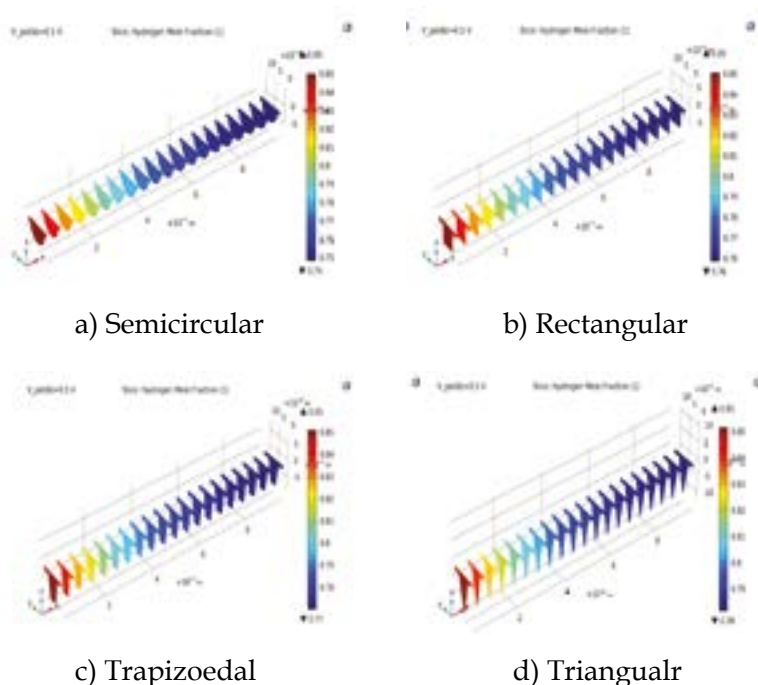
**Figure 3:** The performance of the developed model as a function of different gas flow duct shapes at a cell voltage of 0.5 V.

The spatial distribution of oxygen mole fraction within the air electrode and in its flow duct is depicted in Fig.4. The depletion of oxygen is slowly declines along the main flow channel directions and reaches almost null close to the outlet from its initial value of 0.11. Noticeable depletion is observed in all geometrical ducts but more significant in semicircular ducts. This is because the relative reduction electrochemical reaction and diffusion of oxygen is sluggish than hydrogen fuel.



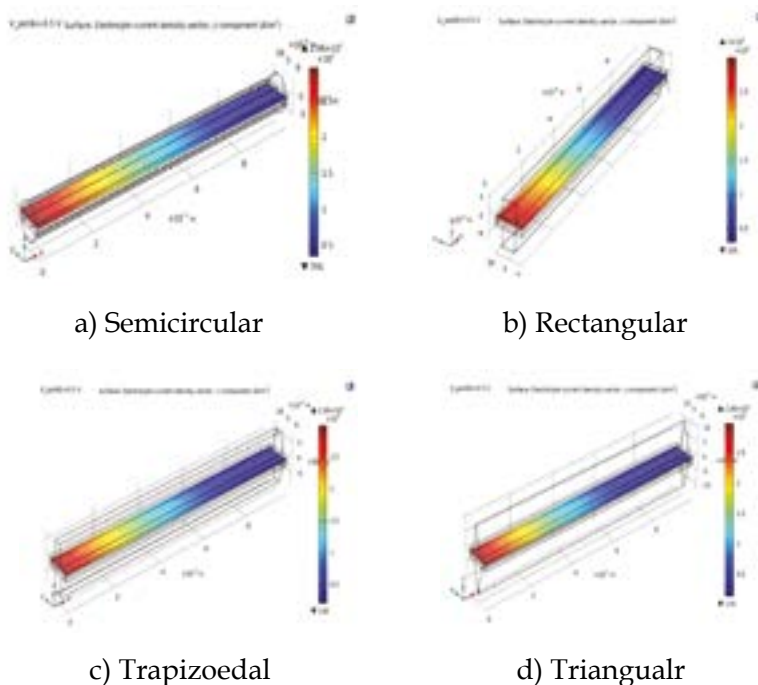
**Figure 4:** The distribution of oxygen mole fraction at different shape of gas flow ducts a cell voltage of 0.5 V.

Figure 5 shows the distribution of hydrogen inside the fuel flow duct and at the anode electrode. As illustrated in the figure, the mole fraction of hydrogen cascades from 0.85, which is an initial value for all types of reactant flow ducts to about 0.75, 0.76, 0.77 and 0.78 at the outlet of semi-circular, rectangular, trapezoidal and triangular ducts, respectively. The amount of hydrogen at the fuel electrode has been also declined along the flow channel directions. Yet, the depletion of hydrogen is not noticeable like that of happening at the air electrode.



**Figure 5:** The distribution of hydrogen mole fraction at different shape of gas flow ducts at a cell voltage of 0.5 V.

Figure 6 has been displayed that the distribution of electrolyte current density at the side of air electrode is non-uniform, underprivileged and almost nil at the cathode outlet because of oxygen depletion. Relatively, the distribution of current is good in semicircular reactant gas flow channels that supplies uniform gas distribution. Consequently, the primary solution to boost the performance of SOFC is increasing the flow rate of cathode that facilitates oxygen mass transfer.

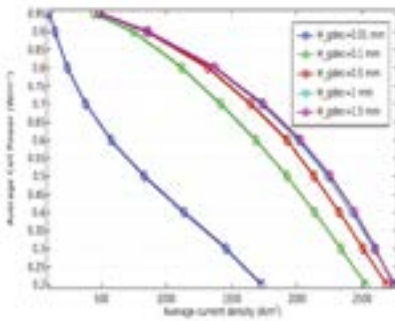


**Figure 6:** Electrolyte current density at different shape of gas flow ducts at a cell voltage of 0.5V.

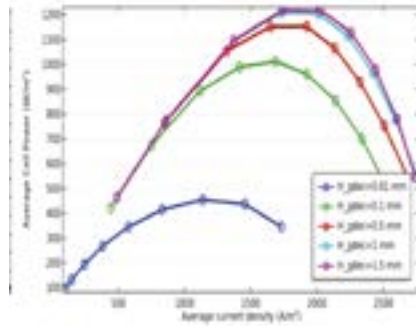
Besides, the performance of P-SOFC has been studied numerically as a function of electrode thickness. The simulation has been conducted using a semicircular duct that gives a maximum power density. Accordingly, the thickness of anode has been simulated at value of 0.01, 0.1, 0.5, 1, and 1.5mm under similar electrolyte thickness (0.1mm). Then after, the performance of the model has been evaluated when the cathode electrode thickness has been changed from 0.01 to 1.5mm using the anode thickness that gives peak power density. The simulation result unveil that air electrode thickness has considerable effect on cell performance than that of anode as can be seen clearly in Fig .7. Connecting with this, a deprived performance has been observed at thinner cathode electrodes. The expected reason associated with this is that the relative oxygen diffusion towards the anode and its electrochemical reactivity is slow compared with hydrogen. Alongside, the chance of supplying a sufficient quantity of air is declined that resulting in sever oxygen deple-



tion. In contrast, the model performance is declining as the anode electrode is going to be thinner especially above 0.5 mm because of having substantial fuel diffusion resistance as illustrated in Fig.8. Yet, the finding also disclosed that the performance of the model is improved when the anode electrode gets thicker up to 0.5mm. This is because the diffusion of gases is augmented when the thickness of the anode electrode increases up to a certain limit. Accordingly, a maximum power density is observed at a cathode thickness of 1.5 and anode of 0.5mm. This is due to as the anode thickness is made thinner the diffusion potential loss is meaningfully diminishing. As a result, the overall cell performance is boosted.

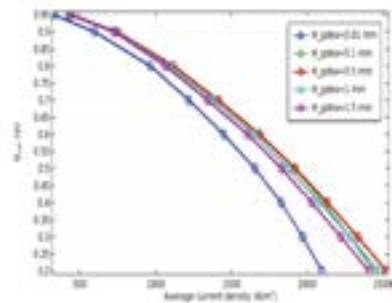


a) Polarization Curve

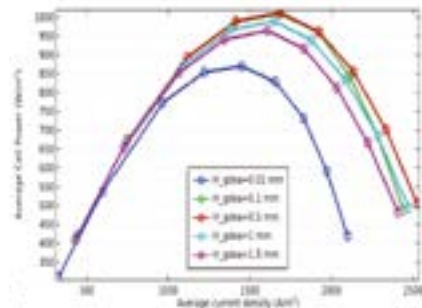


b) Power Curve

**Figure 7:** The performance of the developed model as a function of air electrode thickness.



c) Polarization Curve



d) Power Curve

**Figure 8:** The performance of the developed model as a function of fuel electrode thickness.

#### 4. Conclusion

A three dimensional P-SOFC model has been developed and simulated numerically to investigate the effect of flow channel shape and electrodes thickness on cell performance. Accordingly, the finding of the study disclosed that maximum power density of  $1008.91\text{W/m}^2$  were recorded when the reactant gas channel is constructed in semicircular following rectangular ( $961.32\text{W/m}^2$ ), trapezoidal ( $882.51\text{W/m}^2$ ) and, triangular ( $796.3\text{W/m}^2$ ) shape. In addition, the electrodes thickness analysis confirmed that the air electrode has substantial influence on model performance than that of anode. The finding also disclosed that the performance of the model is improved when the anode electrode gets thicker up to 0.5mm but it is sharply decreasing beyond 0.5mm because of having substantial fuel diffusion resistance. Accordingly, a maximum power density is observed at a cathode thickness of 1.5 and anode of 0.5mm. On the contrary, a deprived performance has been observed at thinner cathode electrode of 0.01mm compared with anode due to higher oxygen depletion and the relative oxygen diffusion towards the anode and its electrochemical reactivity is slow compared with hydrogen.

#### Acknowledgment

This paper has been successfully completed with the support of Gazi University Department of Energy Systems Engineering and Turkey Abroad and Relative Ministry who gives scholarship opportunity to continue my Ph.D. at Gazi University. Hence, we are eager to acknowledge them.

## REFERENCES

Atkinson, A., Barnett, S., Gorte, R. J., Irvine, J. T. S. S., Mcevoy, A. J., Mogensen, M., Vohs, J. (2004). Advanced anodes for high-temperature fuel cells. *Nature Materials*.

Chan, S. H., Khor, K. A., & Xia, Z. T. (2001). *A complete polarization model of a solid oxide fuel cell and its sensitivity to the change of cell component thickness*, 93, 130-140.

Cheddie, D. F. (2013). *Modelling of ammonia-fed solid oxide fuel cells*. 504-511.

Choudhury, A., Chandra, H., & Arora, A. (2013). Application of solid oxide fuel cell technology for power generation - A review. *Renewable and Sustainable Energy Reviews*, 20, 430-442. Retrieved from: <https://doi.org/10.1016/j.rser.2012.11.031>

Etemadi, A., Ghorbani, S., Masoumpour, M., & Dadkhah, M. (2016). The Numerical analysis of an anode-supported high temperature DIR- PSOFC operating conditions with considering the maximum allowable temperature difference. *Journal of Heat and Mass Transfer Research*, 1(2), 15-25.

Fang, X., Zhu, J., & Lin, Z. (2018). Effects of electrode composition and thickness on the mechanical performance of a solid oxide fuel cell. *Energies*, 11(1735), 1-13. Retrieved from: <https://doi.org/10.3390/en11071735>

Ilbas, M., Kumuk, B., Alemu, M. A. M. A., & Arslan, B. (2020). Numerical investigation of a direct ammonia tubular solid oxide fuel cell in comparison with hydrogen. *International Journal of Hydrogen Energy*, 45(60), 35108-35117. Retrieved from: <https://doi.org/10.1016/j.ijhydene.2020.04.060>

Jiang, W., Fang, R., Khan, J. A., & Dougal, R. A. (2006). Parameter setting and analysis of a dynamic tubular SOFC model. *Journal of Power Sources*, 162(1), 316-326. Retrieved from: <https://doi.org/10.1016/j.jpowsour.2006.06.086>

Kakaç, S., Pramuanjaroenkij, A., & Zhou, X. Y. (2007). A review of numerical modeling of solid oxide fuel cells. *International Journal of Hydrogen Energy*. Retrieved from: <https://doi.org/10.1016/j.ijhydene.2006.11.028>

Ke An. (2003). Mechanical Properties and Electrochemical Durability of Solid Oxide Fuel Cells. *Virginia Polytechnic Institute and State University, USA*.

Lan, R., Irvine, J. T. S., & Tao, S. (2012). Ammonia and related chemicals as potential indirect hydrogen storage materials. *International Journal of Hydrogen Energy*, 37(2), 1482-1494. Retrieved from: <https://doi.org/10.1016/j.ijhydene.2011.10.004>

Mench, M. M. (2008). Fuel Cell Engines. In *Fuel Cell Engines*. Retrieved from: <https://doi.org/10.1002/9780470209769>

Minh, N. Q. (2004). Solid oxide fuel cell technology - Features and applications. *Solid State Ionics*, 174, 271-277. Retrieved from: <https://doi.org/10.1016/j.ssi.2004.07.042>

Molla, A., & Ilbas, M. (2020). Direct ammonia fueled solid oxide fuel cells:

A comprehensive review on challenges, opportunities and future outlooks. *International Journal of Energy Technology*, 2, 70–91. Retrieved from: <https://doi.org/https://doi.org/10.32438/IJET.203011>

Multiphysics, C., & Software. *Current Density Distribution in a Solid Oxide Fuel*. Retrieved from: [www.c514omsol.com/model/](http://www.c514omsol.com/model/)

Ricardo De la Torre García, U. of T. I. (2011). Production of Micro-Tubular Solid Oxide Fuel Cells. *University of Trento, Italy*, (April).

S.C Singhal. (2000). Advances in solid oxide fuel cell technology. *Solid State Ionics*, 135(1-4), 305–313. Retrieved from [www.elsevier.com/locate/ssi](http://www.elsevier.com/locate/ssi)

Siddiqui, O., & Dincer, I. (2018). A review and comparative assessment of direct ammonia fuel cells. *Thermal Science and Engineering Progress*, 5(August 2017), 568–578. Retrieved from: <https://doi.org/10.1016/j.tsep.2018.02.011>

Singhal, S. C. (2002). Solid oxide fuel cells for stationary, mobile, and military applications. *Solid State Ionics*, 152–153, 405–410. Retrieved from: [https://doi.org/10.1016/S0167-2738\(02\)00349-1](https://doi.org/10.1016/S0167-2738(02)00349-1)

Singhal, Subhash C., & Kendall, K. (2003). High-temperature Solid Oxide Fuel Cells: Fundamentals, Design and Applications. In *High-temperature Solid Oxide Fuel Cells: Fundamentals, Design and Applications*. Retrieved from: <https://doi.org/10.1016/B978-1-85617-387-2.X5016-8>

Su, S., Gao, X., Zhang, Q., Kong, W., & Chen, D. (2015). Anode-versus cathode-supported solid oxide fuel cell: Effect of cell design on the stack performance. *International Journal of Electrochemical Science*.

Su, S., Zhang, Q., Gao, X., Periasamy, V., & Kong, W. (2016). Effects of changes in solid oxide fuel cell electrode thickness on ohmic and concentration polarizations. *International Journal of Hydrogen Energy*. Retrieved from: <https://doi.org/10.1016/j.ijhydene.2016.04.221>

Walther, D. C., & Ahn, J. (2011). Advances and challenges in the development of power-generation systems at small scales. *Progress in Energy and Combustion Science*. Retrieved from: <https://doi.org/10.1016/j.pecs.2010.12.002>

Wojcik, A., Middleton, H., Damopoulos, I., Van Herle, J., & Van, J. (2003). Ammonia as a fuel in solid oxide fuel cells. *Journal of Power Sources*, 118, 342–348. Retrieved from: [https://doi.org/10.1016/S0378-7753\(03\)00083-1](https://doi.org/10.1016/S0378-7753(03)00083-1)

Xiurong Fang, J. Z. and Z. L., & Cell, F. (2018). *Effects of Electrode Composition and Thickness on*. Retrieved from: <https://doi.org/10.3390/en11071735>

Yu, Z., Liu, S., Zheng, F., & Ding, Y. (2016). Effects of the different supported structures on tubular solid oxide fuel cell performance. *International Journal of Electrochemical Science*, 11(12), 10210–10222. Retrieved from: <https://doi.org/10.20964/2016.12.53>



# CO<sub>2</sub> EMISSION MITIGATION IN A NATURAL GAS/RENEWABLE ENERGY SYSTEM AND IMPACTS ON THE CARBON BUDGET

*Mujeeb Babatunde Adetayo*<sup>1</sup>

---

## Abstract

Meeting energy demand requires diverse supply mix of different energy sources. However, the re-occurring natural disasters like flood and wildfire linked to global temperature increase necessitate the use low carbon energy sources, especially renewable energy. Due to the infeasibility of an abrupt renewable energy transition in the short run, this work investigated the extent of emission reduction associated with a combined natural gas and renewable energy system. The analysis was based on the use of fuel emission factors to calculate the emission and carbon budget from various systems of diverse energy sources. Three cases were considered: Case 1 compared a natural gas/ renewable energy and a full natural gas system. This was used to determine the extent of emission reduction if natural gas and renewables had dominated the

---

<sup>1</sup> PhD Student, Marmara University, Faculty of Engineering, Chemical Engineering

consumption mix between the year 2009 and 2019. Case 2 and 3 are projections based on a 320Gt carbon budget (CB) as at the ending of year 2019. The emission coal dominating consumption mix Case 2 is a mixed system which uses the same consumption ratio as that of the year 2019, while Case 3 is a natural gas/ renewable energy system but with a 5-year transition gap. Using the year 2009 to 2019 data, the fuel emission factors (FEF) for oil, natural gas and coal gave 0.06489, 0.05406 and 0.09277Gt/EJ respectively. Based on these values, Case 1 gave an emission reduction of 88.31 GtCO<sub>2</sub> and 38.03 GtCO<sub>2</sub> for a natural gas/ renewable energy and a full natural gas system respectively. With the year 2019 fossil fuel consumption ratio, Cases 2 and 3 gave 6 and 7 years respectively for a positive carbon budget. With more than 0.55 and 0.65 fossil fuel share for Case 2 and 3 respectively, the positive carbon budget lies within the first 10 years. The result additionally shows that a positive carbon budget of up to 20 years requires a fossil fuel (natural gas) fraction of as low as 0.3 in the consumption mix. All in all, the results show that additional use of carbon capture technologies is required to achieve the net zero emission target as envisaged by global emission control bodies.

**Keywords:** Co2 Emission, Fossil, Fuel, Natural Gas, Renewable Energy, Carbon Budget.

## 1. Introduction

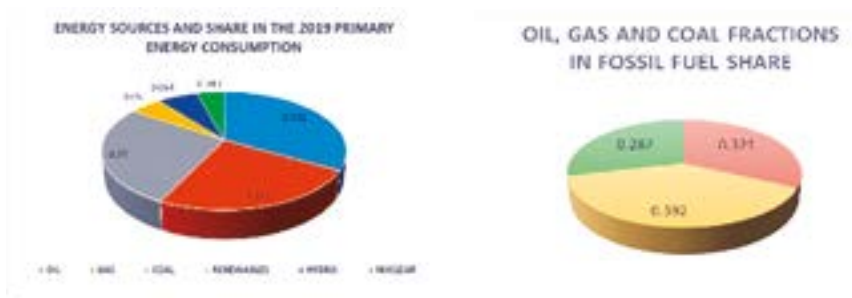
Due to the increasing global population, an option to meeting future energy demand requires diverse range of supplies, including oil, gas, coal, and renewables. However, meeting CO<sub>2</sub> emission reduction goals with such options will be very difficult (Looney, 2020). This is because any energy generation path to be adopted must be that by which carbon emissions will fall sharply as the world seeks to move to a lower carbon energy system consistent with the climate goals (Looney, 2020). Thus, among the fossil fuel energy sources, natural gas with the lowest fuel emission factor is expected to play an important role in supporting renewable resource integration (Mac Kinnon, Brouwer, & Samuelsen, 2018)Brouwer, & Samuelsen, 2018. The aim of this work is to investigate the extent at which the combination of both natural gas and renewable energy sources can help to mitigate CO<sub>2</sub> emissions pending the major goal of full renewable energy transition. According to Mac Kinnon et al. (2018), natural gas has a unique role to play with regards to meeting sustainable energy requirement. This is because it can serve as a means of carbon reductions, and an essential target for displacement with lower-carbon alternatives, depending upon the goal to be realized as well as the strategy and dynamics of operation (Mac Kinnon et al., 2018)2018. Also, the use of natural gas and renewables has been studied and can to a large extent help in reducing emissions in the power sector. For example, natural gas can reduce CO<sub>2</sub> emissions by up to 60% compared with coal when used for power generation (Ang, Röttgers, & Burli, 2018). According to the International Energy Agency (IEA), more than 40% of global CO<sub>2</sub> emissions in 2015 came from electricity and heat generation. In combination with renewables and the use of carbon capture and storage (CCS) technologies, natural gas will be essential in significantly lowering greenhouse gas (GHG) emissions. Also, due to the intermittent nature of renewable energy sources like solar and wind power, natural gas can serve as backup to maintain a steady supply of electricity (Lulek & Sadowska, 2020). Moreover, the petroleum industry flares an approximate of 140 billion cubic meters of natural gas annually, resulting in the discharge of about 400 million tons of CO<sub>2</sub> equivalent into the atmosphere every year (Bereznoy, 2021). This amount of flare gas can serve as a solution



to power generation challenges and can provide the approximate annual electricity consumption of 750 billion kWh required of the African continent (Chang, Zhuo, Meng, Qin, & Yao, 2016). Aside energy waste and drastic environmental impacts reduction, other benefits of gas utilisation in the expense of flaring are in reducing flaring light, noise, and odour, extending flare tip life and improving public relations of oil and gas industries with surrounding communities (Yazdani, Asadi, Dehaghani, & Kazempoor, 2020). Estimate shows that by the end of the year 2019, the total proved reserve of natural gas was 198.8 trillion cubic metres (7019.0 trillion cubic feet). With a billion cubic metres supplying about 6.729 exajoules, such reserve can supply about  $1.3377 \times 10^{15}$  exajoules. With an average annual energy consumption of 583.9 exajoules, these gas resources can suffice the global population for decades (by fuel type-Exajoules & Emissions, 2006). Thus, with the consensus agreement towards oil and coal as major causal of emission rise (Ogbonnaya et al., 2019), the combined natural gas and renewable energy system can serve as a good transition between the present state of mixed energy and full renewable energy system. However, mechanisms must be put in place to narrow the duration of such transition phase such that emission will be reduced and the carbon budget will not get exhausted. By these, the challenges of climate change will be highly mitigated.

**Table 1:** Energy sources and share in the year 2019 primary energy consumption (Ang et al., 2018).

Energy source	Consumption (Exajoules)	Share of primary energy (%)
Oil	193.0	33.1
Gas	141.5	24.2
Coal	157.9	27.0
Renewables*	29.0	5.0
Hydro	37.6	6.4
Nuclear	24.9	4.3
<b>Total</b>	<b>583.9</b>	



a. b. **Figure 1:** (a.) Energy sources and share in the 2019 primary energy consumption; (b.) Oil, gas and coal fraction in fossil fuel (Renewable power includes biofuels and excludes hydro) (Data used in diagram sourced from (Ang et al., 2018)).

Climate change is undoubtedly a major driving force behind environmentally-influenced societal change (Palut & Canziani, 2007). The dangerous impact of this catastrophic human-induced phenomenon depends on various factors which includes magnitude of its change as well as its potential for irreversibility (Solomon, Plattner, Knutti, & Friedlingstein, 2009). Anthropogenic emissions have led to continuous increase in the atmospheric concentrations of key greenhouse gases (Solomon et al., 2009), and abrupt efforts towards net zero emission is required to prevent further devastating climate impacts (Stern, 2006). Thus, the Sustainable Development Goal 13 is about taking urgent action to realizing this emission reduction goal. In line with this, Article 2.1(a) of the Paris Agreement is aimed at “holding the global average temperature increase well below 2°C above pre-industrial levels and pursuing efforts to limit the temperature increase to 1.5°C above pre-industrial levels” (Looney, 2020). To achieve these, there is a finite CO<sub>2</sub> emission (carbon budget) that should be allowed to enter the atmosphere to remain within the target temperature limits. This assumes that the amount of warming that will occur can be approximated by total CO<sub>2</sub> emissions. Excluding CO<sub>2</sub> released by permafrost thawing or methane released by wetlands, the remaining carbon budget is assessed and estimated to be 420 GtCO<sub>2</sub> for the 67th percentile of TCRE (transient climate response to cumulative emissions of carbon) starting from the 1st of January 2018 onward (Rogelj et al., 2018). Based on this figure, an annual fossil fuel emission of 42Gt (by fuel type-Exajoules & Emissions, 2006) as well as those from other unaccounted sources is as-

sumed to leave an approximate carbon budget of 320Gt at the end of year 2019. Moreover, according to Solomon et al. (2009), having a significant decline in global temperature is unclear and not assured even if carbon emissions ceases completely, and hence, the possibility of a short and long-term scale irreversible and adverse climate changes if carbon dioxide emission continues (Solomon et al., 2009). For an effective and long-lasting solution to these challenges (Edenhofer et al., 2014), setting emission mitigation targets (Dong, Hua, & Yu, 2018) is very important and requires frequent monitoring, evaluation, and energy policy adjustment for its successfully realization (Newell, Raimi, & Aldana, 2019). In addition to these, alternative energy for future supply is paramount, and factors such as energy sustainability, economy, efficiency and low environmental impact need to be considered to prevent energy poverty and global energy crises (Ogbonaya, Abeykoon, Damo, & Turan, 2019).

There are numerous works that has been published about means of carbon mitigation as it relates to energy consumption and impact on the carbon budget. Bismark et al. investigated and proposed the emission mitigation pathways for CO<sub>2</sub> emissions from fossil fuel combustion only, based on selected countries which includes the USA, China, Canada, and Nigeria. The author generated an algorithm which was used to propose emission mitigation pathways for the countries investigated to allow them to achieve zero CO<sub>2</sub> fossil fuel emission by the year 2030 (Mac Kinnon et al., 2018)2018. Michael et al. investigated the emissions from natural gas with a focus on power generation. He also proposed a pathway for natural gas generation and infrastructure to maximize environmental benefits and support renewable resources in the attainment of emission reduction (Ogbonaya et al., 2019). Dong et al. in his review laid down procedures and systematic analysis of how China can reach its peak carbon emissions earlier than expected (Dong et al., 2018). The study investigated the five main driving factors of carbon emission peak in China. The factors include transportation, energy-related issues, urbanization, economic development, and foreign direct investment and technology. It also gave a summary of various predictions relating to the subject. Another intensive effort on the present work is that of the Working Group III contribution to the IPCC Fifth Assessment Report (WGIII AR5). The work assessed the relevant options for mitigating climate change through limiting or preventing

greenhouse gas emissions, as well as activities that remove them from the atmosphere (Edenhofer et al., 2014). In addition, Hulme (2016) in his “1.5 °C and climate research after the Paris Agreement” stated the importance of a science–policy interaction and the deployment of limited time and resources in designing flexible mechanisms to pursue more pragmatic and decision-centred applications of climate research (Hulme, 2016). The Paris Agreement is a commitment made by national leaders towards ensuring emission reduction and means by which such will be achieved within given time frames in their respective countries. Besides national commitments, multinational companies including Shell, ExxonMobil, and British Petroleum (BP) also keyed into this agreement and efforts are on-going towards its accomplishment. According to the year 2019 Shell Annual reports, it states that “Shell fully supported the Paris Agreement’s goal to keep the rise in global average temperature this century to well below two degrees Celsius (2°C) above pre-industrial levels and to pursue efforts to limit the temperature increase even further to 1.5°C”. It also supported the vision of a transition towards a net-zero emissions energy system in pursuit of the goal (Lulek & Sadowska, 2020). As a result of these, Shell identified measures like implementation of energy-efficiency where reasonably practicable, developing new fuels for transport such as advanced biofuels and hydrogen, maintaining a focus on using natural gas and renewable electricity to generate power and working with nature-based solutions as possible solutions to tackling climate change challenges (Lulek & Sadowska, 2020). British Petroleum (BP) additionally identified improving energy efficiency, rapid growth in low or zero carbon energy sources, switching to low or zero carbon liquid and gaseous fuels, promoting natural climate solution and restoration as possible measures (Lulek & Sadowska, 2020). In order to bring a sustainable energy future within reach, IRENA 2018 report identified rapid decline in renewable energy costs, improving energy efficiency, widespread electrification, increasingly “smart” technologies, continual technological breakthroughs and well-informed policy making as necessary measures (Ang et al., 2018). According to the ExxonMobil technological report, industrial emissions can be reduced using technologies like low-energy separations, high-efficiency reactors and high-efficiency catalysts that help refiners make cleaner, high-quality transportation fuels more efficiently (Bereznoy, 2021).

Based on the above analysis, lots of opportunities lies in the use of natural gas, and the extent to which emission could be curtailed through its adoption is important to be known. This needs to be investigated, and a realistic mitigation path need to be put in place to meet any emission reduction goal set therefrom. This is necessary because according to the IRENA 2018 report, the carbon mitigation paths of current and planned policies are comparatively slow. According to the report, the paths are such that energy related budget associated with the set global temperature limit of 2°C and 1.5°C will be exhausted under 20 and 10 years respectively (Ang et al., 2018). Based on these, this paper investigated the role of natural gas and renewable energy transition in achieving the emission target, and hence, a long-term positive carbon budget pending net zero energy transition. The analysis was based on the use of fossil fuel emission factors to determine the emissions associated with various systems of diverse energy consumption share as it relates to the energy projection data published by recognized energy organizations. Due to data limitation, average values from available data were used in some aspects of the work where doing so is seen as realistic. Therefore, the result gives a very good approximate of what is expected of the work but may not be a completely accurate representation of it.

## 2. Methodology

Fossil fuels are common energy sources but associated with a high degree of emissions. For a natural gas and renewable energy system, the extent of emission cut which gives a positive carbon budget is examined and compared with a mixed system.

The syntax used for all cases is: "RESOURCES: Oil (O), Gas (G), Coal (C) or Renewables and others (R+) \_EMISSION (E), CARBON BUDGET (CB) or EMISSION REDUCTION(ER)\_FRACTION OF FOSSIL FUEL IN ENERGY MIX/YEAR".

For example, "O\_E\_2009" denotes "OIL\_EMISSION\_2009". It stands for CO<sub>2</sub> emitted from oil consumption in 2009. Also "R+\_E\_2030" denotes "RENEWABLE ENERGY AND OTHER ENERGY SOURCES ASIDE FOSSIL FUELS\_EMISSION\_2030". It stands for CO<sub>2</sub> emitted from consumption of non-fossil fuels in 2030. "GOC/G\_E\_0.843" denotes "GAS, OIL AND COAL SYSTEM/ GAS SYSTEM\_EMISSION\_0.843". It stands

for CO<sub>2</sub> emitted from a gas, oil and coal driven system followed by a wholly gas system, of which the fraction of fossil fuel in the total energy mix is 0.843 or 84.3%.

Three cases are considered:

Case 1 was used to determine the extent of emission reduction if natural gas and renewables had dominated the energy consumed between year 2009 and 2019. The emission reductions were determined for two subcases.

Subcase 1: A fossil fuel/renewable energy system such that fossil fuel is wholly natural gas.

Subcase 2: A full natural gas system.

Case 2 and 3 projects future emissions based on a 320 Gt carbon budget as at year 2019 ending.

Case 2: An oil, gas, coal and renewable energy system which uses the same consumption mix as that of the year 2019.

Case 3: A natural gas/ renewable energy system having its first 5 years (transition window) as that of the 2019 mix.

The fuel emission factors (FEF) used for oil, gas and coal are 0.06489, 0.05406 and 0.09277 Gt/EJ respectively. As shown in Figure 2, these values were determined using emission and consumption data from the year 2009 to 2018. The values translate to the amount of CO<sub>2</sub> emission from the consumption of an exajoule of the fuels. It implies that for every exajoule of oil, gas and coal consumed, 0.06489, 0.05406 and 0.09277 Gt of CO<sub>2</sub> is respectively emitted.

Mathematically,

$$FEF \left( \frac{Gt}{EJ} \right) = \frac{\sum_{i=1}^n \left( \frac{E_i (Gt)}{C_i (EJ)} \right)}{n} = \frac{\sum_{i=1}^n \left( \frac{E_i (Gt)}{C_i (TWh) * 0.0036} \right)}{n}$$

$$C_t = x_i C_T$$

$$C_T = \sum_{i=1}^n C_i = \sum_{i=1}^n x_i C_T$$

$$E_i = FEF_i * x_i C_T$$

$$E_T = \sum_{i=1}^n E_i = \sum_{i=1}^n (FEF_i * x_i C_T)$$

FEF: Fuel Emission Factor (Gt/EJ)

E: CO<sub>2</sub> emission (Gt)

E<sub>T</sub>: Total CO<sub>2</sub> emission (Gt)

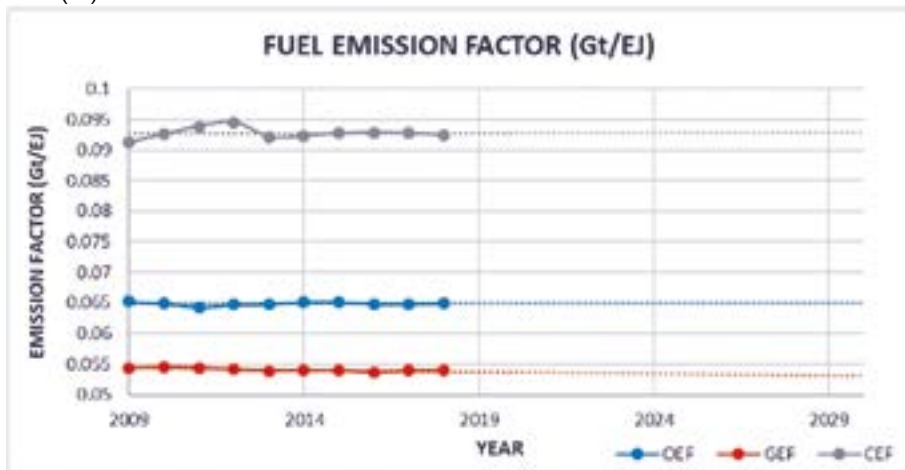
C: Fuel consumption (EJ or TWh)

C<sub>T</sub>: Total fuel consumption (EJ)

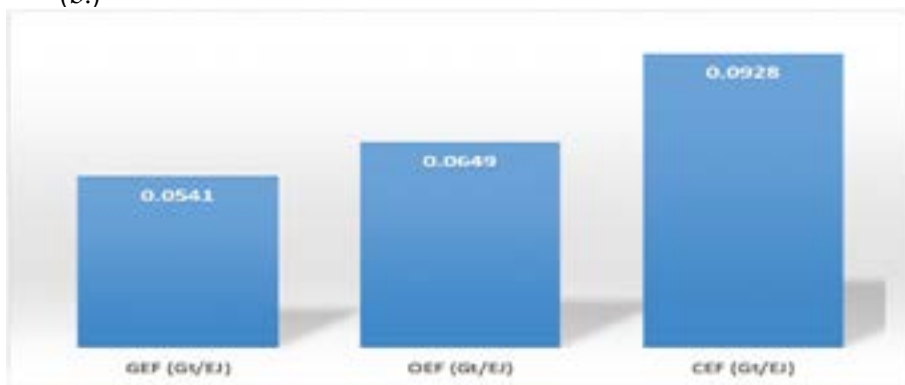
n: Number of years

x: Share of fuel in the consumption mix

(a.)

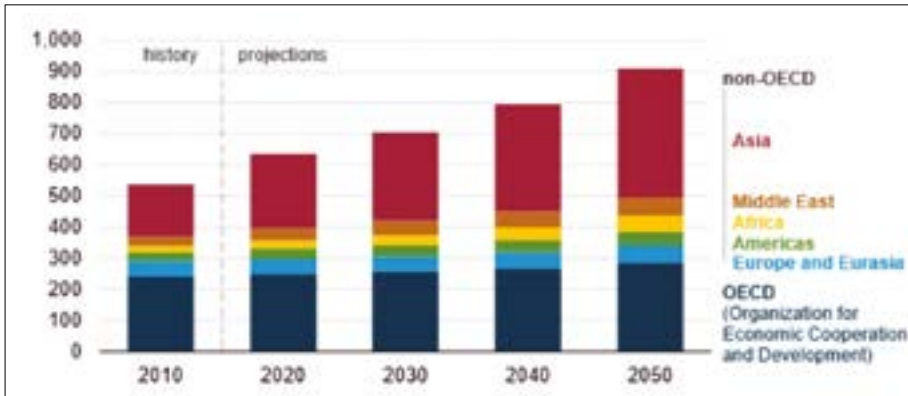


(b.)



**Figure 2:** (a.) Fuel emission factors (FEF) determination from energy consumption and emission data; (b.) Average fuel emission factors (FEF) for natural gas, oil and coal.

The energy consumption projection data used is as given in the International Energy Outlook Report (Osaki, 2019) by the U.S. Energy Information Administration. Accuracy in the results is a function of ratio of fossil fuel to other energy sources and the ratio of oil, gas, and coal in the fossil fuel mix. With the expectation of a continuous shift from fossil fuels to renewables, the fraction of fossil fuel in the 2019 consumption mix is taken as the maximum.



**Figure 3:** Global primary energy history and projection (Osaki, 2019).

The assumptions used in the analysis are:

- i. Fuel emission factors are constant throughout for each fuel type.
- ii. Carbon emission from renewable energy sources is equivalent to carbon captured using clean technologies; both are therefore not accounted for.
- iii. There remains a carbon budget of 320 GtCO<sub>2</sub> as at year 2019 ending based on a 1.5°C temperature limit.

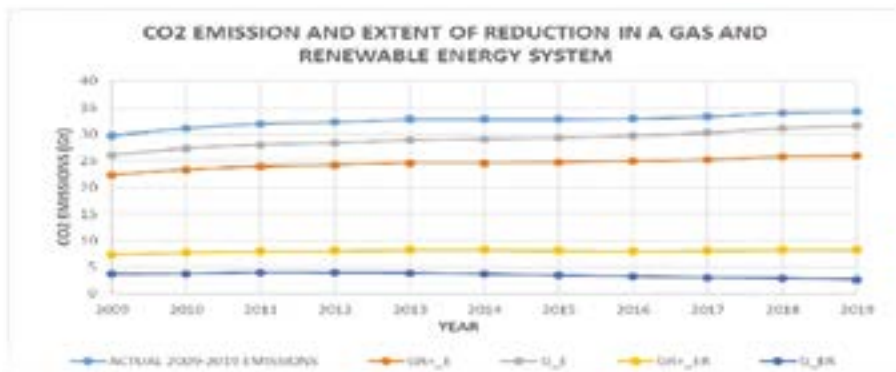
### 3. Results and Discussions

#### 3.1. Energy System Scenarios

Case 1 is a natural gas and renewable energy system for the year 2009 to 2019. It is used to determine the extent of emission reduction if natural gas and renewables had dominated the energy consumed be-



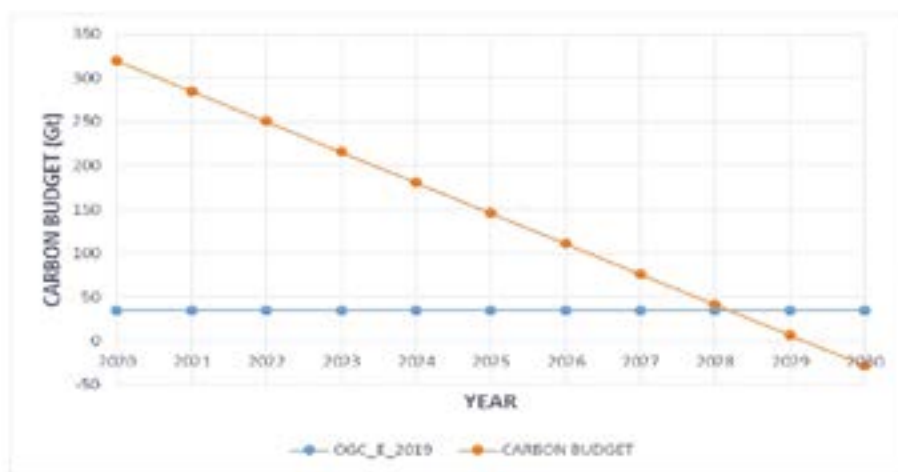
tween year 2009 and 2019. Two subcases were considered: Subcase 1 is a natural gas/renewable energy system while Subcase 2 is a full natural gas system. The control case is the actual emission as calculated for the year range. Figure 4 shows the results for the control and subcases as well as the emission reduction associated with each. While the actual emission gave 357.86 Gt, the full gas and gas/ renewable energy system gave 269.55 and 319.83 Gt respectively. This implies an emission reduction of 38.026 and 88.310 Gt for the full gas and gas/ renewable energy system respectively, as well as a respective annual emission reduction of about 3.8026 and 8.8310 Gt. On a percentage basis, these values accounts for about 9% and 21% respectively of the average annual CO<sub>2</sub> emissions and implies that a gas/renewable energy system could lead to a significant cut in carbon emissions. For fossil fuels, coal with the highest emission factor of 0.09277 Gt/EJ is expected to give the highest emission while natural gas with the lowest emission factor of 0.05406 Gt/EJ is expected to give the lowest. Renewable energy has the least and is the most favourable. However, with the full adoption of renewable energy requiring lot of measures, policies and therefore time to be put in place, a gradual process of partial transition to a gas/ renewable energy system will be a feasible option.



**Figure 4:** Carbon emission in a natural gas and renewable energy system.

Case 2 discusses a fossil fuel/ renewable energy system with the year 2019 consumption ratios used as a case study. According to Table 1, the fossil fuel share in the 2019 primary energy consumption is 84.3%. With the expectation of a shift from fossil fuels to renewables, this 2019

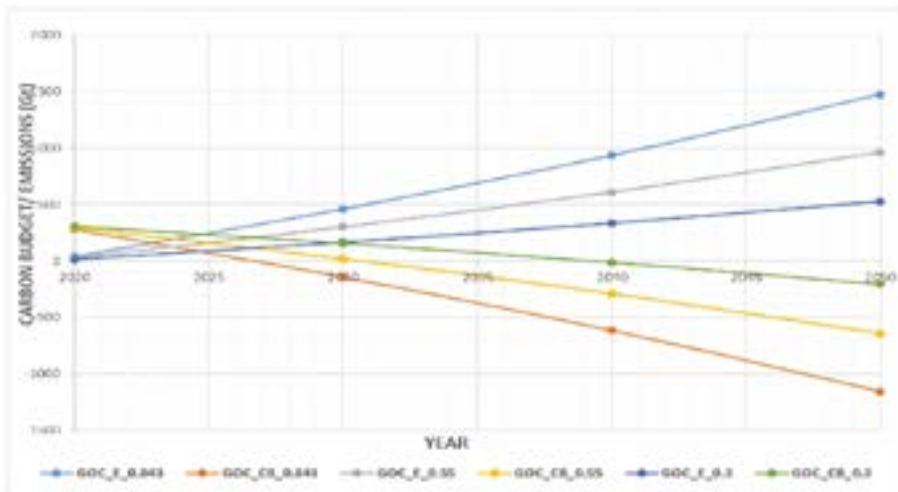
fossil fuel consumption fraction is taken as the maximum possible value. The control case uses the same data and emission pace as that of 2019 and Figure 5 shows that the carbon budget drops to zero in 8 years (year 2028) assuming the year 2019 energy consumption and emissions keeps reoccurring. A major goal of the Paris Agreement is increasing this exhaustion period as much as possible above the 8 years and keeping the carbon budget positive pending net zero emission transition. However, since energy consumption is expected to increase in the coming years, the control case might seem not to give the lowest emission on a business-as-usual scenario. This is because the increase in energy consumption will translate into more need for energy, and hence, increase in the CO<sub>2</sub> emissions. The carbon budget exhaustion period therefore goes below the 8 years earlier determined for the control case as will be seen subsequently. This will be so if the pace remains as that of the year 2019, except there is a shift to lower emitting sources or other approaches like deployment of carbon capture and storage (CCS) technology and other carbon mitigation means.



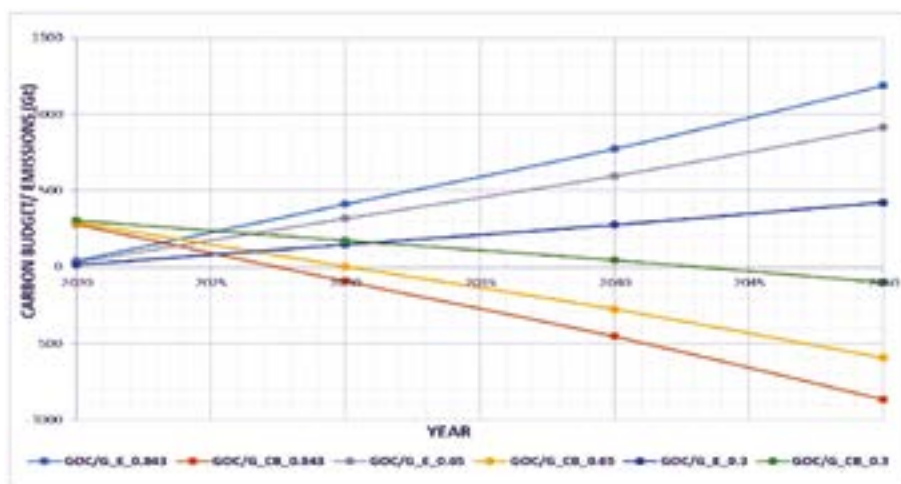
**Figure 5:** Carbon budget exhaustion for the year 2019 emission pace (control case).

Having investigated the control case scenario, we now look into the case of mixed energy systems which uses the projected energy consumption data from which projected emissions were calculated. The assumption of the maximum future fossil fuel percentage of 84.3% in the consumption mix being equal to that of 2019 is used to determine the highest

possible emissions which gives the earliest exhaustion period. With the projected increase in energy consumption, Figure 6 shows that the earliest carbon budget exhaustion is 6 years (year 2026). This is earlier than the 8 years obtained in Figure 5 (control case) because increase in energy consumption was not accounted for in the control case. In order to raise the exhaustion period, there must be a reduction in fossil fuel consumption which implies a shift to lower emitting sources like renewable energy and allowing natural gas consumption to dominate the fossil fuel share. Figure 6 gave the results for various fossil fuel consumption ratios, associated emissions and their corresponding carbon budget exhaustion periods. Different fossil fuel to renewable energy ratio were examined starting from 0.843 fossil fuel share which gave the earliest exhaustion period of about 6 years as mentioned up to a fossil fuel share of 0.1 which gave an exhaustion period of more than 30 years. In-between these two are other fossil fuel to renewable energy ratios with their emissions and impacts on the carbon budget. Figure 7 is an extract from Figure 6, and it shows that any fossil fuel fraction above 0.55 gives a CB exhaustion period of less than 10 years while a fraction of 0.3 gave 20 years. A shift from 0.843 to 0.55 fossil fuel share either with or without any transition window is apparently a tough task which requires extraordinary global efforts and cooperation as well as stringent policies.



**Figure 6:** Emission and carbon budget for a fully mixed system with different fossil fuel consumption ratios.

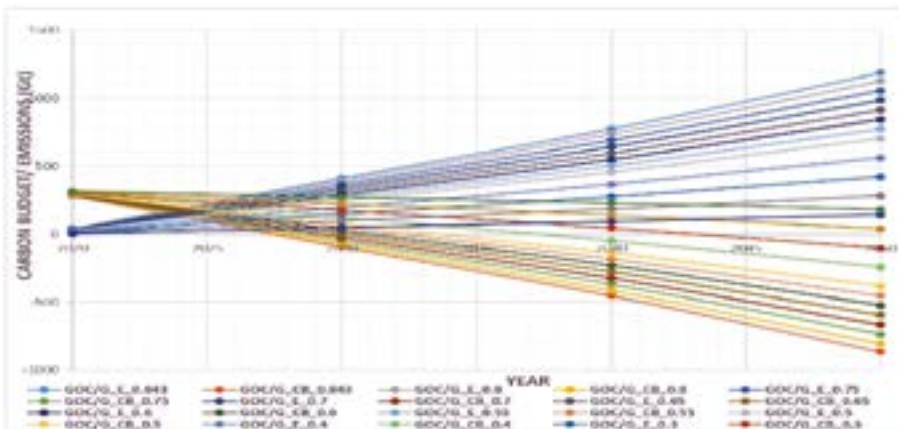


**Figure 7:** Emission and carbon budget for 0.843, 0.55 and 0.3 fossil fuel fractions.

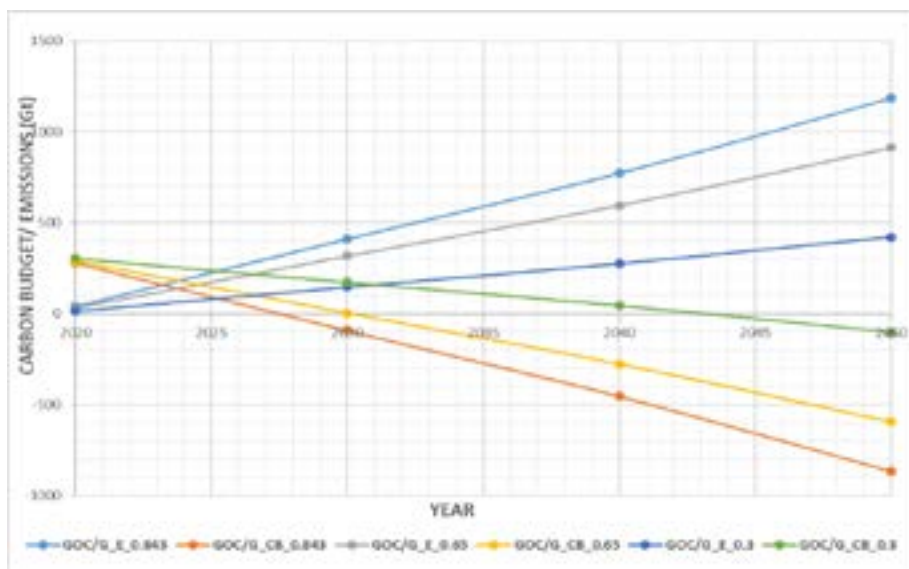
CASES	CB (Gt) by 2020 year ending	CB (Gt) by 2030 year ending	CB (Gt) by 2040 year ending	CB (Gt) by 2050 year ending
GOC_CB_0.843	280.05	-141.911	-615.146	-1155.06
GOC_CB_0.8	282.09	-118.35	-567.446	-1079.82
GOC_CB_0.75	284.46	-90.953	-511.98	-992.34
GOC_CB_0.7	286.83	-63.556	-456.515	-904.846
GOC_CB_0.65	289.2	-36.159	-401.05	-817.357
GOC_CB_0.6	291.57	-8.763	-345.584	-729.868
GOC_CB_0.55	293.94	18.635	-290.119	-642.379
GOC_CB_0.5	296.31	46.031	-234.654	-554.89
GOC_CB_0.4	301.05	100.825	-123.723	-379.912
GOC_CB_0.3	305.78	155.619	-12.792	-204.934
GOC_CB_0.2	310.52	210.413	98.139	-29.956
GOC_CB_0.1	315.26	265.206	209.069	145.022

**Table 2:** CASE 2 (An oil, gas, coal, and renewable energy system which uses the same consumption mix as that of the year 2019).

Case 3 is also a natural gas/ renewable energy system but differs from Case 2 in that it incorporates a 5-year fully mixed energy transition period after which a wholly natural gas system follows. The transition window uses the same energy consumption share as that of the 2019 as given in Table 1. The transition window makes this system very feasible and can be termed a more realistic natural gas/ renewable energy system due to its structure. Figure 8 shows the results of various fossil fuel (natural gas) consumption ratios, associated emissions, and their corresponding carbon budget exhaustion periods. With the incorporated transition period, different natural gas to renewable energy ratio were examined starting from 0.843 fossil fuel share which gave the earliest exhaustion period of about 7 years up to a fossil fuel share of 0.3 which gave an exhaustion period of more than 30 years. In-between these two are other energy ratios with their emissions and impacts on the carbon budget. Figure 9 is an extract of Figure 8 and shows that natural gas fractions above 0.65 leaves the CB exhausted within 10 years. Additionally, Figure 8 shows that only about 0.1 and 0.2 natural gas fraction in the energy consumption mix allows a positive carbon budget beyond 2050. The next is 0.3 natural gas share which hits zero by 2043. Though a propitious result, there is the need to improvise more practical approaches by which the exhaustion period could be raised to allow enough time for net zero emission transition.



**Figure 8:** Emission and carbon budget for a mixed and gas/renewable energy system.



**Figure 9:** Emission and carbon budget for 0.843, 0.65 and 0.3 fossil fuel fractions.

**Table 3:** CASE 3 (A natural gas/ renewable energy system having its first 5 years transition window as that of the 2019 mix).

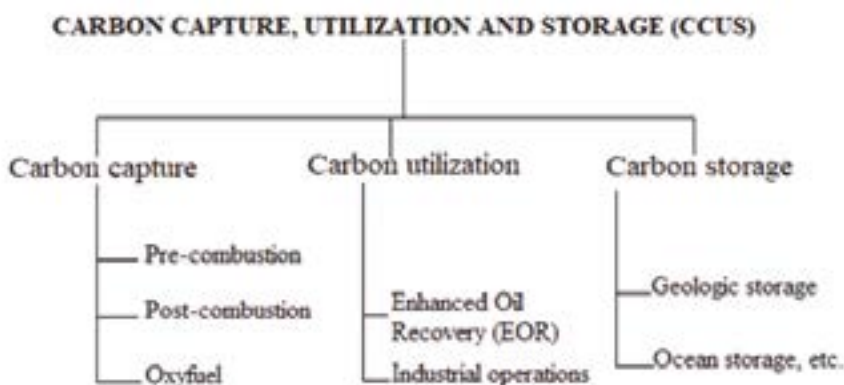
CASES	CB (Gt) by 2020 year ending	CB (Gt) by 2030 year ending	CB (Gt) by 2040 year ending	CB (Gt) by 2050 year ending
GOC/G_ CB_0.843	280.053	-91.947	-453.653	-866.327
GOC/G_E_0.8	282.090	-70.935	-414.191	-805.815
GOC/G_CB_0.75	284.460	-46.501	-368.304	-735.451
GOC/G_CB_0.7	286.829	-22.068	-322.417	-665.088
GOC/G_CB_0.65	289.198	2.366	-276.530	-594.725
GOC/G_CB_0.6	291.568	26.800	-230.643	-524.361
GOC/G_CB_0.55	293.937	51.232	-184.756	-453.998
GOC/G_CB_0.5	296.306	75.666	-138.869	-383.634
GOC/G_CB_0.4	301.045	124.533	-47.095	-242.907
GOC/G_CB_0.3	305.784	173.400	44.679	-102.181
GOC/G_CB_0.2	310.523	222.266	136.452	38.546
GOC/G_CB_0.1	315.261	271.133	228.226	179.273

The results show the huge impact of fossil fuel use on the carbon budget. It is apparent that for significant emission reduction to achieve the target set by global emission control bodies, more mechanisms need to be put in place. Thus, deployment of technologies like direct air capture, Clean Technologies (CT) etc. is necessary. In a gas and renewable energy system, the use of these technologies will further result into significant emission reduction and allow enough time before the carbon budget exhaustion. Some of these technologies are discussed below.

#### **a. Carbon Capture, Utilization and Storage (Ccus) Technology**

Carbon capture, utilization and storage (CCUS) consists of different technologies with which carbon dioxide (CO<sub>2</sub>) emissions from fossil fuel use at large point sources can be captured and transported to safe geological storage, rather than its emission into the atmosphere (Chalmers, Leach, Lucquiaud, & Gibbins, 2009) Lucquiaud, & Gibbins, 2009. Significant amount of emissions can be curtailed with this technology. There is also the prediction that the technology can lead to about 85% emission reduction from power plants. However, there will be some associated energy penalty which will significantly increase the cost of energy production (Pike, 2006). The technology has three interconnecting processes which are efficient carbon capturing, transportation to storage site and utilization or permanent storage and monitoring at selected sites. For CO<sub>2</sub> capture, the three possible mechanisms proposed are Pre-combustion, Post-combustion and Oxyfuel combustion (Pike, 2006). Some other Carbon-Capture techniques are classified as emerging technologies, one of which is the Chemical-Looping Combustion (Technology, 2016). After carbon capture follows either its utilization or storage. CO<sub>2</sub> can be stored in depleted oil and gas reservoirs, unmineable coal beds, saline aquifers and basalts (Leung, Caramanna, & Maroto-Valer, 2014). The captured CO<sub>2</sub> can also be utilized in enhanced oil recovery processes, food processing and chemical industries. The CO<sub>2</sub> being used in industries are those that comes from natural formations, and putting the captured gas to use would result in a net reduction of carbon emission (Tan, 2014). CO<sub>2</sub> utilization could be seen as a better option due to the controversies and risk attached to the effectiveness of its storage in

either geologic formations or aquifers. CCUS is a powerful and effective technology in carbon mitigation from large scale fossil fuel use and Shell's Quest is the world's first known commercial-scale CCUS project. The Shell's Quest design is such that annually, more than one million tons of CO<sub>2</sub> can be captured and stored permanently- an equivalence of the annual emission from 250,000 cars (Leung et al., 2014).

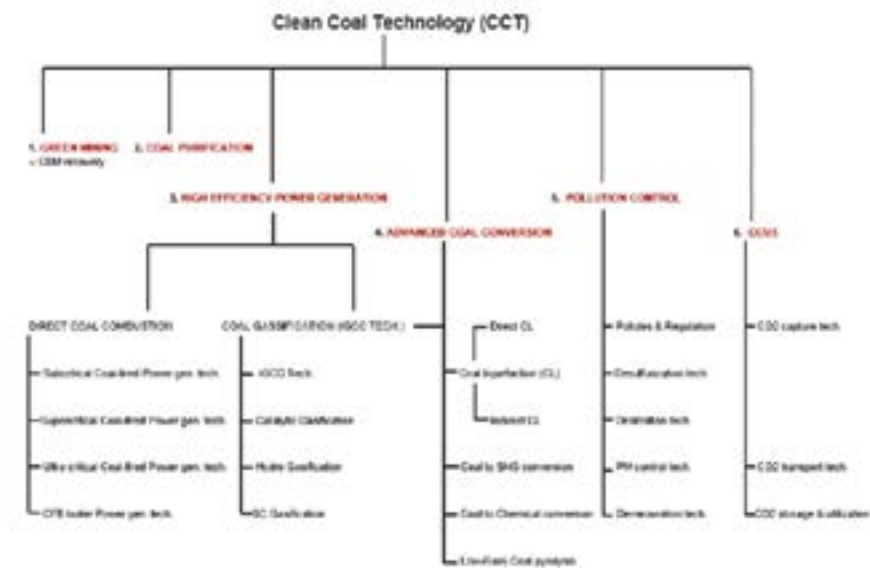


**Figure 10:** Carbon capture, utilization, and storage (CCUS).

### **b. Clean Coal Technology (Cct)**

Technologies that allow coal to be used in an environmentally satisfactory and economically viable way are regarded as clean coal technologies (CCTs) (by fuel type-Exajoules & Emissions, 2006). A basic idea behind the CCTs is the development of more thermally efficient systems which will bring about energy efficiency together with proper handling of the produced flue gasses. Other areas which are regarded as CCTs include green mining, coal purification, advanced coal conversion, and the carbon capture, utilization, and storage (CCUS) technologies. Like the carbon capture technology, the broadest classification of CCT is into three: Pre-combustion, Combustion and Post-combustion. Processes like coal washing, wet scrubbing, gasification, electrostatic precipitation fall under one of these broad classifications (Chang et al., 2016). The various areas of CCT are shown in Figure 11.





**Figure 11:** Clean coal technologies (CCTs) (CBM: Coal bed methane, CFB: Circulating fluidized bed, IGCC: Integrated gasification combined cycle, CL: Coal liquefaction, SNG: Syngas, CCUS: Carbon capture, utilization, and storage). Information in the Figure 11 were extracted from Chang et al. (2016).

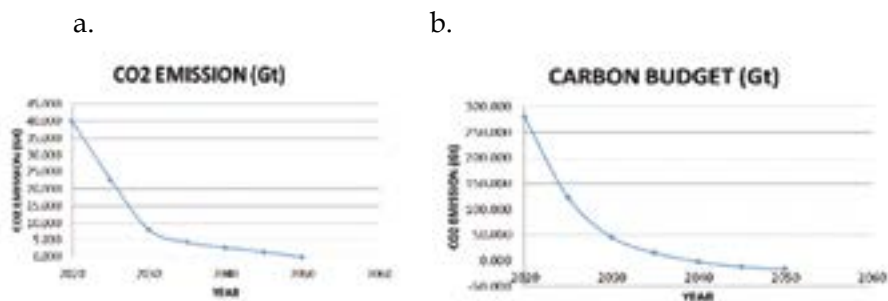
### 3.2. Emission Reduction Paths

Having investigated the impact of the various energy sources on the carbon budget, a gas and renewable energy system is seen to have a significant but perhaps, not enough impact to reaching the emission and temperature reduction targets, except with other measures already explained. The Paris Agreement is aimed at drastic global temperature reduction, but there is still limited knowledge of how to achieve the set goals (Van Vuuren et al., 2018). For effective emission reduction goal realization, two things are necessary: developing realistic pathways and setting a path of how to achieve them. For drastic greenhouse gas (GHG) emissions reduction, different mitigation scenarios have been developed using integrated assessment models (IAMs) (Edenhofer, 2015; Tavoni et al., 2015; Van Vuuren et al., 2007). Previous works have shown that achieving the ambitious targets of the Paris Agreement will require emission reductions combined with net carbon dioxide removal (CDR) from the atmosphere (Edenhofer, 2015; Tavoni et al., 2015; Van Vuuren et al., 2007). These will include zero- and low-carbon

energy transition, energy efficiency increment, carbon capture and storage (CCS) adoption, non-CO<sub>2</sub> GHG emissions reduction, land-use change related emission elimination and stimulating afforestation. Approaches such as carbon capture and storage (CCS) and afforestation are termed carbon dioxide removal (CDR) method and associated with several challenges such as reliance on underground CO<sub>2</sub> storage and competition for land with food production and biodiversity protection (Van Vuuren et al., 2018).

Here, we propose CO<sub>2</sub> reduction targets which will allow an extended positive carbon budget period if achieved based on a gas and renewable energy system. The extent of carbon emission is majorly a function of two things: the fossil fuel consumption ratio (coal: oil: gas) and the ratio of fossil to renewable energy (fossil fuel: renewable energy). A low fossil fuel to renewable energy ratio is expected to give lower emission. For path 1 and 2, fossil fuel where used refers to natural gas from the year 2025 onwards, while that of path 3 refers to the year 2030 onwards.

Path 1 scenario is represented by Figure 12 and the associated values are contained in Table 4. In order to make the path as realistic and feasible as possible, it is made to begin with a mixed system, similar to the year 2019 fossil fuel consumption ratio of 0.843, with 0.321, 0.392 and 0.287 for coal, oil and gas respectively. With the same coal, oil and gas ratio, the fossil fuel consumption shares for the period between the year 2020 and 2025 lies in-between 0.843 and 0.6 which are the respective ratios for the two extreme periods respectively. The fossil fuel (natural gas) consumption shares for the period between year 2025 and 2030 lies in-between 0.6 and 0.2, 2030 and 2035 in-between 0.2 and 0.3, 2035 and 2040 in-between 0.3 and 0.06, 2040 and 2045 in-between 0.06 and 0.03, and finally, 2045 and 2050 in-between 0.03 and 0. The path begins with a fully mixed energy system up to year 2025.



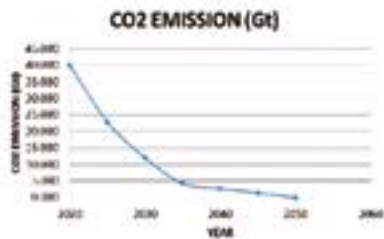
**Figure 12:** Emission reduction path 1: (a.) Emissions (b.) Carbon budget.

**Table 4:** Emission reduction path 1.

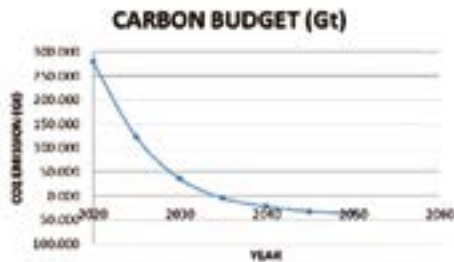
Year	Fossil Ratio	Ct (EJ)	Fossil C (EJ)	Coal C (EJ)	Oil C (EJ)	Gas C (EJ)	C_E (Gt)	O_E (Gt)	G_E (Gt)	Et (Gt)	Syrs Et (Gt)	CB (Gt)
2020	0.843	669.93	564.75	181.28	221.38	162.08	16.82	14.37	8.76	39.95	39.95	280.05
2025	0.6	704.21	422.53	0.00	0.00	422.53	0.00	0.00	22.84	22.84	156.98	123.08
2030	0.2	738.50	147.70	0.00	0.00	147.70	0.00	0.00	7.99	7.99	77.07	46.00
2035	0.1	788.61	78.86	0.00	0.00	78.86	0.00	0.00	4.26	4.26	30.62	15.38
2040	0.06	838.73	50.32	0.00	0.00	50.32	0.00	0.00	2.72	2.72	17.46	-2.08
2045	0.03	899.39	26.98	0.00	0.00	26.98	0.00	0.00	1.46	1.46	10.45	-12.53
2050	0	960.05	0.00	0.00	0.00	0.00	0.00	0.00	0.00	0.00	3.65	-16.18

Path 2 and 3 scenarios are represented by Figure 13 and 14 respectively. The paths use non conservative values and therefore have very early carbon budget exhaustion periods. The associated values are contained in Table 5 and 6 respectively. While Path 2 is similar to 1, Path 3 has the earliest carbon budget exhaustion. It begins with a mixed system, similar to the year 2019 fossil fuel consumption ratio of 0.843, with 0.321, 0.392 and 0.287 for coal, oil and gas respectively. That of year 2025 with a 0.6 fossil fuel share has a coal, oil and gas ratio of 0.333 for each. The period between year 2020 and 2025 takes an average of the values of year 2020 and 2025 while the year between 2025 and 2030 takes an average of the fossil fuel share of 0.6 in year 2025 and 0.3 in year 2030. The fossil fuel (natural gas) consumption shares for the period between year 2030 and 2035 lies in-between 0.3 and 0.2, 2035 and 2040 in-between 0.2 and 0.15, 2040 and 2045 in-between 0.15 and 0.1, and finally, 2045 and 2050 in-between 0.1 and 0.

a.



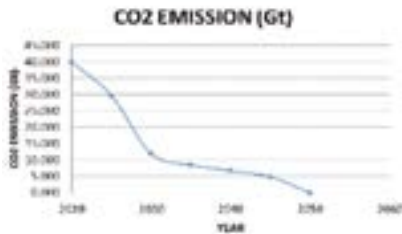
b.

**Figure 13:** Path 2 (a.) Emissions; (b.) Carbon budget.

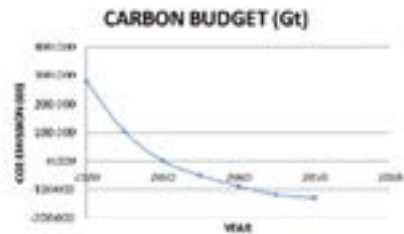
**Table 5:** Emission reduction path 2.

Year	Fossil Ratio	Ct (EJ)	Fossil C (EJ)	Coal C (EJ)	Oil C (EJ)	Gas C (EJ)	C_E (Gt)	O_E (Gt)	G_E (Gt)	Et (Gt)	5yrs Et (Gt)	CB (Gt)
2020	0.843	669.93	564.75	181.28	221.38	162.08	16.82	14.37	8.76	39.95	39.95	280.05
2025	0.6	704.21	422.53	0.00	0.00	422.53	0.00	0.00	22.84	22.84	156.98	123.08
2030	0.3	738.50	221.55	0.00	0.00	221.55	0.00	0.00	11.98	11.98	87.06	36.02
2035	0.1	788.61	78.86	0.00	0.00	78.86	0.00	0.00	4.26	4.26	40.60	-4.58
2040	0.06	838.73	50.32	0.00	0.00	50.32	0.00	0.00	2.72	2.72	17.46	-22.05
2045	0.03	899.39	26.98	0.00	0.00	26.98	0.00	0.00	1.46	1.46	10.45	-32.49
2050	0	960.05	0.00	0.00	0.00	0.00	0.00	0.00	0.00	0.00	3.65	-36.14

a.



b.

**Figure 14:** Path 3 (a.) Emissions; (b.) Carbon budget.**Table 6:** Emission reduction path 3.

Year	Fossil Ratio	Ct (EJ)	Fossil C (EJ)	Coal C (EJ)	Oil C (EJ)	Gas C (EJ)	C_E (Gt)	O_E (Gt)	G_E (Gt)	Et (Gt)	5yrs Et (Gt)	CB (Gt)
2020	0.843	669.93	564.75	181.28	221.38	162.08	16.82	14.37	8.76	39.95	39.95	280.05
2025	0.6	704.21	422.53	140.70	140.70	140.70	13.05	9.131	7.61	29.79	174.35	105.71
2030	0.3	738.50	221.55	0.00	0.00	221.55	0.00	0.00	11.98	11.98	104.42	1.29
2035	0.2	788.61	157.72	0.00	0.00	157.72	0.00	0.00	4.26	8.53	51.26	-49.98
2040	0.15	838.73	125.81	0.00	0.00	125.81	0.00	0.00	2.72	6.80	38.32	-88.30
2045	0.1	899.39	89.94	0.00	0.00	89.94	0.00	0.00	1.46	4.86	29.16	-117.5
2050	0	960.05	0.00	0.00	0.00	0.00	0.00	0.00	0.00	0.00	12.16	-129.6

#### 4. Conclusions

Using different energy consumption scenarios, we have investigated the extent of emission reduction associated with a combined natural gas and renewable energy system. Using the year 2009 to 2019 data, the fuel emission factors (FEF) for oil, natural gas and coal were calculated as 0.06489 Gt/EJ, 0.05406 Gt/EJ and 0.09277 Gt/EJ respectively. These values give an insight into the huge CO<sub>2</sub> emission associated with coal and oil, with the coal emission factor almost doubling that of natural gas. From the least to the most conservative, and with as low as 0.65 fossil fuel fraction in the consumption mix, all the cases considered showed a positive carbon budget only within the first 10 years. Case 2 and 3 additionally shows that a positive carbon budget of up to 20 years requires a fossil fuel (natural gas) fraction of as low as 0.3 in the consumption mix. This implies that a full natural gas/renewable energy system, with its significant emission reduction has limited impact on keeping the carbon budget positive for an extended period. This also shows that maintaining a long term positive carbon budget goes beyond the use of low emitting energy sources. Deploying mechanisms like carbon capture and storage (CCS) technologies to extract already emitted CO<sub>2</sub> will go a long way in complementing such efforts. The proposed natural gas/renewable energy based emission reduction pathways will go a long way in extending the positive carbon budget period if adopted. All in all, meeting the various emission goals requires an abrupt change in the global energy consumption pattern, a speedy transition to less emitting energy sources coupled with the deployment of CCUS technologies. Other approaches include developing new fuels for transport such as advanced biofuels and hydrogen, improving energy efficiency, rapid decline in renewable energy costs, increasing smart technologies, continual technological breakthroughs and well-informed policy making. These should take early effect if significant carbon emission cut and a long term positive carbon budget is to be achieved.

#### Acknowledgement

The author appreciates Türkiye Burslari (YTB), Turkey, for the scholarship opportunity which paved way for this research work.

## REFERENCES

- Ang, G., Röttgers, D., & Burli, P. (2018). *Global Energy Transformation: A Roadmap to 2050*. Abu Dhabi: IRENA. Retrieved from: <http://www.irena.org/publications/2018/Apr>
- Bereznoy, A. (2021). Global Oil & Gas Corporations in the Race for Technological Superiority. *Mirovaia ekonomika i mezhdunarodnye otnosheniia*, 65(5), 59-67.
- by fuel type-Exajoules, C., & Emissions, C. D. (2006). bp Statistical Review of World Energy June 2020.
- Chalmers, H., Leach, M., Lucquiaud, M., & Gibbins, J. (2009). Valuing flexible operation of power plants with CO<sub>2</sub> capture. *Energy Procedia*, 1(1), 4289-4296.
- Chang, S., Zhuo, J., Meng, S., Qin, S., & Yao, Q. (2016). Clean coal technologies in China: current status and future perspectives. *Engineering*, 2(4), 447-459.
- Dong, F., Hua, Y., & Yu, B. (2018). Peak carbon emissions in China: Status, key factors and countermeasures A literature review. *Sustainability*, 10(8), 2895.
- Edenhofer, O. (2015). *Climate change 2014: mitigation of climate change*. Cambridge University Press.
- Edenhofer, O., Pichs-Madruga, R., Sokona, Y., Agrawala, S., Bashmakov, I. A., Blanco, G., Bustamante, M. (2014). Summary for policymakers.
- Hulme, M. (2016). 1.5 C and climate research after the Paris Agreement. *Nature Climate Change*, 6(3), 222-224.
- Leung, D. Y., Caramanna, G., & Maroto-Valer, M. M. (2014). An overview of current status of carbon dioxide capture and storage technologies. *Renewable and Sustainable Energy Reviews*, 39, 426-443.
- Looney, B. (2020). Statistical Review of World Energy, 2020. *Bp*, 69, 66.
- Lulek, A., & Sadowska, B. (2020). Corporate social responsibility (CSR) in the annual reporting of oil companies worldwide modern business management. *Zeszyty Naukowe Akademii Morskiej w Szczecinie*.
- Mac Kinnon, M. A., Brouwer, J., & Samuelsen, S. (2018). The role of natural gas and its infrastructure in mitigating greenhouse gas emissions, im-

proving regional air quality, and renewable resource integration. *Progress In Energy And Combustion Science*, 64, 62-92.

Newell, R., Raimi, D., & Aldana, G. (2019). Global energy outlook 2019: the next generation of energy. *Resources for The Future*, 8-19.

Ogbonnaya, C., Abeykoon, C., Damo, U., & Turan, A. (2019). The current and emerging renewable energy technologies for power generation in Nigeria: A review. *Thermal Science and Engineering Progress*, 13, 100390.

Osaki, K. (2019). US Energy Information Administration (EIA): 2019 Edition US Annual Energy Outlook report (AEO2019). *Haikan Gijutsu*, 61(8), 32-43.

Palut, M. P. J., & Canziani, O. F. (2007). Contribution of working group II to the fourth assessment report of the intergovernmental panel on climate change.

Pike, R. (2006). The chemistry of carbon capture and storage. *JPT, J. Pet. Technol.*, 58, 36-38.

Rogelj, J., Shindell, D., Jiang, K., Fifita, S., Forster, P., Ginzburg, V., Kriegler, E. (2018). Mitigation pathways compatible with 1.5 C in the context of sustainable development. In Global warming of 1.5° C. 93-174. Intergovernmental Panel on Climate Change.

Solomon, S., Plattner, G.-K., Knutti, R., & Friedlingstein, P. (2009). Irreversible climate change due to carbon dioxide emissions. *Proceedings of the National Academy of Sciences*, 106(6), 1704-1709.

Stern, N. (2006). Stern Review: The economics of climate change.

Tan, Z. (2014). Carbon capture and storage. In *Air Pollution and Greenhouse Gases*. Springer, 349-393.

Tavoni, M., Kriegler, E., Riahi, K., Van Vuuren, D. P., Aboumahboub, T., Bowen, A., Jewell, J. (2015). Post-2020 climate agreements in the major economies assessed in the light of global models. *Nature Climate Change*, 5(2), 119-126.

Technology, A. E. C. (2016). Chemical-Looping Combustion.

Van Vuuren, D. P., Den Elzen, M. G., Lucas, P. L., Eickhout, B., Strengers, B. J., Van Ruijven, B., Van Houdt, R. (2007). Stabilizing greenhouse gas con-

centrations at low levels: an assessment of reduction strategies and costs. *Climatic Change*, 81(2), 119-159.

Van Vuuren, D. P., Stehfest, E., Gernaat, D. E., Van Den Berg, M., Bijl, D. L., De Boer, H. S., Harmsen, M. (2018). Alternative pathways to the 1.5 C target reduce the need for negative emission technologies. *Nature Climate Change*, 8(5), 391-397.

Yazdani, E., Asadi, J., Dehaghani, Y. H., & Kazempoor, P. (2020). Flare gas recovery by liquid ring compressors-system design and simulation. *Journal of Natural Gas Science and Engineering*, 84, 103627.





# ENERGY AND EXERGY ANALYSIS OF A TRAPEZOIDAL CONCENTRATED PHOTOVOLTAIC-THERMOELECTRIC SYSTEM

*Aminu Yusuf<sup>1</sup>*

---

## Abstract

Concentrated photovoltaic-thermoelectric hybrid system has high potential to be considered as a clean energy source, because electrical energy is generated by both photovoltaic and thermoelectric module. The hybrid system is a thermodynamic system which has both reversible and irreversible losses. Energy and exergy analysis of the system can lead to identifying the sources of the losses and suggest the ways of improving the system. In this study, a new configuration of the hybrid system is introduced, and its performance is analysed based on first and second laws of thermodynamics. The analysis revealed that losses increase with increase in the optical concentration ratio. Further analysis showed that

---

<sup>1</sup> PhD Student, İstanbul University-Cerrahpasa, Faculty of Engineering, Department of Electrical-Electronics Engineering, ORCID: 0000-0003-4169-6529

losses will greatly be reduced by making the efficiency temperature coefficient of PV as small as possible. It is hoped that the PV manufacturers will give more attention to reducing the efficiency temperature coefficient of PV, as doing so, will lead to improvement in the performance of the PV as well as that of the hybrid system.

**Keywords:** Concentrated Photovoltaic, Thermoelectric, Energy, Exergy, Irreversibilities, Performance Evaluation.

## 1. Introduction

Many countries are increasingly embracing renewable energy sources, this is in-line with the need to cut the CO<sub>2</sub> emissions. One of the most promising technologies through which a clean electrical energy is produced is a photovoltaic (PV) system; it utilises energy from the sun and convert it into electrical energy. Substantial amount of energy is captured from the sun by coupling concentrators to the PV cells. By doing so, electrical output of the PV cells increases as well as high thermal energy is produced. The thermal energy if not utilised or dissipated quickly will raise the temperature of the PV cells. Accordingly, for every rise in the temperature above the standard temperature test conditions, the energy conversion efficiency as well as output power will reduce. Thermal cooling systems such as air-cooled (Agrawal, S. & Tiwari, G. N., 2012), water-cooled (Gomaa, M. R., R. J. Mustafa & H. Rezk., 2019), phase change materials (A. S. Abdelrazik, R. Saidur & F. A. Al-Sulaiman, 2020), nanofluid-cooled (S. Soltani, A. Kasaeian, H. Sarrafha & D. Wen., 2017) have been employed to lower the temperature of the PV system. Alternatively, the excess thermal energy can be harvested by a thermoelectric generator (TEG) when thermally coupled to the PV. Therefore, additional electrical energy will be generated by the TEG (A. Yusuf, N. Bayhan, H. Tiryaki, B. Hamawandi, M. S. Toprak & S. Ballikaya, 2021). The combined system is concentrated photovoltaic-thermoelectric hybrid system (CPV-TE).

A CPV-TE system is a thermodynamic system in which its performance can be evaluated using both first and second laws of thermodynamics. Energy analysis is conducted using law of conservation of energy, and it is a measure of how energy is utilised in a thermodynamic process. While exergy analysis is conducted using the conservation of mass and energy as well as the second law of thermodynamics for the analysis, design, improvement of energy through minimising the losses in the system (A. Duran Sahin, I. Dincer & M. A. Rosen, 2007). Thermodynamic systems have both internal and external irreversibilities which are considered as losses; energy analysis does not account for those internal irreversibilities of a system. While exergy analysis considers both the internal and external irreversibilities, it measures the quality of energy

which is either consumed or destroyed, it identifies points, magnitude and sources of inefficiencies in a thermodynamic system (F. Sarhaddi, S. Farahat, H. Ajam & A. Behzadmehr, 2010).

Energy and exergy analysis of CPV-TE systems have been carried out by many researchers. Li et al. (D. Li, Y. Xuan, Q. Li & H. Hong, 2017), used first and second laws of thermodynamics to determine the energy and exergy output of a CPV-TE system. The analysis showed that a high concentration ratio in combination with a suitable PV cell will improve the system's output efficiency. Singh et al. (S. Singh, O. I. Ibeagwu & R. Lamba, 2018), performed energy and exergy analysis of a CPV-TE system over a wide range of solar radiation. Their results showed that the output power of the system increased by 86% and the exergy efficiency is 8% higher than the energy efficiency when the concentration ratio increases from 1 to 3 (A. Riahi, A. Ben Haj Ali, A. Fadhel, A. Guizani & M. Balghouthi, 2020). Experimentally determined the performances of CPV/T and CPV/T-TE systems. The electrical efficiency of the CPV/T-TE system for a sunny day characterised by an ambient temperature of 33 °C and a solar radiation of 935 W/m<sup>2</sup> increased by 7.46% compared to the CPVT system (S. Shittu, G. Li, X. Zhao, J. Zhou, X. Ma & Y. G. Akhlaghi, 2020). Experimentally studied energy and exergy efficiencies of PV-TE system with micro channel heat pipe. The results showed that the system generated hot water and higher output power compared to standalone PV system. Moreover, the results indicated that thermal insulation at the back of the micro channel heat pipe raises the temperature of the PV, this in turn lowers the overall output performance of the system (E. Yin, Q. Li & Y. Xuan, 2018). Have shown that the efficiency of CPV-TE system increase with increase in the reference efficiency of the PV operating in the system.

In this study, a new trapezoidal copper plate is introduced into CPV-TE system. The copper plate facilitates heat transfer and ensures uniform temperature distribution on the hot side of the TEG. To minimize heat losses, insulation is provided on the sides of the copper plate. Comprehensive energy and exergy analysis are presented, and influence of efficiency temperature coefficient on the efficiencies are determined.

## 2. Proposed Model

The proposed model as shown in Fig. 1 consists of a concentrator, PV cell, TE module, insulation and air microchannel heat sink. In CPV-TE systems, PV is the major source of electrical power and this power strongly depends on the surface temperature of the PV ( $T_{pv}$ ); the performance of the PV increases as the temperature of the PV approaches temperature of the reference test conditions which is usually 25 °C. On the contrary, the performance reduces as the temperature of the PV increases above the temperature of the reference test conditions.

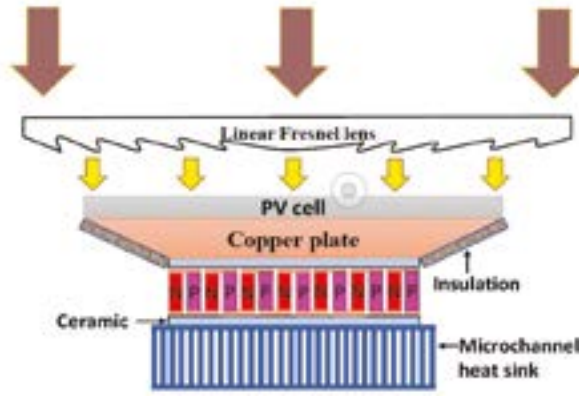


Fig. 1. Simplified concentrated photovoltaic-thermoelectric system.

Energy and exergy efficiencies of the proposed model can be derived using the first and second laws of thermodynamics. The energy balance on the top surface of the PV is given as:

$$CG A_{pv} \tau_g \alpha_{pv} = Q_{conv} + Q_{rad} + P_{pv} + Q_b \quad (1)$$

where the term on the left side is the energy into the CPV-TE system, the first and second terms on the right are the convective and radiative losses, the third and fourth terms are the power generated by the PV and energy absorbed by the TE module via trapezoidal copper plate.

Electrical power generated by the PV given in terms of its energy conversion efficiency is:

$$P_{pv} = CG A_{pv} \tau_g \eta_e (1 - \beta_{pv} (T_{pv} - T_r)) \quad (2)$$

where  $C$ ,  $G$ ,  $A_{pv}$  are the optical concentration ratio, the solar radiation, and area of the PV cell,  $\tau_g$  is the transmissivity of glass,  $\varepsilon$  is the emissivity of the PV cell,  $\alpha_{pv}$  is the absorptivity of PV cell,  $\sigma$  is the Stefan Boltzmann constant,  $T_{pv}$  is the temperatures of the PV cell,  $T_r$  is temperature at standard test conditions,  $\eta_r$ ,  $\beta_{pv}$  are the reference efficiency of PV and the efficiency temperature coefficient of PV.

Now the heat energy on the hot side of the TEG can be obtained by knowing the thermal resistance ( $R_{th1}$ ) between the surface of PV and hot side of the thermoelements as:

$$Q_h = \frac{T_p - T_h}{R_{th1}} \quad (3)$$

While the heat rejected on the cold side of the TEG can be determined if the energy efficiency of TEG is known at a particular temperature difference:

$$Q_c = Q_h (1 - \eta_{TE}) \quad (4)$$

The maximum energy conversion efficiency of a TE module given as a function of figure of merit and temperatures of the hot and cold sides is (K. Gaurav & S. K. Pandey, 2017):

$$\eta_{TE} = \eta_c \frac{T_h (\sqrt{1 + ZT_{av}} - 1)}{T_h \times \sqrt{1 + ZT_{av}} + T_c} \quad (5)$$

where  $\eta_c$  is the Carnot efficiency, temperatures of hot ( $T_h$ ) and cold ( $T_c$ ) sides of thermoelements,  $ZT_{av}$  is the dimensionless figure of merit of thermocouples given as (A. Yusuf & S. Ballikaya, 2020):

$$ZT_{av} = \frac{T_{av} (S_p - S_n)^2}{(\sqrt{\rho_p k_p} + \sqrt{\rho_n k_n})^2} \quad (6)$$

where  $T_{av}$  is the average temperature of hot and cold sides,  $S_{p/n}$  is the Seebeck coefficient,  $\rho_{p/n}$  is the electrical resistivity,  $k_{p/n}$  is the thermal conductivity.

For an air-cooled microchannel heat sink, the rejected heat on the cold side of the TEG can also be given in terms of thermal resistance ( $R_{th2}$ ) between the cold side of thermoelements and cooling air:

$$Q_c = \frac{T_f - T_a}{R_{s,t}} = 2n_{ch} v_{air} A_{ch} \rho_{air} C_p R_{s,t} (T_f - T_a) \quad (7)$$

where  $T_f$  is temperature of the air at the exit of the microchannel heat sink,  $T_a$  is the atmospheric temperature,  $n_{ch}$  is the number of channels,  $v_{air}$  is the mean air speed in the channel,  $A_{ch} = h_f w_{ch}$  is the cross-sectional area of the flow,  $\rho_{air}$  is the density of air,  $C_p$  is the heat capacity of air,  $\dot{V}$  is the volume flow rate of air,  $w_{ch}$  is the width of a channel,  $h_f$  is the height of channel/fin. Table 1 presents the parameters used in this study.

**Table 1.** Parameters of the CPV-TE and cooling system.

Parameter	Symbol	Value
Absorptivity of PV	$\alpha_{pv}$	0.9
Area of monocrystalline silicon PV cell	$A_{pv}$	$2.37 \times 10^{-2} \text{ m}^2$
Area of TE module	$A_{TE}$	$1.6 \times 10^{-3} \text{ m}^2$
Area of thermoelement	$A_{n/p}$	$2.36 \times 10^{-6} \text{ m}^2$
Atmospheric temperature	$T_a$	293 K
Density of air	$\rho_{air}$	$1.225 \text{ Kg m}^{-3}$
Efficiency temperature coefficient of PV cell	$\beta_{pv}$	$1 \times 10^{-3} - 5 \times 10^{-3} \text{ K}^{-1}$
Heat capacity of air	$C_p$	$1007 \text{ J Kg}^{-1} \text{ K}^{-1}$
Height of fin	$h_f$	$25 \times 10^{-3} \text{ m}$
Kinematic viscosity of air	$\mu_w$	$1.516 \times 10^{-5} \text{ m}^2 \text{ s}^{-1}$
Length of heat sink	$L_{hs}$	$50 \times 10^{-3} \text{ m}$
Number of channels	$n_{ch}$	$N_f + 1$
PV cell efficiency	$\eta_r$	$10 \times 10^{-2} - 25 \times 10^{-2}$
Stefan Boltzmann constant	$\sigma$	$5.67 \times 10^{-8} \text{ W m}^{-2} \text{ K}^{-4}$
Solar irradiance	$G$	$1000 \text{ W m}^{-2}$
Temperature of the sun	$T_s$	5777 K
Thermal conductivity of copper	$K_{cu}$	$401 \text{ W m}^{-1} \text{ K}^{-1}$
Thermal conductivity of ceramic	$K_{cer}$	$25 \text{ W m}^{-1} \text{ K}^{-1}$
Thermal conductivity of PV cell	$K_{pv}$	$148 \text{ W m}^{-1} \text{ K}^{-1}$
Thermal conductivity of tedlar	$K_t$	$0.2 \text{ W m}^{-1} \text{ K}^{-1}$
Thermal conductivity of air	$K_{air}$	$26.3 \times 10^{-3} \text{ W m}^{-1} \text{ K}^{-1}$



Thermal conductivity of glass	$K_g$	$1.1 \text{ W m}^{-1} \text{ K}^{-1}$
Thermal conductivity of grease	$K_{gr}$	$8 \text{ W m}^{-1} \text{ K}^{-1}$
Thickness of copper plate	$L_{cu}$	$3 \times 10^{-3} \text{ m}$
Thickness of PV cell	$L_{pv}$	$1.35 \times 10^{-4} \text{ m}$
Thickness of tedlar	$L_t$	$7.5 \times 10^{-5} \text{ m}$
Thickness of glass	$L_g$	$3 \times 10^{-3} \text{ m}$
Thickness of layer of thermal grease	$L_{gr}$	$5 \times 10^{-4} \text{ m}$
Thickness of base of the heat sink	$L_b$	$10 \times 10^{-3} \text{ m}$
Thickness of copper electrode	$L_{ele}$	$1 \times 10^{-4} \text{ m}$
Thickness of ceramic plate	$L_{cer}$	$5 \times 10^{-4} \text{ m}$
Transmissivity of glass	$\tau_g$	0.95
Volume flow rate		$4.718 \times 10^{-3} \text{ m}^3 \text{ s}^{-1}$
Width of heat sink	$w_{hs}$	$50 \times 10^{-3} \text{ m}$
Width of fin	$w_f$	$223 \times 10^{-6} \text{ m}$
Width of channel	$w_{ch}$	$482 \times 10^{-6} \text{ m}$
Wind velocity	$v$	$1 \text{ m s}^{-1}$

The thermal resistance of the microchannel heat sink is given as (R. Chein & G. Huang, 2004):

$$R_{in} = R_b + R_{cap} + R_{fin} \quad (8)$$

where  $R_b$ ,  $R_{cap}$ ,  $R_{fin}$  are the thermal resistance of the base of the heat sink, capacitive resistance, and thermal resistance due heat conduction by the fins and convection from the fins to the flowing air, respectively defined as:

$$R_b = \frac{L_b}{K_b A_b} \quad (9)$$

$$R_{cap} = \frac{1}{n_{ch} v_{air} A_{ch} \rho_{air} C_p} \quad (10)$$

The thermal resistance that is associated with the fluid flow and the dimension of the channels/fins is the  $R_{fin}$ , and is given as [18]:

$$R_f = \frac{1}{h_{air} (A - A_f (1 - \eta_f))} \quad (11)$$

where  $A$  is the total surface area of all the fins and un-finned portion,  $A_f$  represent the surface area of all the fins,  $\eta_f$  is the efficiency of a fin. These parameters are respectively given as:

$$A = L_{hs} [w_{hs} + N_f (2h_f + w_f)] \quad (12)$$

$$A_f = 2 N_f L_{hs} h_f \quad (13)$$

$$\eta_f = \frac{\tanh(mh_f)}{mh_f} \quad (14)$$

where  $L_{hs}$ ,  $w_{hs}$  are the length and width of heat sink,  $w_f$  is width of a fin,  $N_f = (w_{ch} L_{hs} - w_{ch}) / (w_{ch} + w_f)$  is the number of fins,  $m = \sqrt{2 h_{air} / (K_{hs} w_f)}$ ,  $K_{hs}$  is the thermal conductivity of the material of the heat sink which in this case is copper, while the forced air heat transfer coefficient ( $h_{air}$ ) can be obtained as:

$$h_{air} = \frac{K_{air} N_v}{D_{ch}} \quad (15)$$

where  $K_{air}$  is the thermal conductivity of air,  $D_{ch}$  is the hydraulic diameter of a channel and is given as:

$$D_{ch} = \frac{2(h_f w_{ch})}{(h_f + w_{ch})} \quad (16)$$

For a laminar flow, the Nusselt number ( $N_u$ ) can be calculated as (T. L. Bergman & F. P., 2011):

$$N_u = -1.047 + 9.326 G_a \quad (17)$$

where the function aspect ratio ( $G_a$ ) is given as

$$G_a = \frac{\left(\frac{w_{ch}}{h_f}\right)^2 + 1}{\left(\frac{w_{ch}}{h_f} + 1\right)^2} \quad (18)$$

The corresponding friction factor ( $f$ ) in the channels and Reynolds number ( $Re_{Dch}$ ) are denoted as:

$$f = 4 \frac{(19.64 G_s + 4.7)}{\Re_{Dch}} \quad (19)$$

$$\Re_{Dch} = \frac{v_{av} D_{ch}}{\mu_w} \quad (20)$$

where  $\mu_w$  is the Kinematic viscosity of the fluid.

Since the system is a forced air-cooled, the power consumed by the cooling fan should be taken into consideration. The higher the power consumed by the fan, the higher the cooling it will provide. In this study, the power consumed by the fan is considered as a constraint, therefore, its performance is limited. However, the dimension of the microchannel heat sink is optimized for optimal performance. Power consumed by the fan is given as a product of volume flow rate and pressure drop across the heat sink (T. Cui, Y. Xuan & Q. Li, 2016):

$$P_{fan} = 0.5 f v_{av}^3 n_{ch} \rho_{av} A_{ch} \frac{L_{hs}}{D_{ch}} \quad (21)$$

The net output power of the system which is the useful exergy output is given as:

$$\dot{E}x_{useful} = P_{pv} + Q_h \eta_{TE} - P_{fan} \quad (22)$$

The exergy into the CPV-TE is given as:

$$\dot{E}x_i = C G A_p \left[ 1 - \frac{4}{3} \frac{T_s}{T_c} + \frac{1}{3} \left( \frac{T_s}{T_c} \right)^4 \right] \quad (23)$$

where  $T_s$  is the temperature of the sun, and the term in the square bracket is the exergy of solar radiation given by Patela [21].

The energy and exergy efficiencies of the system are respectively given as:

$$\eta_{sys} = \frac{\dot{E}x_{useful}}{C G A_{pv}} \quad (24) \quad \psi_{sys} = \frac{\dot{E}x_{useful}}{C G A_p \left( 1 - \frac{4}{3} \frac{T_s}{T_c} + \frac{1}{3} \left( \frac{T_s}{T_c} \right)^4 \right)} \quad (25)$$

### 3. Results and Discussion

Generally, efficiency temperature coefficient of PV cells is given by manufacturers, and its typical value is in the range of  $0.001 \text{ (K}^{-1})$  –  $0.005 \text{ (K}^{-1})$ . To understand the influence of the efficiency temperature coefficient of the PV on the energy and exergy efficiencies of the CPV-TE system, four different values of the efficiency temperature coefficients are used to compute the efficiencies. The variation of temperature of the PV with the optical concentration ratio is shown in Fig. 2. At optical concentration ratio,  $C = 1$ , one can see that irrespective of the value of the efficiency temperature coefficient, the temperatures are almost the same. The influence of the efficiency temperature coefficients increases with increase in the value of the optical concentration ratio. At  $C = 8$ , the PV with the lowest efficiency temperature coefficient has the lowest surface temperature of the PV.

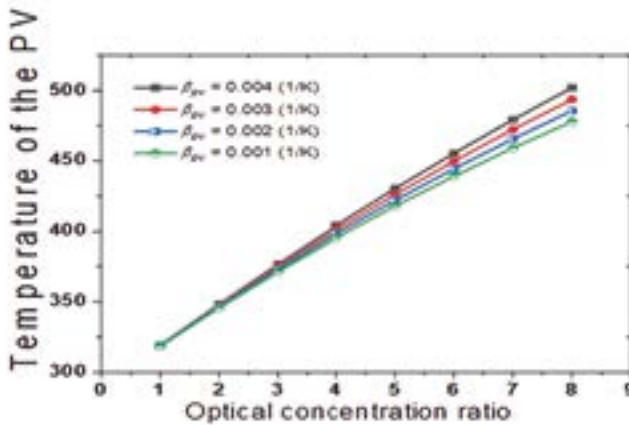


Fig. 2. Temperature of PV against optical concentration ratio for different efficiency temperature coefficients of the PV.

It will be recalled that the efficiencies of the PV are strongly dependent on the surface temperature of the PV. As shown in Figs. 3 and 4, the PV with the highest efficiency temperature coefficient ( $\beta_{pv}$ ) of PV has the lowest energy and exergy efficiencies. This is due to the high surface temperature of PV with  $\beta_{pv} = 0.004 \text{ (K}^{-1})$  in comparison to when the efficiency temperature coefficient is low. In both Figs. 3 and 4, the efficiencies are

monotonically decreasing functions of the optical concentration ratio, and the exergy efficiencies are higher than the corresponding energy efficiencies. It can be seen that, even at maximum optical concentration ratio, reasonable efficiencies are obtained for the PV with  $\beta_{pv} = 0.001 \text{ (K}^{-1}\text{)}$ .

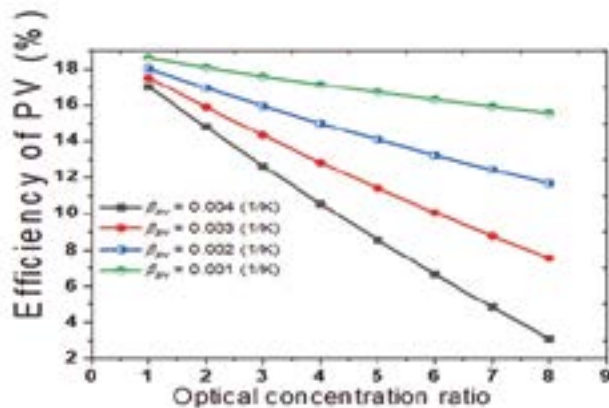


Fig. 3. Energy efficiency of PV against optical concentration ratio for different efficiency temperature coefficients of the PV.

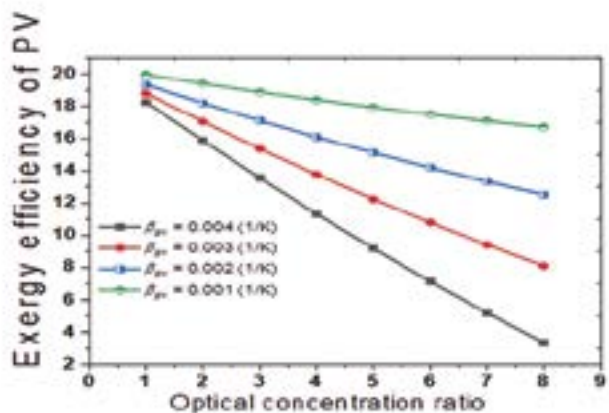


Fig. 4. Exergy efficiency of PV against optical concentration ratio for different efficiency temperature coefficients of the PV.

The energy and exergy efficiencies of TE module have different behaviour from that of the PV. This is because the performance of the TE module increases with temperature. The highest values of the energy

and exergy efficiencies of the TE module are obtained for PV with  $\beta_{pv} = 0.004 \text{ (K}^{-1}\text{)}$  as shown in Figs. 6 and 7, while the lowest values are obtained for PV with  $\beta_{pv} = 0.001 \text{ (K}^{-1}\text{)}$ . Both efficiencies increase and then decrease with increase in the optical concentration ratio. This is because the TE module has maximum amount of energy it can convert into electrical energy. After the point of the maximum power energy is exceeded, further increase in the heat input will not amount to any significant increase in the amount of power generated by TE module.

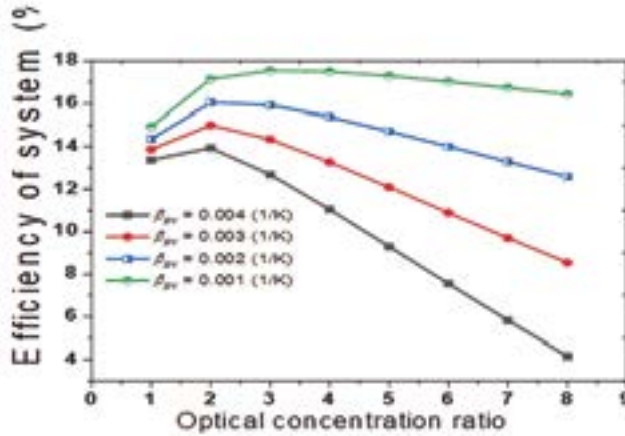


Fig. 5. Energy efficiency of PV against optical concentration ratio for different efficiency temperature coefficients of the PV.

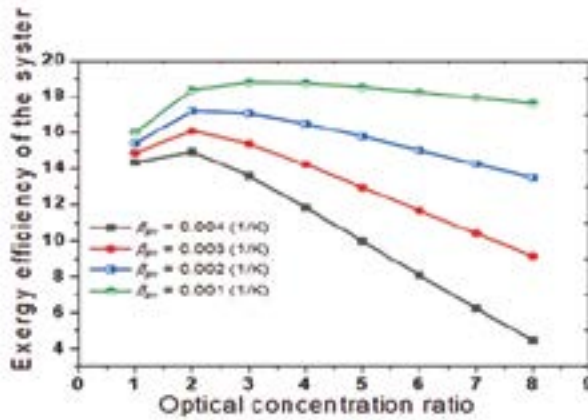


Fig. 6. Exergy efficiency of TEG against optical concentration ratio for different efficiency temperature coefficients of the PV.

Now the net energy and exergy efficiencies of the system are given in Figs. 7 and 8. One can see that the efficiencies have the combined behaviours of the PV and the TE module. Since the PV is the major source of the power in the CPV-TE system, the system with the lowest efficiency temperature coefficient has the highest energy and exergy efficiencies. Likewise, in all cases, the efficiencies reduce with increase in the optical concentration ratio. It is found that a CPV-TE with efficiency temperature coefficient of  $\beta_{pv} = 0.001 \text{ (K}^{-1}\text{)}$ , will have a reasonable energy and exergy efficiencies even when operated at high concentration ratio.

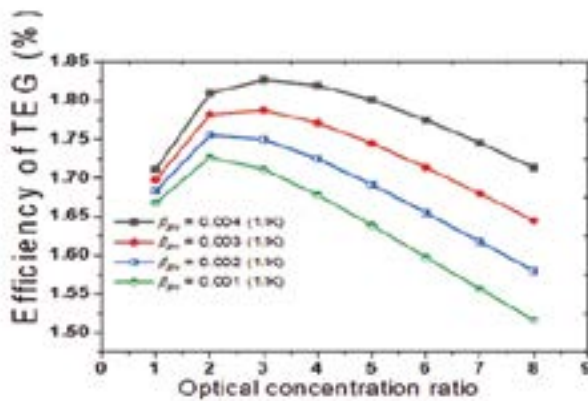


Fig. 7. Energy efficiency of PV against optical concentration ratio for different efficiency temperature coefficients of the PV.

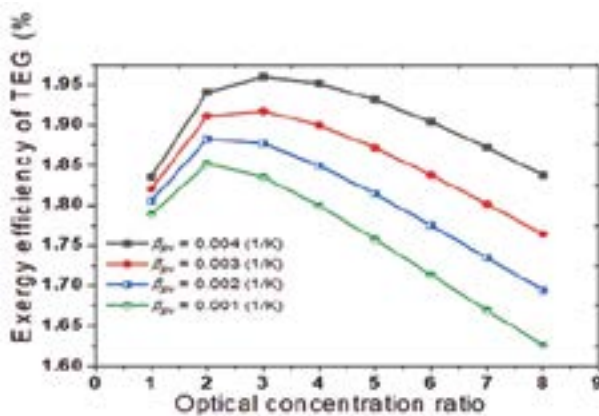


Fig. 8. Exergy efficiency of the system against optical concentration ratio for different efficiency temperature coefficients of the PV.

#### 4. Conclusion

Thermodynamic systems have both internal and external losses, and these losses if not checked, will severely affect the performance of the system. These losses can be reduced and the performance of the system can be improved through energy and exergy analysis. Here, a concentrated photovoltaic-thermodynamic system is analysis based on energy and exergy performance. The results have shown that the energy and exergy efficiencies of the system diminish with rise in the value of the optical concentration ratio, this indicates the presence of high losses at high concentration ratio/temperature. These losses could be reduced by making the performance of the PV less sensitive to high temperature. In other words, both the energy and exergy efficiencies improve when the efficiency temperature coefficient of the PV is low. Thus, the general conclusion is that the efficiency temperature coefficient of PV should be as small as possible for a better performance of a highly concentrated photovoltaic-thermoelectric system.



## REFERENCES

Agrawal, S. & Tiwari, G. N. (2012). Exergoeconomic analysis of glazed hybrid photovoltaic thermal module air collector. *Solar Energy*, 86(9), 2826-2838. doi: 10.1016/j.solener.2012.06.021.

Gomaa, M. R., R. J. Mustafa & H. Rezk. (2019). An experimental implementation and testing of a concentrated hybrid photovoltaic/thermal system with monocrystalline solar cells using linear Fresnel reflected mirrors. *Int J Energy Res*, 4862. doi: 10.1002/er.4862.

A. S. Abdelrazik, R. Saidur & F. A. Al-Sulaiman. (2020). Thermal regulation and performance assessment of a hybrid photovoltaic/thermal system using different combinations of nano-enhanced phase change materials. *Solar Energy Materials and Solar Cells*, 215, 110645. doi: 10.1016/j.solmat.2020.110645.

S. Soltani, A. Kasaeian, H. Sarrafha & D. Wen. (2017). An experimental investigation of a hybrid photovoltaic/thermoelectric system with nanofluid application. *Solar Energy*, 155, 1033-1043. doi: 10.1016/j.solener.2017.06.069.

A. Yusuf, N. Bayhan, H. Tiryaki, B. Hamawandi, M. S. Toprak & S. Balikaya. (2021). Multi-objective optimization of concentrated Photovoltaic-Thermoelectric hybrid system via non-dominated sorting genetic algorithm (NSGA II). *Energy Conversion and Management*, 236, 114065. doi: 10.1016/j.enconman.2021.114065.

A. Duran Sahin, I. Dincer & M. A. Rosen. (2007). Thermodynamic analysis of solar photovoltaic cell systems. *Solar Energy Materials and Solar Cells*, 91(2-3), 153-159. doi: 10.1016/j.solmat.2006.07.015.

F. Sarhaddi, S. Farahat, H. Ajam & A. Behzadmehr. (2010). Exergetic performance assessment of a solar photovoltaic thermal (PV/T) air collector. *Energy and Buildings*, 42(11), 2184-2199. doi: 10.1016/j.enbuild.2010.07.011.

D. Li, Y. Xuan, Q. Li & H. Hong. (2017). Exergy and energy analysis of photovoltaic-thermoelectric hybrid systems. *Energy*, 126, 343-351. doi: 10.1016/j.energy.2017.03.042.

S. Singh, O. I. Ibeagwu & R. Lamba. (2018). Thermodynamic evaluation of irreversibility and optimum performance of a concentrated PV-TEG cogenerated hybrid system. *Solar Energy*, 170, 896-905. doi: 10.1016/j.solener.2018.06.034.

A. Riahi, A. Ben Haj Ali, A. Fadhel, A. Guizani & M. Balghouthi. (2020). Performance investigation of a concentrating photovoltaic thermal hybrid solar

system combined with thermoelectric generators. *Energy Conversion and Management*, 205, 112377. doi: 10.1016/j.enconman.2019.112377.

S. Shittu, G. Li, X. Zhao, J. Zhou, X. Ma & Y. G. Akhlaghi (2020). Experimental study and exergy analysis of photovoltaic-thermoelectric with flat plate micro-channel heat pipe. *Energy Conversion and Management*, 207, 112515. doi: 10.1016/j.enconman.2020.112515.

E. Yin, Q. Li & Y. Xuan. (2018). Optimal design method for concentrating photovoltaic-thermoelectric hybrid system. *Applied Energy*, 226, 320–329. doi: 10.1016/j.apenergy.2018.05.127.

K. Gaurav & S. K. Pandey. (2017). Efficiency calculation of a thermoelectric generator for investigating the applicability of various thermoelectric materials. *Journal of Renewable and Sustainable Energy*, 9(1), 014701. doi: 10.1063/1.4976125.

A. Yusuf & S. Ballikaya. (2020). Modelling a Segmented Skutterudite-Based Thermoelectric Generator to Achieve Maximum Conversion Efficiency. *Applied Sciences*, 10(1), 408. doi: 10.3390/app10010408.

A. S. Al-Merbaty, B. S. Yilbas & A. Z. Sahin. (2014). A model study for cyclic thermal loading and thermal performance of a thermoelectric generator: Thermal performance of a thermoelectric generator. *Int. J. Energy Res.*, 38(10), 1351–1360. doi: 10.1002/er.3152.

M. B. Kleiner, S. A. Kuhn & K. Habberger. (1995). High performance forced air cooling scheme employing microchannel heat exchangers. *IEEE Trans. Comp., Packag., Manufact. Technol. A*, 18(4), 795–804. doi: 10.1109/95.477466.

R. Chein & G. Huang. (2004). Thermoelectric cooler application in electronic cooling. *Applied Thermal Engineering*, 24(14-15), 2207–2217. doi: 10.1016/j.applthermaleng.2004.03.001.

T. L. Bergman & F. P. (2011). *Incropera, Eds., Fundamentals of heat and mass transfer*, Hoboken, NJ: Wiley.

R. W. Knight, D. J. Hall, J. S. Goodling & R. C. Jaeger. (1992). Heat sink optimization with application to microchannels. *IEEE Trans. Comp., Hybrids, Manufact. Technol.*, 15(5), 832–842. doi: 10.1109/33.180049.

T. Cui, Y. Xuan & Q. Li. (2016). Design of a novel concentrating photovoltaic-thermoelectric system incorporated with phase change materials. *Energy Conversion and Management*, 112, 49–60. doi: 10.1016/j.enconman.2016.01.008.

R. Petela. (2003). Exergy of undiluted thermal radiation. *Solar Energy*, 74(6), 469–488. doi: 10.1016/S0038-092X(03)00226-3.



# BİYODİZEL ÜRETİMİ İÇİN YENİLENEBİLİR KAYNAKLARDAN KATALİZÖRLERİN ELDE EDİLMESİ

*Elnura Artykbaeva<sup>1</sup>*

---

## Özet

Son zamanlarda, fosil kaynaklarının yetersizliği ve sera gazı emisyonları gibi çevrenin kaygıları nedeniyle alternatif bir yakıt dikkat çekmektedir. Biyodizel son zamanlarda yenilenebilirliği, sürdürülebilirliği ve petrol bazlı dizel ile karşılaştırıldığında asgari miktarda CO<sub>2</sub>, SO<sub>2</sub> ve hidrokarbon emisyonu ile petrol dizel yakıtının ümit verici bir alternatifi haline gelmiştir. Biyodizel, yağ asitlerinin monoalkil esterlerinden oluşan petrol dizeli için yenilenebilir bir alternatiftir ve petrol dizeli ile benzer fiziksel özelliklere sahiptir, ancak yenilenebilir, biyolojik olarak parçalanabilir, toksik olmayan ve düşük emisyonlar da dahil olmak üzere benzersiz avantajları vardır. Biyodizel genellikle bitkisel yağların veya hayvansal yağların katalizörlerin varlığında kısa zincirli alkollerle (genellikle metanol) transesterifikasyonuyla üretilir. Heterojen katalizör, ayırma ve yeniden kullanılabilirlik avantajları nedeniyle, transesterifi-

---

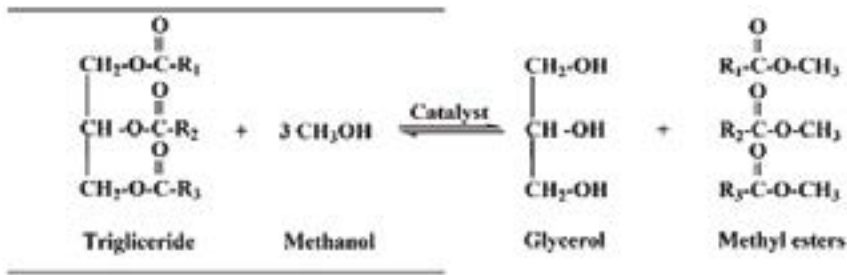
<sup>1</sup> Yüksek Lisans Öğrencisi, Kocaeli Üniversitesi Mühendislik Fakültesi, Kimya Mühendisliği

kasyon reaksiyonunda ikili bir rol oynar. Son zamanlarda, yenilenebilir kaynaklardan türetilen heterojen katalizörler daha fazla dikkat çekmiştir. Açıklanan yenilenebilir kaynaklar arasında kabuklar, kemikler, bitki ya da ağaçtan elde edilen küller, doğal kaynaklar, büyük ölçekli endüstriyel atıklar bulunur. Bu malzemelerden hazırlanan katalizörler biyodizel ürününü daha sürdürülebilir, çevre dostu ve uygun maliyetli hale getirebilir. Bu çalışmada, yenilenebilir kaynakların biyodizel üretiminin katalitik işleminde katalizör olarak kullanılması olasılığını araştırıldı. Yenilenebilir kaynakların biyodizel üretimi için düşük maliyetli katalizör olarak yeniden kullanılması, kirletici maddelerin en aza indirilmesi, biyodizelin üretim maliyetlerinin azaltılması ve biyodizelin tamamen ekolojik olarak üretilmesi sürecinin azaltılması açısından incelenmiştir.

**Anahtar Kelimeler:** Biodizel, Yenilenebilir Kaynaklar, Heterojen Katalizör.

## 1. Giriş

Son zamanlarda, fosil kaynaklarının yetersizliği ve sera gazı emisyonları gibi çevre sorunları nedeniyle alternatif bir yakıt dikkat çekmektedir (L. Wan, H. Liu & D. Skala, 2014; B. Ali et al., 2018). Biyodizel son zamanlarda yenilenebilirliği, sürdürülebilirliği ve petrol bazlı dizel ile karşılaştırıldığında asgari miktarda CO<sub>2</sub>, SO<sub>2</sub> ve hidrokarbon emisyonu ile petrol dizel yakıtının ümit verici bir alternatifi haline gelmiştir (B. Ali et al., 2018). Ek olarak, biyodizel, motor modifikasyonu olmadan doğrudan motora uygulanabilen fosil dizel ile benzer fizikokimyasal özelliklere sahiptir (S. Niu et al., 2018). Biyodizel endüstrisinde en çok kullanılan ticari teknoloji, temel koşullarda triasilgliserit (C<sub>14</sub>-C<sub>20</sub>) 'yi C<sub>1</sub>-C<sub>2</sub> alkollerle transesterize etmektir (D. Y. C. Leung et al. 2010). Transesterifikasyon reaksiyonu şu şekilde temsil edilir:



Genel olarak, K (Na) hidroksit gibi çözünebilir bazlar, hafif koşullar altında oldukça yüksek katalitik aktivitelerinden dolayı transesterifikasyon reaksiyonu için katalizör olarak kullanılır (F. Su and Y. Guo, 2014). Maalesef, bu homojen katalizörler reaktörlere olduğu kadar zor geri dönüşümlerine de aşındırıcıdır. Sonuç olarak, metal oksitler, karışık oksitler, destekli alkali metaller, zeolitler, hidrotalsitler vb. gibi heterojen katalizörler, daha az korozyon, kolay ayrılma ve düşük çevre kirliliği nedeniyle homojen bazların yerini almak üzere geniş çapta incelenmiştir (M. kumar and M. P. Sharma, 2016).

Son zamanlarda, kataliz alanı, yüksek katalizörlerin yüksek üretim maliyeti ve metal kayıpları nedeniyle katalitik işlemlerin genel sürdürülebilirliğini arttırmak için yüksek hacimli yenilenebilir kaynaklardan türetilen heterojen katalizörlerin kullanılması ve geliştirilmesine büyük

önem vermektedir (J. A. Bennett, K. Wilson & A. F. Lee, 2016; S. H. Y. S. Abdullah et al., 2017). Tepkime sırasındaki yüksek aktiviteleri ve seçimlerinin yanı sıra, yenilenebilir kaynaklar kaynaklı katalizörler ucuz bir şekilde sentezlenebilir, bu da biyodizel üretiminin maliyetini daha da azaltır. Ayrıca, katalizörlerde özellikle katı atıklarda yenilenebilir malzemelerin kullanılması, çevre sorununu da kısmen çözebilir ve bertarafı ile ilişkili maliyetleri azaltabilir, bu da bu yenilenebilir malzemelere katma değer anlamına gelir (S. H. Y. S. Abdullah et al., 2017). Geçtiğimiz birkaç yılda, bazı makalelerde çeşitli yenilenebilir malzemeler gözden geçirilmiştir. İnceleme literatürlerinin çoğu, biyokütle, yumurta kabuğu, nano gözenekli materyaller ve benzeri gibi yenilenebilir tek malzemeler üzerine odaklanmıştır ve vurguları da büyük oranda atık malzeme üzerine konurken, yenilenebilir malzemelerin sınıflandırılması çok açık değildir. Yenilenebilir kaynakların uygulanmasında kritik bir rol oynayan, araştırma ilerlemelerini, zorluklarını ve yenilenebilir kaynaklardan türetilmiş heterojen katalizörlerin gelecekteki fırsatlarını kapsamlı bir şekilde gözden geçirmektir. Bu makale biyodizel üretimi için farklı yenilenebilir kaynaklar tarafından sınıflandırılan çeşitli katalizörlerin uygulamaları araştırılmıştır. Kökenlerine göre, bahsettiğimiz yenilenebilir kaynaklar; kabuklar (yumurta kabuğu ve yumuşakça kabuğu), kemikler, bitki / ağaçtan küller vb. Ayrıca, gelecekteki zorluk ve katalizörün yenilenebilir kaynaklardan geleceği de göz önünde bulundurulur.

## **2. Biyodizel Üretimi için Kabuk Türevi Katalizörler**

### **2.1 Kabuklar**

Yumuşakçalardan elde edilen büyük miktarda kuş yumurtası ve et tüketimi nedeniyle, katı atık bertarafı sorununa neden olan büyük miktarda atık kabukları üretilir. Bu kabuk esas olarak  $\text{CaCO}_3$  içerdiğinden,  $\text{CaO}$  600-1000°C yüksek sıcaklıkta elde edilebilir (B. L. Salvi & N. L. Panwar, 2012). Bu nedenle, bu atık kabukları basitçe kalsine edilebilir ve biyodizel üretimi için katalizör olarak kullanılabilir Kuş yumurta kabuklarının  $\text{CaO}$ 'nun güvenilir kaynakları olduğu kanıtlanmıştır (Y.

H. Tan et al., 2015). En yaygın kuş kabuğu, tavuk yumurtasıdır (M. Balakrishnan et al., 2011). Transesterifikasyon reaksiyonu için ilk kalsine edilmiş tavuk kabuğu katalizörü, Wei ve diğ. çalışmalarında yumurta kabuğundan elde edilen CaO katalizörü 1000°C’de 2 saat kalsine edildikten sonra biyodizel için yüksek katalitik performans göstermiştir (%95 biyodizel verimi) (Z. Wei, C. Xu, and B. Li, 2009). Ayrıca, katalizörün katalitik aktivitesi ilk 13 döngüde kademeli olarak azaldı ve 17.döngüden sonra kalsiyum hidroksitin görünümü nedeniyle tamamen deaktive oldu. Yenilemeyen yağların transesterifikasyonu için kalsine tavuk yumurta kabuğu da kullanılmıştır (S. B. Chavan et al., 2015). Reaktiflerle temas eden CaO türevinden önce yenmeyen yağlarda serbest yağ asidini çıkartmak için asit katalizli bir esterleşme reaksiyonu yapılmalıdır (B. Ali et al., 2018). Ördek yumurta kabuğu, tavuk yumurta kabuğu ile benzer bileşenleri sergiler. Yin ve diğ. kalsine atık ördek kabuğunun, biyodizel sentezinde umut vaat eden başka bir CaO katalizörü olduğu sonucuna varmışlardır (X. Yin et al., 2016). Kuş yumurta kabukları arasında, boyutu sadece yarım tavuk yumurtasına eşdeğer olan bıldırcın yumurtası en küçüğüdür Cho ve diğ. hurma yağı transesterifikasyonu için asitle muamele edilmiş bıldırcın yumurta kabuğu katalizörünü araştırmışlar (Y. B. Cho & G. Seo, 2010). Yoğun kütikül tabakasını çıkarmak için asitle muamele edilmiş HCl çözeltisi ile kullanıldıktan ve daha sonra 800°C’nin üzerinde kalsine edildikten sonra, sentezlenen katalizör 5 tekrarlı kullanım sırasında sürekli olarak yüksek dönüşüm (% 98’in üzerinde) tutabilir. Üstelik hazırlanan bıldırcın yumurta kabuğu CaO, CH<sub>3</sub>OK’tan daha yüksek katalitik performans sergilemiş, çünkü katalizör yüzeyindeki büyük gözenekler, yalnızca büyük miktarda güçlü bazik bölge sağlamakla kalmayıp ayrıca yağ moleküllerinin geçişini kolaylaştırmış. Bir devekuşu yumurtası, dünyadaki en büyük kuş yumurtasıdır ve her devekuşu yumurta kabuğu yaklaşık 15 cm uzunluğunda, 13 cm genişliğinde ve 1.4-2.0 kg ağırlığındadır. 1000°C’de kalsine edildikten sonra, elde edilen CaO, daha küçük partikül büyüklüğü nedeniyle kalsine tavuk yumurta kabuğuna (% 96 vs %94) kıyasla daha yüksek aktivite göstermiştir (Y. H. Tan et al., 2015). Özetle, tüm bu atık yumurta kabuğu CaCO<sub>3</sub>’ten oluşur ve CaO için kaynak malzeme olarak başarıyla kullanılabilir. Bu yumurta kabukları arasında, içerdiği CaO miktarı ve hazırlanan CaO’nun yüzey

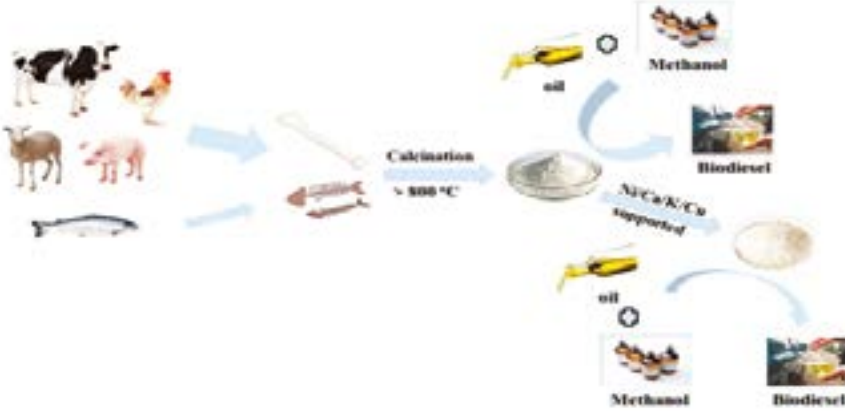


alanı esas olarak katalitik aktivitesine neden olur. Yumurta kabuğunun doğrudan kullanımına ek olarak, mikrodalga ve ultrasonik yöntemler gibi reaksiyon hızını artırmak için biyodizel sentezinde yardımcı transesterifikasyon teknikleri indüklenmiştir (P. Adewale, M.-J. Dumont & M. Ngadi, 2015; I. Choedkiatsakul, K. Ngaosuwan & S. Assabumrungrat, 2013). Mikrodalga, temel olarak elektromanyetik radyasyondur (0.3 ve 300 GHz arasındaki frekanslar), doğrudan reaktiflere enerji aktarabilir ve böylece yoğun lokalize ısıtmaya neden olur ve ön ısıtma basamağı elimine edilir ve reaksiyon daha kısa sürede tamamlanabilir (P. Adewale, M.-J. Dumont & M. Ngadi, 2015). Khemthong ve ark. mikrodalga koşulu altında (900W mikrodalga gücü), yağ asidi metil ester (FAME) verimi, kalsine edilmiş tavuk yumurta kabuğu katalizörü üzerinde 4 dakikada bile % 96.7'ye ulaşabildiğini bulmuşlar (P. Khemthong et al., 2012).

Tipik bir yumuşakça kabuğu olarak salyangoz kabuğunun ana bileşeni kalsiyum karbonattır (N. A. Oladoja & Y. D. Aliu, 2009). Kalsine salyangoz kabuğunun (900°C'de), atık kızartma yağı transesterifikasyonu ve biyodizel verimi sırasıyla %87,28 ve %99,58 dönüşüm ile mükemmel aktivite göstermiştir (A. Birla, B. Singh, S. N. Upadhyay & Y. C. Sharma, 2012). İstiridye kabuğu 700°C'nin üzerindeki kalsinasyon yoluyla CaO'ya dönüştürülebilir ve % 73.8 verim ile soya fasulyesi yağının transesterifikasyonu için başarıyla kullanılmıştır (N. Nakatani, H. Takamori, K. Takeda & H. Sakugawa, 2009). Biyodizel üretimi için atık yengeç ve kırışık (Anadara granosa) kabuklarını CaO'nun öncülleri olarak başarıyla kullanmıştır. 900°C'de kireçlenmeden sonra, karşılık gelen biyodizel saflığı yengeç kabuğu için %96.5'e ulaşabilirken, kırışık kabuğu için %97.48 verim elde edilmiştir (P.-L. Boey, G. P. Maniam, S. A. Hamid & D. M. H. Ali, 2011). Pers Körfezi kıyılarında toplanan atık midyeler, 950°C'den yüksek kalsinasyon sıcaklıklarında CaO'ya dönüştürülebilen bir başka CaCO<sub>3</sub> kaynağıdır. Biyodizel üretimi için CaO katalizörleri elde etmek için atık midyenin kabuğu için benzer bir strateji kullanılmıştır (R. Rezaei, M. Mohadesi & G. R. Moradi, 2013). Sonuçlar, 1000°C'de kalsine edildikten sonra elde edilen katalizör, ticari CaO'ninkinden daha yüksek aktivite sergilemiş ve biyodizel verimi % 86'ya kadar ulaşabilir (S. Sirisomboonchai et al., 2015).

## 2.2 Kemikler

Hayvan kemikleri, biyodizel sentezinde hammadde olarak kullanılabilir et üretiminden elde edilen bir çeşit yaygın atık ürünüdür (Şekil 1’de).



Şekil 1. Biyodizel sentezinde hayvan kemiklerinin kullanımı.

Biyodizel sentezi için besleme stoğu olarak balık kemiğinin kullanımı ilk önce kalsine balık kemiğinin yüksek katalitik performansının esas olarak yüksek kalsinasyon sıcaklığında  $\beta$ -tri-kalsiyum fosfat oluşumundan kaynaklandığını bulunmuştur (R. Chakraborty, S. Bepari & A. Banerjee, 2011). Bir başka çalışmalarda, atılan balık parçaları sadece hammadde yağı olarak değil aynı zamanda katalizör olarak da kullanılması ve iki aşamalı bir işlemle biyodizel sentezinde denenmiştir (D. Madhu, B. Singh & Y. C. Sharma, 2014). Esterleştirme reaksiyonu gerçekleştirilmiş ve atık balık yağının biyodizel’e yüksek dönüşümü (% 96’nın üzerinde) elde edilmiş. Evcil hayvan kemikleri, esas olarak  $\text{Ca}_3(\text{PO}_4)_2$  ve  $\text{CaCO}_3$  içerir, ayrıca triasilgliseritten biyodizel üretmek için de kullanılabilir. Örneğin, koyun kemiğindeki  $\text{Ca}_3(\text{PO}_4)_2$ ,  $800^\circ\text{C}$ ’de hidroksiapatite dönüştürülebilir ve bu hazırlanan malzeme üzerinde %96,78’lik bir yüksek metil ester (ME) dönüşümü elde edilebilir (A. Obadiah et al., 2012). Soya yağı transesterifikasyonu için aktif katalizörler elde etmek için kalsine atık sığır kemiğinden yararlanılmıştır (S. M.

Smith et al., 2013). Sentezlenen katalizörün katalitik aktivitesinin esas olarak CaO içeriğine bağlı olduğunu bulunmuş. Başka bir çalışmada, atık kızartma yağından elde edilen biyodizel üretiminde atık hayvan kemiği kullanılmıştır. Katalizör olarak doğrudan kullanıma ek olarak, hayvan kemiği, gözenekli yapısı ve adsorpsiyon kabiliyeti nedeniyle iyi destek olarak kabul edildi. Biyodizel üretiminde, destek olarak atık hayvan kemiklerinden elde edilen doğal hidroksiapatit kullanan bir dizi heterojen katalizör araştırılmıştır. Örneğin, atık balık (*Lates calcarifer*) kemik destekli bakır katalizörü ve oleik asit esterifikasyonunun katalizindeki uygulaması bildirilmiş. Başka bir çalışmada, balık pulu türevli hidroksiapatit, %59.90 Ni/Ca asit katalizörün balık pulu ve % 98,40 biyodizel verimi elde edilmiştir. Kalsine edilmiş hayvan kemiği, katalizörlerin sentezi için potasyum tuzlarına ( $K_2CO_3$  ve KOH gibi) destek olarak da kullanılabilir. Deneysel sonuçlar, hazırlanan katalizörlerin, yüksek toplam bazlıkları nedeniyle yüksek katalitik aktiviteye (elde edilen verimin % 96'nın üzerinde) sahip olduğunu ortaya çıkardı (J. Nisar et al., 2017).

### 2.3 Bitki / Ağaç Kaynaklarından Elde Edilen Katalizör

Atık bitki / ağaç kaynaklarının katalitik malzemelere uygulanması son zamanlarda çok dikkat çekmiştir (M. Balakrishnan, V. S. Batra, J. S. J. Hargreaves & I. D. Pulford, 2011). Bitki / ağaç kaynaklarından elde edilen kül içinde bulunan çok miktarda alkali veya alkali toprak elementleri nedeniyle, biyodizel üretimi için çeşitli kül bazlı katalizörler araştırılmıştır. Tropikal ülkelerde bol miktarda tarımsal katı atık olan yağ hurma külü (kazan külü), hurma yağı fabrikası tüketimi için buhar ya da elektrik üretmek üzere yağ hurma elyafı, çekirdeği, kabukları ve boş meyve demetlerinin yakılmasından sonra üretilir. Külün ana inorganik elemanı, temel olarak biyodizel sentezi için yüksek katalitik aktivitesine katkıda bulunabilecek K'dır (Retrieved from: <https://pubs.acs.org/doi/abs/10.1021/ef8007954>). *Lemna perpusilla* Torrey, göletlerin su yüzeyinde doğal olarak yetişen çok küçük bir su otudur. *Rafine Jatropa curcas* L.'de kullanılan *Lemna perpusilla* Torrey külü, yağ transesterifikasyonu ortak yanmadan elde edilen kül 550°C'de kalsine edilmiş.

Maksimum yağ dönüşümü %89.43 olmuştur. *Lemna perpusilla* Torrey külünün yüksek performansı, esas olarak yüksek potasyum içeriğinden (%11.3) kaynaklanmaktadır. Benzer şekilde, yüksek potasyum içeren kakao kabuğu ile *Jatropha* yağı transesterifikasyonu yüksek katalitik aktivite göstermiştir (V. Vadery et al., 2014). Odun külü de yüksek alkali bir malzemedir. *Jatropha* yağının transesterifikasyonunda esas olarak  $\text{Ca}_2\text{SiO}_4$ ,  $0.05\text{Ca}_3(\text{PO}_4)_2$ ,  $\text{Ca}_3(\text{PO}_4)_2$  ve yüksek ester dönüşümünden (% 97-99) oluşan odun külünün elde edilebileceğini buldu (B. L. Salvi & N. L. Panwar, 2012).

Başka bir çalışmada huş kabuğundan elde edilen külü (bir tür odun külü) kullanmışlar ve elde edilen sonuçlar huş kabuğundan elde edilen odun külünün CaO'dan oluştuğunu ve bunun da iyi katalitik performansla yol açtığını göstermiş (B. K. Uprety, at al, 2016). Kalsine edilmiş muz kabuğu külü başka bir tür yeni kül bazlı katalizör olarak değerlendirilmiş (M. Gohain, at al, 2017). Sadece açık havada yanmış ve bir Muffle fırınında kalsine edilmiş, elde edilen kül, biyodizel üretimi için oldukça etkili sonuçlar vermiş.  $\text{K}_2\text{O}$  ve CaO varlığı, yüksek katalitik aktivitesine bağlanır. Külün katalizör olarak doğrudan kullanılmasına ek olarak, transesterifikasyon reaksiyonunda kül bazlı katalizörün aktivitesini arttırmak için bir dizi modifiye yöntem araştırılmıştır (W. W. S. Ho, at al., 2012; W. W. S. Ho, at al., 2014).

### 3. Sonuç

Bu makalede biyodizel sentezinde heterojen katalizörlerin sentezi için hammadde olarak kullanılacak yenilenebilir kaynaklar araştırıldı. Yukarıdaki bölümlerde anlatıldığı gibi, yenilenebilir kaynaklardan heterojen katalizörlerin kullanılması biyodizelin sentezini daha sürdürülebilir hale getirebilir ve çevre sorunlarına karşı koyabilir. Yukarıdaki araştırmada, yenilenebilir kaynaklardan türetilmiş katalizörün katalitik aktivitesini etkilemek için üç anahtar nokta olduğu düşünülmektedir: (1) yenilenebilir kaynak malzemenin türü, (2) modifikasyon yöntemleri ve (3) kalsinasyon sıcaklığı. Yenilenebilir kaynak malzemenin türü, biyodizel üretimi için uygulamasında önemli bir rol oynamıştır.

Bununla birlikte, birçok yenilenebilir malzeme kalsinasyondan sonra bile hiçbir katalitik aktiviteye sahip değildir. Katalizör olarak kullanılmadan önce değiştirilmeleri gerekir. Değişiklik yöntemleri iki gruba ayrılabilir. Bir grup, yardımcı yöntemler olsa da (yardımcı çözücü, hidrasyon, mikrodalga, vb.) Yenilenebilir kaynak materyalden türetilmiş katalizörün katalitik etkinliğini arttırmak içindir. Diğer grup, biyodizel sentezinde aktif hale getiren aktif fazları ( $H_2SO_4$ , K, Ca tuzları vb.) Yükleme için özel yapısını (geniş yüzey alanı gibi) kullanmaktır. Kalsinasyon sıcaklığı da katalitik aktivitede önemli bir rol oynar. Çünkü CaO katalizörünün yüzey alanı kalsinasyon sıcaklığından belirgin şekilde etkilenebilir. Bu katalizörler transesterifikasyon reaksiyonunda kabul edilebilir bir katalitik etkinlik sergilemelerine rağmen, bu yeşil katalizörler için hala zorluklar vardır. İlk olarak, CaO,  $K_2O$ , Ca veya K destekli katalizör gibi çok sayıda yenilenebilir kaynak katalizörü genellikle reaksiyon ortamında deaktivasyon, zehirlenme ve sızıntı problemleri vardır.

Örneğin, yenilenebilir kaynaklardan türetilen saf CaO katalizörü için devre dışı bırakma nedenleri aşağıdaki gibidir: (1)  $CO_2$  ve  $H_2O$  havada mevcut ve katalizörün CaO yüzeyiyle reaksiyona giren reaktif; (2) reaksiyon sırasında katalizör yüzeyinde kalsiyum digliseroksit oluşumu ve (3)  $Ca^{2+}$  iyonlarının CaO yüzeyinden süzülmesi. Bu problemi çözmenin bir yolu CaO ile MgO, ZnO,  $SiO_2$  gibi diğer oksitler arasında kompozit oksitler oluşturmaktır. Bu nedenle, gelecekteki çalışmalarımızda transesterifikasyon reaksiyonu için daha kararlı ve yüksek verimli kompozit oksitler katalizörü bulmak çok daha önemli bir yöntem olacaktır. Yenilenebilir kaynakların katalizörlerinin çevresel faydaları, büyük miktarda çözücü veya tehlikeli / toksik kimyasallar, enerji yoğun ısı veya basınç sistemleri veya pahalı ticari katkı maddeleri kullanılarak sentezlenmeleri durumunda ihmal edilebilir. Biyodizel üretimi için katalizörler alanını daha fazla keşfetme ihtiyacına rağmen, yenilenebilir kaynaklardan türetilen katalizörler üzerinde yoğun ve çeşitli araştırmalar yapılması potansiyeli, endüstriyel seviyede biyodizel üretimi için heterojen bir katalizör olarak potansiyelini göstermektedir.

## KAYNAKÇA

L. Wan, H. Liu & D. Skala. (2014). Biodiesel production from soybean oil in subcritical methanol using  $\text{MnCO}_3/\text{ZnO}$  as catalyst. *Appl. Catal. B Environ.*, 152-153, 352–359. doi: 10.1016/j.apcatb.2014.01.033.

B. Ali, S. Yusup, A. T. Quitain, M. S. Alnarabiji, R. N. M. Kamil & T. Kida. (2018). Synthesis of novel graphene oxide/bentonite bi-functional heterogeneous catalyst for one-pot esterification and transesterification reactions. *Energy Convers. Manag.*, 171, 1801–1812, doi: 10.1016/j.enconman.2018.06.082.

S. Niu, Y. Ning, C. Lu, K. Han, H. Yu & Y. Zhou. (2018). Esterification of oleic acid to produce biodiesel catalyzed by sulfonated activated carbon from bamboo. *Energy Convers. Manag.*, 163, 59–65. doi: 10.1016/j.enconman.2018.02.055.

D. Y. C. Leung, X. Wu, and M. K. H. Leung. (2010). A review on biodiesel production using catalyzed transesterification. *Appl. Energy*, vol. 87, 4, 1083–1095. doi: 10.1016/j.apenergy.2009.10.006.

F. Su and Y. Guo. (2014). Advancements in solid acid catalysts for biodiesel production. *Green Chem.*, 16(6), 2934–2957. doi: 10.1039/C3GC42333F.

M. kumar and M. P. Sharma. (2016). Selection of potential oils for biodiesel production. *Renew. Sustain. Energy Rev.*, 56, 1129–1138. doi: 10.1016/j.rser.2015.12.032.

J. A. Bennett, K. Wilson & A. F. Lee. (2016). Catalytic applications of waste derived materials. *J. Mater. Chem. A*, 4(10), 3617–3637. doi: 10.1039/C5TA09613H.

S. H. Y. S. Abdullah *et al.* (2017). A review of biomass-derived heterogeneous catalyst for a sustainable biodiesel production. *Renew. Sustain. Energy Rev.*, 70, 1040–1051. doi: 10.1016/j.rser.2016.12.008.

R. Shan, C. Zhao, P. Lv, H. Yuan & J. Yao. (2016). Catalytic applications of calcium rich waste materials for biodiesel: Current state and perspectives. *Energy Convers. Manag.*, 127, 273–283. doi: 10.1016/j.enconman.2016.09.018.

M. Balakrishnan, V. S. Batra, J. S. J. Hargreaves & I. D. Pulford. (2011). Waste materials – catalytic opportunities: an overview of the application of large scale waste materials as resources for catalytic applications. *Green Chem.*, 13(1), 16–24. doi: 10.1039/C0GC00685H.

B. L. Salvi & N. L. Panwar. (2012). Biodiesel resources and production technologies – A review. *Renew. Sustain. Energy Rev.*, 16(6), 3680–3689. doi: 10.1016/j.rser.2012.03.050.

Y. H. Tan, M. O. Abdullah & C. Nolasco-Hipolito. (2015). The potential of waste cooking oil-based biodiesel using heterogeneous catalyst derived from various calcined eggshells coupled with an emulsification technique: A review on the emission reduction and engine performance. *Renew. Sustain. Energy Rev.*, 47, 589–603. doi: 10.1016/j.rser.2015.03.048.

Z. Wei, C. Xu, and B. Li. (2009). Application of waste eggshell as low-cost solid catalyst for biodiesel production. *Bioresour. Technol.*, 100(11), 2883–2885. doi: 10.1016/j.biortech.2008.12.039.

S. B. Chavan, R. R. Kumbhar, D. Madhu, B. Singh & Y. C. Sharma. (2015). Synthesis of biodiesel from *Jatropha curcas* oil using waste eggshell and study of its fuel properties. *RSC Adv.*, 5(78), 63596–63604. doi: 10.1039/C5RA06937H.

X. Yin, X. Duan, Q. You, C. Dai, Z. Tan & X. Zhu (2016). Biodiesel production from soybean oil deodorizer distillate using calcined duck eggshell as catalyst. *Energy Convers. Manag.*, 112, 199–207. doi: 10.1016/j.enconman.2016.01.026.

Y. B. Cho & G. Seo. (2010). High activity of acid-treated quail eggshell catalysts in the transesterification of palm oil with methanol. *Bioresour. Technol.*, 101(22), 8515–8519. doi: 10.1016/j.biortech.2010.06.082.

Y. H. Tan, M. O. Abdullah, C. Nolasco-Hipolito & Y. H. Taufiq-Yap. (2015). Waste ostrich- and chicken-eggshells as heterogeneous base catalyst for biodiesel production from used cooking oil: Catalyst characterization and biodiesel yield performance. *Appl. Energy*, 160, 58–70. doi: 10.1016/j.apenergy.2015.09.023.

P. Adewale, M.-J. Dumont & M. Ngadi. (2015). Recent trends of biodiesel production from animal fat wastes and associated production techniques. *Renew. Sustain. Energy Rev.*, 45, 574–588. doi: 10.1016/j.rser.2015.02.039.

I. Choedkiatsakul, K. Ngaosuwan & S. Assabumrungrat. (2013). Application of heterogeneous catalysts for transesterification of refined palm oil in ultrasound-assisted reactor. *Fuel Process. Technol.*, 111, 22–28, Jul., doi: 10.1016/j.fuproc.2013.01.015.

P. Khemthong *et al.* (2012). Industrial eggshell wastes as the heterogeneous catalysts for microwave-assisted biodiesel production. *Catal. Today*, 190(1), 112–116. doi: 10.1016/j.cattod.2011.12.024.

N. A. Oladoja & Y. D. Aliu. (2009). Snail shell as coagulant aid in the alum precipitation of malachite green from aqua system. *J. Hazard. Mater.*, 164(2), 1496–1502. doi: 10.1016/j.jhazmat.2008.09.114.

A. Birla, B. Singh, S. N. Upadhyay & Y. C. Sharma. (2012). Kinetics studies of synthesis of biodiesel from waste frying oil using a heterogeneous catalyst derived from snail shell. *Bioresour. Technol.*, 106, 95–100. Feb., doi: 10.1016/j.biortech.2011.11.065.

N. Nakatani, H. Takamori, K. Takeda & H. Sakugawa. (2009). Transesterification of soybean oil using combusted oyster shell waste as a catalyst. *Bioresour. Technol.*, 100(3), 1510–1513. doi: 10.1016/j.biortech.2008.09.007.

P.-L. Boey, G. P. Maniam, S. A. Hamid & D. M. H. Ali. (2011). Utilization of waste cockle shell (*Anadara granosa*) in biodiesel production from palm olein: Optimization using response surface methodology. *Fuel*, 90(7), 2353–2358. doi: 10.1016/j.fuel.2011.03.002.

R. Rezaei, M. Mohadesi & G. R. Moradi. (2013). Optimization of biodiesel production using waste mussel shell catalyst," *Fuel*, 109, 534–541. doi: 10.1016/j.fuel.2013.03.004.

S. Sirisomboonchai *et al.*. (2015). Biodiesel production from waste cooking oil using calcined scallop shell as catalyst. *Energy Convers. Manag.*, 95, 242–247. doi: 10.1016/j.enconman.2015.02.044.



R. Chakraborty, S. Bepari & A. Banerjee. (2011). Application of calcined waste fish (*Labeo rohita*) scale as low-cost heterogeneous catalyst for biodiesel synthesis," *Bioresour. Technol.*, 102(3), 3610–3618. doi: 10.1016/j.biortech.2010.10.123.

D. Madhu, B. Singh & Y. C. Sharma. (2014). Studies on application of fish waste for synthesis of high quality biodiesel. *RSC Adv.*, 4(59), 31462–31468. doi: 10.1039/C4RA03590A.

A. Obadiah, G. A. Swaroopa, S. V. Kumar, K. R. Jeganathan & A. Ramasubbu. (2012). Biodiesel production from Palm oil using calcined waste animal bone as catalyst. *Bioresour. Technol.*, 116, 512–516. doi: 10.1016/j.biortech.2012.03.112.

S. M. Smith *et al.* (2013). Transesterification of soybean oil using bovine bone waste as new catalyst. *Bioresour. Technol.*, 143, 686–690. doi: 10.1016/j.biortech.2013.06.087.

J. Nisar *et al.* (2017). Enhanced biodiesel production from *Jatropha* oil using calcined waste animal bones as catalyst. *Renew. Energy*, 101, 111–119. doi: 10.1016/j.renene.2016.08.048.

Process Optimization for Biodiesel Production from Waste Cooking Palm Oil (*Elaeis guineensis*) Using Response Surface Methodology | Energy & Fuels. Retrieved from: <https://pubs.acs.org/doi/abs/10.1021/ef8007954> (15.08.2020).

V. Vadery *et al.* (2014). Room temperature production of *jatropha* biodiesel over coconut husk ash. *Energy*, 70, 588–594. doi: 10.1016/j.energy.2014.04.045.

B. K. Uprety, W. Chaiwong, C. Ewelike & S. K. Rakshit. (2016). Biodiesel production using heterogeneous catalysts including wood ash and the importance of enhancing byproduct glycerol purity. *Energy Convers. Manag.*, 115, 191–199. doi: 10.1016/j.enconman.2016.02.032.

M. Gohain, A. Devi & D. Deka. (2017). *Musa balbisiana* Colla peel as highly effective renewable heterogeneous base catalyst for biodiesel production. *Ind. Crops Prod.*, 109, 8–18. doi: 10.1016/j.indcrop.2017.08.006.

W. W. S. Ho, H. K. Ng & S. Gan. (2012). Development and characterisation of novel heterogeneous palm oil mill boiler ash-based catalysts for biodiesel production," *Bioresour. Technol.*, 125, 158–164. doi: 10.1016/j.biortech.2012.08.099.

W. W. S. Ho, H. K. Ng, S. Gan & S. H. Tan. (2014). Evaluation of palm oil mill fly ash supported calcium oxide as a heterogeneous base catalyst in biodiesel synthesis from crude palm oil. *Energy Convers. Manag.*, 88, 1167–1178. doi: 10.1016/j.enconman.2014.03.061.



**JEOLOJİ ÇALIŞMALARI**  
*GEOLOGY STUDIES*



# EVALUATION OF THE ASSOCIATIONS BETWEEN GROUNDWATER FLUCTUATIONS AND SOIL SALINITY USING LANDSAT IMAGERIES AND GEOSTATISTICAL METHODS

*Behnam Khorrami*<sup>1</sup>

---

## **Abstract**

Marand plain is one of the most critical areas in northwestern Iran regarding its groundwater status. Almost all of the residents' potable and cultivation water need is catered by groundwater. In this study, the Spatio-temporal variations of groundwater and its associations with soil salinity were investigated. The hydrograph and kymograph analysis were done to unearth the temporal variations of groundwater level and salinity respectively. According to the hydrograph of the region, the water table of the aquifer has experienced a descending trend with an annual decline of 96 cm from 2003 to 2011. The kymography analysis suggests that there is an ascending trend in the electrical conductivity

---

<sup>1</sup> PhD Student, Dokuz Eylul University, The Graduate School of Natural and Applied Sciences, Geographic Information Systems, ORCID: 0000-0003-3265-372X

(EC) of the groundwater with more than 17 microsiemence increase in the same period. The salinity index extracted from Landsat TM processing is an indicator of the soil salinity of the plain. The area-averaged time series of the Soil Salinity Index (SSI) also shows an increasing trend at the same period which is in almost complete agreement with the variations of groundwater EC ( $r = 0.92$ ). The SSI also turned out to be highly correlated with the water table fluctuations with a correlation of -0.75. The spatial variability maps of the study area were generated using the Kriging interpolation technique. According to the spatial maps, it's also found that the southern part of the region has suffered the most water level fall while the central and western areas show water level rise. The EC map also suggests that the salinity level has decreased in the west and a small part of the east through the central plain shows a salinity increase.

**Keywords:** Groundwater Degradation, Soil Salinity, Marand Plain, GIS, Landsat.

## 1. Introduction

Water resources stored in aquifers beneath the land have been playing a vital role in supporting human beings' water needs either in agricultural or industrial sectors for many decades. These resources have a critical stance in arid and semi-arid regions (Sahfiei, 2008) of the world on account of the increased need for freshwater as a result of population growth, on one hand, and the climate changes impacts on the other hand so that the majority of the aquifers located in these regions now are facing with grave challenges. About 99 percent of the world's liquid water is stored in underground strata which are used by one-third of the total population (Jackson et al., 2001). In arid and semi-arid regions, the dearth of precipitation and surface waters lead to the utmost reliance of these areas to groundwater resources in supplying the required water for human use in agriculture, household, and industry (Khorrami and Gunduz, 2018) which in recent years has brought out the decline of the groundwater table.

There is a bilateral interaction between groundwater and surface water resources. The groundwater fluctuations can impact the quality of water in terms of increased salinity which may be detrimental to human life as well as agricultural products. It may also change the quality of soil by the interactions between groundwater and surface soil which is deemed an unpleasant aspect of groundwater shrinkage especially for agricultural and environmental applications (Elhag, 2016; Asfaw et al., 2018). Soil salinization is considered a global problem, especially in arid and semi-arid regions. The negative impacts associated with soil salinity are manifested as the lowered quality of soil and water thus, diminished quality and quantity of crops (Hashem et al., 2010; Abbas et al., 2013; Didi et al., 2019) with an estimated yield loss of 30 and 80 % in moderate and high saline farms respectively (Ibrakhimov et al., 2007). The depth and salinity of groundwater are among the main causative factors of soil salinization (Ibrakhimov et al., 2007). Assessment of the temporal and spatial changes of GROUNDWATER and soil quality is a necessary practice to guarantee sustainable development plans. The association between groundwater fluctuations with water quality and soil characteristics like soil moisture, soil salinity, and vegetation cover-



age is widely studied worldwide (Ibrakhimov, 2005; Bristow et al., 2006; Abbas et al., 2013; Yan et al., 2015; Korkmaz et al., 2015; Abliz et al., 2016; Fontes Júnior and Montenegro, 2017; Horriche and Benabdallah, 2020; Jarraya Horriche and Benabdallah, 2020).

Remote sensing materials and techniques accompanied by the analytical capabilities of Geographic Information Systems (GIS) have paved the way for more convenient and costly-effective monitoring of ground-water fluctuations and soil characteristics. The satellite imageries provide a useful means for detecting and mapping soil salinity based on the reflective characteristics of the soil surface. The suitability and accuracy of this approach for remote assessment of soil salinity have been approved through several studies in recent years (e.g. Lhissou et al., 2014; Elhag, 2016; Azabdaftari and Sunarb, 2016; Elhag and Bahrawi, 2017; Nguyen et al., 2020; Ghazali et al., 2020). On account of the bare role of groundwater and soil quality in sustaining economic and environmental progress, it seems mandatory to surveil the water quantity and quality in aquifers and the quality of soils in farmlands.

Locating on the arid belt of the world, Iran has been engaging with groundwater crisis in the aftermath of changes in the global and regional climate and mismanagement of the resources in recent decades so that most of the aquifers across the country are in a dicey situation regarding groundwater quantity and quality as well (Nabavi, 2018). There are 609 aquifers in Iran, from which the number of aquifers categorized under the 'restricted' class has increased from 150 in 2000 (Larijani, 2005) to 402 in 2018 (MOE, 2019). The majority of water need in the Marand plain is supplied from its aquifer mostly for drinking and cultivation purposes. Farming is the main income source for the residents of the region. The extraction of groundwater storage has increased sharply in recent years due to a lack of precipitation and insufficient surface water. Thus, groundwater is an important water supply for this area. The current study aims mainly at monitoring the groundwater fluctuations and their associated impacts on groundwater salinity as well as soil salinity and green coverage over time using satellite imageries and in situ observation.

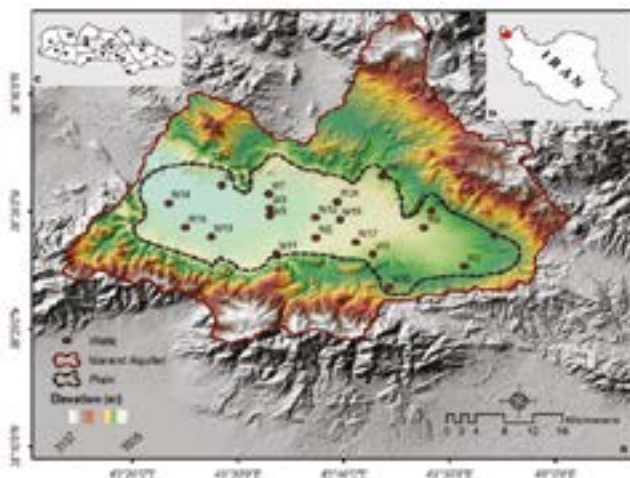
## 2. Methodology

### 2.1 Study Area

The Marand plain, in the center of the Marand aquifer, is located within the geographic coordinates of 45-15 to 46-05 E and 38-18 to 38-46 N (Khorrami et al., 2018) in the province of East Azerbaijan, NW Iran (Figure 1). More than two-thirds of the Marand aquifer is mountainous with the maximum, minimum, and elevation ranges of 3137 m, 1005 m, and 2132 m respectively. With an average elevation of 1050m, the Marand plain is located in the southern part of Marand county (Khorrami and Gunduz, 2019). The Marand plain is known as a part of the Caspian Sea basin in the north (Najib, 2002). The region has a semi-arid climate, with a mean annual precipitation of 236 mm and a maximum temperature of 40.6°C in summer, and a minimum temperature of -22.5°C in winter (Lashkaripour et al., 2005).

### 2.2. Materials and Methods

The required groundwater quantitative and qualitative database for this study was obtained from the Regional Water Company. Checking and organizing the data, 20 wells with a suitable temporal and spatial overlap were selected for 9 years from 2003 to 2011. The location of the sampling wells is shown in Figure 1.



**Figure 1.** The geographic location of the Marand plain with the sampling wells (a), the location of the plain in NW Iran (b), and the Thiessen network of the groundwater wells (c).

The Landsat TM (5) imageries with the scan characteristics of pass:169 and row:33, were received from the USGS web portal (<https://earthexplorer.usgs.gov/>). The selection of TM imageries was done according to the image selection criteria such as the minimum cloud coverage and maximum temporal similarity.

### 2.2.1. Groundwater Hydrography

The water table in a given aquifer responds to any change in the storage of the aquifer so that storage increase rises the water table and vice versa. This response of an aquifer can be illustrated and studied through groundwater hydrography assessment (Kumar, 2014). A hydrograph is a kind of chart in which the correspondent temporal changes of the water table are drawn to get an overview of groundwater level trends within a specific time.

To fit the selected wells to the spatial extent of the area, the Thiessen network was established in the ArcGIS environment. The Thiessen technique generates polygons as boundaries around each sampling point (target) which contains any point relating to that target (Huisman and De by, 2009). Table 1 has the characteristics of the applied wells in this study. Using the individual polygon areas and the water level of the correspondent wells, the mean annual values of groundwater level for each well were calculated and consequently, the plain's hydrograph was drawn.

**Table 1.** The characteristics of the applied piezometric wells.

ID	Well Name	Location ID	UTM (X)	UTM (Y)	Thiessen Area (km <sup>2</sup> )
1	Abarghan	W <sub>1</sub>	579250	4257600	32.77
2	Asadagi	W <sub>2</sub>	575050	4257700	42.95
3	Bahram	W <sub>3</sub>	562400	4254600	29.13
4	Charchar	W <sub>4</sub>	563650	4267000	29.27
5	Dolatabad	W <sub>5</sub>	569500	4258750	48.60
6	Galeban	W <sub>6</sub>	548012	4264039	46.05
7	Hosein Beig	W <sub>7</sub>	554550	4257200	23.16
8	Kandlaj	W <sub>8</sub>	564700	4249400	25.82
9	KoshkSaray	W <sub>9</sub>	549050	4254650	31.32
10	Markid	W <sub>10</sub>	554500	4260400	22.66

11	Qamish Agol	$W_{11}$	541550	4265450	42.82
12	Qaraje Mohammad	$W_{12}$	548150	4261850	12.39
13	Qaraje Mohammad	$W_{13}$	548150	4260750	26.73
14	Qirkhlar	$W_{14}$	534200	4262650	57.80
15	Gazafar	$W_{15}$	536500	4258800	38.08
16	Sari Tape	$W_{16}$	570550	4261450	20.23
17	Marand	$W_{17}$	560050	4256500	26.63
18	Qishlaq	$W_{18}$	540100	4257400	47.68
19	Yalguz Agaj	$W_{19}$	557850	4260050	19.83
20	Yamchi	$W_{20}$	557700	4262700	37.91

### 2.2.2. Groundwater Kymography

Water salinity is defined as the number of dissolved ions and particles in water. The groundwater salinity in an aquifer is evaluated using the Electrical Conductivity (EC) measurements and is a very important quality index due to its impacts on human life. The EC records of the selected wells in the study area were used to study the fluctuations of the groundwater salinity. Kymography is a process like a hydrography analysis, which represents the space-time water quality changes in an aquifer using the chemical analysis results of water samples (Rostamzadeh et al., 2016).

### 2.2.3. Spatial Variability

#### *Geostatistics*

GIS has got a great potentiality in geographic/environmental data analysis especially in water resources studies thanks to its robust analytical capability. One of the most used analytical tools in GIS is geostatistics by which the spatial structure of geo-related data is examined to be used in data analysis (Rajaei and Pouraslan, 2015). In general, geostatistics is a process with which the value of a sampled parameter is estimated for an unknown location using the values measured in known locations (Khor-

rami and Gunduz, 2019). There are different interpolation methods in geostatistics to use regarding the characteristics and nature of the data. Taking its high accuracy (Qahroodi, 2002) into account, the Kriging technique was applied to the groundwater wells to derive temporal maps of the water level and salinity of the Marand plain. The Kriging interpolation model is an estimation technique based on the 'weighted moving average' which is described as the following expression:

$$Z_{s0} = \sum_{i=1}^N \lambda_i Z_{si} \quad (1)$$

Where  $Z_{si}$  is the measured value at the  $i$ th location,  $\lambda_i$  is an unknown weight for the measured value, and  $S_0$  is the prediction location and  $N$  is the number of measurements (Qahroodi, 2002). Since the weights ( $\lambda_i$ ) in this method depend on both the distance between the samples and their spatial autocorrelation, Kriging goes through a two-step process: 1. Spatial autocorrelation analysis of the sample points 2. Surface prediction (Interpolation) (Meena, 2017). In this study, the step procedure followed for databases to create the desired surface map layers.

### *Change Detection*

Change detection is a detection process of changes/differences in the quantity or quality of a feature in a period of time (Lu et al., 2004). This technique is applied in a GIS environment comparing two raster layers representing the same feature or quality with the same spatial location during different times. The raster layers created for each parameter of the study were used to generate change detection maps so that the spatial extent of the variations that occurred for each parameter was revealed.

### *Soil Salinity Index*

The traditional approach of measuring soil salinity is based on the EC measurements from soil samples of a given area (Rhoades, 1990). Though the field observations are accurate, the restriction associated with this traditional approach makes it laborious and extravagant in data analysis and studies. Image processing has become an impressive method in gaining information about the Earth's surface features with-

out direct contact (Aggarwal, 2004). Based on the spectral signature of soil particles on satellite imageries, characteristics of the surface soil such as moisture content, vegetation coverage, soil quality, etc. can be detected and studied through image processing. In the current study, the salinity of the surface soil of the study area was evaluated based on the salinity index derived from the Landsat 5 (TM) imageries. Soil Salinity Index (SSI) is one of the widely used remotely sensed indicators (Dehni and Lounis, 2012; Abbas et al. 2013; Allbed et al. 2014) which is calculated by the following formulas:

$$SSI = \sqrt{R \times NIR} \quad (2)$$

R and NIR stand for the 'Red' and 'Near Infrared' respectively which correspond with Bands 3 and 4 of Landsat TM imageries.

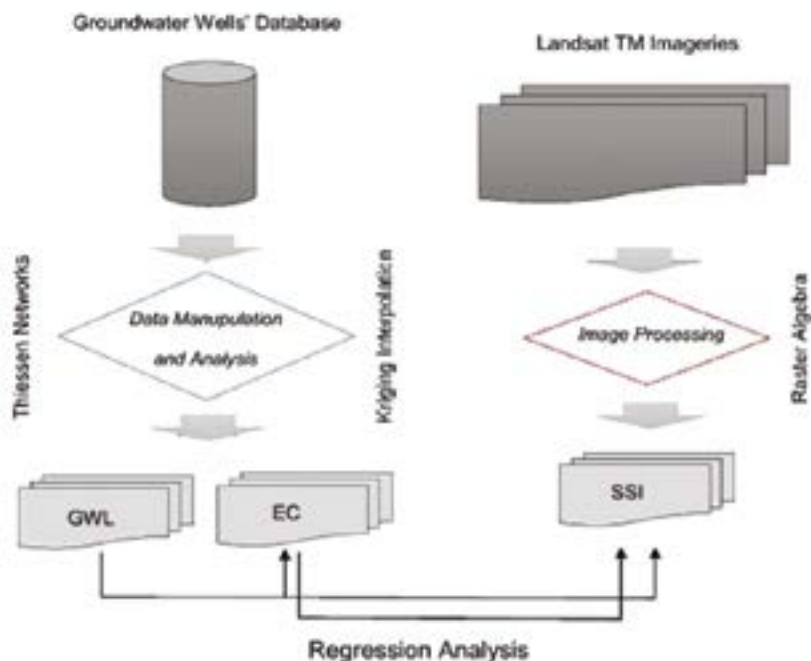


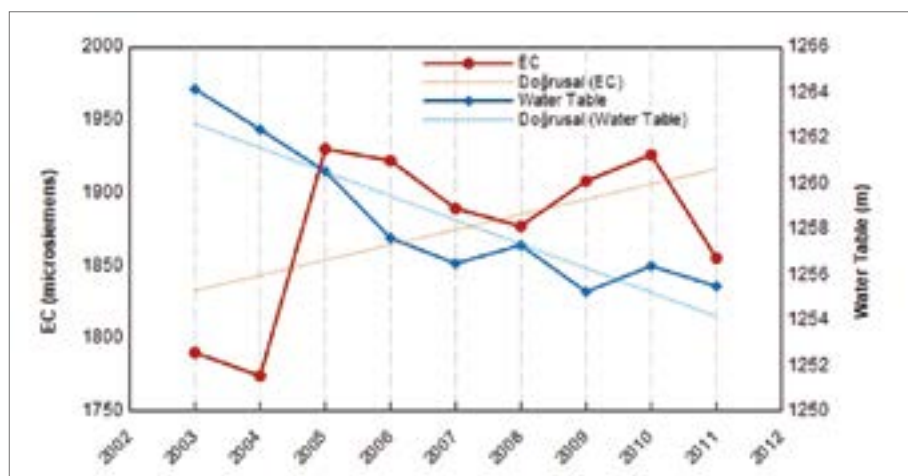
Figure 2. Graphical Illustration of the study workflow.

### 3. Results and Discussion

#### 3.1. Investigating the temporal fluctuations of the water table and EC

To discover the temporal variations of the plain's groundwater quantity and quality, hydrograph and kymograph graphs were used respectively to have an overview of their trends. The resulted hydrograph depicts a descending trend in the water level of the aquifer with an approximate decline of 8.6 m from 2003 to 2011, which corresponds to an annual drop of 96 cm. The aquifer's kymograph shows a total amount of 65 microsiemens increase which equals about 7 microsiemens per year.

Figure 3, shows the temporal interactions between groundwater and salinity. Based on this graph, there is a strong interactive association between the water table and EC fluctuations ( $R: -0.66$ ). The graph reveals that the more the groundwater level shrinks during the time, the more the water salinity increases. This is in agreement with the findings of Sarah (1997). Although, a number of influential parameters impact the variations of the groundwater electrical conductivity, the increase of the water salinity in the Marand plain can mainly be associated with the groundwater depletion due to the excessive water withdrawal particularly for agricultural purposes (Lashkaripour et al., 2005).



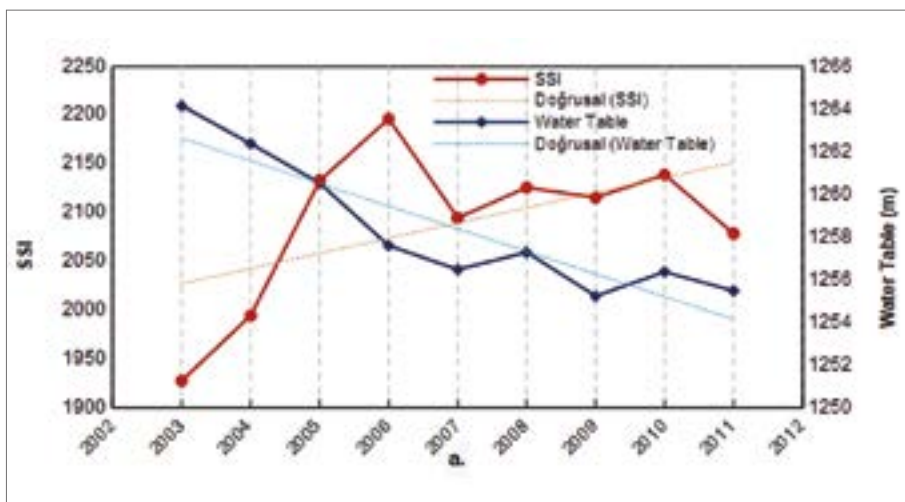
**Figure 3.** Temporal Interactions between the water table and groundwater salinity

### 3.2. Associations of SSI with the water table and EC

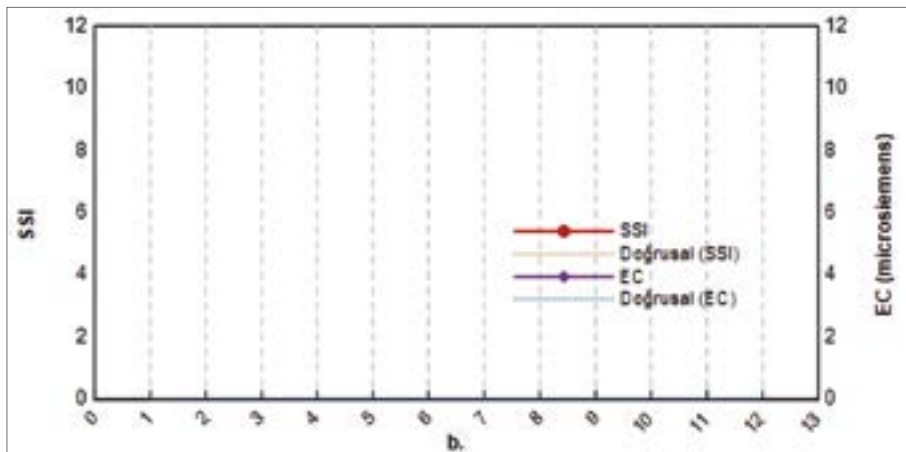
The temporal associations between the variations in groundwater level and salinity with soil salinity were analyzed through simple statistical analysis of regression modeling. The association between the groundwater EC and soil salinity index (SSI) (Figure 4) shows a very high agreement with a correlation of 0.9 which suggests that the soil salinity of the study area is controlled directly by the groundwater salinity so that the variations of groundwater salinity can be modeled perfectly based on remote sensing imageries of Landsat satellite.

The temporal interactions between the groundwater level and soil salinity also indicate a high negative correlation ( $R: -0.72$ ) which accentuates that the soil quality of the plain is affected by the variations of groundwater. The increase in the level of groundwater brings about a decrease in soil salinity and vice versa. And this is mainly because of the side-effects of the groundwater variations.

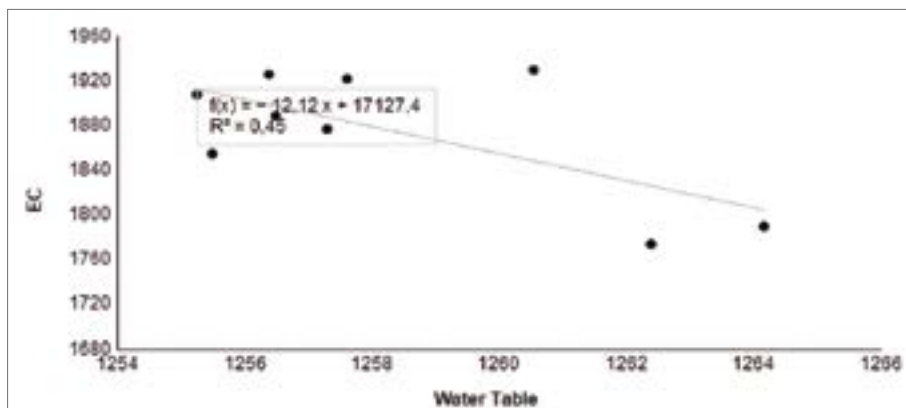
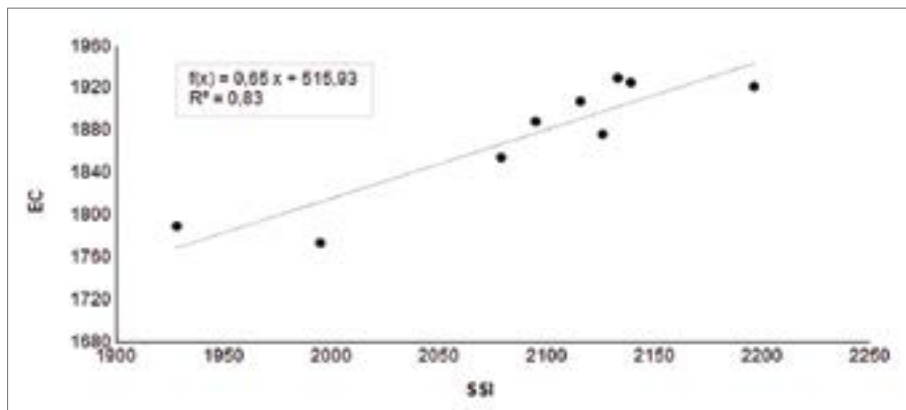
The linear regression graphs of EC-SSI, EC-water table, and water table-SSI are given in Figures 5-a, b, and c respectively. The associations of all the graph variables are statistically significant at 0.01 level. The regression coefficient for EC and SSI is the highest (0.83) which again indicates the best performance of the model in predicting each variable. The regression model for water table-EC and water table-SSI seems also good with regression coefficients of 0.44 and 0.52 respectively.

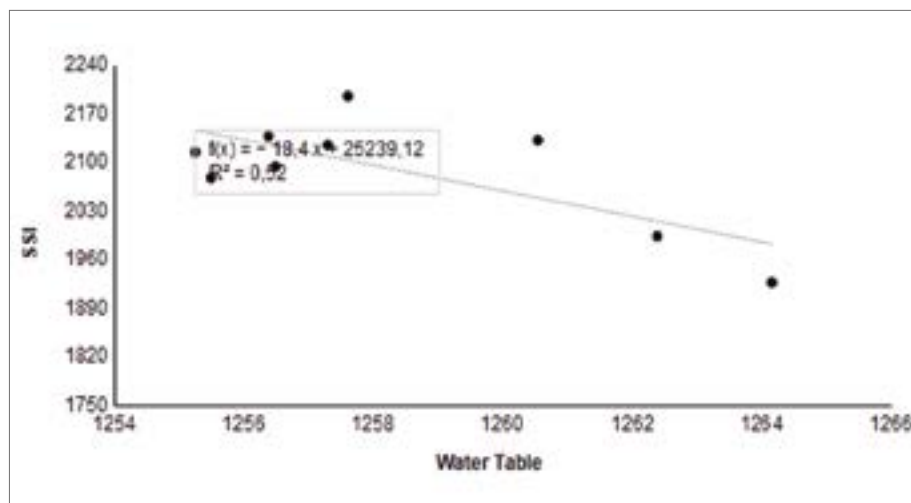






**Figure 4.** Temporal Interactions between Soil Salinity and water table (a) and soil and water salinity (b).

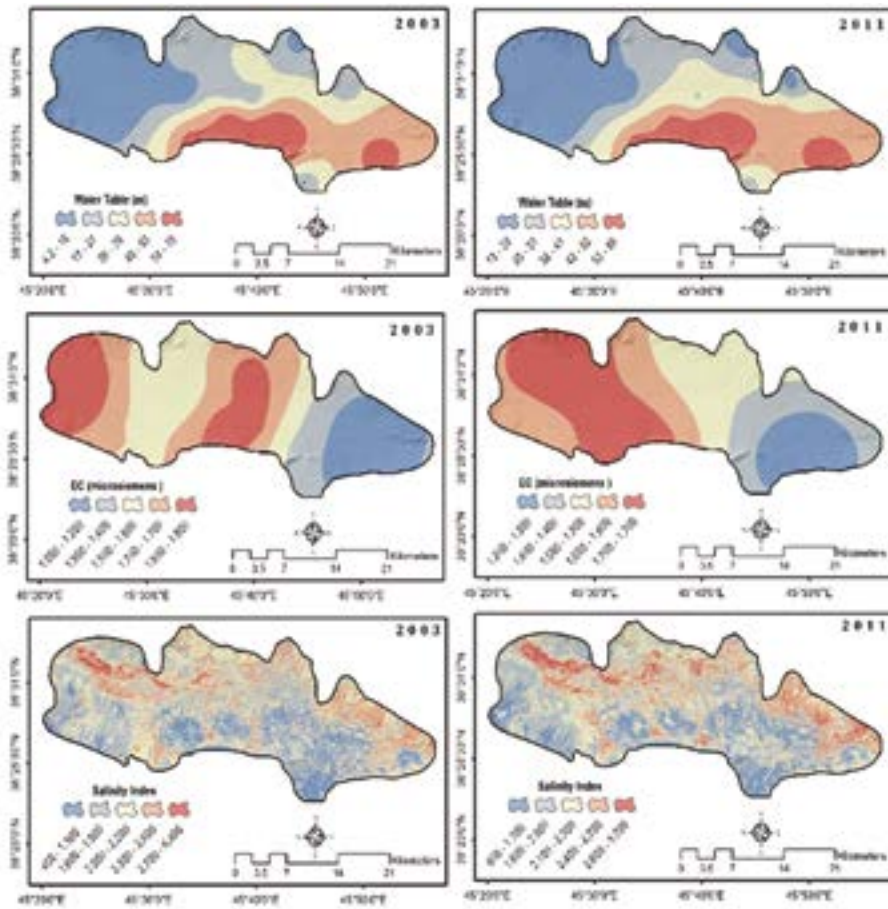




**Figure 5.** The Statistical association between the study variables.

### 3.3. Spatial Variability of the SSI, EC, and the Water Table

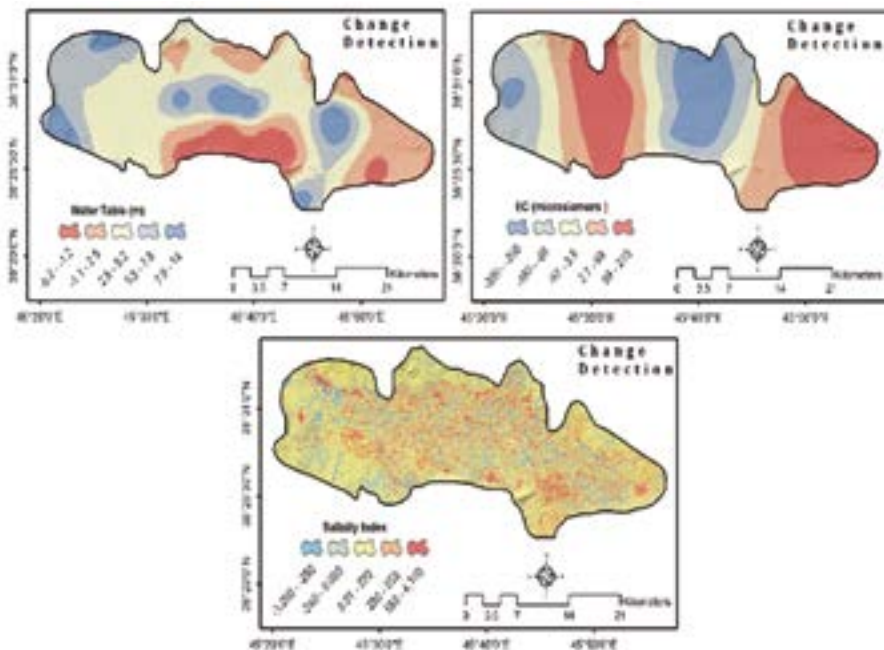
The variability of groundwater level, EC, and SSI in the spatial domain was investigated by portraying the spatial dispersion of the variables using the Kriging Geostatistical method. Figure 6 shows the spatial distribution of groundwater level, EC, and SSI. According to the maps, the eastern and central southern parts of the plain are more problematic concerning their water table status where the highest water level decline has occurred. The western and central northern parts, on the other hand, show a water level increase. Since the changes mimic the surface slope of the plain with a dominant east-west pattern (Lashkaripour et al., 2005), It can be inferred that the surface topography of the plain affects the discovered spatial pattern of groundwater level changes. Furthermore, the volume of the agricultural activities is high in the westerly flank of the plain which yields in the over-exploitation of the aquifer storage and as a results groundwater decline in the west. The EC maps also portray almost the same pattern as water table maps. The water salinity map of 2011 indicates that the severity of water salinity level has shifted mainly to the west which is ascribed to the groundwater decline in the west of the plain. SSI maps for 2003 and 2011 depict almost the same pattern with more concentration of the increased salinity in 2011.



**Figure 6.** Spatial Illustration of the variations of the water table, groundwater, and soil salinity during 2003 to 2011.

In order to unearth the transpired changes in the spatial context, the changes detection technique was applied to the raster layers of corresponding parameters. The change detection maps are illustrated in Figure 7. According to that, the highest decline in groundwater level was revealed to be 8.2 m which has occurred in the central south of the plain. The western and central parts show water level rise during the same period. The salinity change map indicates that the salinity rate has decreased in the west and a small section of the east while the center shows a salinity increase. Looking at figure 7, slight spatial relation is seen between groundwater level and salinity changes so that the decreasing wa-

ter level associates with salinity increase in the west. On the contrary, the zones of water salinity rise overlay the zones with water level rise in the south. The change detection map of SSI shows increased salinity which is chiefly vivid in the east of the plain. The decreased salinity index values are also more concentrated in the western parts. Although the visual interpretation of the SSI variations is challenging due to the small-scale changing zones apparent in the SSI change map, the overall variations seem harmonious with that of the water table and EC.



**Figure 7.** Spatial Illustration of the variations of the water table, groundwater, and soil salinity over the study area from 2003 to 2011.

#### 4. Conclusions

Groundwater plays a critical role in sustaining the water need of different sectors in the Marand plain. The main recharging source for the groundwater aquifer of the plain is precipitation whose dramatic variations on account of the climate change impacts have caused severe

challenges for the residents of the region. The variations of groundwater quantity and quality impact the soil coverage. The main activity of the residents of the region is agriculture therefore knowledge of the quantity and quality of groundwater and soil of the region is of utmost importance for the continuation of the economic activities as well as normal human life which necessitates monitoring of the groundwater variations and its associations with soil quality. In this premise, assessment and analysis of the fluctuations of groundwater level and quality were set as the main goal for the current study to find the temporal and spatial variations of groundwater salinity and its possible interactions with groundwater level fluctuations. The associations of the varying groundwater level and salinity with soil salinity were also investigated. The results from hydrography analysis indicate that during the study span (from 2003 to 2011), the Marand aquifer has suffered from an annual water table drop of about 96 cm. The kymography analysis also resulted in the 17 microsiemence increase in the groundwater salinity over the same time. The regression modeling resulted in a high association between the groundwater level fluctuations and that of water EC and soil salinity. To sum up, the findings of this study suggest that using remotely sensed data integrated with GIS tools, is a suitable means to implement groundwater and soil quality surveillance practices to provide useful information regarding the Spatio-temporal changes of these parameters over time.

## REFERENCES

- Abbas, A., Khan, S., Hussain, N., Hanjra, M. A., & Akabar, S. (2013). Characterizing soil salinity in irrigated agriculture using a remote sensing approach. *Physics and Chemistry of the Earth*, 55–57, 43–52. <https://doi.org/10.1016/j.pce.2010.12.004>.
- Abliz, A., Tiyp, T., Ghulam, A., Halik, Ü., Ding, J. L., Sawut, M. & Abliz, A. (2016). Effects of shallow groundwater table and salinity on soil salt dynamics in the Keriya Oasis, Northwestern China. *Environmental Earth Sciences*, 75(3), 260.
- Aggarwal, S. (2004). Principles of remote sensing. In Satellite remote sensing and GIS applications in agricultural meteorology. Proceedings of a training workshop held 7–11 July 2003 in Dehra Dun (India), AGM-8, WMO/TD-No. 1182 (p. 423).
- Allbed, A., Kumar, L. & Sinha, P. (2014). Mapping and modelling spatial variation in soil salinity in the Al Hassa Oasis based on remote sensing indicators and regression techniques. *Remote Sensing*, 6(2), 1137–1157. <https://doi.org/10.3390/rs6021137>.
- Asfaw, E., Suryabhadgavan, K. V. & Argaw, M. (2018). Soil salinity modeling and mapping using remote sensing and GIS: The case of Wonji sugar cane irrigation farm, Ethiopia. *Journal of the Saudi Society of Agricultural Sciences*, 17(3), 250–258.
- Azabdaftari, A. & Sunarb, F. (2016). Soil salinity mapping using multi-temporal landsat data. The International Archives of the Photogrammetry. *Remote Sensing and Spatial Information Sciences*, 7, 3–9.
- Bristow, K. L., Narayan, K. A., Kemei, J. K. & Charlesworth, P. B. (2006). Groundwater Level and Salinity in the Trent Road Area, North Burdekin Water Board: An update to June 2005. CSIRO Land and Water Science Report 24/06 July 2006. Retrieved from: <http://www.clw.csiro.au/publications/science/2006/sr24-06.pdf>.
- Dehni, A., Lounis, M. (2012). Remote sensing techniques for salt affected soil mapping: application to the Oran region of Algeria. *Procedia Eng.* 33, 188–198.
- Didi, S., Housni, F. E., del Toro, H. B., & Najine, A. (2019). Mapping of

soil salinity using the Landsat 8 image and direct field measurements: A case study of the tadla plain, Morocco. *Journal of the Indian Society of Remote Sensing*, 47(7), 1235-1243.

Elhag, M. (2016). Evaluation of different soil salinity mapping using remote sensing techniques in arid ecosystems, Saudi Arabia. *Journal of Sensors*, 2016.

Elhag, M. & Bahrawi, J. A. (2017). Soil salinity mapping and hydrological drought indices assessment in arid environments based on remote sensing techniques. Geoscientific Instrumentation. *Methods and Data Systems*, 6(1), 149.

Fontes Júnior, R. V. D. P. & Montenegro, A. A. D. A. (2017). Temporal dependence of potentiometric levels and groundwater salinity in alluvial aquifer upon rainfall and evapotranspiration. *RBRH*, 22.

Ghazali, M. F., Wikantika, K., Harto, A. B. & Kondoh, A. (2020). Generating soil salinity, soil moisture, soil pH from satellite imagery and its analysis. *Information Processing in Agriculture*, 7(2), 294-306.

Horriche, F. J. & Benabdallah, S. (2020). Assessing Aquifer Water Level and Salinity for a Managed Artificial Recharge Site Using Reclaimed Water. *Water*, 12(2), 341.

Hosam, H., Bayoumi, E. A. F. & Istva'n, P. (2010). Relationship between environmental impacts and modern agriculture. *O' buda University E-Bulletin*, 1(1), 87-98.

Huang, C., Wylie, B., Yang, L., Homer, C. & Zylstra, G. (2002). Derivation of a tasselled cap transformation based on Landsat 7 at-satellite reflectance. *International journal of remote sensing*, 23(8), 1741-1748.

Huisman, O. and De by, R. (200). "Principles of geographic information systems". An introductory textbook, The International Institute for Geo-Information Science and Earth Observation (ITC), The Netherlands.

Ibrakhimov, M. (2005). Spatial and temporal dynamics of groundwater table and salinity in Khorezm (Aral Sea Basin), Uzbekistan. Cuvillier.

Ibrakhimov, M., Khamzina, A., Forkutsa, I., Paluasheva, G., Lamers, J. P. A., Tischbein, B. & Martius, C. (2007). Groundwater table and salinity: Spatial and temporal distribution and influence on soil salinization in

Khorezm region (Uzbekistan, Aral Sea Basin). *Irrigation and Drainage systems*, 21(3-4), 219-236.

Jackson, R.B. Carpenter, S.R. Dahm, C.N. McKnight, D.M. Naiman, R.J. Postel, S.L. and Running, S.W. (2001). Water in a changing world. *Ecological Applications*, 11(4), 1027-1045.

Jarraya Horriche, F., & Benabdallah, S. (2020). Assessing Aquifer Water Level and Salinity for a Managed Artificial Recharge Site Using Reclaimed Water. *Water* (20734441), 12(2).

Khan, N.M., Rastoskuev, V.V., Sato, Y., Shiozawa, S., 2005. Assessment of hydro saline land degradation by using a simple approach of remote sensing indicators. *Agric. Water Manage.* 77,

Khorrami, B and Gunduz, O. "Analyses of meteorological drought and its impacts on groundwater fluctuations, a case study: Marand Plain (Iran)". *Pamukkale University Journal of Engineering Sciences*. doi: 10.5505/pajes.2019.63600.2019.

Khorrami, B. Roostaei, S. & Valizadeh, K. (2018). Assessment of Groundwater-Level Susceptibility to Degradation Based on Analytical Network Process (ANP). *International Journal of Environment and Geoinformatics*, 5(3), 314-324.

Korkmaz, N., Mehmet, G. & Asik, S. (2015). Temporal and spatial variations of groundwater level and salinity: A case study in the irrigated area of Menemen Plain in Western Turkey. *Hungarian Agricultural Engineering*, (28), 39-43.

Kumar, C. P. (2014). Groundwater data requirement and analysis. *National Institute of Hydrology*.

Larijani, K. M. (2005). Irans Water Crisis; Inducers, Challenges and Counter-Measures. ERSA 45<sup>th</sup> congress of the European Regional Science Association, Aug 2005, Vrije University, Amsterdam, Netherlands.

Lashkaripour, G. R., Asghari-Moghaddam, A., & Allaf-Najib, M. (2005). The effects of water table decline on the groundwater quality in Marand Plain, Northwest Iran. *Iranian Int. J. Sci*, 6(1), 47-60.

Lhissou, R., El Harti, A, & Chokmani, K. (2014). Mapping soil salinity



in irrigated land using optical remote sensing data. *Eurasian Journal of Soil Science*, 3(2), 82.

Lu D, Mausel P, Brondizio E and Moran, E. (2004). Change detection techniques. *International journal of remote sensing*, 25(12), 2365-2401.

Meena, R.S. (2017). Approximating Soil Physical Properties Using Geo-Statistical Models in Lower Kosi Basin, Of Ganga River System, India Prone to Flood Inundation. *International Journal of Civil Engineering and Technology (IJCIET)*, 8(5),1445-1459.

Ministry of Energy (MOE), 2018. Statistica on water resources. Retrieved from: <http://isn.moe.gov.ir/Statistical-Reports>

Najib, M. (2002). Hydrogeology of Marand plain and the Impacts of Groundwater level changes on water quality. MSc Dissertation, University of Sistan and Balouchestan, Zabol, Iran.

Nguyen, K. A., Liou, Y. A., Tran, H. P., Hoang, P. P. & Nguyen, T. H. (2020). Soil salinity assessment by using near-infrared channel and Vegetation Soil Salinity Index derived from Landsat 8 OLI data: a case study in the Tra Vinh Province, Mekong Delta, Vietnam. *Progress in Earth and Planetary Science*, 7(1), 1-16.

Qahroodi, Tali M. (2002). Kriging Interpolation Method, *Geography Researches*, 43, 95-108.

Rajaei, T. & Pouraslan, F. (2015). Spatiotemporal Groundwater Level Forecasting in Davarzan Plain. *Hydro geomorphology*,1(4), 1-19.

Rhoades, J. D. (1990). Determining soil Salinity from Measurements of Electrical conductivity. *Communications in Soil Science and Plant Analysis*, 21(13-16), 1887-1926. Doi: <https://doi.org/10.1080/00103629009368347>.

Rostamzadeh, H. Nikjoo, M. Asadi, E. & Jafarzadeh, J. (2016). A Survey on the Quality of Drinking Water in the Populated Areas of Ardabil Plain Using a Combination of Multi-Criteria Decision Making Models and Geo-statistics in the GIS Environment. *Hydro geomorphology*, 1(3), 43-60.

Sahfiei, Kh. (2008). Guidelines to Derive Aquifer Kymographs using Thiessen's Method, the Bureau of research and management of watersheds (Energy Ministry of Iran), Groundwater Department.

Sarah, I.O. (1997) Irrigation and land degradation: Implications for agriculture in Turkmenistan, central Asia. *Journal Arid Environments*, 37, 65-179.

Yan, S. F., Yu, S. E., Wu, Y. B., Pan, D. F., She, D. L. & Ji, J. (2015). Seasonal variations in groundwater level and salinity in coastal plain of eastern China influenced by climate. *Journal of Chemistry*, 201.



# **RARE EARTH ELEMENTS IN INDONESIA: PRELIMINARY DISCUSSION ON REGULATION, RESOURCES AND FUTURE POLICY PARADIGM**

*Syamsul Hidayat<sup>1</sup>*

---

## **Abstract**

This paper seeks to discuss Rare Earth Elements (REE) in Indonesia. This study elaborates required issues and puts regulations, resources and policy paradigm in one frame of discussion and analysis. In the new existing regulation, it is clearly stated that REE is grouped in metallic mineral group. This emphasized is positive for REE business permits and can avoid conflict of management in the field. Resources data from various studies and potential resources that have not been researched in detail indicate that amount of REE resources and reserves in Indonesia can still continue to grow. Export restriction for REE and initiation of Indonesia's long-term REE based strategic projects can be considered as part of policy paradigm. Considering unrenewable resource of REE and

---

<sup>1</sup> PhD Student, Eskisehir Osmangazi University, Faculty of Engineering and Architecture, Mining Engineering

limit existing resources anticipation in the future, creative approach to discover and extract new resources is another new reasonable paradigm. Characteristics of Indonesian nature are unique factors that encourage complexity of environmental protection and it will be significant challenge for the environmental protection action plan.

**Keywords:** REE, Regulation, Resources, Policy Paradigm.

## 1. Introduction

The issue of Rare Earth Elements (REE) is one of the serious concerns in Indonesia's mining policy. Researches on REE that have been continuously promoted in the last few years will also continue to be carried out for the next years. Valuable information in the previous research will become as additional input points and references for the Indonesian government related to the management of REE in the future. In addition to other resources, tailings and by-products of raw material processing are among of REE resources in Indonesia. REE resources are also getting special attention because of the strategic benefits of this commodity for industries such as transportation, electronics, military and etc. Downstream processing of mineral policy approach and strategic issues of REE at international level have encourage influence effects on mineral policy, including policy on REE in Indonesia.

Studies related to REE in Indonesia are commonly conducted separately according to the existing topics. There are studies related to technical issues of mineral content, issues related to technical enrichment, analysis refer to different kind of resources and other various issues. Rosita et. al., (2020), characterized three Indonesian coal fly ashes obtained from coal-fired power plants in Indonesia, the characterization results showed that the ashes had a critical REY (rare-earth elements and yttrium) content exceeding 38 % (Rosita, et al., 2020). Purwadi et. al., (2019) conducted study on REE in tin mining tailings. Tailing samples were collected from two tin mine tailings in Bangka Island. Results showed that the tailing samples were identified as quartz and contained a high amount of erbium between 111.6 and 3768.4  $\mu\text{g/g}$  (Purwadi, et al., 2019) Maulana et. al., (2014) reported the geochemistry of rare earth elements (REE) in the weathered crusts of granitic rocks at Mamasa and Palu Region, Sulawesi Island. The result shows that the total REE content of the weathered crust are relatively elevated compared to the parent rocks (Maulana, et al., 2014). Warmada et al. (2007) reported fluid inclusion, Rare-Earth Element and stable isotope study of Carbonate Minerals from the Pongkor Gold – Silver Deposit, West Java. The study shows that the abundance of rare earth and yttrium (REY) in carbonate samples is very low ( $\Sigma\text{REY}$  mostly  $< 2$  ppm) (Warmada, 2007). Putra and Sobirin (2018)

reported result of mapping Apatite-Ilmenite Rare Earth Element mineralized zone in Sijuk Distric, Belitung Island. Alteration, geological structure, and lithology data were used as variables. The study concluded that utilization of this mineral in Sijuk district is still not very good even though the statistical data shows the amount of potential abundance of apatite-ilmenite mineral in that location (Putra, M. I. J., Sobirin, 2018).

Study on REE from multiple perspectives is urgently to be performed. It is important because of interests of resource utilization and scope policy related to REE in the future under the Indonesian new mining law. Based on several important issues of mining such as implementing of downstream processing of minerals, mining policy critical issues, technical and general issues of studies on REE that have been carried out, it is necessary to conduct study on REE in Indonesia which lays down regulations, resources and projections of policy opportunities in one frame of discussion and analysis.

## **2. Material and Methods**

This paper contains study of REE and its related issues, by taking case studies in Indonesia. Literature study based on published journals and conferences and reports from various sources is the approach to achieve the objectives. Data and information on regulation, resources and policy approach related to REE were collected from previous sources to support discussion in the paper. Based on collected data and information, substantial analysis and conclusion are submitted in the end.

## **3. Result**

### **3.1. Policy and Regulation**

Indonesia's mining policy entered new phase when Law 4/2009 was issued. This law was valid for 11 years until an amendment was made with the enactment of Law 3/2020. The Omnibus Law 2020 also contains articles related to mining policy. Many new issues are regulated in these 2 laws, one of the important issues is the obligation to process raw material domestically. Classification of Mineral commodities into 5 groups of

minerals, namely radioactive minerals, metallic minerals, non-metallic minerals, rocks and coal provides details between groups and for differentiating permits in the field. These two laws generally classify mineral commodities in same manner but in their derived rules there are differences in details of each group. The difference lies in the details of which minerals are classified in radioactive group and which minerals are classified in metallic group, this detail directly related to REE.

Rules related to REE can be referred to the Mining Law and its derivative regulation. Mining business, according to article 34 of Law 4/2009, can be operated into five classified groups as mentioned above consisting of radioactive minerals, metallic minerals, non-metallic minerals, rocks, and coal (Republik Indonesia, 2009). Law 4/2009 has been amended through Law 3/2020 and the Omnibus Law 2020. The updated derivative rules concerning the elaboration of these groups of mining commodities are contained in the Government Regulation No. 96/2021 (Presiden Republik Indonesia, 2021; Republik Indonesia, 2020). Mineral grouping that are indirectly related to REE in the old regulations is contained in Government Regulation No. 23/2010 which has been revised several times, fifth revised was issued as Government Regulation No. 8/2018 (Presiden Republik Indonesia, 2018; Presiden Republik Indonesia, 2010). Types of radioactive minerals and metallic minerals in that old regulation are mentioned in article 2 paragraph 2a stated that radioactive minerals include radium, thorium, uranium, monazite, and other radioactive minerals. Under the old rules as can be seen in above article, mineral such as monazite (which can contain REE) are still included in the radioactive minerals group. According to new regulation types of radioactive minerals and metallic minerals are mentioned in Government Regulation No. 96/2021 article 2 (Presiden Republik Indonesia, 2021). In article 2 paragraph 1a stated that radioactive minerals Include uranium, thorium, and other radioactive minerals. Article 2 Paragraph 1b states that metallic minerals include: aluminium, antimony, arsenic, basnasite, bauxite, beryllium, iron ore, bismuth, cadmium, cesium, gold, galena, gallium, germanium, hafnium, indium, iridium, chrome, kcbai, chromite, lithium, rare earth elements, magnesium, manganese, molybdenum, monazite, nickel, niobium, osmium, iron sands, palladium, silver, platinum, rhodium, ruthenium, selenium, zinc, senodm, cinnabar,



strontium, tantalum, tellurium, copper, tin, titanium, vanadium, tungsten, and zirconium; (Presiden Republik Indonesia, 2021). Based on the above list, metal minerals consist of 48 types, monazite minerals (that can contain REE) which were previously included in the radioactive minerals group are now included in metallic minerals group. In addition, in this new regulation it is emphasized that REE is included in the metallic minerals group, this also did not exist in the old regulation.

In fact, until now there has been no Mining Business Permit issued specifically for REE, but it issued for monazite minerals ( $[(Ce, La, Pr, Nd, Th, U)(PO_4)_3]$  and xenotime ( $PO_4$ ) and xenotime ( $PO_4$ ) (Pusat Sumber Daya Mineral, 2019). In terms of mineralogy, REE content in monazite is more than 90% while the radioactive element is less than 5%, based on this percentage monazite can be included in metallic mineral commodities, so that its exploitation is same as other metal commodities (Pusat Sumber Daya Mineral, 2019). Minerals that containing REE (monazite, zircon and xenotime) are secondary minerals from the main minerals such as tin, gold, bauxite and nickel laterite. Therefore its business management cannot be equated with management of common mineral commodities (Pusat Sumber Daya Mineral, 2019). However, the obligation to process raw materials domestically is still regulated in Law 3/2020 articles 102-104, which is most likely to be related directly or indirectly to REE. Such assertions would relate directly or indirectly to REEs in terms of for example by-products or residues from the processing of copper metal minerals and nickel tailings. Further rules related to By-product or residue from metal mineral processing will be listed in other derivative rules such as regulations at the level of ministerial regulations.

### 3.2 REE Resources in Indonesia

Locations of REE are distributed on the big islands of Indonesia such as Sumatra, Kalimantan, Java, Sulawesi and Papua. Exact amounts of resources in all locations have not been identified because field research is still being performed. Resource values of several locations have been identified. Based on the type, REE resource potential in Indonesia can be divided into 2 (two) types, namely placer deposit and lateritic deposit (Pusat Sumber Daya Mineral, 2019).

### 3.2.1 Placer Deposit Type

As an associated mineral for tin, REE placer-type is often found in tin resource locations, namely on the tin granite route that passes through the Riau Islands, Bangka Belitung Islands and the southern part of West Kalimantan. The potential of placer REE is inseparable from the estimation of tin potential because the two are very closely related, deposited together in alluvial tin deposits, especially those found in Bangka Belitung and Riau Islands, both on land (on shore) and in waters (off shore) (Pusat Sumber Daya Mineral, 2019).

Referring to the 2014 tin exploration data, total potential resources of placer tin ore deposits both from land and offshore in the areas Bangka, Belitung and Kundur reached 7.010.075.409 m<sup>3</sup> with details 189.323 tons of monazite, 21.876 tons of xenotim and 1.226.268 tons of zircon (Pusat Sumber Daya Mineral, 2019). The Geological Resource Center-Geological Agency in 2014 conducted study to determine the potential of REE resources in tailings deposits at Bangka Island using the remote sensing interpretation method. The result of the study shows that the thickness of tailings deposit is 4 - 6 m<sup>2</sup>, the total area of tailings deposit is 500.000 ha, so the volume is 5.500.000.000 m<sup>3</sup>. Total REE content is 9,5 g/m<sup>3</sup>, the REE tonnage reached 52.387.500.000 g or 52.000 tons (Pusat Sumber Daya Mineral, 2019).

### 3.2.2 Residual/Lateric Deposit Type

This type is a type of deposit that has begun to be developed in several REE producing countries. The potential for the lateritic type of REE in Indonesia is quite large, if pointed out from geological and climatic point of view the conditions of Indonesia allow the occurrence of lateritic deposits. Several investigation activities have been carried out by PSDMBP/CCGMR (Pusat Sumber Daya Mineral Batubara dan Panas Bumi / Center for Coal and Geothermal Mineral Resources) and BATAN/NNEA (Badan Tenaga Nuklir Nasional / National Nuclear Energy Agency) related to sediment (Pusat Sumber Daya Mineral, 2019). Table 1 contains recapitulation results from various research sources related to the calculation of hypothetical resources for REE deposits of residual/lateritic type, referenced and modified from (Pusat Sumber Daya Mineral, 2019).

**Table 1.** REE Resources Residual Type /Lateritic.

No.	Location	Province	Inferred Resources			Data Source
			Ore (Ton)	REE Content (ppm)	REE (Ton)	
1.	Parmonangan	North Sumatera	4.426.115, 4	-	19.917	PSDMBP/ CCGMR
2.	Ketapang	West Kalimantan	1.928.640	-	219	PSDMBP/ CCGMR
3.	Taan	West Sulawesi	7.319.193	859-1.416	-	Sikadana dkk, 2018, BATAN/NNEA
4.	Banggai	Central Sulawesi	1.515.056	-	443	PSDMBP/ CCGMR

### 3.2.3 Ion Adsorption dan Inside Coal Deposit Type

The potential of ion adsorption type of REE resources, especially those found in kaolin deposits in Belitung Island, cannot be calculated because of the limited data obtained from hand drilling and test wells. Although the result of chemical analysis has shown the presence of REE content, this potential is still an indication of REE (Pusat Sumber Daya Mineral, 2019). Currently, research on the potential of REE in Indonesian coal is still very limited. However, based on geological conditions and the amount of Indonesia's coal potential, it is estimated that the potential of REE in Indonesian coal is quite significant (Pusat Sumber Daya Mineral, 2019).

In summary, the potential of minerals containing REE in Indonesia in general is as follows: first, Monazite minerals ( $(\text{REE, Th})\text{PO}_3$ ) and Xenotim minerals ( $\text{YPO}_4$ ) are by-products of tin ore processing. Second, Zirconium silicate minerals (Zr, Th, Y, Ce) ( $\text{SiO}_2$ ) are by-products of tin and gold ores processing and in zircon sands. Third, rare earth ferrotitanates minerals (REE, Ca, Na) (Ti, Fe) ( $\text{O}_2$ ) are residues from the processing of Bauxite into alumina. Fourth, nickel laterite ores (52 ppm Sc, 18 ppm Nd, 60 ppm Pr, 8 ppm Dy), are by-product of nickel laterite ore

processing through hydrometallurgical processes (HPAL-high pressure acid leaching). Fifth, other potential minerals such as granite, coal ash/FABA (monazite (Ce, La, Y, Th) phosphate) and others (Kementrian Energi dan Sumber daya Mineral Republik Indonesia, 2020).

Amount of monazite and xenotime resources, amount of red mud deposits containing REE, and amount of nickel limonite reserves that REE can be obtained from its inside can be summarized from the available data. Indonesia already has monazite resources of 185.179 tons of metal which can be further calculated as reserves (Kementrian Energi dan Sumber daya Mineral Republik Indonesia, 2020). Indonesia already has xenotime resources of 20.734 tons of metal which can be further calculated as reserves (Kementrian Energi dan Sumber daya Mineral Republik Indonesia, 2020). REE will also be obtained from Red Mud (residue from processing of bauxite into alumina), in 2024 it is predicted that 18 million tons of red mud deposits will be available from the existing process activities (Kementrian Energi dan Sumber daya Mineral Republik Indonesia, 2020). REE in Indonesia also has the potential to be obtained from by-products of nickel laterite. Indonesia is recorded to have proven reserves of nickel limonite ore of 359 million tons (Kementrian Energi dan Sumber daya Mineral Republik Indonesia, 2020).

In addition to studies conducted by institutions as described above, studies on REE are also conducted by researchers from others institutions based on various different interest. Study on characteristics of REE from various sources can provide an overview of the general content of REE in each different location. In the study of Rosita et. al., (2020), three Indonesian coal fly ashes (which obtained from Tuban, Indramayu, and Paiton-1 coal-fired power plants in Indonesia) were characterized and subjected to sequential physical separation processes. Three Indonesian coal fly ashes were characterized as potential REY (rare-earth elements and yttrium) sources. An REY enrichment process is required before they can be recovered. Of the three samples, that originating from South Sumatera coal combustion in the Indramayu coal-fired power plant had a unique character because of its relatively high contents of  $\text{Fe}_2\text{O}_3$  and  $\text{CaO}$ . It was found that the REY content increased as the particle size of the ash decreased (Rosita, W. et al., 2021). Handoko and Sanjaya; (2018)

reported characteristics and genesis of Rare Earth Element (REE) in western Indonesia. The research shows that the potential REE mines can be found in several different locations in Indonesia, such as Tin Island, Sumatera, and Kalimantan. Most of them are composed of monazite, zircon, and xenotime as rare earth minerals. Monazite is known for its elevated number of radioactive elements, so study about radioactive content and more environment friendly ore processing becomes compulsory. Rare earth element found in several different deposit forms; secondary deposit and primary deposit. Secondary deposit that occurred in the given area in ion-absorption clay and placer deposit form derived from weathering of primary deposit. In addition, primary deposit is discovered in the area in the form of pegmatite and granitic rocks (Handoko, A. D., & Sanjaya, E., 2018).

Same issue as the above studies is regarding the characteristics of minerals and their composition. Harjanto et. al., (2013), reported some basic characteristics of mineralogy and chemical composition of the REE minerals associated with tin ores. The main REE minerals in such ores include monazite and xenotime, which contain small amounts of radioactive elements such as thorium (Th) and uranium (U). Potential methods of REE mineral beneficiation and extraction are discussed. Processing techniques of REE minerals associated with tin ore includes concentration and extraction process. Concentration of REE minerals associated with tin ore may utilize the combination of magnetic and high tensions separator process. Modification and optimization of the concentration process in tin ore processing plant should be undertaken to produce higher grade REE minerals products. Further evaluation to select the extraction process of minerals concentrate to individual REE compounds should be undertaken based on their mineralogy, physical and chemical characteristics (Harjanto, S., Virdhian, S., & Afrilinda, E., 2013).

Studies on the technical processing of materials in order to obtain REE elements in its inside can provide more reference and options so that can be determined which are more optimally applied in the field. Bahti et. al., (2011) reported extraction and chromatographic studies on rare-earth elements (REEs) from their minerals, applied for REE in Indonesia. Resulted from the study critical point and recommendation are as

follows: 1. Development and improvements in digestion and separation methods have been done and the resulted methods could be adopted for further development into the technology for up-scaled production of rare-earth elements. 2. Extraction and chromatographic methods have been shown to be prospective for further development as the technology for the preparation of pure rare-earth element products. 3. Rare-earth mineral deposits, which are abundant and spread out of Indonesian archipelagos, must be exploited and processed for optimal economic benefit (Bahti, H. H., Mulyasih, Y., & Anggraeni, A., 2011). Prameswara et. al., (2021) Studied leaching behavior and kinetic of light and heavy REE from Zircon Tailings in Indonesia. The objective is to determine the effects of several operating conditions in the leaching process. In this study, REMs (Rare Earth Metals) were extracted from zircon tailings. The optimum REM leaching conditions of the zircon tailing alkaline fusion products occurred at an HCl concentration of 2 M, leaching temperature of 80° C, and S/L (solid-liquid) ratio of 10 g/100 mL for 1 h (Prameswara, G. et al., 2021).

### 3.3. Policy Paradigm

Indonesia's mining policy for last 12 years has provided opportunities to perform downstream processing of minerals. It can be seen from Law 4/2009 and Law 3/2020. The impacts of Indonesia's mining policies related to the downstream process of minerals are the obligatory for raw material processing domestically and export ban. Hidayat (2021) emphasized that the production of certain mineral types has changed significantly due to the export ban policy which also has contributed to the mining sector's contribution to Indonesian exports (Hidayat, S., 2021). PWC (2019) reported that the production of nickel and bauxite has also continued to increase after the relaxation of the ban on exports of nickel ore and washed bauxite by the Indonesian Government at the beginning of 2017. Another factor contributing to the increase is the production from the new nickel smelters that have been coming on-line since 2017 together with higher global nickel prices driven by increased demand for the electric vehicle industry (Price Water House Coopers, 2019).

In the Law 3/2020, the obligation to process raw materials domestically is still regulated. The consequence of the policy based on this Law is encourage multiplier effects to the mining activities in Indonesia. The effects under consideration can be seen in export ban, process of building smelter facilities, the availability of local infrastructure to support the smelter industry, fluctuations in export volume of metal commodities, environmental protection process and etc. The policy also has impacts on REE. REE Resources on tailings and by-products of metal processing have also received special attention in Indonesia's mining policy. Export ban, utilization of REE for long-term domestic strategic industries, creative approach to discover and to extract new resources and environmental protection strategies are challenges and opportunities for future policy paradigm of REE in Indonesia.

Discover alternative resources and proper environmental protection management are interesting issues related to REE. Recycling as a different approach to obtaining new REE resources has also been the subject of scientific discussion. Electronic waste, for example, can be an alternative source to obtain REE in addition to conventional methods of extracting from earth, but it has not been as significant resource. Klinger (2018) stated that annually less than 1% of rare earth elements consumed are recycled, meaning that we are accumulating untapped stockpiles in our electronic waste (Klinger, J. M., 2018). Charalampides et. al., (2016) emphasized that the mining and processing of rare earth metals usually result in significant environmental defects. Many deposits are associated with high concentrations of radioactive elements such as uranium and thorium, which requires separate treatment and disposal. The accumulation of rare earth elements in soils has occurred due to pollution caused by the exploitation of rare earth resources and the wide use of rare earths as fertilizers in agriculture (Charalampides, G. et al., 2016).

#### **4. Discussion**

The existing derivative regulation of Law 3/2020 governing REE is Government Regulation No. 96/2021. The difference between this regulation and the previous regulation is about the grouping of mineral commodities. In this regulation it is clearly stated that REE is grouped

in metallic minerals group. This grouping is positive for clarity of REE management permits under metallic minerals and can avoid conflict of management. But this problem should not only be end in the clear classification of REE in to metallic group. Positioning REE only as a metal group without consider the strategic importance of these minerals in international market demand and without consider their opportunities for domestic strategic demand is same as to eliminate opportunity for improvisation in policy. Indonesia should move to the next step regarding management of REE. Derivative regulation regarding REE in Indonesia have to pay close attention using comprehensive different points of view. Management authority and another strategic action plan must be positioned in same level of interest.

REE resources and reserves in Indonesia are increasingly being encouraged to be researched in recent years. Resources data both from various studies and potential resources that have not been researched in detail indicate that amount of REE resources and reserves in Indonesia can still continue to grow. Advance research under the initiation of official government institutions and/or under the initiation of companies that have potential deposits/resources will likely continue to be carried out in the future. Under the existing policy, Indonesia will be able to produce centralized data related to the source and amount of REE. Centralization of data will be useful for future management.

Export ban on raw materials is a crucial issue in Indonesia's new mining policy and it gives impacts on fluctuations of export volume of Indonesian metal commodities. The application of export restriction for REE can be considered as part of policy paradigm. It should not only to stimulate domestic processing and refining activities and to restrict export volumes, but also more than that, the paradigm can be more strategic. It can be accompanied by the pioneering of Indonesia's long-term REE based strategic projects. This paradigm will not only involve stakeholders in the mining sector but also will involve cross-sectoral such as Minister of Industry, Minister of Education, Minister of Research and Education, Minister of Trade, market practitioners and others. This paradigm will be closely related to triple helix of innovation vision of the country. Activities that only focus on discovering, extracting, process-



ing of raw materials and selling should be considered as conventional paradigm. The availability of REE resources and other material deposit should be considered as basic capital to build technology and national strategic industries in the future.

Transfer of processing technology can also be a new paradigm. Transfer of technology for processing equipment, whether on small or large scale, can become a part of Indonesia's long-term strategy, not only for REE sector but also for other materials sectors. Applied technology of processing equipment from other countries, especially from the countries of mining investors, as much as possible is necessary to encourage transfer of processing technology mechanism. This is antithesis of conventional paradigms that only focus on rent, import and use. This approach will involve many activities such as agreements, human resources and research capabilities building, policies, research budget allocation, and will involve stakeholders from Indonesia, industry and concerned country.

According to current studies, Indonesia still not apply creative approach to discovery and extract new REE resources. Availability of human resources and technology play important rule to discovery new resources and to increase amount of resources list. Some existing mining companies can directly operate enrichment of REE from their tailings and by-product of metal processing. Joint activities to discovery amount of REE from these two resources with existing companies or third party also can be considered. Considering unrenewable resource of REE and limit existing resources anticipation in the future, creative approach to discovery and extract new resources is reasonable alternative approach and another new paradigm. Creative approach to discovery beside above mentioned conventional resources can be applied, for example recycling of electronic waste. The technology has been not widely available in Indonesia, but it can be planed for middle or long period. Capacity building related to human resources and technology must be applied as soon as possible in this concern if Indonesia plane to become REE and Industry based country in the future.

Environment always become important issue for sustainability of mining industries activities. Characteristics of Indonesian nature posi-

tioned in equator region that more rainfall, earthquake and vulnerable land stability are unique factors that encourage complexity of environmental protection action in the field. Soil and water pollution are critical concern in this issue. Protection of environmental carrying capacity for human life and other elements of ecosystem should take part in planning agenda. All existing factors should be put in one frame which is equally important in environmental protection planning.

## 5. Conclusion

Putting the Law and regulation, resources, and future policy paradigm in one study framework for REE can help to understand, to provide solutions and some specific recommendations on this issue in a more comprehensive perspective. The existing derivative regulation of law 3/2020 governing REE is Government Regulation No. 96/2021. It is clearly stated that REE is grouped in metallic mineral group. This emphasized is positive for REE business permits and can avoid conflict of management in the field. REE resources and reserves in Indonesia have been encouraged to be researched in recent years. Amount of REE resources and reserves can still continue to grow. Export restriction for REE and initiation of Indonesia's long-term REE based strategic projects can be considered as part of policy paradigm. Generally, Indonesia is still implementing conventional paradigm that focus on discovering, extracting, processing of raw materials and selling, still not apply deep concern to perform REE and other material resources as basic capital to build technology and national strategic project. Creative approach to discovery and extract new resources still not become serious concern. Considering unrenewable resource of REE and limit existing resources anticipation in the future, creative approach to discovery and extract new resources is reasonable alternative approach and another new paradigm for Indonesia, for example, in electronic waste, recycling. Characteristics of Indonesian nature positioned in equator region that more rainfall, earthquake and vulnerable land stability are unique factors that encourage complexity of environmental protection action in the field. That will be significant challenge for the environmental protection action plan.

## REFERENCES

Rosita, W., Bendiyasa, I. M., Perdana, I., & Anggara, F. (2020). Sequential particle-size and magnetic separation for enrichment of rare-earth elements and yttrium in Indonesia coal fly ash. *Journal of Environmental Chemical Engineering*, 8(1), 103575.

Purwadi, I., van der Werff, H., & Lievens, C. (2019). Reflectance spectroscopy and geochemical analysis of rare earth element-bearing tailings: A case study of two abandoned tin mine sites in Bangka Island, Indonesia. *International Journal of Applied Earth Observation and Geoinformation*, 74, 239-247.

Maulana, A., Yonezu, K., & Watanabe, K. (2014). Geochemistry of rare earth elements (REE) in the weathered crusts from the granitic rocks in Sulawesi Island, Indonesia. *Journal of Earth Science*, 25(3), 460-472.

Warmada, I. W., Lehmann, B., Simandjuntak, M. & Hemes, H. S. (2007). Fluid inclusion, rare-earth element and stable isotope study of carbonate minerals from the Pongkor epithermal gold-silver deposit, West Java, Indonesia. *Resource Geology*, 57(2), 124-135.

Putra, M. I. J., Sobirin. (2018). Mapping Apatite-Ilmenite Rare Earth Element Mineralized Zone using Fuzzy Logic Method in Sijuk District, Belitung. *International Journal of Remote Sensing and Earth Sciences (IJReSES)*, 15(1), 1-14.

Republik Indonesia. (2009). Undang-Undang Republik Indonesia Nomor 4 Tahun 2009 Tentang Pertambangan Mineral dan Batubara [ Republic of Indonesia, 2009. Law Number 4 of 2009 on Mineral and Coal Mining].

Republik Indonesia. (2020). Undang-Undang Republik Indonesia Nomor 3 Tahun 2020 Tentang Perubahan Atas Undang-Undang Nomor 4 Tahun 2009 Tentang Pertambangan Mineral dan Batubara [ Republic of Indonesia, 2020. Law Number 3 of 2020 Concerning Amendments to the Law Number 4 Year 2009 Regarding Mineral and Coal Mining]

Presiden Republik Indonesia. (2021). Peraturan Pemerintah Republik Indonesia No. 96 Tahun 2021 Tentang Pelaksanaan Kegiatan Usaha Pertambangan Mineral dan Batubara. [ President of the Republic of Indonesia. 2021. Government Regulation of the Republic of Indonesia No. 96 of 2021 about the Implementation of Mineral and Coal Mining Business Activities]

Presiden Republik Indonesia. (2010). Peraturan Pemerintah Republik Indonesia No. 23 Tahun 2010 Tentang Pelaksanaan Kegiatan Usaha Pertambangan Mineral dan Batubara. [ President of the Republic of Indonesia. 2010. Government Regulation of the Republic of Indonesia No. 23 of 2010 about the Implementation of Mineral and Coal Mining Business Activities]

Presiden Republik Indonesia. (2018). Peraturan Pemerintah Republik Indonesia

Nomor 8 Tahun 2018 Tentang Perubahan Kelima atas Peraturan Pemerintah No. 23 Tahun 2010 Tentang Pelaksanaan Kegiatan Usaha Pertambangan Mineral dan Batubara. [ President of the Republic of Indonesia. 2018. Government Regulation of the Republic of Indonesia Number 8 of 2018 concerning the Fifth Amendment to Government Regulation No. 23 of 2010 about the Implementation of Mineral and Coal Mining Business Activities]

Pusat Sumber Daya Mineral, Batubara dan Panas bumi Badan Geologi Kementerian Energi dan Sumber Daya Mineral. (2019). Potensi Logam Tanah Jarang di Indonesia. [Center for Mineral, Coal and Geothermal Resources, Geological Agency of the Ministry of Energy and Mineral Resources Republic of Indonesia. (2019). Potential of Rare Earth Elements in Indonesia]

Kementrian Energi dan Sumber daya Mineral Republik Indonesia. (2020). Booklet Tambang Tanah Jarang 2020 [Ministry of Energy and Mineral Resources of the Republic of Indonesia. (2020). Rare Earth Mining Booklet 2020] Retrieved from: <https://www.esdm.go.id/id/booklet/booklet-tambang-tanah-jarang-2020>(15.09.2020).

Handoko, A. D., & Sanjaya, E. (2018). Characteristics and genesis of Rare Earth Element (REE) in western Indonesia. In IOP Conference Series: Earth and Environmental Science (118(1), 012077). IOP Publishing.

Harjanto, S., Virdhian, S., & Afrilinda, E. (2013). Characterization of Indonesia rare earth minerals and their potential processing techniques. *J. Rare Earth*, 52, 99-108.

Bahti, H. H., Mulyasih, Y., & Anggraeni, A. (2011). Extraction and chromatographic studies on rare-earth elements (REEs) from their minerals: the prospect of REEs production in Indonesia. In Proceedings of the 2nd International Seminar on Chemistry, 421-430.

Prameswara, G., Trisnawati, I., Mulyono, P., Prasetya, A., & Petrus, H. T. B. M. (2021). Leaching Behaviour and Kinetic of Light and Heavy Rare Earth Elements (REE) from Zircon Tailings in Indonesia. *JOM*, 73(4), 988-998.

Hidayat, S. (2021). Indonesia's Mining Policy: Particular Discussions on Curent Issues IV. International Istanbul Scientific Research Congress, Proceedings Book, 257-264.

Price Water House Coopers. (2019). *Mining in Indonesia Investment and Taxation Guide*.

Klinger, J. M. (2018). Rare earth elements: Development, Sustainability and Policy Issues. *The Extractive Industries and Society*, 5(1), 1-7.

Charalampides, G., Vatalis, K., Karayannis, V., & Baklavaridis, A. (2016). Environmental Defects and Economic Impact on Global Market of Rare Earth Metals. In IOP Conference Series: Materials Science and Engineering (161(1), 012069). IOP Publishing.



**MİMARLIK VE MÜHENDİSLİK ÇALIŞMALARI**  
*ARCHITECTURE AND ENGINEERING STUDIES*



# KÜLTÜR VE POLİTİKANIN OSMANLI DÖNEMİNDEN GÜNÜMÜZE KADAR KUZAY KIBRIS TÜRK CUMHURİYETİ KONUTLARININ ÜZERİNDE ETKİSİ

*Ziba Sami<sup>1</sup>*

---

## Özet

Mimarlıkta bir bina türü olarak konut başlangıçtan bu yana, çağlar boyunca farklı faktörlerle etkilenmiştir. Bu faktörlerin önemlilerinden kültür ve politikadan bahsetmek mümkündür. Bu çalışma kapsamında, Kuzey Kıbrıs Türk Cumhuriyeti'ndeki konutlar Osmanlı imparatorundan günümüze kadar kültür ve politika açısından incelenmiştir. Osmanlı imparatorluğu döneminde sahip olduğu alanlarda değişiklik olmadığını biliyoruz peki mimari konusunda bu nasıl devam ediyor ve Kıbrıs'ta yaşayan insanlar kendi yaptıkları konutları yapmayı devam ediyorlar mı yoksa konut yaptıklarından politikadan etkileniyorlar mı? Araştırma kapsamında Osmanlı döneminin etkisi, daha sonra İngiliz ve ardından olan savaşların etkisi; İki toplumun uzun süre beraber yaşadıkları sonra ayırması konutların üzerinde nasıl bir iz bıraktığını ve etkileri

---

1 PhD Student, Yıldız Teknik Üniversitesi, Mimarlık Fakültesi, Mimari Tasarım



üzerinde yapılmıştır. Genel bir bakış açısıyla, konutun tarihsel süreçteki durumu, literatür çalışması ve çeşitli yayınlardan incelenmiştir. Bundan hareketle araştırma üç ana bölümden oluşmaktadır. Birincisi konut tanımı ve tarih sürecinde gelişimi, ikinci bölümde kültür ve politikanın faktörleri mimarlıkta incelenmesi ve üçüncü bölümde ise değerlendirme ve olgular konutlar üzerinde ele alınmıştır.

**Anahtar Kelimeler:** Konut(lar), Kültür, Politika, Kıbrıs, Tarih.

## 1. Giriş

Konutlar, toplumun kültürel ve politika değişkenlerinin ve değerlerinin maddi / fiziksel ifadesidir ve tasarım ve mekân kullanımı kavramı ile bağlantılı kişisel ve psikolojik işlevleri temsil eder. Geleneksel olarak, konut kavramı, bir toplumun sosyo-kültürel, politik ve ekonomik özelliklerinin yansımalarını bütünleştirir ve gösterir, çünkü konut yapıları, mevcut belirli çevresel koşullarla benzersiz bir şekilde ilişkili olan özellikleri sergiler. Bu, genel olarak konut ve özelde toplu konut ile ilgili her geleneksel ortamın kendi özel imajına ve kimliğine sahip olduğu anlamına gelir (Hoşkara vd, 2009: 81).

Konutlar kültür açısından toplumun alt ve üst sınıf tabakalarının aile yaşamlarını yansıtan fiziksel kanıtlardır. Konut, bir ailenin insancıl (beşeri) yaşamının fonksiyonel ihtiyaçlarını fiziksel olarak karşılayan hacimleri içerir. Nüfusun artışı, zorunlu ve istekli göçlerin, kırsal alanlardan kentlere akışı ve bunu tetikleyen sanayideki gelişim, konut açığının boyutlarını günümüze taşımıştır. Bu süreçteki tüm kültürel ve politika gelişmeler konutların üzerinde önemli izler bırakmıştır. Kıbrıs, Doğu Akdeniz bölgesinde oldukça küçük bir kara parçası olmasına rağmen, tarihsel akış içerisinde 3000 yıldan daha uzun bir süre Afrika, Orta Doğu, Anadolu ve Avrupa'dan gelen yerleşimcileri çekmiştir. Bunun nedeni, adanın doğal kaynakları, uygun iklimi ve bölgedeki stratejik önemidir. Öte yandan, ada yabancıların yerleşmesine, ekonomik güçlülere ve toplumsal çekişmelere sahne olmuştur. Bu yönden konut yapımı kendini yenileyerek günümüze kadar değerini korumuştur (Qurresh, 2004: 1).

Ada son süreçte her ne kadar yönetim açısından iki bölgeye ayrılmış olmasına rağmen, tarihi süreçte tek ada ve onu oluşturan toplumların kırsal alan konutlardaki mimari anlayışı aynıdır. Ancak; Venedik, Lüzinya, Osmanlı ve İngiliz sömürge sürecinde kentsel mekânda bu yönetimlerin kültürel ve politika durumu yansıtır konutlar yapmışlardır. Kıbrıs'ın konutları üzerinde oldukça geniş araştırma mevcuttur ama konutların tarih boyunca kültür ve politika açısından etkilenmesi hakkında şimdiye kadar bir araştırma yapılmamıştır ve bu araştırma yapılmasına neden olmuştur.

## 2. Konutun Tanımı

Konut, insanoğlunun en temel ihtiyaçlarından biridir. Çünkü insanoğlu, kendini iklimin, doğanın ve diğer bütün canlıların olumsuz etkilerine karşı koruyabileceği bir ortama ihtiyaç duymaktadır. Bu ihtiyacı, geçmişten günümüze sürekli olarak modernleştirdiği bir yapılanma ile gidermeye çalışmaktadır. Konuta duyulan ihtiyaç zamanla bir arada yaşam olgusunu, sonrasında ise kentleşme sürecini ortaya çıkarmıştır. Kentleşme tarihi süreç içerisinde kendine özgü bir yapılanmaya gitmiş ve kültürden kültüre değişiklikler göstermiştir. Ancak, 20. yüzyıla gelindiğinde bu farklı özellikler ve zenginlikler küreselleşme olgusuyla birlikte yavaş yavaş kaybolmaya başlamış, ülkeler arası farklılıklar süreci yerini ülkeler arası benzerlikler sürecine bırakmıştır (Kayserili vd, 2014: 253).

## 3. Konutun Tarihi Süreçteki Gelişimi

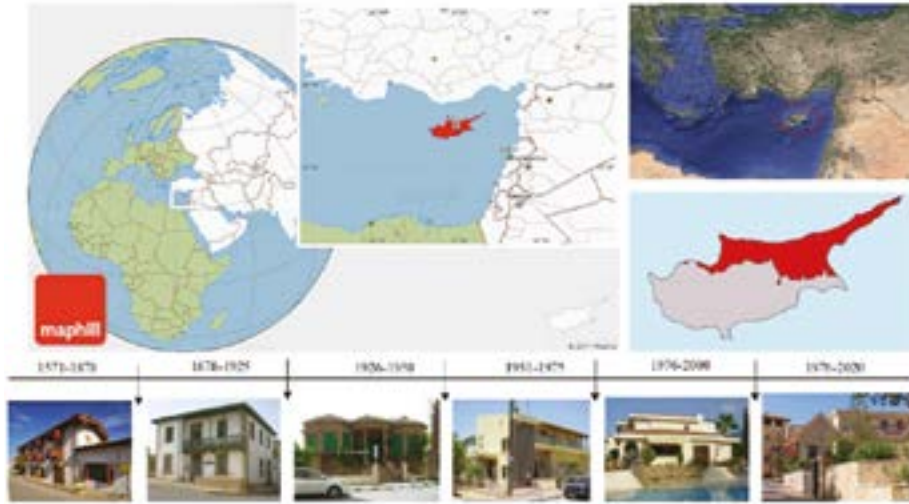
İnsanlığın bilinen en eski zamanlarından bu yana insanoğlunun en önemli temel ihtiyaçlarından biride barınma olmuştur. Bu ihtiyacı etkileyen unsurlar ilk etapta yağmurdan, soğuktan, yabani hayvanlardan ve benzeri dış faktörlerden korunma, mahremiyetin sağlanması, depolama ve eşyayı saklama güdüsü şeklinde sıralanabilir. İlk zamanlar, ilkel barınakların yapıldığı alanlar serbest mal iken, yani ücret ödemeyi gerektirmeyen, parsellenip satılarak rant elde edilmeyen ve imar/iskan vb. kavramlar ile izne bağlanma ve teşkilatlanmaları söz konusu olmadığı dönemlerde yapılan konutlarda kullanım değeri önem arz etmektedir. Kullanılan malzemelerin belli bir üretim organizasyonuna ihtiyaç duyması ile birlikte emek maliyeti önemli yer tutmaya başlamıştır. Ağaçların işlenmesi, taşların yontulması vb. ihtiyaçlar, mesleki teşkilatlanma ve iş bölümünü gerekli kılmıştır. Konutların yapılmasında ekseriyetle kullanım değeri ön planda olmakla birlikte döneme göre değişim değeri de önem arz edebilmektedir. Kullanılan malzemelerde ise döneme göre değişkenlikler görülebilmektedir (Tağraf, 2019: 1).

## 4. Kıbrıs Adasının Tanımı

Kıbrıs, Akdeniz'in üçüncü büyük adasıdır. Adanın kuzeyinde Türkiye, doğusunda Suriye, güneydoğusunda İsrail, Filistin ve Lübnan, güneyinde Mısır en yakın komşularıdır (Şekil.1). Kıbrıs Adası, Akdeniz'in

kuzeydoğu bölgesinde 34° 33' ve 35° 41' kuzey enlemleri ve 32° 17' ve 34° 35' doğu boylamları, bazı kaynaklara göre ise Akdeniz'in kuzey doğusunda 38° 34' ve 35° 41' kuzey enlemleriyle 32° 20' ve 34° 35' doğu boylamları arasında yer almaktadır (Alasya, 1998; Hakeri, 1993).

Adanın toplam yüzölçümü 9235 km<sup>2</sup> dir. KKTC yüzölçümü ise 3242 km<sup>2</sup> dir. Ülkenin nüfusu 1996 nüfus sayımına göre 205587 kişidir. Adada yerleşme M.Ö 1500 yıllarında başlamış ve adaya çeşitli devletler hâkim olmuştur. Ada Osmanlıların yönetimine 1572 yılında girmiştir. Osmanlıların adaya hâkim olmasıyla şehirler daha da gelişmiştir. Ada, 1878 de İngiliz yönetimine girmiştir. Adanın İngiliz yönetimine girmesiyle başlayan Türk – Rum kavgası günümüze kadar devam etmiştir (Çitçi, 2013: 225).



Şekil 1. Kıbrıs Konumu ve Konutların Değişimi (Kaynak: Yazar).

### 5. Osmanlı Dönemi Konut Tarzı (1571-1878)

“Kıbrıs’ın Anadolu ile olan yakın ilişkisi tarihi boyunca kendini gösteren önemli bir noktadır. Bunun en uzun ve. Etkili olanı ise, adanın Osmanlılar tarafından fethedilmesiyle başlayan ve 307 yıl süren devridir. (1571-1878) Bu dönemde Osmanlılar adaya kendi yönetim, ekonomi ve sosyal organizasyon sistemlerini getirmişlerdir. Osmanlı döneminde adada özellikle paşaların, devlet görevlilerinin ve yetkililerinin kentler-

de oturacakları yeni konutlar yapılmış, dini ve kültürel binalar inşa edilmiştir” (Yeşilada ve Atun, 1990; Quriesh. 2004: 28).

Adada 1571 yılında başlayan Osmanlı dönemi ile Kıbrıs’ın yeniden imarı ve gelişimi için Anadolu’dan nüfus getirilerek kent ve kırsal kesimlere yerleştirilmiştir. Bu dönemde, Türk mimarisi tarzında birçok cami, han, hamam, çeşme, tekke ve konutlar inşa edilmiş; bunlar arasında da halen yaşamlarını sürdüren konutlar önemli yer almıştır. Bu evlerde, geleneksel Türk Evî’nin dış sofalı plan tipi yaygın olarak kullanılmıştır. Evlerin sokakla olan teması, cumbalar aracılığı ile sağlanmış; odalar, çok amaçlı olarak tasarlanmıştır. Odalar, ortak mekân olarak kullanılan sofaya (sundurmaya) açılmaktadır. Sofa sadece odaları birbirine bağlayan dar bir dolaşım alanı değil, iklime de uygun olacak şekilde ya odaların önünde yer alan bir yarı açık mekân, ya da odalar arasında yer alan bir iç Mekân konumundadır (Çoğaloğlu, 2016: 50). Evlerde iç kısmının dışardan görünmesini engelleyen önlemler alınmış, güvenliği sağlayacak şekilde sokak cephelerinde yer alan göz hizasının üzerindeki küçük pencereler, yüksek bahçe duvarları, masif kapılarla korunan giriş mekânları ile merdivenin gizli bir Yerde olmasına özen gösterilmiştir (Andız, 1999; Bağışkan, 2005).

Kıbrıs’ın Osmanlı Dönemi’nden (1571-1878) günümüze gelen XIX. Yüzyıl Türk Evleri, adanın zengin kültür mirası içinde önemli bir yer teşkil etmektedirler. Evlerde, yaşam kültürü ile biçimlenen ve cephe karakteristiği oluşturan cumbalar, özellikle başkentin tarihi kent dokusunda simgesel bir öge olarak görülmektedirler. Kıbrıs’ın Osmanlı Dönemi’nden (1571-1878) günümüze gelen XIX. Yüzyıl Türk Evleri, adanın zengin kültür mirası içinde önemli bir yer teşkil etmektedirler. Evlerde, yaşam kültürü ile biçimlenen ve cephe karakteristiği oluşturan cumbalar, özellikle başkentin tarihi kent dokusunda simgesel bir öge olarak görülmektedirler (Turkan, 2018: 556).

## 6. İngiliz Dönem Konut Tarzı (1878- 1960)

1878 yılından 1960 yılına kadar süren İngiliz dönemi, Kıbrıslı Türkler için zorluklarla dolu bir dönem olmuştur. Bu dönemde nüfus Türkler aleyhine bozulmuştu. Bunun başlıca sebebi ise saldırılar, ekonomik ve siyasi baskılar sonucu çok sayıda Türk vatandaşının adayı terk et-

mesi, yani göç etmek zorunda kalmasıydı (Kızılyurek, 1983). İngiliz Dönemi'n de Rumlar ve Türklerin değişik bölgelerde yaşadıkları görülmektedir (Çoğaloğlu, 2016: 53). Kıbrıs adası 1878 – 1960 arasında geçen 82 yıl boyunca İngiliz yönetiminde kalmıştır. Bu süre içinde Sanayi İnkılâbı, Dünya savaşları (I ve II. Dünya savaşları) gibi önemli olaylar meydana gelmiştir. Bu olayların sonunda başta sanayi olmak üzere teknoloji, kültür, eğitim, sağlık alanda önemli gelişmeler olmuştur. İngiliz sanayisindeki hızlı gelişmeler Kıbrıs konut mimarisinde de kendisini göstermiştir. Daha önce konutların yapı malzemesi olarak kullanılan taş-toprak, kerpiç, ahşap malzemenin yerini betonarme yapı binalar almaya başlamıştır. İngilizler döneminde yapı malzemesinde meydana gelen değişikliğin yanında aynı zamana iç dekorasyonunda da önemli değişiklikler olmuştur. Osmanlı dönemindeki duvardaki dolapların ve sedirlerin yerini hareketli mobilyalar almaya başlamıştır. Yalın yer döşemeleri yerine İngiliz döneminde, ahşap, mermer, karo-mozaiik gibi yer döşemeleri gibi değişiklikler yanında konutların alt katına da pencereler girmiş ve bunlar daha büyük tutulmuştur (Mor ve Çitçi, 2013: 235).

İngiliz dönemindeki ev planları basittir. Adadaki evlere ‹balkon› eklenmesi anlayışı, İngilizler döneminde yerleşmiştir. Özellikle, 1880 yılından itibaren günümüzde de görüldüğü gibi, pekçok balkonlu ev inşa edilmiştir (Qurish, 2004: 31). Geleneksel Türk Evi plan tiplerinden iç sofalı plan tipi yaygın olarak kullanılan konutların cepheleri İngiliz Koloni mimari tarzındadır (Dağlı, 1990; Balkan, 1998). Yapı teknolojisindeki gelişmelerin binalara yansması, bunların yanı sıra, başta İngiltere olmak üzere gelişmiş batılı ülkelerle yapılan ticaretin artması, mimar-mühendis teknisyen gibi yapı kalitesini artıran elemanların çoğalmaya ve hatta yetismeye başlaması, yeni binaların ve kuşkusuz özellikle konutların planlı bir biçimde yapılmasına etken olmuştur (Qurish, 2004: 32).

## 7. Kıbrıs Cumhuriyeti Dönemi (1960-1975)

Genel olarak inşaat sektörü ve özel olarak da konut sektörü 1960 öncesinde düzenleyici kurumlara sahip değildi. Konutla ilgili ilk kural ve plan 1960 yılında Kıbrıs Cumhuriyeti'nin kurulmasıyla birlikte geti-

rildi (Yörücü ve Keleş, 2007: 78). Bu dönemde hükümet, inşaat işlerinin çoğu özel sektör tarafından yapılmasına rağmen, birkaç daire inşa etti. 1963 ile 1968 yılları arasında Kıbrıslı Türk yetkililer inşaat faaliyetlerini azalttı. 1963'ten 1974'e kadar Kıbrıslı Türkler zorla göç ettirildi veya Kıbrıslı Rumların görüşüne göre homojen yerleşim bölgeleri oluşturmayı "seçti"; Kıbrıslı Türkler topraklarını, köylerini ve evlerini terk ederek ya küçük gettolarda yaşamak için göç ettiler (Sözen, 1998: 13).

Adanın her yerine veya diğer ülkelere dağılmış daha güvenli yerleşim bölgelerinde. 1965'te Kıbrıs Türk yönetimi, en azından bazı mülteci ailelerinin yaşam koşullarını iyileştirmek için bir Mülteci Konut projesi geliştirdi. 1963-1974 yılları arasında kendi köylerinden (103 köy) daha güvenli bölgelere (gettolar) kaçan kendi ülkelerinde evlerini kaybeden ve mültecileri terk eden Kıbrıslı Türklerin sayısı 25.000'dir (BM Güvenlik Konseyi Raporu, 1964). Ortaya çıkan konut ihtiyacı, Lefkoşa, Gazimağusa, Girne, Limasol (Limasol) ve Baf'a (Baf) taşınan köylü göçmenler için inşa edilen konutlarla tamamlandı. Buna ek olarak, bazıları adadaki diğer belirli yerlere yerleştirildi. "Altı yıl içinde 65 farklı kent- sel ve kırsal yerleşimde 1513 konut birimi inşa edilmiş ve eve ihtiyacı olan ailelere tahsis edilmiştir (1966'da 130 birim; 1967'de 206; 1968'de 512; 1969'da 424; 1970-71: 241). Bu birimlerden 247'sinde bir yatak odası varken geri kalanında iki yatak odası vardı. Taban alanı 46 m<sup>2</sup> ile 70 m<sup>2</sup> arasında değişmekte olup, 1513 ünitenin 503'ü prefabrik, geri kalanı ise inşaat malzemesi olarak tuğla kullanılmıştır. Şu anda bu konut birimlerinin çoğu hala oturulabilir durumda ve düşük gelirli aileler tarafından işgal ediliyor. Hükümet bunları tahsis eder birimleri uygun ailelere ulaştırır ve kira tahsil etmez." (Gazioğlu, 1994).

Günümüz konutları olarak nitelendirilebilecek bu konutlarda ilk göze çarpan özellik konutların dikey olarak yükselmesidir. Konutların kat sayısı 3 veya 4 olmakla birlikte Maraş'ta 1960 yılında sonra yapılan konutlar ise 10-15 katlı olabilmektedir. Maraş turistik amaçlı bir yer olduğu için konutlar daha çok bahçe içlerinde yapılmışlardır. Hava sirkülasyonu sağlamak amacıyla karşılıklı pencere ve kapılar yanında yeterince ışıktan da faydalanmak amacıyla pencereler büyük tutulmuştur. Ancak hızlı kentleşme nedeniyle kısa bir sürede yapılan betonarme yapıları bu konutlar kent merkezlerinde genellikle 120 m<sup>2</sup> oturum alanına

sahiptirler. Öte yandan kentlerin dış alanlarında yapılan villa tipi konutlar birbirine asla benzemedikleri gibi bir villanın farklı yerlerinde değişik mimari tarzları görmek mümkündür. Özgün mimarileri yanında çatı süslemelerinde ve dizaynına ayrı bir önem verilmiştir. Genellikle yuvarlak olarak inşa edilen bu konutlara yumuşak bir görünüm vermeye çalışılmıştır (Çitçi, 2013: 18).

Yeni tip konutlar direk güneşten korunmak için bir kemer içine alınmış ve binanın çevresi süslü taş duvarlarla çevrilmişlerdir. Yüksek olmayan bu duvarların üstünde yine yükseltisi fazla olmayan demir parmaklıklar konulmuştur. Yeni tip konutlarda çatılar genellikle ya terastır ya da az eğimli kiremitle kaplıdır. Isıyı yansıtmak amacıyla konutların dış cephesindeki ana renk beyaz olması sebebiyle kentler uzaktan bakıldığında zaman beyaz evler olarak görünürler (Çitçi, 2013: 18). İnsanların ekonomik gücü ve kişisel tercihlerini kullanarak barınmalarını sağlamak için gerekli konut miktar ve kalitesi belirli bir anda var olan miktar ve kalitesinden farklı ise aradaki bu fark konut ihtiyacını doğurabilir (Keleş, 1976: 99).

## **8. Kıbrıs Türk Federe Devleti - Kuzey Kıbrıs Türk Cumhuriyeti Dönemi**

1970'lerin sonlarında yeni bir konut talebinin ortaya çıkması ve bu nedenle 1978'de hükümet bir Sosyal Konut Kanunu çıkararak konut piyasasına müdahale etmek zorunda kaldı. Sosyal, ekonomik ve kültürel düzeylerde hissedilen değişen ihtiyaçlara cevap verebilmek için yeni konut geliştirmeleri ancak 1980'lerden sonra kentsel gelişimin ana bileşenlerinden biri haline geldi. Bu dönemden itibaren konut ortamları, her ikisi de yasal çerçeve içinde farklı özellikler ve sorunlar sunan toplu konut ve bireysel konut olmak üzere iki farklı eğilim göstermiştir. Bir sonraki bölümde, Kuzey Kıbrıs'ta konutla ilgili yasal çerçeve değerlendirilecek ve 1980'lerden sonraki çeşitli konut gelişmeleri derinlemesine tartışılacaktır (Hoşkara vd., 2009: 86-87).

1974 yılında Kıbrıs'ta yaşanan siyasi değişimlerle birlikte oluşan yeni toplu durum gereğince yapılan nüfus değişimi neticesinde Güney'deki Türkler Kuzey'e, Kuzey'deki Rumlar Güney'e göç etmişlerdi.



Yapılan bu değişim neticesinde Rumların Kıbrıs'ın Kuzey bölgesinde bırakmış oldukları konut sayısı, Güneyden Kuzeye göç eden Türk nüfusuna yeterli derecede olmasından dolayı konut arayışına gidilmemiş; uzunca bir süre konut üretimi durmuştur. Adanın 1974 yılında Türk müdahalesinin ardından siyasi olarak ikiye ayrılması, Türk ve Kıbrıslı Rumların güneyden kuzeye veya kuzeyden güneye göçüne yol açtı. Nüfus hareketi, 2 Ağustos 1975 tarihli Gönüllü Nüfus Yeniden Gruplandırılması Anlaşması'nın bir sonucu olarak ve Birleşik Kıbrıslı Türklerin gözetiminde adanın kuzeyine taşındı ve tahminen 180.000 Kıbrıslı Rum adanın güneyine taşındı. Bu olay her iki tarafın da konut ihtiyacını değiştirdi, çünkü güneyden kuzeye Türk göçmen sayısının kuzeyden güneye göç eden Rumlara göre daha az olması nedeniyle kuzeydeki mevcut konut stoku talebi aştı ve böylelikle adanın kuzey kesiminde 1970'lerin sonu ve 1980'lerin başında çok az yeni inşaat yapıldı (Gazioğlu, 1996).

Bu dönemde ekonomik yaşantının çöküntüye uğraması, hayat pahalılığının artması sonucunda kötüleşen yaşam koşulları içerisinde bireylerin kendi konutlarını yapmaları zorlaştı, hatta imkânsız hale geldi. Daha çok işyeri ve resmi binaların inşa edildiği görülmektedir (Balkan, 1998). Konut ihtiyacı bu dönemde devletin aracılığı ile inşa edilen dar gelire sahip ailelerin barınma ihtiyaçlarını giderebilecek biçimde maliyeti düşük, küçük ve standartlaştırılmış plan tipine sahip sosyal konutlarla giderilmiştir. Bununla birlikte devlet dışında kooperatifler kurularak bireylerin ihtiyaçları doğrultusunda konutlar üretilmeye çalışılmıştır. Bu dönemdeki konutların bir kısmı devlet ve kooperatifler tarafından inşa edilirken, bir kısmı da özel sektör tarafından inşa edilmiştir (Çoğaloğlu, 2016: 61).

Modern konutların plansızca inşa edilmesi sonucunda görsel açıdan oldukça olumsuz bir görüntüye bürünmeye başlayan, binaların yeşil alan, bahçe ve otopark gibi olması gereken özellikleri, binaları inşa eden müteahhitlerin ekonomik hırslarının sonucunda tamamen göz ardı edilmektedir. Bunun sonucunda çocukların oyun oynayacağı bir bahçesi olmayan, otomobillerin park edebilmesi için gerekli otoparklardan yoksun ve yeşil alanların olmadığı düzensiz bir kentleşme ortaya çıkmaktadır. Oysa gelişmiş ülkelerde konut kooperatifleri kurulur ve bu kooperatifler kâr amacı gütmeyenler (Türkoğlu, 2007: 259).

## 9. Kıbrıs Konutları Etkileyen Faktörler

Mimari uygulamalar arasında idari binaların inşası, Kıbrıs'ta yönetimin farklı dönemlerdeki değişim ve sürekliliğinin önemli göstergesi olmuştur. Kıbrıs'ta hüküm süren farklı yönetimlerin politik ve ideolojik yansımalarının en somut olanlarının bugüne en yakın dönemlerde daha iyi izlenebildiği söylenebilir. Örneğin İngiliz Sömürge Mimarisi, çoğunlukla politik karar alıcılar tarafından sadece ötekine karşı üstünlüğün sıradan üretimini ve yeniden üretimini başlatmak ve sürdürmek için değil, yöneticiler tarafından bütün taraflar için "imparatorluğu görünür ve somut hale getirmek" amacıyla araç sallaştırılmıştı. İngiliz Koloni İdaresinin sonlanarak Kıbrıs Cumhuriyeti'nin adanın idari yapısını oluşturduğu 1960-63 dönemi ve Kıbrıslı Türkler için kısa ömürlü Kıbrıs Cumhuriyeti'nden Kuzey Kıbrıs Türk Cumhuriyeti'nin kuruluşuna (1983) kadar olan süre özel bir dönemi kapsamaktadır (Gürdallı ve Koldaş, 2017: 749).

## 10. Kültür

Kıbrıs sorunu, bir siyasal bütünleşme sorunu olarak tanımlanabilir. Etnik oluşum ve farklılaşmanın kültürel alanda seyrettiği durumlarda, siyasal bütünleşmenin üniter devlet sistemiyle, kültürel alanı terk ettiği durumlarda ise federal bir devlet yapısıyla sağlanabileceği söylenebilir (Tamçelik, 2008: 306).

Konut planlaması, kullanıcının sosyal ve kültürel nitelikleri ve çevre faktörlerinin etkileri ile biçim bulabilmekte; planlayıcının yalnız kendi programlaması ile ihtiyaçlara cevap veren fiziki ve yaşamsal yeterliliğe ulaşamamaktadır (Çoğaloğlu, 2016: 9).

Kültür, toplumların zaman içerisinde oluşturduğu düşünce ve inanç anlayışıdır. Bir insan topluluğunu diğer bir topluluktan ayıran değerler, inançlar, normlar, varsayımlar ve davranış biçimini oluşturan kültür; öğrenilir, tek bir bireye ait değil, toplumun tüm bireyleri ile paylaşılır, kuşaktan kuşağa aktarılır, bir olgunun başka bir olgu tarafından simgelenir, birbirine bağlı pek çok unsurun oluşturduğu bir yapıdır. Bu unsurlardan birinde veya bir kısmında oluşan değişiklik diğer kısımlarımda değişikliğine sebep olarak, uyarlanabilir, ait olduğu

toplumu bir takım ölçüler içerisine sokarak sınırlandırabilir (Gür, 2000). Kültür, değişken bir olgudur ve zamanla değişime uğrar. Buna bağlı olarak mimarlık olgusu da değişime uğramaktadır. Konutlar, kullanıcının gelenekleri, alışkanlıklarını ve bununla birlikte beğenilerinin bir genel toplamı olan yaşam kültürleri ile uyum sağlamaları gerekmektedir (Turkan, 2006). Mimaride yaşam kültürünün yeri toplumun gelenek ve beğenilerinin konutta yansısıyla ortaya çıkar. Yaşam biçimi kültürel faktörlere göre, konut planlamasındaki farklı fonksiyonların oluşumuna dolaysız olarak etki etmektedir. Bu etkilerle ortaya çıkan modeller de toplumların kültürel yansımaları olarak konut tiplerini oluşturmaktadır (Çoğaloğlu, 2016; 12).

### 11. Politika

Hızlı kentleşme, nüfusun artışı, ihtiyaçların değişmesi, göç gibi etkenlerden dolayı konut ihtiyacı süreklilik gösterir. Konut ihtiyacının yeterli nitelik ve nicelikte konut ile karşılanamaması konut sorununu Hızlı kentleşme, nüfusun artışı, ihtiyaçların değişmesi, göç gibi etkenlerden dolayı konut ihtiyacı süreklilik gösterir. Konut ihtiyacının yeterli nitelik ve nicelikte konut ile karşılanamaması konut sorununu (Önver, 2016: 7).

Kıbrıs'taki tarihî görüşler, yaşanan siyasi ihtiyaçlar tarafından tayin edilmek ve pratik siyasete çözümler üretebilmek için hizmet edebilir. Aksi takdirde hayata yabancı olan bir tarih ilmi, sırf antikacı zihniyetiyle hareket eder ki bu da istenen bir şey değildir. Ancak asıl siyasi tarih, gerçek mesuliyetine tam manasıyla müdriktir ve bundan dolayı mazinin tozlarına yeniden hayat vermesini bilir. İşte bu suretle hayata yabancı ve hayata yakın tarih ilmî birbirinden ayrılır. Kıbrıs örneğinde de olduğu gibi gerçek siyasi tarih ilmi, cevap verilmesine şiddetle ihtiyaç duyulan soruları sorar veya bunları tartışılması için ortaya atar. Ancak bu sayede toplumlar kendi yaşantılarını daha derin ve esaslı olarak anlayabilmeleri mümkün olur (Tamçelik, 2010: 107).

KKTC devleti, iskân, topraklandırma ve eşdeğer mal politikalarının Kuzey Kıbrıs'taki inşaat sektörünün durumunu ve gelişimini doğrudan etkilediği görüşü doğrultusunda, öncelikle bu politikaların anlaşılması gerektiği düşünülmektedir. Bu bağlamda, 1974 sonrasında Kıbrıs Türk

yönetiminin izlediği mülkiyetle ilgili konut politikaları, özetle aşağıdaki gibi gerçekleşmiştir:

- 1974 sonrası oluşan iki bölge yapı sonucunda Kuzey’de terk edilen konutlar, eşdeğerden, TMT, mücahitlik, TBK puanlarından ve tahsisten hak sahibi olanlara önceleri kullanım amaçlı dağıtılmış, daha sonraları tapuları da verilmiştir.

- Konut dışındaki taşınmaz mallar da (arsalar, arsa nitelikli araziler, kuru ve sulu tarım arazileri vb.) önceleri kullanım amaçlı dağıtılmış, daha sonraları ise bunların da tapuları eşdeğer, TMT, mücahitlik, TBK puanları karşılığı ve tahsisten hak sahibi olanlara verilmiştir.

- Tapuları dağıtılan bu araziler üzerine mevcut düzenlemelere uygun olarak, tarım arazisi, arsa veya arsa nitelikli arazi ayrımı yapılmaksızın “yol ulaşan her araziye”, inşaatlar yapılabilmektedir; bu uygulama günümüzde de devam etmektedir.

Daha iyi anlaşılması açısından konuyla ilgili bazı ayrıntılar notlarda ayrıca sunulmaktadır. Yukarıda kısaca özetlenen ve notlarda ayrıntılarıyla açıklanmaya çalışılan tüm bu mal ve mülk dağıtım durumlarına bakıldığında, halen Kuzey Kıbrıs’ta mevcut mal / mülk tipleri aşağıdaki gibi sınıflandırılabilir:

- Türk malları (orijinal – 1960’dan beri Türkler tarafından mülk edinilmiş Türk malları - 1960 Kıbrıs Cumhuriyeti kayıtlarına göre tapu sahibi)

- Rum malları (orijinal – 1960’dan beri Rumlar tarafından mülk edinilmiş mallar - 1960 kayıtlarına göre genelde Rumlara olmak üzere başka şahıslara ait olan ve 1974 sonrası terkedilerek Kuzey’de boş kalan ve çeşitli uygulamalarla Ada’nın Kuzeyinde yaşayan Türklere dağıtılan ve daha sonra KKTC tapusu verilen mallar)

A. 1974 sonrası Güney’den Kuzey’e göç etmiş olan Kıbrıslı Türklere “eşdeğer” karşılığında (Güneydeki malları karşılığında) dağıtılan, terkedilmiş – genelde – Rum malları;

B. 1974 sonrasında genelde Türkiye’den göç edenlere “tahsisten” dağıtılan (karşılığı olmayan) terkedilen Rum malları (karşılıksız satılan puanlar karşılığı dağıtılan tapular);

C. TMT, mücahitlik ve TBK puanları karşılığında dağıtılan (aslında

hizmet dışında maddi bir karşılığı olmayan) terkedilmiş Rum malları (Hoşkara, 2007).

Konut politikaları ise ekonomik, toplumsal, kültürel ve siyasal alanlar ile yakından ilişkilidir. 21. yüzyılda konut politikası kapitalist sistemin özünde var olan adaletsiz gelir dağılımını dengelemede sosyal politikanın bir aracı olarak kullanılabilme özelliğinden daha baskın olarak, ekonominin canlanması için inşaat sektörünün lokomotif olarak kullanılması, finans piyasalarının hareketlenmesini sağlanması için kullanılmaktadır. Devletlerin konut politikalarının doğuşunda ve gelişmesinde birincil etmen barınma ihtiyacının karşılanmasında karşılaşılan sorunlar ve bu sorunların toplumsal, ekonomik ve siyasal etkilerinin azaltılması, mümkünse yok edilmesidir (Önver, 2016: 6).

## 12. Değerlendirme

Dönemi karakteristik özelliklerini şöyle söyleyebiliriz:

Osmanlı mimarisi (1571-1878) ile yapılan Konaklar ve bulundukları caddeler otantik dokunun yansıtıldığı etkileyici manzaralar sunar. Cumbaların tamamına yakını, oda genişliğince, bir yönde (sokağa) taşan, düz çıkma şeklindedir Ahşap eli böğründelerle de ahşap konsollara destek sağlanmıştır. Ön köşelerde yer alan kare kesitli ahşap dikmelerle, taban girişlerinden en öndeki, alçı sıva kaplı Cumba cephesine çerçeve teşkil etmektedir. (Turkan, 2018).

1878 ile 1925 tarihleri arası, Kıbrıs'ta İngiliz Dönemi olmakla birlikte önceki dönem olan Osmanlı Dönemi (1571-1878)'nin planlama etkilerinin konutlarda halen devam ettiği görülmektedir. Bu zaman diliminde kent yaşamını sürdüren bireylerin ihtiyaçlarını karşılamak üzere inşa edilen konutlar, Kıbrıs'ın Osmanlı Dönemi'nin iç sofalı Geleneksel Türk Evi plan tipine sahiptirler. Sofanın iki yanında sıralanan odalar sofaya açılmaktadır.

Bu yıllara ait konutlar, cumbaları, kemerleri ve yığma yapım sistemi ile Osmanlı Dönemi konut mimarisinin genel özelliklerini taşımaktadırlar. 1900-1925 tarihleri arasındaki konutlar genellikle iki kattan oluşup, zemin ile üst kat aynı plan tipine sahiptir. Zemin katta sofa

(sundurma) ve sofanın sağ ve sol tarafında yer alan yaşama, yemek yeme ve servis mekânları, üst katta ise yatma mekânları bulunmaktadır. Yapı malzemesi; büyük oranda yerel ve bölgesel kaynaklardan sağlanmış olan Sarıtaş (kumtaşı) ve kolay elde edilmesinin yanı sıra ısı iletkenliği düşük, enerji tasarrufu yüksek, doğaya uyumlu kerpiç kullanılmıştır. Çatı malzemesi, ahşap kirişleme, hasır, kamış, toprak ve oluklu kiremit olan konutların döşeme malzemeleri ise toprak, yerel mermer ve taştır. Sıva malzemesi de alçıdan ibarettir. Bu döneme ait konutlarda, cumbalarla birlikte balkonlar da görülmektedir. Çıkma ve balkonları taşıyan C-S kıvrımlara sahip genellikle taş malzemeden yapılmış konsollar, değişik süslemelere sahip olup konutların önemli bir cephe elemanını teşkil etmiştir. Cepheler, önceki dönemin yalınlığına karşın, İngiliz Koloni Mimarisi etkileri ile detaylarla hareketlendirilmiştir (Çoğaloğlu, 2016: 133).

1926-1950 tarihleri arasındaki konutlarda, plan düzenlemesinin, bir önceki dönemin İç Sofalı plan tipinin temelinde devam ettiği görülmektedir. Sofanın iki yanında sofa boyunca uzanan ve sofaya açılan odalar yanı sıra sofaya hol veya koridor aracılığı ile bağlanan odaların oluşturduğu plan şeması, İç Sofalı planın değişimi ile döneme tipoloji oluşturmuştur. Önceki dönemde görülen cumbalar da bu dönemde değişime uğrayarak balkona dönüşmüştür. Böylece üst katların sokak ve yakın çevre ile ilişkisi, açık mekânlarla sağlanmıştır. Genellikle tek katlı olarak ve ayrıık nizamda tasarlanan konutlar, kendi ihtiyaçları doğrultusunda iklim özellikleri, yöresel malzemeyle ve tarihi doku zarara uğratılmadan inşa edilmişlerdir.

Detay, biçim, malzeme ve estetiğe özen gösterilerek yapılan konutların yapı malzemelerinin büyük bir kısmı yerel kaynaklardan çıkarılan sarı taş olmuştur. Bu çeyrek zaman diliminin son yıllarında, betonarme karkas sistemin kullanılmaya başlanması ile birlikte, plan şemalarında farklı form anlayışları ortaya çıkmıştır. Genellikle yalın plan tiplerine sahip konutlarda, çokgen biçimli mekânlar dikkat çekmektedir. Tek katlı olarak inşa edilen konutlar, yüksek tavana, etrafında bahçeye ve üzeri kapalı teraslara sahiptirler. Konutlarda doğal havalandırmayı sağlayan dikdörtgen formlu pencereler ve düz atkılı veya kemerli kapılar bulunmaktadır. Çatılarında, oluklu kiremit yerine Marsilya tipi

kiremit kullanılmaya başlanan konutlarda, döşeme malzemesi olarak da ahşap ve renkli desenli karo mozaikler görülmektedir (Çoğaloğlu, 2016: 180).

Yaptığımız araştırmalara göre bu dönemdeki konutların planları, önceki dönemlerdeki yaşam kültürüne uygun geleneksel şemaların aksine kullanıcıların ihtiyaç ve sosyal durumlarına göre kullanıcıya özel tasarlanmış, modern mimari örnekleri olarak görülmektedir. 1950'li yılların başlarından itibaren Kıbrıs'la mimarların adaya gelip mimari proje hizmeti vermeye başlamaları, plan şemalarında geleneksellikten moderne değişimi etkileyen önemli bir faktör olmuştur.

Betonarme karkas yapım sisteminin kullanılması da plan şemalarına esneklik getirmiş ve daha organik biçimlerdeki şemalara olanak sağlamıştır. Planı oluşturan mekânlarda ise işleve özel tasarım niteliği de bu dönemin özelliğidir. Plan şemalarındaki organik şekiller ve esneklik cephelere de hareket sağlamıştır. Bu dönemde eğimli çatıların yanı sıra betonarme karkas sisteminin olanaklarıyla düz çatılarda gözlemlenmektedir. Bu dönemde, duvar malzemesi olarak tuğla, kapı pencere doğraması ve teras-balkon korkuluğu olarak demir profil, alüminyum, hazır dış cephe sıvaları gibi çağdaş yapı malzemeleri kullanılmış; geleneksel malzemelerden taş ve ahşap ise estetik cephe elemanı olarak yer almıştır (Çoğaloğlu, 2016: 240).


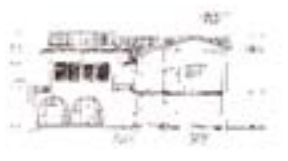

Dönemin ilk yılları bir önceki dönemin etkisini taşımaktadır (1976-2000). Daha sonraki yıllarda ise toprağın değer kazanması ve ekonomik üretimin standartlaşmayı öne çıkarması ile birçok kişiyi barındıran çok katlı konut yapıları yanı sıra standart plan şemalarına sahip konut sitelerinin inşaatı başlamıştır. Yaşam gereksinimlerine göre özel tasarımla oluşturulan plan şemaları, bu periyodda oldukça azalma göstermiştir.

Çok katlı yapılardaki konutlarda hol veya koridorla bağlanan gündüz ve gece bölümlerindeki mekânların dizisi şeklinde şemalıdan plan ve az katlı yarı veya tam müstakil konutlarda alt katta gündüz bölümüne ait mekânlar ile üst kattaki iki veya üç adet yatak odasından ibaret gece bölümü mekânlarının oluşturduğu tip plan, dönemin standart plan tipolojilerini teşkil etmektedir.







Dönemin son yıllarında, az sayıda da olsa kullanıcı gereksinimleri-







ne göre tasarlanarak, daha işlevsel ve fiziksel çevre koşullarına uygun, kullanıcıya özel planlar görülmektedir 1976-2000 dönemindeki konutlarda, çağdaş yapı malzemeleri kullanımı yaygınlaşmış, geleneksel malzemeler yalnızca dekoratif amaçlı olarak az miktarda kullanılmıştır. Dönemin çok katlı yapıları, betonarme düz dam ile bitirilmiş, az katlı konutlarda ise genellikle beşik tipi olmak üzere kiremit kaplı eğimli çatı örtüsü kullanılmıştır. Plan şemalarındaki yalın çizgiler cephelere yansımış, hareketten yoksun cephe karakterleri ortaya çıkmıştır (Çoğaloğlu, 2016: 300). Tablo 1’de konutların Osmanlı döneminden günümüze kadar politika ve kültür açısından değişimleri incelenmiştir:











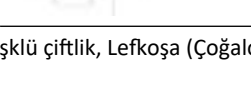
**Tablo 1.** KKTC Osmanlı döneminden günümüze kadar değerlendirme (Kaynak: Yazar).







Yıl	Cephe	Plan	Kültür ve Politika Özellikleri
1571-1878	 		<ul style="list-style-type: none"> <li>▪ Konutlar Osmanlı mimarisinden etkilenmiş ve bu konutlar Türk kültürüne yakın bir şekilde kurulmuştur.</li> <li>▪ Politika açısından ada Osmanlı devletinden etkilenmiştir ve adada göçmenler sayısı arttığı için çok sayıda konut yapılmıştır.</li> </ul>
	Barbarlık Müzesi, Kütüphane Sokak No:8, Surlar içi, Lefkoşa (Saçaklı Ev) (Çoğaloğlu, 2016: 88)		




1878-1925			<ul style="list-style-type: none"> <li>■ Kültür açısından konutlar bu dönemde İngiliz kültüründen etkilenmiştir ve konutlar basit bir şekilde yapmaya başlamıştır. Konutların iç tasarımları İngiliz kültüründen etkilenerek değişmeye başlamıştır ve duvarlardaki dolaplar mobilyaya dönüşmüştür.</li> <li>■ Politika açısından konutların kullandıkları malzeme ve yapı teknoloji değişmeye başlamıştır. Malzeme Osmanlı döneminde ahşap ve taş kullanırken, bu dönemde betonarme kullanmaya başlamışlardır.</li> </ul>
			
			

1926-1950	 		<ul style="list-style-type: none"> <li>▪ Kültür açısından bu dönemde cumbalar da değişime uğrayarak balkona dönüşmüştür. Sokak ve yakın çevre ile ilişkisi, açık mekânlarla sağlanmıştır, yöresel malzemeyle ve tarihi doku zarara uğratılmadan inşa edilmişlerdir.</li> </ul>
	 		<ul style="list-style-type: none"> <li>▪ Politika açısından bu dönemde çok az sayıda yeni konutlar inşa edilmiştir ve konutlar sadeleşmiştir.</li> </ul>
	<p>Selim Caddesi, No:42, Köşklü çiftlik, Lefkoşa (Çoğaloğlu, 2016: 135)</p>	<p>Abdullah Paşa Sokak No:3, Surlar içi, Mağusa (Çoğaloğlu, 2016: 158)</p>	

1951- 1975	 	 	<ul style="list-style-type: none"> <li>■ Kültür açısından KKTC yaşayan insanlar kendi kültürlerini konutlarında devam ediyorlar.</li> <li>■ Politika açısından ise inşaat sektörlerinin gelişimleri birlikte çok konut yapılmıştır ama bu konutlar savaştan sonra yapıldıkları için sade bir şekilde yapılmıştır.</li> </ul>
	<p>Server Somuncuoğlu, Sokak No:4, Köşklü çiftlik, Lefkoşa (Çoğaloğlu, 2016: 183)</p>		
	 		<p>Ekonomik üretimin standartlaşmayı öne çıkarması ile birçok kişiyi barındıran çok katlı konut yapıları yanı sıra standart plan şemalarına sahip konut sitelerinin inşaatı başlamıştır.</p>
<p>Mustafa Karakuş Sokak No:25, Mağusa (Çoğaloğlu, 2016: 234)</p>			
 	 	<p>Mehmet Akif Caddesi, No:36, Köşklü çiftlik, Lefkoşa (Çoğaloğlu, 2016: 96)</p>	

1976- 2000	 	<ul style="list-style-type: none"> <li>Adada yaşayan insanların kültür ve yaşamları değişmesiyle birlikte konutlarda değişmeye başlamış ve daha detayli ve geniş konutlar yapılmaya başlamıştır.</li> <li>Politika açısından ülkede güvenlik hakımı olduğu için binalar daha büyük ve geniş yapılmış ve geçmiş dönemlere göre detail binalara eklenmiş ve mimarlık açısından konutlar zenginleşmeye başlamıştır.</li> </ul>
	<p>Konya Sokak No:2-4-6, Lefkoşa (Çoğaloğlu, 2016: 242)</p>	
	 	
1976- 2000	<p>Konya Sokak No:2-4-6, Lefkoşa (Çoğaloğlu, 2016: 99)</p>	
	 	
	<p>Kuru Dere Sokak No:9, Lefkoşa (Çoğaloğlu, 2016: 290)</p>	

2000-2020	 	<ul style="list-style-type: none"> <li>Politika açısından ülkenin tanımlanmasıyla birlikte ve ülkenin güvenliği ve ekonomik açısından iyi durumda olmasıyla birlikte inşaat sektörü artmış ve komşu ülkelerden göçmenler bu adayı yaşam için tercih etmişlerdi. Bu yüzden 2-3 katlı konutlar apartmanlara dönüşmüşlerdi. Hata 2012 yılında politika açısından Ankara'da destek almıştır (Tamçelik, 2012: 2)</li> </ul>
	<p>Sakarya Caddesi, Golden konutları ve Terrace Park'ın komşu, Mağusa (<a href="https://doveconstruction.com">https://doveconstruction.com</a>).</p>   <p>Merkez Sakarya, Mağusa, Golden konutları (doveconstruction.com )</p>	

### 13. Sonuç

KKTC dünyada en önemli adaylarındandır ve tarih sürecinde farklı uyruklara misafirlik yapmıştır bu yüzden zengin bir geçmişe sahiptir. Osmanlı döneminde ada tamamen Türklerin egemenliğindeymiş. Bu dönemde kültür ve politika açısından iyi durumda olduğundan dolayı adada yaşayan insanlara konut, cami vs. binalar yapılmıştır. Bu dönemde konutlar Osmanlı kültürünü taşır ve benzer bir şekilde yapılmıştır. Osmanlı döneminde Kıbrıs'ta kendi yöntemlerle değişimler yapmışlar ama bu değişimler pozitif yöndedir. İngilizlerin politikaları ve kültürleri konutlarda yansımıştır. İngilizler Kıbrıs'a geldikleri dönem malzeme açısından, iç tasarım ve mobilya açısından değişime uğramıştır. Binalar-

da betonarme kullanımı ve iç tasarımda ise duvardaki dolaplar mobilyaya dönüşmüştür. Savaş döneminde ise konutlar çok az sayıda yapılmış ve yapılan konutlar sade bir şekilde yapılmıştır. Savaş döneminden sonra ada iki bölüme ayrıldıktan dolayı, adada yaşayan Türkler kuzeye toplanırlardır. Bu yüzden kendi kültürlerini tekrar konutlarında devam etmişlerdir. Ancak ilk senelerde göçmen insanlar adaya döndükleri için çok sayıda konuta ihtiyaç duyulmuştur böylece konutlar bu dönemde aşırı bir şekilde yapılmış ve bu konutlar sade bir şekilde ve katlar artmıştır. Ada iki bölüme ayırmasına rağmen Güney Kıbrıs'ta hala Türk kültürü ve Osmanlı döneminden gelen konutların kültürleri devam ediyor. Son dönemlerde ise politika iyi bir durumda olduğundan dolayı diğer ülkelerden de göç etmeye başlamışlardı ve böylece aşırı bir şekilde konut inşaatı artmıştır.

## KAYNAKÇA

Alasya, H.F. (1988). Tarihte Kıbrıs. Ankara: Kıbrıs Türk Kültür Derneği Genel Merkezi.

Andız, S. (1999). Kıbrıs'ta Vakıf Tarihi Eserler. Lefkoşa: Kuzey Kıbrıs Türk Cumhuriyeti, Vakıflar ve Din İşleri Dairesi. Vakıflar Genel Müdürlüğü.

Bağışkan, T. (2005). Kıbrıs'ta Osmanlı-Türk Eserleri. Lefkoşa: Kuzey Kıbrıs Müze Dostları Derneği.

Balkan, E. A. (1998). Tarihsel süreç içerisinde Kuzey Kıbrıs Türk Cumhuriyetinde toplum ve mimarlık. İstanbul.

Dağlı, U. U. (1990). Lefkoşa-Ara bahmet mahallesi konutları morfolojik analizi (Yüksek Lisans Tezi). İstanbul Teknik Üniversitesi, Fen Bilimleri Enstitüsü, İstanbul.

Çoğaloğlu, M. (2016). Kuzey Kıbrıs'ta XX. Yüzyıl Konutlarının Plan Değişimi ve Gelişimi Üzerine Bir İnceleme: Lefkoşa, Mağusa Ve Girne Örneklemesi (Yüksek Lisans Tezi). Lefkoşa.

Gazioğlu, A. C. (1994). Kıbrıs'ta Türkler. Lefkoşa: Kıbrıs Araştırma ve Yayın Merkezi.

Hakeri, B. H. (1992). Kıbrıs Türk Ansiklopedisi. Lefkoşa: Kıbrıs Gazetesi.

Hoşkara, Ş. (2007). Annan Planı Sonrasında Kuzey Kıbrıs'ta İnşaat Sektörüne, Mimarlık ve Planlamaya Eleştirel Bir Bakış. Kentleşme Dergisi, 334. Erişim adresi: [http://www.mimarlikdergisi.com /index.cfm?sayfa=mimarlik&DergiSayi=52&RecID=1296](http://www.mimarlikdergisi.com/index.cfm?sayfa=mimarlik&DergiSayi=52&RecID=1296)

Gürdallı, H. & Koldaş, U. (2017). Kıbrıs Cumhuriyeti'nden Kuzey Kıbrıs Türk Cumhuriyeti'nin İnşasına Giden Süreçte Lefkoşa'da Mekânın ve Mimarının Siyasi Dönüşümü: 1963-1983. Journal of History Culture and Art Research, 6(4), 748-772. doi:<http://dx.doi.org/10.7596/taksad.v6i4.1104>

Quriesh, A. A. (2004). K.K.T.C.'de Toplu Konut Üretimi Üzerine Araştırma (Yüksek Lisans Tezi). Yakın Doğu Üniversitesi Fen Ve Sosyal Bilimler Enstitüsü.

Kocaman, S., Kayserili, A. & Kaya, F. (2014). Kültürel Coğrafya Açısından Bir Araştırma: Tarihi Kağızman Evleri, Doğu Coğrafya Dergisi, 19(32), 145- 170.

Kızılyürek, N. (1983). Kıbrıs sorununda iç ve dış etkenler. Lefkoşa: Işık Kitabevi Yayınları.

Önver, M. Ş. (2016). Konut ve Konut Politikası. IJOPEC Yayıncılık. İstanbul. Türkiye.

Mor, A. ve Çitçi, D. (2013). KKTC’DE Kentleşme. Doğu Coğrafya Dergisi, 18, 225- 245.

Sözen, A. (1998). The Cyprus Conflict and the Negotiations: A Political and International Law Perspective. Ankara.

Türkoğlu, H. D. (2007). Konut Alanlarının Yenilenmesinde Kooperatif Modeli. Ayşegül Mengi, (Ed.). Kent ve Planlama Geçmişi Korumak Geleceği Tasarlamak. Ankara: İmge Yayınları.

Tağraf, N. K. (2019). İstanbul’da Konut Sektörü Ve Tarihsel Gelişimi (Yüksek Lisans Tezi). İstanbul Üniversitesi, İstanbul.

Tağra, N. K. (2019). İstanbul’da Konut Sektörü Ve Tarihsel Gelişimi (Yüksek Lisans Tezi). İstanbul Üniversitesi Sosyal Bilimler Enstitüsü, İstanbul.

Turkan, Z. (2018). Kıbrıs’ta Osmanlı Dönemi XIX. Y.Y. Türk Evlerinde Bir Karakteristik: Cumba. Tarih Kültür ve Sanat Araştırmaları Dergisi, 7(1), 565- 577.

Tamçelik, S.( 2008). Kıbrıs’ta Türklerle Rumların Toplumsal Çatışma Düzlemi ve Bununla İlgili Ahlakî ve Mantıksal Değerleri. Hacettepe Üniversitesi Türkiye Araştırmaları (HÜTAD), 8, 285 – 320.

Tamçelik, S.(2012). Kuzey Kıbrıs Gelecek Vizyonu, Eko Avrasya dergisi, (Editör yazısı), 1-4.

Tamçelik, S. (2010). Kıbrıs Meselesinde Metodolojik Sorunlar Ve Çözüm Önerileri, Zeitschrift Für Die Welt Der Türken, Journal Of World Of Turks.

Yeşilada, F. & Atun, M. (1990). Traditional Building Construction and Materials in Cyprus. The Lusignan House. Nicosia.

Yorucu, V. & Keleş, R. (2007). The Construction Boom and Environmental Protection in Northern Cyprus as a Consequence of the Annan Plan, Construction Management and Economics.

Erişim adresi: <https://doveconstruction.com/sky-sakarya>.

Erişim adresi: <https://doveconstruction.com/magusa-merkez-sakarya-apartman-golden-residence-yasam>





# BLOCKCHAIN TECHNOLOGY IN THE EDUCATION SYSTEM

*Saadia Elgati*<sup>1</sup>

---

## **Abstract**

Blockchain is an emerging and innovative technology that brought many benefits to many sectors. Education is one of the most important sectors that have a great effect on economic growth. Integrating blockchain technology in the education field will have a significant impact on its improvement especially nowadays during the coronavirus pandemic when most schools and universities moved to online systems. Many solutions have been proposed to address education challenges. In this paper, we introduce the blockchain features that play a significant role in improving the education industry. We present blockchain-based applications in education and we discuss and analyze a variety of existing enabling technologies that were developed to be used in education systems and compare them in terms of blockchain key features. We also

---

<sup>1</sup> PhD Student, Sakarya University, Faculty of Computer and Information Sciences, Computer Engineering, ORCID: 0000-0002-8852-3433

introduce the advantages of integrating blockchain technology in the education system. Finally, we list the challenges of using blockchain in education systems and provide some directions for improving the education system.

**Keywords:** Blockchain, Education, Security, Smart Contracts.

## 1. Introduction

Blockchain was first launched in 2008 and used as a peer-to-peer electronic cash system for Bitcoin cryptocurrency (Nakamoto, 2008). Blockchain is a public distributed ledger in which the data is distributed among users in a way that makes it difficult to tamper with. Recently, due to its extensive features, blockchain has gained a significant attention, and it is not only used in finance industry but also in many other sectors such as education, healthcare, insurance, real estate, and commerce industry. Education is one of the most important fields and the main key aspect for the growth of other industries as well. Currently online learning has become a recognized means of teaching. Increasing numbers of students from different backgrounds and places are taking the opportunity to study online especially after the coronavirus pandemic most universities chose to educate online nowadays. However, due to the lack of trust and certification, online education is currently facing major challenges that may have undesirable consequences. Therefore, the use of blockchain in the education system is becoming a necessary condition to increase the potential of educational institutions. To improve the education system, many implementations have been developed; however, its success is still incomplete. It is desirable to make full use of the potential of blockchain technology in education. The proven characteristics and advantages of blockchain technology can solve most of the problems currently faced by the higher education system. In this paper we attempt to investigate blockchain based applications in education and introduce its benefits and drawbacks. The remainder of this paper is organized as follows: Section 2 provides an overview of the characteristics of the blockchain. In section 3, different blockchain based applications in education system are introduced. In section 4, the existing blockchain based projects in education are presented. In section 5, we list the advantages and obstacles of blockchain technology in the education and provide some future directions. Finally, we conclude in section 6.

## 2. Characteristics of The Blockchain

Before we discuss Blockchain applications in education it is necessary to mention the characteristics or the key features of the blockchain that education will benefit from. Blockchain's features are as follows: decen-

tralization, traceability, immutability, currency properties, consensus and smart contract.

Decentralization is the process of distributing data among nodes in different places in a peer to peer network so no single entity retains the control. Data transmission, verification, confirmation, storage, maintenance and similar operations will be based on a distributed structure framework. Data is grouped into blocks that are linked to each other forming a chain, and each node in the network has the same exact copy of data. In this structure, no trusted authority is needed (Nakamoto, 2008; Yumna et al., 2019).

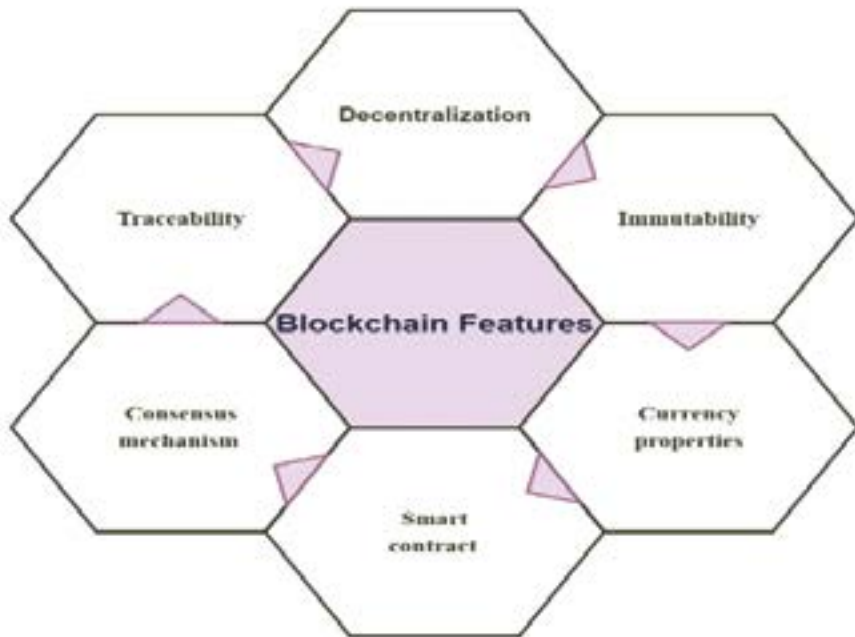
Traceability is that all transactions on blockchain are bundled into blocks. Each block is connected to the previous and the next block through a cryptographic hash. Every block contains the hash of the previous block. Therefore, every data is trackable (Chen et al., 2018; Lin et al., 2017).

Immutability is the ability of blockchain to keep data untampered. Due to its linked structure, each block contains the hash of the previous one making it impossible to change data that is already included in the blockchain. Because any change in the data will lead a change of the block hash which is considered as the unique ID of the block, and it will be immediately detected since all blocks are linked through block hashes (Aste et al., 2017).

Currency properties, bitcoin was the first cryptocurrency issued. In blockchain technology, cryptocurrency is a digital currency that is created using different mining algorithms. While validating blocks the miner who solves the block will get rewarded a cryptocurrency (Nofer et al., 2017).

Consensus mechanism is a fault tolerant process that is used in blockchain technologies to achieve the agreement on data among nodes in a distributed network. There are many consensus algorithms such as proof of work (PoW) proof of state (PoS) and practical byzantine fault tolerance (PBFT) (Bach et al., 2018).

Smart contract is a self-executing program stored on the blockchain and run when some predefined conditions are met and according to the terms of the agreement between the entities of the contract without involving any intermediary. It is secure, fast, efficient and accurate (Buterin, 2014).



**Figure1:** Blockchain features.

**Figure1:** Blockchain features.

### 3. Blockchain Applications in Education

The education sector is facing the same problems that have plagued it for years. For example, lack of transparency, inadequate student and teacher accountability, lack of true desire for students to study, ineffective paper-based record-keeping methods and fake academic certificates. The blockchain has the potential to improve education and address these issues. There are various areas of blockchain applications in education.

#### *Transparent Record Keeping*

Using the blockchain, the data is stored in a database that is spread across multiple locations. The blockchain records blocks into a sequential order as well as timestamps. Thus, when data is entered cannot be altered.

### *Authenticated Certificates*

Besides maintaining records, blockchain is used to monitor and facilitate schools and university accreditation and prevent certificates falsification. Even if the certificates are lost, they can be easily verified. Educational records stored on the blockchain can be accessed and transmitted swiftly to other schools and organizations, including potential employers. To provide others access to a student's profile, all they have to do is share a link or his digital address. Because the full history of changes with signatures is maintained on the blockchain, this approach provides complete legitimacy of credentials and student data.

### *Student Data Privacy and Consent*

Most educational institutions require students' guardians to sign many types of forms to allow schools to use student data, but they may not be able to distinguish between the forms they signed for consent, nor do they know where or when these forms will be used. To address this, Gilda, Shlok, and Mehrotra, Maanav proposed a methodology for implementing blockchain innovation using hyperledger fabric and composer. This framework is used to create a digital agreement that may be completed without the usage of a third-party legally binding document (Gilda & Mehrotra, 2018).

### *Student Accountability*

Teachers can utilize blockchain smart contracts to enter into digital agreements with learners over the fulfillment of their assignments. The agreement spells out all of the assignment criteria, such as the directions, requirements, and deadlines. When students finish the work and meet all of the criteria of the agreement, they may be granted automatic entry to the next section of the course or get credit and a certificate of completion. Basically, smart contracts can help provide independent learning in a typical classroom setting, as well as provide the incentive factor that is sometimes lacking in traditional educational systems.

Automated evaluation is used. For instance, the course learning outcomes accomplishment values, the course name and weight can be included in the block. The transformation of student achievement assessment results to post-job competence evaluation results may also be done, and student competency evaluation results will be given to the

curriculum, ensuring the program's continual quality development. In the block, diplomas of graduated students as well as information that has been used to create an index capacity of graduate requirements during the learning process are included. Therefore, in contrast to the previous crude approval based solely on the diploma, there is the ability to approve the structure of the learning process, verify the gold content of the diploma, and categorize different students who receive the diploma. Learning outcomes may originate from a variety of sources, including educational institutions, professional experience, online studies, and other learning methods. Because of the outcomes-oriented educational concept, learners can receive a diploma if they meet the institution's graduate requirements index points (Duan et al., 2017).

### *Motivating Students and Teachers*

To inspire students and urge professors to participate to the educational process by generating new learning materials and contributing in research, cryptocurrency and tokenized credits can be utilized to create effective incentive systems. Smart contracts can be created to reward fulfilled activities with cryptocurrency. Teachers will be able to further motivate students by awarding extra credit to best performers. Tokenized credits can be used to pay for tuition, buy school supplies and other instructional resources, and cover other educational costs. Rewarding students for finishing a particular major and getting a university credential could drastically reduce the percentage of students who drop out before completing their education (N. Szabo, 1997).



**Figure2:** Blockchain based education application.



#### 4. Blockchain Based Projects in Education

Although there are various blockchain based applications to be used in the education field only few institutes and universities have applied the blockchain technology in their education systems. In the following we discuss the available blockchain based projects.

**Edgecoin:** Is the first blockchain educational project that aims to solve payment problems by providing a decentralized payment system open for educational institutions to make transactions such as paying for educational services. This includes paying enrollment fees, books, accommodation, rental of transport and other educational items needed. Edgecoin is run on stellar blockchain using PoS consensus. It is secure, fast and efficient (Chen et al., 2018).

**Tutellus:** Is a blockchain platform that seeks to minimize education cost for students and bring motivation for both students and teachers since it pays students for learning and remunerates teachers for the value they provide. It is based on Ethereum blockchain and it aims to reduce the poverty through education. In addition, Tutellus project attempts to lower the gap between education and employment thus solving the lack of opportunities of jobs (Guustaaf et al., 2021).

**Sony Global Education (SGE):** Is a blockchain-based system that securely stores and shares student data. It allows educational and training organizations to contribute data to the system and makes it verifiable. It grants organizations required rights to analyze the data to identify trends in education and training in the population and evaluate the effectiveness of various education and training programs. The key features of this project are: extremely reliable data storage, flexible access control, tamper-proof learning history records, and data sharing with different organizations. SGE is based on Hyperledger Fabric blockchain (Turkanović, 2018; Sharples, 2016; Ocheja, 2018).

**TeachMePlease (TMP):** Is a project that runs on DISCIPLINA blockchain. It provides a platform that allows effective cooperation between students, teachers and educational institutions. It also allows students to choose classes according to their needs, communicate with each other and manage their process. Meantime, it provides educational institutions the ability to access to course creation tools, assignments, academic

history of students, and pricing. TMP keeps a unified database based on the performance of each user. This helps to create rating of users of the platform (Kuvshinov, 2018).

**Blockcerts:** Is an open source project that was developed by MIT and Learning Machine. Using blockchain, it allows official records to be issued, viewed and verified in a secure manner. It provides e-certificates and diplomas that can be verified instantly and free of cost anywhere in the world. It is based on Bitcoin blockchain technology. It gives to the users the ability to hold and share their own digital records that are cryptographically signed (Hameed, 2019).

**GradeBase:** Is a project based on Bitcoin blockchain technology that provides a system that enables the verification of educational records and qualifications in a quick and easy way. It includes a QR code in students CVs, LinkedIn and online profiles. When it is scanned the record or qualification will be verified instantly with the same standards all over the world. Thus, preventing all types of frauds (Hameed, 2019).

**Echolink:** Is a system built on EKO blockchain which is a public blockchain that uses proof of professional stake consensus (PoPS) protocol. It provides verified information about education, skills and work experience. EchoLink system enables storing professional and other related data in an immutable format on blockchains. Multiple public, shared and private blockchains are supported and accessible through Echolink system (Williams & Dolan, 2020).

**Origin-Stamp:** Is a web based, trustworthy timestamping service that stores anonymous, tamper-proof time stamps for any digital information using the decentralized Bitcoin blockchain. Users can use Origin-Stamp to hash files, emails, or plain text, then save the hashes in the Bitcoin blockchain, as well as retrieve and validate time stamps that have been committed to the blockchain. Origin-Stamp is free and simple to use, allowing anyone, such as students, researchers, authors, journalists, or artists, to demonstrate that they were the original source of certain material at a specific point in time (Hepp et al., 2018).

**APII:** Employers and recruiters must verify educational and job experience, which is a costly and time-consuming process. To verify an individual's claims regarding their education and work, the recruiting

industry uses various verifications across organizations and intermediaries. APPII intended to change the cross-referencing process by giving the candidate control over the process, allowing for faster and less expensive checks. APPII guarantees that verifying a candidate's experience is a one-time event, with the record of the verification securely and completely accessible to anybody or any organization (Retrieved from: <https://appii.io>)

**ODEM:** Is a platform that connects students, professors, and other stakeholders in order to provide appropriate services and courses. Furthermore, ODEM offers potential in the obstacles that students experience in acquiring a solid education. Because employing a block-chain-based infrastructure can boost educational development while also being low-cost and simple to manage (Alam & Benaida, 2020).

**Parchment:** Is a platform to evaluate academic qualifications, process programs, and generate certificates. Students can simply communicate their academic performance with potential employers (Alam & Benaida, 2020). This is the most extensively used electronic credential service, which enables students, academic institutions, and businesses to effortlessly apply, verify, and exchange their credentials in a secure environment. Its platform has facilitated the transfer of more than thirty million transcripts and other certifications between millions of people and thousands of colleges and universities around the world (Alam & Benaida, 2020).

**TrueRec:** Is a project developed by the SAP Innovation Center Network that permits academic accomplishments to be recorded on the Ethereum public blockchain and allows users to store professional and academic credentials, which are granted by academic institutions, in the TrueRec app on their device. When a new credential or document is issued by TrueRec, the user receives it as a TRU file, with the credential's digital fingerprint (hash) stored on the blockchain. Because the credential itself isn't stored on the blockchain, the individual's privacy is safeguarded. At the same time, because the blockchain is the one source of truth, anyone may quickly check the credential's validity after obtaining it from the user (Dias, 2018).

**BitDegree:** BitDegree offers software and technology-related online courses. With tokenized bursaries, students are incentivized to learn.

The platform offers a gamified atmosphere where learners are given a character and must complete quests to explore the virtual world. When they achieve substantial learning and course completion goals, they are rewarded and recognized by future employers who are also registered on the platform. The blockchain stores all academic certifications, which are aggregated in the student's profile. Companies wishing to hire new computer specialists with fresh insights can keep an eye on the students' progress and select the best candidate (Steiu, 2020; Schnorr, 1991).

**Table1:** Comparison of educational projects.

Project/ Feature	Decentralization	Traceability	Immutability	Smart contract	currency	con- sensus
<b>Edge- coin</b>	Uses DApp based on stellar blockchain.	Yes	Immutable platform.	Edgecoin executes a transaction using a smart contract-driven payment system.	EDGT token	Proof of Stake (PoS).
<b>SGE</b>	Uses decentralized, distributed ledger system.	Provides anonymous data	Tamper free records	Uses smart contract to manage data access.	-	Hyper-Ledger Fabric.
<b>Teach-MePle-ase</b>	Uses its own decentralized blockchain (DISCIPLINA).	Yes	Immutable.	Uses smart contracts to ensure secure transactions.	Disciplina coin	Delegated proof of Stake (DPoS).
<b>Tutellus</b>	Decentralized and collaborative EdTech platform.	Yes	Immutable platform.	The system will run on smart contract-based regulations.	TUT token	Sharding.
<b>Block-certs</b>	Implemented in Bitcoin decentralized blockchain.	Yes	Immutable.	Uses smart contract to secure academic credentials.	-	Proof of Work (PoW).

<b>Grade-Base</b>	Based on Bitcoin decentralized blockchain.	Yes	Immutable.	Uses smart contracts to verify qualifications.	-	Proof of Work (PoW).
<b>Echolink</b>	<i><b>EKO decentralized Blockchain Application Platform and Services.</b></i>	Yes	Immutable.	Uses smart contract to bind entities.	Echolink-Token	Proof of Professional Stake (PoPS).
<b>Origin-Stamp</b>	Based on Bitcoin decentralized blockchain.	Yes	Immutable.	-	-	Proof of Work (PoW).
<b>APII</b>	Decentralized platform.	No	Immutable.	Uses smart contract to ensure teachers and students' academic backgrounds and qualifications.	-	Proof of Work (PoW).
<b>ODEM</b>	Built on Ethereum decentralized blockchain.	No	Immutable.	Uses smart contracts to manage payments.	ODE Token.	Proof of Stake (PoS).
<b>Parchment</b>	Decentralized platform.	No	Immutable.	-	-	Proof of Work (PoW).
<b>TrueRec</b>	Uses Ethereum decentralized blockchain.	No	Immutable.	Uses smart contracts (scripting) functionality to make online contractual agreements easier.	-	Proof of Stake (PoS).
<b>BitDegree</b>	Uses Ethereum decentralized blockchain.	Yes	Immutable.	Uses smart contract to ensure the exchange of tokens between the sponsor and the student.	BDG Token.	Proof of Stake (PoS).

## 5. Benefits of Blockchain on The Education System and Challenges

### 5.1. Advantages

Degree fraud, education verification, and the difficulty of translating and comparing the same degrees across different learning institutions are all issues that universities, individuals, and companies confront today (Elendner et al., 2016). In addition, the expenses of printing, validating, and archiving degrees and certifications are very costly. While e-learning is becoming increasingly popular, there is currently no standard guidelines that are acknowledged by all enterprises, countries, or institutions for the verification of certification and validation of competences. The incapacity to validate skills contributes to the wide gap in the employment. The education industry requires solutions that make validation, verification, and aggregation of person's educational record much easier as well as enable the user to look for jobs and employ competent candidates. Therefore, since blockchain is a secure, fast, and cost-effective mechanism to organize records and data such as degrees, e-learning certificates, blockchain-based educational projects solved all of the concerns. The education system will be disrupted by blockchain-enabled products and services. We classify the advantages of blockchain on education as follows:

**Building trust between parties:** The blockchain strategy would make a connection between multiple smart devices due to its advanced features. Only confirmed devices could interact with the system, and miners would have to confirm every block first (Turkanović et al., 2018).

**Minimize cost:** Since the blockchain does not rely on any third parties, the costs are reduced. Authors in demonstrated how blockchain helps to reduce the costs of storage, transactions and educational records management and maintenance. By using private or public networks, the fees of the traditional way of storing data in cloud can be minimized. Basically, the blockchain reduces all costs that are associated with certificates verification and processing (Hölbl et al., 2018).

**Reduce time:** It saves a significant amount of time. The transaction time is reduced from weeks to seconds using the blockchain. For example, in the traditional system, when a student wants to enroll in a univer-

sity, he spends a significant amount of time filling out forms and waiting for a response from the university administration.

**Security:** Due to its infrastructure, the blockchain provides security to users, data, and other agents.

**Educational Institution duties:** In educational institutions, blockchains have the potential to change certain functions. The blockchain would be an excellent format for granting qualifications and experience, as it would eliminate the role of the institution administrator as the delivery site. This would also reduce a stream of profits for the institution, possibly lowering costs or allowing those services to be distributed everywhere. Higher education institutions around the world are currently introducing blockchain courses to their students, recognizing the benefits of technology advancements. Many countries with blockchain educational institutions include the United States, Canada, and Denmark. Cornell University in the United States was one of the first universities to include blockchain courses in its program.

**Transparency and accountability:** The blockchain helps to improve both transparency and accountability since all records are stored in one place and accessible easily from any location (Arenas & Fernandez, 2018).

## 5.2. Challenges and Future Directions

Even though blockchain has many advantages for improving the education industry, there are many concerns that must be considered. The main challenge is related to the scalability of blockchain to handle large amount of data. There are many solutions proposed to solve this issue but still the blockchain suffers from scalability bottlenecks. Another problem is relevant to blockchain's privacy and security. Malicious threats and data leakage are two examples of security and privacy risks that could arise when using blockchain technology. The cost of using blockchain in education is the third main challenge, which includes the cost of processing power, the cost of changing existing infrastructure, and the cost of handling large amounts of data. The fourth problem is associated with trust. Institutions of higher learning are still hesitant to

share their data on a blockchain network. Furthermore, the immutability of blockchain, which is a key attribute of the technology, may represent a barrier to its acceptance in the field of education. It may be difficult for educational institutions to implement new information storage laws or correct invalid information due to immutability. Another issue with blockchain technology is that it is still in its infancy. Some immaturity issues, such as poor usability and confusing configuration, still affect blockchain. In addition, educational institutions are of centralized nature including decentralized blockchain into their systems will affect their process.

Blockchain is one of the most significant innovative technologies recently. It will most likely take a long time for the technology to gain widespread acceptance. This is because there are a number of issues that must be addressed before the technology can be used in the education field.

A significant area where blockchain might be of a considerable advantage is collaboration and partnership among educational institutions. As previously mentioned, some educational institutions are experimenting blockchain as a secure and reliable ledger to track their students' academic accomplishments. This includes not only keeping track of students' certificates, but also their various learning results and competences. A future research project in this area would look into how blockchain could be used to help educational institutions collaborate and partner more effectively. Smart contracts can be used to record and share students' information. Furthermore, a current issue with blockchain technology is the lack of usefulness of its products. Also, there is a lack of terminology clarity of the technology. Moreover, many complex settings, such as the primary keys and public keys may be required to be stored by the user for security reasons. For users in the education field, blockchain has entirely new terminology that can be difficult to grasp. The usability of blockchain products must be improved by creating simple interfaces so that people with no technical knowledge can understand and use the system.

To solve the scalability issues multiple solutions were proposed. Therefore, integrating such solutions into the blockchain based educational applications, will help improving them at large extent.



## **6. Conclusion**

Applying blockchain technology into the education sector is still in its early phases. In this paper, we introduced the key feature of blockchain that the education sector can benefit from and we also presented existing blockchain based educational applications. Finally, the benefits and challenges that face integrating blockchain into educational systems are discussed. Meantime we gave some few directions for future projects in this sector. Although there are plenty of solutions proposed there is every time new challenges that appear. This paper can serve as an overview of the application of blockchain in the education in general, its advantages and drawbacks and provide a clear insight into the different projects available that educational institutions could use.

## REFERENCES

- Nakamoto, S. (2008). Bitcoin: A peer-to-peer electronic cash system.
- Yumna, H., Khan, M. M., Ikram, M. & Ilyas, S. (2019). Use of blockchain in education: a systematic literature review. In Asian Conference on Intelligent Information and Database Systems. Springer, Cham.
- Chen, G., Xu, B., Lu, M. & Chen, N. S. (2018). Exploring blockchain technology and its potential applications for education. *Smart Learning Environments*, 5(1), 1-10.
- Lin, I. C. & Liao, T. C. (2017). A survey of blockchain security issues and challenges. *Int. J. Netw. Secur.*, 19(5), 653-659.
- Aste, T., Tasca, P., & Di Matteo, T. (2017). Blockchain technologies: The foreseeable impact on society and industry. *Computer*, 50(9), 18-28.
- Nofer, M., Gomber, P., Hinz, O., & Schiereck, D. (2017). Blockchain. *Business & Information Systems Engineering*, 59(3), 183-187.
- Bach, L. M., Mihaljevic, B., & Zagar, M. (2018, May). Comparative analysis of blockchain consensus algorithms. In 2018 41st International Convention on Information and Communication Technology, Electronics and Microelectronics (MIPRO), IEEE.
- Buterin, V. (2014). A next-generation smart contract and decentralized application platform. *White paper*, 3(37).
- Chen, G., Xu, B., Lu, M., & Chen, N. S. (2018). Exploring blockchain technology and its potential applications for education. *Smart Learning Environments*, 5(1), 1-10.
- Guustaaf, E., Rahardja, U., Aini, Q., Maharani, H. W., & Santoso, N. A. (2021). Blockchain-based Education Project. *Aptisi Transactions on Management (ATM)*, 5(1), 46-61.
- Turkanović, M., Hölbl, M., Košič, K., Heričko, M., & Kamišalić, A. (2018). EduCTX: A blockchain-based higher education credit platform. *IEEE Access*, 6, 5112-5127.
- Sharples, M., & Domingue, J. (2016). The blockchain and kudos: A distributed system for educational record, reputation and reward. In European conference on technology enhanced learning. Springer, Cham.
- Ocheja, P., Flanagan, B., & Ogata, H. (2018). Connecting decentralized learning records: a blockchain based learning analytics platform. In Proceedings of the 8th international conference on learning analytics and knowledge.

Kuvshinov, K., Nikiforov, I., Mostovoy, J., Mukhutdinov, D., Andreev, K., & Podtelkin, V. (2018). *Disciplina: Blockchain for education*. Yellow Paper. Retrieved from: <https://disciplina.io/yellowpaper.pdf>.

Hameed, B., Khan, M. M., Noman, A., Ahmad, M. J., Talib, M. R., Ashfaq, F & Yousaf, M. (2019). A review of Blockchain based educational projects. *Framework Journal*, 28, 30.

Arenas, R., & Fernandez, P. (2018). CredenceLedger: A permissioned blockchain for verifiable academic credentials. In 2018 IEEE International Conference on Engineering, Technology and Innovation (ICE/ITMC). IEEE.

Williams, A., & Dolan, E. (2020). Application of Blockchain Technology in e-LoA Technopreneurship Journal. *Aptisi Transactions on Technopreneurship (ATT)*, 2(1), 98-103.

Hepp, T., Schoenhals, A., Gondek, C., & Gipp, B. (2018). OriginStamp: A blockchain-backed system for decentralized trusted timestamping. *It-Information Technology*, 60(5-6), 273-281.

Employee background checks and CV verification underpinned by blockchain technology. Retrieved from: <https://appii.io/>

Alam, Tanweer, and Mohamed Benaïda. (2020). Blockchain and Internet of Things in Higher Education." Tanweer Alam, Mohamed Benaïda." Blockchain and Internet of Things in Higher Education. *Universal Journal of Educational Research*, 8, 2164-2174.

Elendner, H., Trimborn, S., Ong, B., & Lee, T. M. (2016). The cross-section of crypto-currencies as financial assets: An overview.

Hölbl, M., Kamisalić, A., Turkanović, M., Kompara, M., Podgorelec, B., & Herićo, M. (2018). EduCTX: an ecosystem for managing digital micro-credentials. In 2018 28th EAAEIE Annual Conference (EAAEIE). IEEE.

Arenas, R., & Fernandez, P. (2018). CredenceLedger: A permissioned blockchain for verifiable academic credentials. In 2018 IEEE International Conference on Engineering, Technology and Innovation (ICE/ITMC). IEEE.

Atienza-Mendez, C., & Bayyou, D. G. (2019). Blockchain technology applications in education. *International Journal of Computing and Technology*, 6(11).

Alammary, A., Alhazmi, S., Almasri, M., & Gillani, S. (2019). Blockchain-based applications in education: A systematic review. *Applied Sciences*, 9(12), 2400.

Hameed, B., Khan, M. M., Noman, A., Ahmad, M. J., Talib, M. R., Ash-

faq, F. & Yousaf, M. (2019). A review of Blockchain based educational projects. *Framework Journal*, 28, 30.

Malibari, N. A. (2020). A Survey on Blockchain-based Applications in Education. In 2020 7th International Conference on Computing for Sustainable Global Development (INDIACom), 266-270. IEEE.

N. Szabo. (1997). The idea of smart contracts, Nick Szabo's Papers and Concise Tutorials, 6.

Delgado-von-Eitzen, C., Anido-Rifón, L., & Fernández-Iglesias, M. J. (2021). Application of Blockchain in Education: GDPR-Compliant and Scalable Certification and Verification of Academic Information. *Applied Sciences*, 11(10), 4537.

Alam, S. (2021). A Blockchain-based framework for secure Educational Credentials. *Turkish Journal of Computer and Mathematics Education (TURCOMAT)*, 12(10), 5157-5167.

Dias, E. F. G. (2018). Ethereum smart contracts for educational certificates (Doctoral dissertation).

Steiu, M. F. (2020). Blockchain in education: Opportunities, applications, and challenges. First Monday.

C. P. Schnorr. (1991). Efficient signature generation by smart cards. *Journal of cryptology*, 4(3), 161-174,

Retrieved from: <https://www.bitdegree.org>.

Gilda, S., & Mehrotra, M. (2018). Blockchain for student data privacy and consent. In 2018 International Conference on Computer Communication and Informatics (ICCCI), 1-5.

Duan, B., Zhong, Y., & Liu, D. (2017). Education application of blockchain technology: Learning outcome and meta-diploma. In 2017 IEEE 23rd International Conference on Parallel and Distributed Systems (ICPADS), 814-817.



# CLIMATE DATA ANALYSIS: A REVIEW OF AI METHODS IN DROUGHT PREDICTION AND EVAPOTRANSPIRATION ESTIMATION

*Yasser Zouzou*<sup>1</sup>

---

## Abstract

Humans have been systematically recording climate data since the mid-nineteenth century. Moreover, the use of satellites to collect climate data has significantly increased the available data in this field. Data analysis tools aimed for climate data analysis are in constant development to keep up with the exponential increase in collected climate data. The need for robust data analysis methods for climate data is in greater demand with the increasing interest in climate change. This paper reviews the recent developments and applications of data science tools for climate data analysis and prediction. The paper focuses on studies in two fields: drought forecasting and evapotranspiration estimation. Several research regarding drought forecasting using various drought indices

---

<sup>1</sup> Master's Student, Erciyes University Engineering Faculty, Civil Engineering, ORCID: 0000-0002-9690-3882

and machine learning (ML) models are examined. Evapotranspiration estimation using ML models trained on limited climatic variables instead of empirical methods that require numerous measurements is also reviewed. The studies emphasize the potential of machine learning in the field of climate data analysis due to the ability of ML to deal with large datasets and non-linearities.

**Keywords:** Climate Analysis, Climate Databases, Drought Forecast, Evapotranspiration Estimation, Artificial Intelligence, Machine Learning.

## 1. Introduction

Climate data analysis and prediction have been practised way before the emergence of the term data science. Records of temperature covering most of the earth date back to 1880. Early data was collected using sensors in dedicated measurement towers. With the invention of satellites, special weather satellites were introduced to monitor the climate of the earth. This allowed for a larger flow of climate data, consequently increasing the demand on data analysis tools oriented for climate datasets. More recently, data retrieved through numerical climate simulations started to compose the largest portion of available climate data. Fig. 1 shows the size and source of climate data currently available and the prospected size in the future. Due to the importance of climate data, more specifically climate predictions, great efforts have been put to utilize the available data to provide clear descriptions of the current climatic state of the earth and obtain accurate predictions for the future states. This has led to the exploitation of AI tools in climate data analysis and prediction.

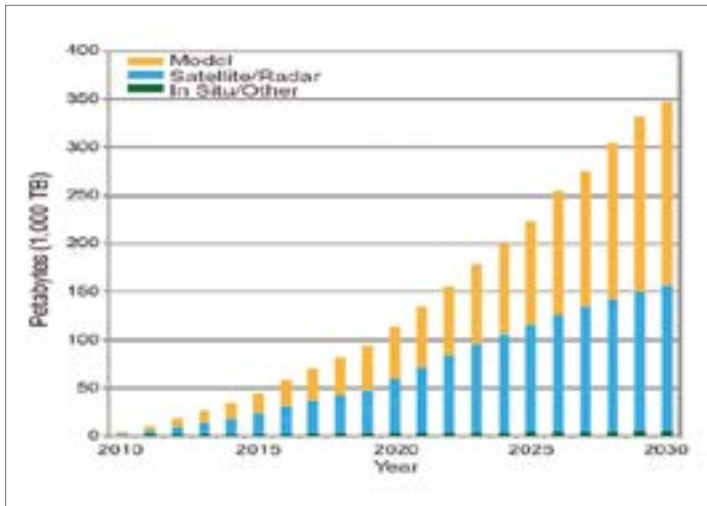


Fig. 1. Sizes and sources of climate data (Overpick et al., 2011).

This paper will review recent applications of data science tools in particularly two climate science areas of study: early drought warning and evapotranspiration prediction.



## 2. Drought Prediction

Droughts have immense humanitarian and economic impacts on countries. The estimated global losses caused by droughts in the 20 years between 1998-2017 are \$1.5 billion (Huntingford et al., 2019)<sup>likely</sup> requiring considerable adaptation to cope with future altered weather patterns. Machine learning (ML). Moreover, in the 2010-2012 Somalia famine, which was mainly caused by drought, 258,000 people lost their lives (Checchi & Robinson, 2013). These numbers emphasize the criticality of drought and the necessity of early drought prediction. Having the ability to predict a drought allows for precautional measures to be taken earlier, consequently minimizing casualties and losses. Climate scientists have used various indices to categorize droughts according to their severity. Precipitation, temperature, and evaporation are the main variables used in most indices to describe drought conditions. Drought prediction has been a researched subject for decades. Earlier attempts to predict droughts used statistical models applied on historical data to retrieve relationships between different climatic variables and drought indices. However, due to the various variables that drought depends on, along with the complex and nonlinear nature of drought relationship with those variables, statistical models were not sufficient in defining these correlations. In recent years, machine learning models were utilized to forecast droughts. The advantage of ML models is their ability to find patterns and correlations between numerous variables even in cases of nonlinearity. This, however, requires large climate datasets to train models, which is widely available thanks to satellite data. In this section, a number of studies in this area will be examined.

Belayneh et al. predicted droughts in the Awash river basin based on the Standard Precipitation Index (SPI) using machine learning models (Belayneh, Adamowski, and Khalil 2016). The Awash River basin (Fig. 2) is located in Ethiopia. The basin was divided into upper, middle, and lower basins for modelling purposes. The SPI index used in this study classifies water availability conditions depending on precipitation measurements only. SPI value ranges between -2 for extremely dry to 2 for extremely wet. Drought occurs when SPI values stay negative for a prolonged period of time.

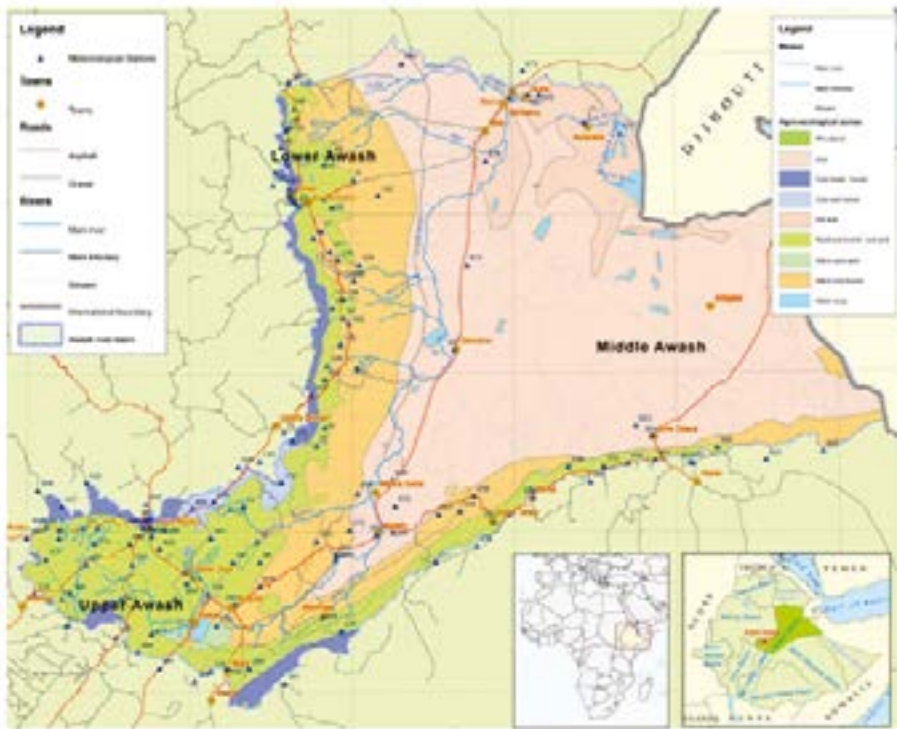


Fig. 2. The Awash River basin in Ethiopia (Belayneh et al., 2016).

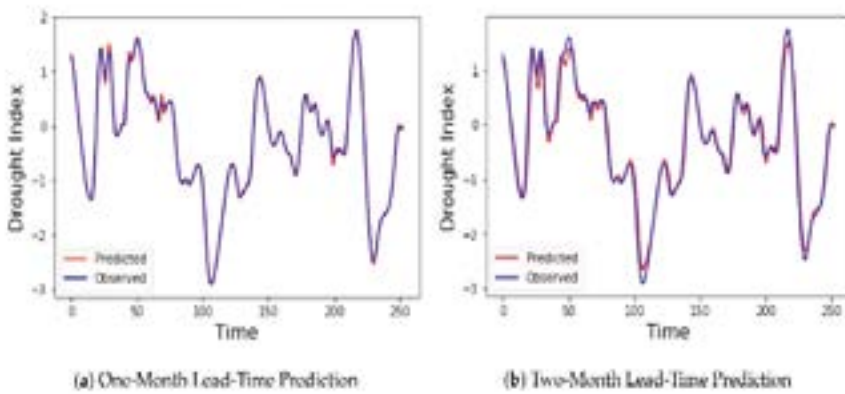
Belayneh et al. used Support Vector Regression (SVR), Autoregressive Integrated Moving Average (ARIMA), and Artificial Neural Networks (ANN) to model SPI time series for drought prediction. WA-SVR and WA-ANN models were also used in this study, where the WA indicates that inputs have been transformed using denoising wavelet transforms. Results show that SVR and ANN models were superior to ARIMA models in 1- and 3-months lead forecasts. Moreover, applying wavelet transforms on the input time series improved the performance of both SVR and ANN models. Fig 3. Shows a comparison between observed SPI values and values predicted by the best WA-SVR model for a 1-month lead forecast. Finally, the authors concluded that for this case study, ANN models are most suitable for drought prediction using SPI. SVR models have the potential of giving better results if a comprehensive parameter selection scheme is available as a more robust alternative to trial and error.



**Fig. 3.** 1 month lead SPI forecast results for the best WA-SVR model (Belayneh et al., 2016).

Agana et al. investigated the use of deep belief networks (DBN) for drought forecasting using the standardized streamflow index (SSI) (Agana & Homaifar, 2018). SSI classifies drought conditions based on river streamflow measurements. SSI is standardized using the same method to standardize SPI, therefore a drought is assumed to happen when the index remains negative for some time and ends when it retains positive values. This study was applied on a dataset of monthly streamflow measurements for the years between 1906-2014 in the Colorado River basin in the USA. In order to reduce noise in data, empirical mode decomposition (EMD) was used to decompose the time series data into signals of different frequencies (intrinsic mode functions (IMF)). Then, using detrended fluctuation analysis (DFA), the main frequencies (IMFs) were used to reconstruct the time series. This procedure allows for irrelevant variations in the time series (noise) to be excluded, ensuring better performance of the machine learning models. Deep belief networks are neural network-based models constructed of several restricted Boltzmann machines (RBM). DBNs are trained in two phases. First, unsupervised learning allows for the initialization network parameters with reasonable values to decrease convergence time in subsequent optimization. Then, available data is used to train the model (supervised learning). Results were compared to SVR and multi-layer perceptron (MLP) models. It was shown that data denoising using EMD-DFA scheme decreased

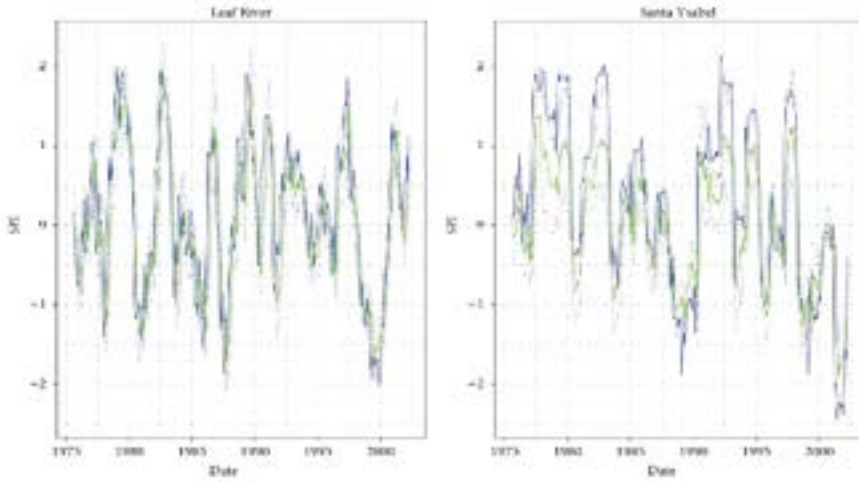
prediction errors significantly for all models. For 1-month lead predictions, EMD-DBN and EMD-SVR models showed similar results. However, for 2-month lead forecasts EMD-DBN models were superior. This shows the importance of pretraining neural networks for parameter initialization. Fig. 4 shows 1-month and 2-month lead-time predictions of the EMD-DBN model compared to observations in one of the stations on the Colorado river.



**Fig. 4.** Observations and predictions of an EMD-DBN model in one of the stations (Agana & Homaifar, 2018).

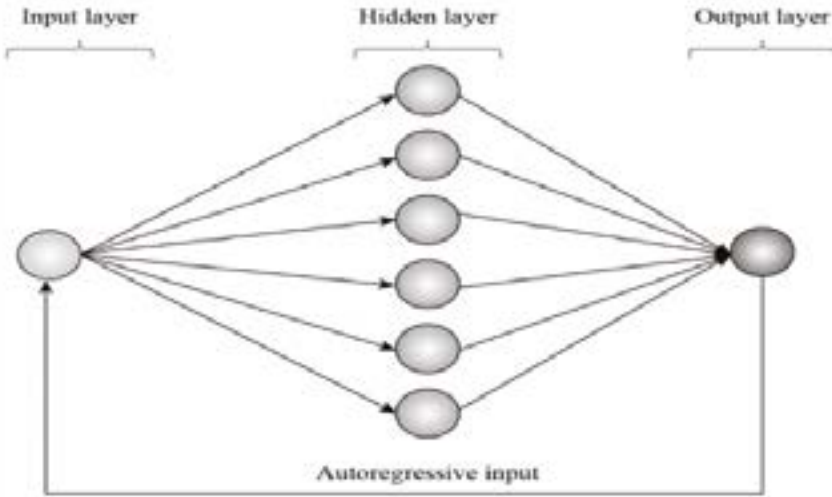
P. Maca and P. Pech investigated drought prediction in Leaf River and Santa Ysabel Creek basins in the USA using two types of neural networks: feed forward multilayer perceptron (sANN) and integrated neural network model (hANN) (Maca and Pech 2016). Unlike the two previous research, this study used two drought predicting indices: standardized precipitation index (SPI) and standardized precipitation evaporation index (SPEI). SPEI takes into consideration both precipitation and potential evapotranspiration to assess drought severity. Input data was normalized using max-min normalization, which transforms the data to a 0-1 range. The sANN model is a normal feedforward MLP with one hidden layer in this case. The hANN model, however, consists of five MLP models stacked together, where the output of every model serves as the input for the next model. Results show that there is high correlation between SPEI and SPI indices, therefore drought forecasts using the two indices were almost identical. Regarding the machine

learning models, the integrated neural network model was found to be superior to the normal MLP model in all test cases. Fig. 5 shows the SPI predictions and model predictions of one of the hANN models for both basins.

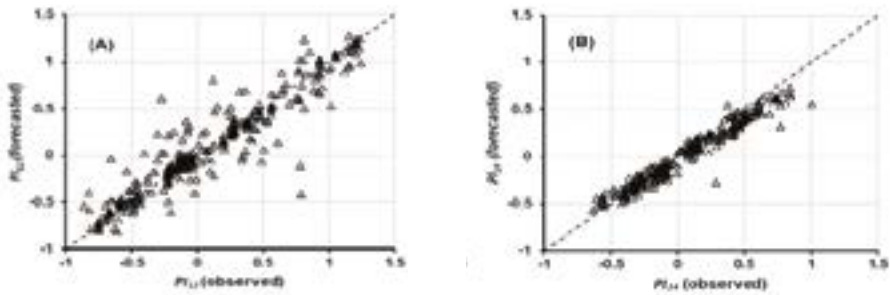


**Fig. 5.** Observations and predictions of an hANN model: The green line represents model predictions and the blue line represents observations of SPI (Maca and Pech, 2016).

A. Alsumaiei and M. Alrashidi forecasted droughts in Kuwait, which is located in a hyper-arid area, using non-linear autoregressive neural networks (NAR) (Alsumaiei and Alrashidi 2020). The precipitation index (PI) was used to predict droughts in this study. Similar to the SPI, negative values of PI indicate droughts, with -1 indicating the most extreme drought. NAR models are recurrent neural networks, meaning that some outputs are sent back as inputs, that integrate autoregressive models to predict time series data (Fig. 6). 12-month and 24-month scale PI values were used for next-time-step PI prediction. It was shown that NAR models produced acceptable accuracies, with models using 24-month scale PI values being more accurate (Fig. 7).



**Fig. 6.** Conceptual illustration of nonlinear autoregressive neural networks (NAR) (Alsumaiei & Alrashidi, 2020)



**Fig. 7.** Scatter plot of PI observations and NAR forecasts (Alsumaiei & Alrashidi, 2020)

### 3. Evapotranspiration Estimation

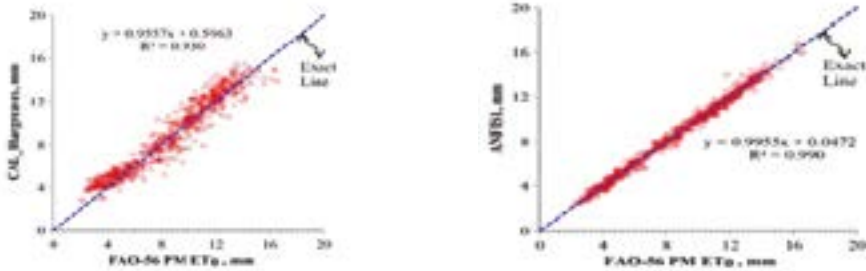
Evapotranspiration is the loss of moisture from earth by evaporation of free water and transpiration from plants. Evapotranspiration measurements are necessary to determine the water loss from crops and soil to subsequently plan irrigation schemes according to demands (Droogers & Allen, 2002).

Measuring evapotranspiration is hard due to the variety of factors influencing this process. These factors include solar radiation, temperature, soil properties, plant properties, humidity, etc. In order to normalize evapotranspiration measurements, Food and Agriculture Organization of the UN (FAO) recommends the use of the FAO-56 PM equation to calculate reference evapotranspiration (ET<sub>0</sub>). ET<sub>0</sub> is the evapotranspiration that occurs from a surface with certain properties and specific crops. Then, the evapotranspiration relevant to a certain area can be derived by knowing the correlations between soil and crop types and evapotranspiration. The FAO-56 PM equation, however, requires many climatic measurements and physical properties, which are not always available. This complexity of evapotranspiration measurement has induced research in estimating its values from easily obtainable climatic measurements, such as temperature and wind speed, using different machine learning models.

V. Nourani et al. thoroughly reviewed the use of artificial intelligence tools for reference evapotranspiration estimation, focusing on studies that apply a Wavelet transform on input variables (Nourani et al. 2014). M. Chia et al. provide a more recent review of ET<sub>0</sub> estimation using AI methods (Chia et al., 2020). M. Chia et al. focused in their review on hybridization methods. Hybridization is the use of data from different resources or a combination of different machine learning models to predict target variables with better consistency and less errors. In this section, a number of recent research on the previously mentioned subject will be examined.

H. Citakoglu et al. estimated monthly mean reference transpiration in Turkey from several combinations of input variables using adaptive network based fuzzy inference system (ANFIS) and artificial neural network (ANN) models (Citakoglu et al., 2014) air temperature, relative humidity, and solar radiation, recorded at stations in Turkey, are used as inputs to the ANFIS and ANN models so as to calculate ET<sub>0</sub> given by the FAO-56 PM (Penman-Monteith. Measurements spanning between 20-45 years were collected from 275 stations in Turkey. Monthly mean ET<sub>0</sub> was calculated in these stations using the recommended FAO-56 PM equation. Then, ANFIS and ANN models were applied to predict monthly mean ET<sub>0</sub> values from different combinations of climatic vari-

ables and results were compared to empirical estimation methods. H. Citakoglu et al. concluded that solar radiation, air temperature, wind speed, and relative humidity are the most effective input features for estimating ET<sub>0</sub>. Moreover, ANFIS models were found to be marginally better than ANN models in this respect. Fig. 8 shows a comparison of ANFIS model predictions and the calibrated Hargreaves empirical method.



**Fig. 8.** Monthly mean ET<sub>0</sub> predictions and measurements (Citakoglu et al., 2014) air temperature, relative humidity, and solar radiation, recorded at stations in Turkey, are used as inputs to the ANFIS and ANN models so as to calculate ET<sub>0</sub> given by the FAO-56 PM (Penman-Monteith).

Left: calibrated Hargreaves equation. Right: ANFIS model.

X. Wen et al. set a measuring station in a specific site in Ejina basin in China to measure meteorological data required for daily ET<sub>0</sub> estimation using the FAO-56 PM equation (Wen et al. 2015) **particularly in extremely arid regions. The objective of this research was to evaluate the use of a support vector machine (SVM.** Then, support vector regression (SVR) models were used to estimate daily ET<sub>0</sub> values. The measuring period was 146 days, whereby the first 102 days were used as training data and the remaining 44 values as a training set. The results show that even though the dataset was significantly small, SVR models were able to estimate ET<sub>0</sub> with acceptable accuracies. Results show that models that took in maximum and minimum daily temperatures and solar radiation as inputs gave the most accurate results. It is worth mentioning that all used methods tended to underestimate ET<sub>0</sub> values in comparison with FAO-56-PM. This study shows that AI techniques can be efficient even when only small datasets are available.



Z. Yin et al. used support vector regression and extreme learning machines (ELM) to predict future variations in ET<sub>0</sub> (Yin et al., 2017). Evapotranspiration is dependent on various meteorological variables, and these variables are in continuous variation because of climate change and global warming. Predicting future variations in ET<sub>0</sub> allows for planning and preparations to be made to cope with these variations. This study was conducted on the headwater region of the Heihe river in China. Combined data from local weather stations and the simulated global climate model (GCM) for the years 1961-2005 were used in this study. Projected climatic variables, such as temperature, humidity, wind speed etc., for the years 2010-2099 were obtained from GCM too. Data between 1961-1990 was used to train the model, and data for years 1991-2005 was used to test the models. Results from the testing phase showed that there is high correlation between FAO-56-PM ET<sub>0</sub> values and GCM-based values, which renders future GCM projections suitable for ET<sub>0</sub> prediction. Z. Yin et al. concluded that both models showed similar accuracies in ET<sub>0</sub> prediction. Fig. 9 shows boxplots of future predictions divided to short-term, mid-term, and long-term.

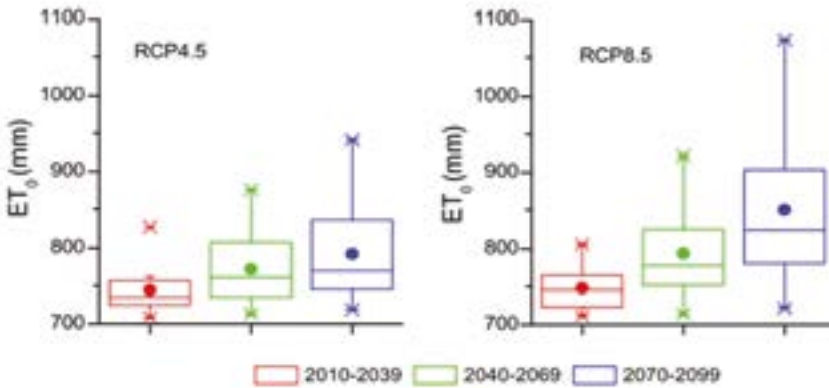


Fig. 9. ET<sub>0</sub> projections based on two different GCM scenarios (Yin et al., 2017).

C. Carter and S. Liang compared ten machine learning models to predict ET values using data collected from satellite sensors (GLASS, MODIS) and data from measuring towers obtained from Fluxnet and Ameriflux (Carter & Liang, 2019). The dataset used for this study contained instances from different locations around the world. The study

focused on the training times of the different methods and their resulting accuracies. Data was split twice, firstly to a small training set and larger validation and test sets, to test training times, and secondly into a large training set and smaller validation and test sets, for calculation of final accuracy and errors. Models with training time of 10 min or more per iteration in the first data split were excluded. This study emphasized the potential of satellite data inclusion in ML models for ET<sub>0</sub> estimation.

Haijiao Yu et al. investigated the uncertainty of artificial intelligence methods in estimating daily reference evapotranspiration (Yu et al. 2020). Whereas other papers were concerned about the potential of different AI models for ET<sub>0</sub> estimation and their accuracies, this paper attacked the problem from a more scientific way. Authors investigated the influence of different variables on AI models and the variation of ET<sub>0</sub> estimations, taking a step towards proving the practical and scientific AI solutions for reference evapotranspiration estimation. The study was conducted on a dataset belonging to Altay Prefecture province in China. Probability distributions were fitted to the variables in order to generate large amounts of random input data. Then, various variables and models were combined to study the effect of every variable on models. It was shown that wind speed, solar radiation, and max/min temperatures were the most contributing variables to the variation of ET<sub>0</sub> estimates (Fig. 10). These results were scientifically verified through the explanation of energy transformation and evapotranspiration demands.

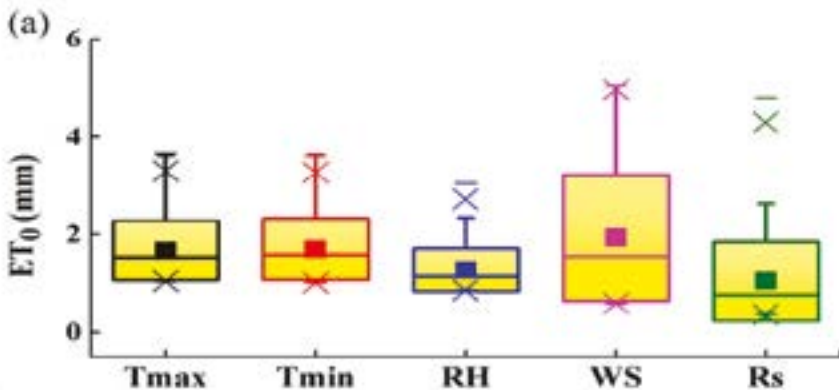
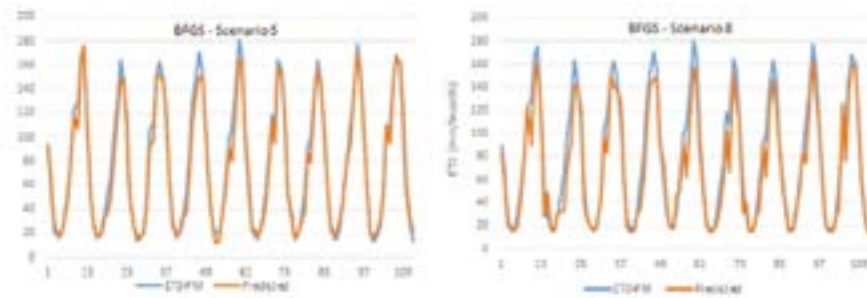


Fig. 10. ET<sub>0</sub> variations related to different variables (Yu et al., 2020).

M. Sattari et al. included kernel-based machine learning methods in their comparison of different ML models for monthly evapotranspiration estimation (Sattari et al., 2021). The study was conducted on data collected from weather stations in the province of Corum, Turkey. Data constituted of measurements from 312 months, spanning between 1993-2018, of which 200 were used as training data and 112 as test data. The study concluded that kernel-based ML models, like gaussian processes, returned good results, however, Broyden-Fletcher-Goldfarb-Shanno artificial neural network (BFGS-ANN) showed the lowest errors between all models (Fig.11).



**Fig. 11.** ET0 time series prediction vs observation for two variable combination scenarios (Sattari et al., 2021).

#### 4. Conclusion

Artificial intelligence has taken a large portion of research in climate science. The nonlinearity of meteorological variables and their dependency on many other properties and variables render machine learning models beneficial and efficient in this field. Moreover, climatical data is available in large datasets, which is necessary for ML applications. The previously reviewed papers showed that drought forecasts can be done with acceptable accuracies using various data transform schemes and machine learning models. Furthermore, reference evapotranspiration can also be estimated with high accuracy using easily measurable variables, allowing for ET0 estimation in undeveloped areas.

Future studies should first be more data focused than model focused. Most studies focus on model types and parameters, ignoring the scientific bases influencing predictions. Secondly, integrating the available prediction methods with AI driven methods should be studied to take a step towards practical application. These steps will allow for the creation of robust models that integrate empirical and data-driven methods to produce reliable results for real-world application.

## REFERENCES

Agana, N. A. & Homaifar, A. (2018,). EMD-Based Predictive Deep Belief Network for Time Series Prediction: An Application to Drought Forecasting. *Hydrology*, 5(1). doi: 10.3390/hydrology5010018.

Alsumaiei, A. A., & Alrashidi, M. S. (2020). Hydrometeorological Drought Forecasting in Hyper-Arid Climates Using Nonlinear Autoregressive Neural Networks. *Water (Switzerland)*, 12(9). doi: 10.3390/W12092611.

Belayneh, A., J. A. & Khalil, B. (2016). Short-Term SPI Drought Forecasting in the Awash River Basin in Ethiopia Using Wavelet Transforms and Machine Learning Methods. *Sustainable Water Resources Management*, 2(1), 87-101. doi: 10.1007/s40899-015-0040-5.

Carter, C. & Liang, S. (2019). Evaluation of Ten Machine Learning Methods for Estimating Terrestrial Evapotranspiration from Remote Sensing. *International Journal of Applied Earth Observation and Geoinformation*, 78, 86–92. doi: 10.1016/j.jag.2019.01.020.

Checchi, F. & Robinson, W. C. (2013). *Mortality among Populations of Southern and Central Somalia Affected by Severe Food Insecurity and Famine during 2010-2012*.

Chia, M. Y., Huang, Y. F., Koo, C. H. & Fung, K. F. (2020). Recent Advances in Evapotranspiration Estimation Using Artificial Intelligence Approaches with a Focus on Hybridization Techniques — A Review.

Citakoglu, H., Cobaner, M., Haktanir, T. & Kisi, O. (2014). Estimation of Monthly Mean Reference Evapotranspiration in Turkey. *Water Resources Management*, 28(1), 99–113. doi: 10.1007/s11269-013-0474-1.

Droogers, P. & Allen, R. G. (2002). Estimating Reference Evapotranspiration under Inaccurate Data Conditions. *Irrigation and Drainage Systems*, 16, 33–45.

Huntingford, C., Jeffers, E. S., Bonsall, M. B., Christensen, H. M., Lees, T. & Yang, H. (2019). Machine Learning and Artificial Intelligence to Aid Climate Change Research and Preparedness. *Environmental Research Letters*, 14(12). doi: 10.1088/1748-9326/ab4e55.

Maca, P. & Pech, P. (2016). Forecasting SPEI and SPI Drought Indices Using the Integrated Artificial Neural Networks. *Computational Intelligence and Neuroscience* 2016. doi: 10.1155/2016/3868519.

Nourani, V., Baghanam, A. H., Adamowski, J. & Kisi, O. (2014). Applications of Hybrid Wavelet-Artificial Intelligence Models in Hydrology: A Review. *Journal of Hydrology*, 514, 358–77. doi: 10.1016/j.jhydrol.2014.03.057.

Overpick, J. T., Easterling, D. R., Meehl, G. A. & Bony, S. (2011). Climate Data Challenges in the 21st Century. *Science*, 331, 700–702.

Sattari, M. T., Apaydin, H., Band, S. S., Mosavi, A. & Prasad, R. (2021). Comparative Analysis of Kernel-Based versus ANN and Deep Learning Methods in Monthly Reference Evapotranspiration Estimation. *Hydrology and Earth System Sciences*, 25(2), 603–18. doi: 10.5194/hess-25-603-2021.

Wen, X., Si, J., He, Z., Wu, J., Shao, H. & Yu, H. (2015). Support-Vector-Machine-Based Models for Modeling Daily Reference Evapotranspiration With Limited Climatic Data in Extreme Arid Regions. *Water Resources Management*, 29(9), 3195–3209. doi: 10.1007/s11269-015-0990-2.

Yin, Z., Feng, Q., Yang, L., Deo, R. C., Wen, X., Si, J. & Xiao, S. (2017). Future Projection with an Extreme-Learning Machine and Support Vector Regression of Reference Evapotranspiration in a Mountainous Inland Watershed in North-West China. *Water (Switzerland)*, 9(11). doi: 10.3390/w9110880.

Yu, H., Wen, X., Li, B., Yang, Z., Wu, M. & Ma, Y. (2020). Uncertainty Analysis of Artificial Intelligence Modeling Daily Reference Evapotranspiration in the Northwest End of China. 176(August). doi: 10.1016/j.compag.2020.105653.



# DEEP LEARNING MODEL FOR AUTOMATED DIAGNOSIS OF SEIZURE USING EEG SIGNALS

*Huda M. S. Algharib*<sup>1</sup>

---

## Abstract

A seizure (or epileptic seizure) is a brain disorder includes serious symptoms such as involuntary movements and consciousness disorders. Electroencephalogram (EEG) is prominently used to measure and monitor the electrical activity of the brain. The interpretation of EEG signals helps to understand the pathophysiology of the brain, hence assisting in the diagnosis brain abnormalities and disorders. However, the EEG signals are extremely difficult to interpret due to their nonlinear and non-stationary nature. Diagnosis and monitoring of the disease using the conventional machine learning techniques require a lot of domain expertise and sound knowledge of data mining to learn a robust model. More recently, deep learning methodologies have shown promising improvement in the recognition accuracy of EEG signals. In this study, a new deep learning model is developed for Computer-Aided Diagno-

---

<sup>1</sup> Ankara University, Faculty of Engineering, Department of Computer Engineering, ORCID: 0000-0003-4811-2856

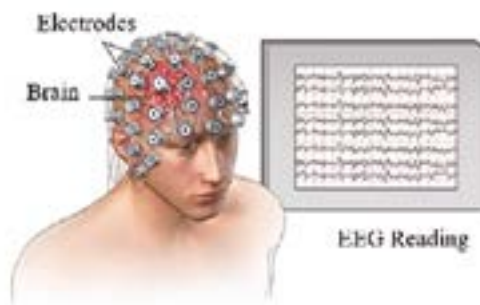


sis (CAD) of seizures based on EEG signals. The proposed 1DCNN-BiGRU model combines one-dimensional convolutional neural network (1DCNN) with Bidirectional Gated Recurrent Unit (BiGRU) to extract the spatial and temporal features from EEG signals, and then utilizes a dense layer with softmax activation function to classify the features. The proposed model is validated and tested using Bonn University database, achieving high classification accuracies.

**Keywords:** Seizure Detection, EEG, Deep Learning, CNN, GRU, BiGRU.

## 1. Introduction

The brain is a vital organ that represents the center of the human body and controls important tasks such as movement, emotions, communication, language, thinking and memory, in addition to, its responses to the environmental demands and changes. All these tasks can be achieved via the chemical and electrical signals of the brain. However, many of the brain disorders are mainly linked to the abnormal changes in electrical brain activity such as epileptic seizures. Several screening techniques have been developed to diagnose epileptic seizures, including MRI, EEG, Magnetoencephalography (MEG) and Positron Emission Tomography (PET) (Kulaseharan et al., 2019; Zazzaro et al., 2019; Klink et al., 2019). The EEG is more preferred than the other techniques because it can monitor the neural or the electrical brain activity over a period of time and exhibit clear rhythms in the frequency domain in addition, it is economical and portable (Subasi et al., 2019). Figure 1 shows how an EEG device records the electrical activity of the brain. It contains metal electrodes that can detect brain activity when placed on a subject's scalp. The electrodes transform the electrical activity into patterns, commonly called brain wave, and then the EEG device sends the data to a computer or cloud server.



**Figure 1:** EEG Machine records the brain waves.

Figure 2 illustrates a graphical representation of the electrical activity of the brain and its corresponding EEG signal for healthy persons and seizure patients. Normally, neurons (also called brain cells or nerve cells) communicate via electrical signals which are normally regulated

during the normal activity of the brain (see Figure 2 (A)). However, the uncontrolled electrical discharges in a group of brain cells cause seizures (Harvard Health Publications, 2014; American Epilepsy Society). This abnormal activity may happen in one group of cells on one side of the brain (Focal-onset seizures) or groups of cells on both/all sides of the brain at the same time (Generalized- onset Seizures). A seizure can be a single event due to an acute cause, such as medication. When a person has recurring seizures, this is known as epilepsy. Focal and generalized onset seizures usually have different causes, and it is important for the neurologist to get an accurate seizure diagnosis in order to determine the most appropriate type of treatment for the patients and identify the cause of the seizures. The traditional method for seizure detection is conducting the direct visual inspection of EEG signals by neurologists. However, this technique is laborious and time-consuming, in addition to; it is limited in identifying abnormalities since the EEG signals are highly complex and difficult to be visually interpreted. Hence, the development of machine learning techniques is very essential to automatically classify these EEG signals correctly with very less time. The traditional machine learning techniques, need a lot of domain expertise and sound knowledge of data mining to learn a robust model, they also only perform well for a limited data. Nowadays, with the increase in the availability of data, the traditional machine learning techniques may not perform very well. For this reason, many researchers have resorted to deep learning techniques to analyze and interpret the EEG signals. A further advantage of using deep learning models is that these models are developed using extensive open-source toolboxes and libraries that written in Python. This advantage has facilitated for the researchers to recreate the previously obtained results and contribute to other works.\_

Since 2016, researchers have embarked on the area of diagnosing epileptic seizure using deep learning models, such as Convolutional Neural Networks (CNN) and Recurrent Neural Networks (RNN). These deep learning models have shown promising improvement in the accuracy of EEG signals identification and classification as reviewed in the next section.



**Figure 2:** An illustration of the brain activity of healthy subject compared to seizure patient.

## 2. Literature Review

This section introduces an overview of the different architectures of deep neural networks in the field of epileptic seizure detection and diagnosis. In literature, the 1DCNNs have been employed by many researchers for the purpose of seizure detection and classification. The authors in have been used 1DCNN for the feature extraction procedure and they reported classification accuracy of 83.86% (Thomas et al., 2018). In another research the 1DCNN to classify the seizure events in multi-channel EEG signals (Boonyakitantont et al., 2019). To increase the accuracy, the signals from each channel are segmented into 4-second intervals first, and then each 3-second are overlapped with the previous segment. The classification accuracy of this method on CHB-MIT database was 99.07%. In the Empirical Mode Decomposition (EMD) technique was used for feature extraction, and 1DCNN was employed to achieve a high accuracy in the multi-class classification task. Another study on seizure detection and diagnosis using a 13-layer one-dimensional deep convolutional neural network (1DCNN) and 300 signals of five persons from the University of Bonn dataset, a classification accuracy of 88.67% was achieved (Daoud et al., 2018; Acharya et al., 2018). The authors in developed an ensemble of Pyramidal One-Dimensional Convolutional Neural Network (P-1DCNN) models for epilepsy Detection with an accuracy of 99.10% (Ullah et al., 2018).

With the goal of improved classification of EEG signals, the 2DCNN was employed by many researchers. In one study a new 2DCNN model was proposed to extract the spectral and temporal features of EEG signals and used them to learn the general structure of seizures (Hossain et al., 2019). In the EEG signals with 32 channels were divided into windows, each with a 2-second width, and then converted them into spatial representation (Bouaziz et al., 2019). The resulting images were used as input to the 2DCNN network. The researchers in used pre-trained Convolutional Neural Networks named (LeNet, AlexNet, and GoogLeNet/Inception-V1) for focal and non-focal epilepsy seizure classification (Taqi et al., 2017). The three models were applied on Bern-Barcelona dataset and each model achieved 100% classification accuracy. Ahmedt-Aristizabal et al. proposed automatic diagnosing of epilepsy from the facial images by extracting the semiological patterns of facial states and classify them (Ahmedt-Aristizabal et al., 2018). A 16 layers 2DCNN model called Visual Geometry Group (VGG-16) was employed in their study. The model was trained primarily by well-known datasets, followed by 1DCNN and LSTM networks in the final few layers, and achieved 95.19% classification accuracy.

In another researches, deep learning techniques that have a different structure from CNNs such as Recurrent Neural Networks (RNNs) were employed for epileptic seizure detection. This class of networks includes long short-term memory (LSTM) approaches and gated recurrent units (GRUs). The authors in have employed the both types of RNNs with sigmoid classification for epileptic Seizure detection, and they achieved a classification accuracy of 96.82% and 96.67% using LSTM and GRU, respectively (Chen et al., 2018).

Hussein et al. developed a deep (LSTM) network to learn the high-level representations of the EEG signals. These representations were fed as inputs to one FC time-distributed Dense layer to extract most robust EEG features relevant to epileptic seizures (Hussein et al., 2018). The proposed method using Bonn dataset achieved 100% accuracy of the two-class, three-class, and five-class EEG classification problems. The authors in designed a deep LSTM network to learn and model discriminative temporal patterns from EEG raw data (Ahmedt-Aristizabal

et al., 2018). Using 10-fold cross-validation scheme on Bonn dataset, they achieved 95.54% validation accuracy and 91.25% test accuracy. In another study, the authors in developed a new approach that integrates the Independently RNN (IndRNN) with a dense structure and an attention mechanism for the seizure/non-seizure classification (Yao et al., 2019). They conducted ten cross-validation experiments on the noisy CHB-MIT data set, and the accuracy arrived at 88.70%. Talathi used the spectral features from 51 EEG sub-segments as input to a 4-layer GRU network with a softmax FC layer. The length of each sub-segment was 80 samples and they achieved 98% accuracy (Talathi, 2017).

In this study, a deep learning-based computer-aided diagnosis (CAD) system is proposed for the automated detection and diagnosis of epileptic seizure. An eight-layer 1DCNN-BiGRU model, including dense layer with softmax activation function is presented for features extraction and classification of EEG signals.

### 3. Materials and Methods

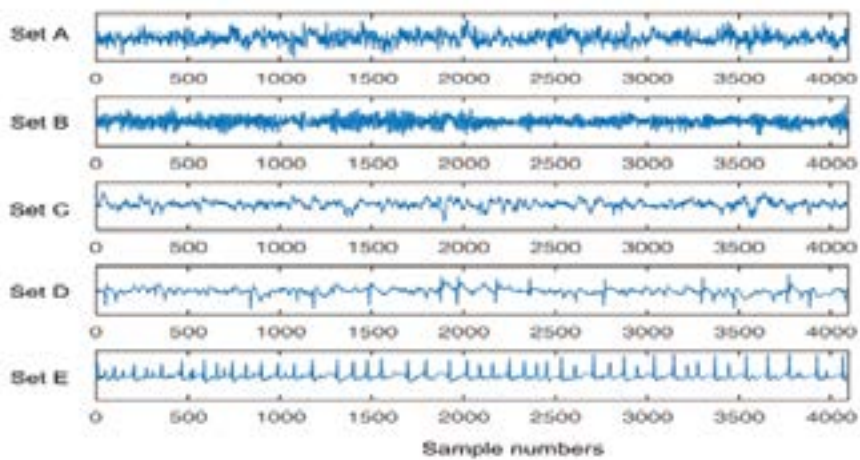
In this section, we describe the used dataset and the proposed deep learning model for the classification of epileptic seizure EEG signals.

#### 3.1. EEG Dataset Description

The EEG dataset used in this research was recorded at Bonn University (Andrzejak et al., 2001). The complete database includes five sets (denoted A–E); each having 100 single-channel EEG records with duration of 23.6 seconds. Each record in the dataset consists of 4097 samples (see Figure 3). The EEG segments were cut out from continuous multichannel EEG recordings after removing the artifacts due to eye movements or muscle activity via visual inspection. Sets A and B were obtained from five healthy subjects with eyes open and closed, respectively. Sets C and D were obtained from patients during seizure-free intervals (i.e., preictal) from the hippocampal half sphere and epileptogenic zone, respectively. Set E was obtained from the same patients during the seizure activity. The detail is given in Table 1.

**Table 1:** The details of University of Bonn epilepsy dataset.

Set Name	A	B	C	D	E
Participant's condition	Healthy	Healthy	Epileptic	Epileptic	Epileptic
Target class	Normal	Normal	Preictal	Preictal	Seizure
Number of records	100	100	100	100	100
Duration of each record	23.6s	23.6s	23.6s	23.6s	23.6s
Number of samples in each record	4097	4097	4097	4097	4097
Description	Eyes opened recording	Eyes closed recording	Recorded during the Pre-seizure from the hippocampal half sphere	Recorded during the Pre-seizure from the epileptic area	Recorded during the seizure activity

**Figure 3:** The sample EEG signals from Bonn University database.

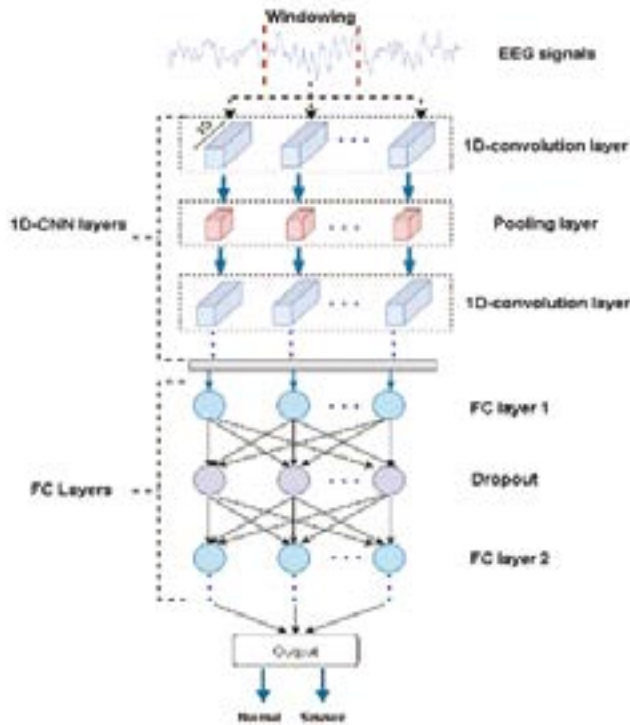
### 3.2. Deep Learning

#### 3.2.1. One Dimensional Convolutional Neural Networks (1DCNNs)

These networks have a straightforward structure which makes them suitable for processing the EEG signals for detection of epileptic seizures. In 1D architecture, EEG signals in the form of one dimensional are used as input to the 1D-CNNs. Figure 4 shows a general form of a 1D-CNN used for epileptic seizure detection. In 1D convolutional operation, the output size  $O$  of the feature map along the dimension is given by

$$O = (I - F + P) / S \quad (1)$$

Where  $I$  the length of the input vector,  $F$  is the length of the filter,  $P$  is the amount of zero padding and  $S$  is the stride.

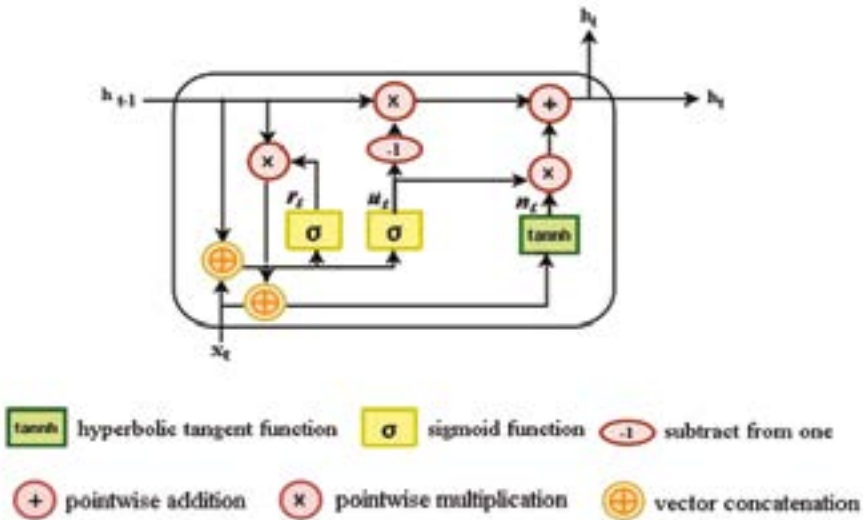


**Figure 4:** Typical 1D-CNN model for epileptic seizure detection.



### 3.2.2 Bi-directional Gated Recurrent Unit Neural Network (Bi-GRU)

The BiGRU is improved GRU model that has the ability to learn information from previous and subsequent data to use them to influence the current inputs (Liu et al., 2021). In particular, the bi-GRU model combines two unidirectional GRUs in opposite directions, one GRU that moves forward starting from the beginning of the data sequence, the other GRU that moves backward starting from the ending of the data sequence. This process allows learning information from both future and past data when dealing with the current data. Figure 5 illustrates the inner structure of GRU cell.



**Figure 5:** The inner structure of GRU cell.

The calculation process in the GRU cell is defined as follows (Cho et al., 2014):

$$\begin{aligned}
 r_t &= \sigma(W_r[h_{t-1}, x_t] + b_r) \\
 u_t &= \sigma(W_u[h_{t-1}, x_t] + b_u) \\
 n_t &= \tanh(W_n[r_t \odot h_{t-1}, x_t] + b_n) \\
 h_t &= (1 - u_t) * h_{t-1} + u_t * n_t
 \end{aligned} \quad (2)$$

Where  $x_t$  is input signal feature for time  $t$ ,  $w_t$  is the weight matrix in the corresponding gate,  $b_t$  is the bias in the corresponding gate,  $r_t$  denotes the reset factor which controls the influence level of  $h_{t-1}$  on  $h_t$ ,  $u_t$  denotes the update factor which controls the update of the memory state.

The BiGRU cell can be defined as follows (Liu et al., 2021):

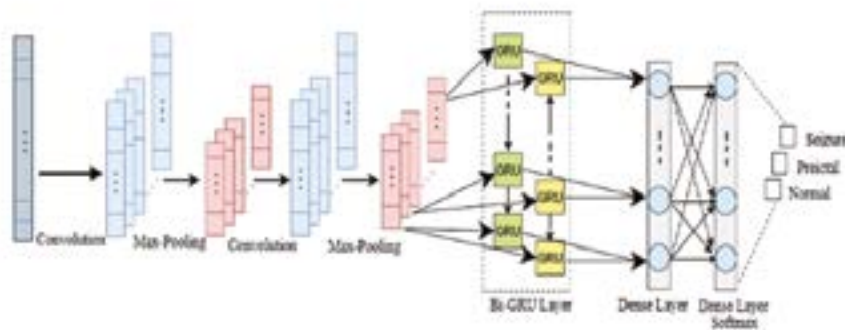
$$\begin{aligned}\vec{h}_t &= GRU_{\text{fwd}}(x_t, \vec{h}_{t-1}) \\ \overleftarrow{h}_t &= GRU_{\text{bwd}}(x_t, \overleftarrow{h}_{t+1}) \\ h_t &= \vec{h}_t \oplus \overleftarrow{h}_t\end{aligned}\quad (3)$$

Where  $\vec{h}_t$  and  $\overleftarrow{h}_t$  are the states of the forward GRU and the backward GRU, respectively,  $\oplus$  indicates the operation of concatenating two vectors.

### 3.2.3. Proposed 1DCNN-BiGRU Model

The developed deep 1DCNN-BiGRU model consists of eight-layers as illustrated in Figure 6. The proposed deep model extracts the spatio-temporal features from the raw EEG signals using two 1D-CNN layers, and each convolution layer is followed by a Max-pooling layer to extract only the most significant features and control the overfitting. To capture the temporal information from the feature maps, a BiGRU layer is applied. The stride size is assigned to 1 and 2 for the Convolution and Max-pooling processes, respectively. The input layer (denoted layer 0) contains the raw EEG signals. The next layer is the convolution layer which performs the convolution operation on the input signal with 32 filters of size 5, resulting in feature maps of size  $4094 \times 32$ . Then, a Max-pooling layer with a kernel of size 2, is applied to these feature maps, reducing the size of the feature map by half (i.e., from  $4094 \times 32$  to  $2047 \times 32$ ). After that, the reduced feature maps are convolved in the third layer with 64 filters of size 3. In layer 4, a Max-pooling of size 2 is applied to the output feature maps from layer 3, reducing the size of the feature map from  $2045 \times 64$  to  $1022 \times 64$ . After that, the extracted features are fed as inputs to the GRU layer. In layer 6 (Max-pooling layer), the size of the feature maps is reduced and the output of this layer is processed in

the Dense layer (Layer 7). The softmax activation function in the output layer (Layer 7) performs the classification task, where the EEG data are classified in ternary (Normal vs Preictal vs Seizure) or binary (Seizure vs non-seizure and Normal vs. Epileptic) depending on the classification problem. The details of the proposed deep architecture are given in Table 2. The parameters of each layer were determined using the brute force technique.



**Figure 6:** The architecture of the proposed 1D-CNN-BiGRU model.

#### 4. Experimental Results and Discussion

In this section, the execution details of the proposed CNN-BiGRU model and the specification of the experiment hardware are given. Then the obtained results of our CAD system are presented and discussed.

**Table 2:** The parameter values of each layer of the proposed CNN-BiGRU model.

No	Layer type	Kernel Size	Parameters	Output Shape
0	Input	-	-	4098×1
1	Conv1D	32×5	stride=1 activation = ReLU	4094×32
2	MaxPooling1D	2	stride=2	2047×32
3	Conv1D	64×3	stride=1 activation = ReLU	2045×64
4	MaxPooling1D	2	stride=2	1022×64

5	Bi-GRU	32	-	1022×32
6	MaxPooling1D	2	stride=2	511×32
7	Dense	-	-	50
8	Dense	-	activation=Softmax	(2,3)

#### 4.1. Experimental Setup

The EEG signals of Bonn database are evaluated by using the 10-fold cross validation technique in this study. 90% of the data are used for training of the proposed CNN model, and remaining 10% as testing. The model is trained using only 20 epochs where each epoch defines one-iteration through the entire training dataset. In order to avoid over-fitting, the training data after each epoch are split into two parts: 90% to train the model, and the remaining 20% to validate the CNN-BiGRU model. Our model was developed using open-source software library called Keras. The library provides numerous components such as layers, activation functions, and optimizers necessary to design and evaluate a deep architecture model. The whole experiment was carried out on a computer with Intel(R) Core(TM) i7-4712MQ 2.30 GHz CPU, 8 GB RAM and NVIDIA GeForce 920M 2 GB graphics card.

#### 4.2. Results

To show the effectiveness of the CNN-BiGRU model, we considered three experiment cases: (i) Normal vs Preictal vs Seizure (AB vs CD vs E, A vs D vs E, B vs D vs E), (ii) Normal vs Epileptic (AB vs CDE), (iii) Seizure vs non-seizure (A vs E, B vs E, AB vs E, C vs E, D vs E, CD vs E). In addition, we compare the obtained results using a Bonn dataset with the results of the state-of-the-art methods.

##### 4.2.1. Experiment 1: Normal vs Preictal vs Seizure Classification

In this experiment, the EEG signals are classified into three classes (i.e. a ternary classification problem). We select different combinations for this classification which are ((i) normal (AB) vs Preictal (CD) vs sei-

zure (E), (ii) normal (A) vs Preictal (D) vs seizure (E), (iii) normal (B) vs Preictal (D) vs seizure (E)). From the results in Table 3, it can be observed that the classification using normal signals that recording during closed eye (B dataset) is better than the normal signals that recording during open eye (A dataset).

**Table 3:** Classification results of the proposed model for Normal vs Preictal vs Seizure.

			Predicted			Accuracy	Precision	Recall	F1-Score
			AB	CD	E	(%)	(%)	(%)	(%)
AB-CD-E	Original	AB	200	0	0	100	100	100	100
		CD	0	200	0				
		E	0	0	100				
			Predicted						
			A	D	E				
A-D-E	Original	A	100	0	0	99.00	100	98.50	98.52
		D	2	98	0				
		E	1	0	99				
			Predicted						
			B	D	E				
B-D-E	Original	B	100	0	0	100	100	100	100
		D	0	100	0				
		E	0	0	100				

#### 4.2.2. Experiment 2: Normal vs Seizure Epileptic Classification

In this experiment, the EEG signals are classified into two classes which are (normal (AB) vs Epileptic (CDE)). The obtained results using 10-fold cross-validation are shown in Table 4. As show, the proposed model achieves high classification accuracy with mean of 100%.

**Table 4:** Classification results of the proposed model for Normal vs epileptic.

			Predicted		Accuracy	Precision	Recall	F1-Score
			AB	CDE	(%)	(%)	(%)	(%)
AB-CDE	Original	AB	200	0	100	100	100	100
		CDE	0	300				

### 4.2.3. Experiment 3: Seizure vs Non-Seizure

This experiment involves six combinations for the binary classification of EEG signals ((i) normal (A) vs seizure (E), (ii) normal (B) vs seizure (E), (iii) normal (AB) vs seizure (E), (iv) Preictal (C) vs seizure (E), (v) Preictal (D) vs seizure (E), (vi) Preictal (CD) vs seizure (E)). The results in Table 5 confirm the robustness of the proposed model with mean accuracies of 99.50% and 100%.

**Table 5:** Classification results of the proposed model for Seizure vs non-seizure.

			Predicted		Accuracy	Precision	Recall	F1-Score
			A	E	(%)	(%)	(%)	(%)
A-E	Original	A E	100	0	100	100	100	100
			0	100				
			Predicted B E					
B-E	Original	B E	100	0	100	100	100	100
			0	100				
			Predicted AB E					
AB-E	Original	AB E	200	0	100	100	100	100
			0	100				
			Predicted C E					
C-E	Original	C E	100	0	99.50	99.00	100	99.50
			1	99				
			Predicted D E					
D-E	Original	D E	100	0	99.50	99.00	100	99.50
			1	99				
			Predicted CD E					
CD-E	Original	CD E	200	0	100	100	100	100
			0	100				

### 4.2.4. Comparison with State-of-The-Art Methods

Many methods have been proposed for the Automated classification of EEG signals. According to our knowledge, a very little work has been proposed to extract both spatial and temporal features from EEG sig-

nals. The spatiotemporal features are very important for accurate classification of Seizure patients as investigated in this work. The comparison with state-of-the-art methods in Table 6 shows that our model has better performance in terms of accuracy.

**Table 6:** Results obtained using State-of-the-art Methods on Bonn EEG dataset.

Study	Preprocessing	DL Network	Number of Layers	K-fold	Classifier	Datasets	Accuracy
[11]	Normalization	1DCNN	13	10	Softmax	B-D-E	88.67
[12]	DA	P-1DCNN	14	10	Softmax	A-E	100
						AB-CDE	99.50
						AB-CD-E	99.10
[21]	Autocorrelation	GRU	4	NA	LR	AB-CD-E	98.00
[23]	CWT	2DCNN	5	10	Softmax	A-E	99.50
						B-E	99.50
						C-E	98.50
						D-E	98.50
						A-D-E	99.00
[17]	DWT+ Segmentation+ Normalization	1DCNN	4	5	Sigmoid	CD-E	97.27
		LSTM	3				96.82
		GRU	3				96.67
[19]	-	LSTM	2	10	Sigmoid	A-E	97.00
						B-E	92.50
						C-E	92.00
						D-E	91.00
[24]	Normalization	1DCNN	15	10	Softmax	B-D-E	98.67
Ours	-	1DCNN-Bi-GRU	8	10	Soft-max	A-E	100
						B-E	100
						C-E	99.50
						D-E	99.50
						AB-E	100
						CD-E	100
						AB-CDE	100
						A-D-E	99.00
						B-D-E	100
						AB-CD-E	100

### 4.3. Merits and Drawbacks of the New Model

The main advantages of this work include:

- 1) An eight-layered deep model has been developed to accurately classify Seizure patients.
- 2) The proposed deep model effectively extracts both discriminative spatial and temporal patterns from the raw EEG data without any pre-processing step.
- 3) The model is validated using 10-fold cross validation technique.
- 4) High classification accuracy compared with State-of-the-art techniques is an attestation to the robustness of the developed model.

Despite its advantages, this work does exhibit some limitations which include:

- 1) The proposed model was trained and tested using a relatively small database, and this work lacks of huge EEG datasets.
- 2) The proposed CNN-BiGRU model combines CNN with BiGRU cells, which they are costly to compute.

## 5. Conclusion

Detection the brain abnormalities and disorders using EEG signals is very important challenge. The accurate detection of epileptic seizures can help to provide suitable treatment to the patients, and hence enhances the quality of their life. In addition to that, the early stage of seizure detection helps the patient to take medication immediately and prevent seizure. In this study, we developed a new deep 1DCNN-BiGRU that relies on 1D CNN and BiGRU layers for the automated detection of seizure. Two convolutional layers, each containing a set of filters, are applied to the input EEG data to capture the hierarchical or spatial features. The output of the convolutional layers is then fed into a BiGRU layer which contains multiple memory cells to discover the temporal dependencies in the extracted features. We demonstrated that our model outperforms the state-of-the-art methods in the task of seizure detection and diagnosis using EEG signals.



## REFERENCES

- Kulaseharan, S., Aminpour, A., Ebrahimi, M. & Widjaja, E. (2019). Identifying lesions in paediatric epilepsy using morphometric and textural analysis of magnetic resonance images. *NeuroImage: Clinical*, 21, 101663.
- Zazzaro, G., Cuomo, S., Martone, A., Montaquila, R. V., Toraldo, G. & Pavone, L. (2019). Eeg signal analysis for epileptic seizures detection by applying data mining techniques. *Internet of Things*, 100048.
- Klink, N. V., Mooij, A., Huiskamp, G., Ferrier, C., Braun, K., Hillebrand, A. & Zijlmans, M. (2019). Simultaneous meg and eeg to detect ripples in people with focal epilepsy. *Clinical Neurophysiology*, 13(7), 1175–1183.
- Pianou, N. & Chatziioannou, S. (2019). Imaging with pet/ct in patients with epilepsy. In *Epilepsy Surgery and Intrinsic Brain Tumor Surgery*. Springer, 45–50.
- Subasi, A., Kevric, J. & Canbaz, M. A. (2019). Epileptic seizure detection using hybrid machine learning methods. *Neural Computing and Applications*, 31(1), 317–325.
- Harvard Health Publications, Harvard Medical School, 2014. Seizure overview. Retrieved from: <http://www.health.harvard.edu/mind-and-mood/seizure-overview>.
- American Epilepsy Society, Facts and figures. Retived from: [https://www.aesnet.org/for\\_patients/facts\\_figures](https://www.aesnet.org/for_patients/facts_figures).
- Thomas, J., Comoretto, L., Jin, J., Dauwels, J., Cash, S. S. & Westover, M. B. (2018). Eeg classification via convolutional neural network-based interictal epileptiform event detection, in 2018 40th Annual International Conference of the IEEE Engineering in Medicine and Biology Society (EMBC), 3148–3151.
- Boonyakitanont, P., Lek-uthai, A., Chomtho, K. & Songsiri, J. (2019). A comparison of deep neural networks for seizure detection in eeg signals. *bioRxiv*, 702654.
- Daoud, H. G., Abdelhameed, A. M. & Bayoumi, M. (2018). Automatic epileptic seizure detection based on empirical mode decomposition and deep neural network. *International Colloquium on Signal Processing & Its Applications (CSPA)*, 182–186.
- Acharya, U. R., Oh, S. L., Hagiwara, Y., Tan, J. H. & Adeli, H. (2018). Deep convolutional neural network for the automated detection and diagnosis of seizure using eeg signals. *Computers In Biology And Medicine*, 100, 270–278.
- Ullah, I., Hussain, M. & Aboalsamh, H. (2018). An automated system for epilepsy detection using eeg brain signals based on deep learning approach, *Expert Systems with Applications*, 107, 61–71.
- Hossain, M. S., Amin, S. U., Alsulaiman, M. & Muhammad, G. (2019). Applying deep learning for epilepsy seizure detection and brain mapping visualization. *ACM Transactions on Multimedia Computing, Communications, and Applications (TOMM)*, 15(1), 1–17.

Bouaziz, B., Chaari, L., Batatia, H. & Quintero-Rinc' A. (2019). Epileptic seizure detection using a convolutional neural network in Digital Health Approach for Predictive, Preventive, Personalised and Participatory Medicine. *Springer*, 79–86.

Taqi, A. M., Al-Azzo, F., Mariofanna, M. & Al-Saadi, J. M. (2017). Classification and discrimination of focal and non-focal eeg signals based on deep neural network. *International Conference on Current Research in Computer Science and Information Technology (ICCIT)*, 86–92.

Ahmedt-Aristizabal, D., Fookes, C., Nguyen, K., Denman, S., Sridharan, S. & Dionisio, S. (2018). Deep facial analysis: A new phase I epilepsy evaluation using computer vision. *Epilepsy & Behavior*, 82, 17–24.

Chen, X., Ji, J., Ji, T. & Li, P. (2018). Cost-sensitive deep active learning for epileptic seizure detection. *International Conference on Bioinformatics, Computational Biology, and Health Informatics*, 226–235.

Hussein, R., Palangi, H., Ward, R. & Wang, Z. J. (2018). Epileptic seizure detection: a deep learning approach. arXiv preprint arXiv:1803.09848.

Ahmedt-Aristizabal, D., Fookes, C., Nguyen, K. & Sridharan, S. (2018). Deep classification of epileptic signals. *Annual International Conference of the Engineering in Medicine and Biology Society (EMBC)*, 332–335.

Yao, X., Cheng, Q. & Zhang, G.-Q. (2019). Automated classification of seizures against nonseizures: A deep learning approach. arXiv preprint arXiv:1906.02745.

Talathi, S. S. (2017). Deep recurrent neural networks for seizure detection and early seizure detection systems. arXiv preprint arXiv:1706.03283.

Andrzejak, R. G., Lehnertz, K., Rieke, C., Mormann, F., David, P., Elger, C. E. (2001). Indications of nonlinear deterministic and finite dimensional structures in time series of brain electrical activity: Dependence on recording region and brain state. *Physical Review E*, 64, 061907.

Türk, Ö., Özerdem, M. S. (2019). Epilepsy Detection by Using Scalogram Based Convolutional Neural Network from EEG Signals. *Brain Sci.*, 9, 115.

Abiyev, R., Arslan, M., Idoko, J.B., Sekeroglu, B. & Ilhan, A. (2020). Identification of epileptic eeg signals using convolutional neural networks. *Appl. Sci*, 10, 4089.

Cho, K., Merriënboer, B. V., Gulcehre, C., Bahdanau, D., Bougares, F., Schwenk, H., & Bengio Y. (2014). Learning phrase representations using RNN encoder-decoder for statistical machine translation. *Proceedings of the 2014 Conference on Empirical Methods in Natural Language Processing (EMNLP)*, 1724–1734.

Liu, X., Wang, Y., Wang, X., Xu, H., Li, C. & Xin, X. (2021). Bi-directional gated recurrent unit neural network based nonlinear equalizer for coherent optical communication system. *Optics express*, 29(4), 5923–5933. Doi: <https://doi.org/10.1364/OE.416672>



# DEEP CAMOUFLAGED OBJECT SEGMENTATION

*Rabeb Hendaoui*<sup>1</sup>

---

## Abstract

In natural environments, camouflaged targets are difficult to detect since they look so similar to the surroundings. Detecting these camouflaged objects is, therefore, a difficult task and more challenging than traditional object detection/segmentation. It is conceivable that effective camouflaged object detection algorithm could be applied as a pest control tool in agriculture, or as a way to detect infection or tumor in medical images. Despite that camouflaged object detection have a wide range of useful applications, but the problem of detecting them has been less studied. Our paper presents a novel deep network that alleviates this problem using a multilevel attention network. First, we extract features based on a modified ResNet network, then an inception module is designed to enhance features from multiscale receptive fields for a better feature representation. Our proposed multi-attention module generates

---

<sup>1</sup> PhD Student, Karadeniz Technical University, Faculty of Engineering, Computer Engineering

better discriminative feature representations and combines semantic and spatial information from different levels to find and distinguish the camouflaged object far better from its surroundings. Our experiments carried out on a camouflaged object dataset demonstrate that our approach outperforms the state-of-the-art methods.

**Keywords:** Camouflage Patterns, Object Segmentation, Deep Learning.

## 1. Introduction

A very rapid and successful expansion has taken place in computer vision research in the last few years. This has been accomplished in a variety of areas, including object detection. Different object detection algorithms have been developed in the literature to tackle diverse visual object detection problems with differing properties and characteristics. Objects can camouflage themselves and hide their signatures in their surroundings. Due to camouflage, object detection becomes more challenging. The camouflage effect refers to a way to integrate the target's signature into the background, as illustrated in Figure 1. Camouflage is a way prey hides from predators by changing their patterns, textures, and colorations to match the surroundings. Human vision systems can't adequately discern a camouflaged object. Detecting hidden foreground objects from background images is achieved using camouflage detection methods. Biologically, some animals are camouflaged in the environment by having unique characteristics. Objects that are camouflaged look almost identical to their surroundings. Objects camouflaged in this manner are the same color as their surroundings, and their texture is destroyed so that it blends into the surroundings. As a result, such camouflaged objects are difficult to detect. Because of the complexity of the problem, fewer works have been conducted using computer vision techniques.



**Figure 1.** A visual illustration of camouflaged images: (a) The image shows the coloration and texture of the scorpion with surrounding, (b) In the image one hunter is disguised in the background.

Two types of camouflage images exist, natural and artificial. Here are the explanations;

**Natural camouflage:** Animals, insects, and humans use natural camouflage to hide and avoid being detected by predators. A camouflaged organism stands a better chance of surviving predators, which allows it to reproduce and carry on its species. As shown in Figure 2, various animals have evolved camouflage as a way to blend in with their environment, a natural adaptation.



**Figure 2.** Examples of types of camouflage: First row for natural camouflage and second row for artificial camouflage.

**Artificial camouflage:** It is the use of cloth or covers colors to simulate camouflaged textures to blend in with their surrounding environment as shown in Figure 2. For example, this involves hiding soldiers and weapons with textured patterns on the battlefield.

Camouflaged objects are rarely studied. This problem was attempted to be solved using low-level features such as texture and color, which led to unsatisfactory performance results from researchers in this field. Oftentimes, hand-crafted features are successful in simple cases but are prone to failure in more difficult ones. Meanwhile, the state-of-the-art methods were tested using images of too low resolution, which are not sufficient to provide high accuracy. The lack of a standard dataset makes it difficult to compare different results fairly, which is another issue that plays an important role. Additionally, none of the approaches provide an evaluation criterion to determine the efficiency of the experiments.

It is crucial to conduct more in-depth studies to detect camouflaged objects more accurately. Since the advent of deep learning in the last

decade, algorithms using convolutional neural networks or CNNs have been producing results close to human levels in many computer vision approaches. Instead of low-level features, deep networks extract high-level semantic features. Hence, high-level image information and context for detecting camouflaged objects must be integrated into a new network.

Based on our analysis and to address the limitations mentioned above, this study proposes a deep neural network for detecting camouflaged objects from images by utilizing multiple attention networks. The inception module is designed to improve the representation of features. An attention module that generates finer details and detects ambiguous camouflaged objects is also proposed. In particular, the transformation attention module is beneficial for detecting small-scale camouflaged objects. Multiscale rich semantic features are extracted by the channel attention module. The spatial attention module extracts shallow features that are beneficial. In experiments conducted on camouflaged object datasets (CAMO), we demonstrate that our proposed method acquires the best results when compared with the state-of-the-art approach.

The rest of this paper is organized as follows. In section 2, we discuss existing detection methods for camouflaged objects. Section 3 explains the proposed method. In Section 4, the experiment results are described. In section 5, we discuss some potential applications. Lastly, we conclude.

## 2. Related Works

Earlier works (Tankus & Yeshurun, 2001) introduced the Darg operators to enhance areas whose shading corresponds to convex (3D) objects to distinguish them from flat backgrounds that appeared to have similar features (like color and texture). Darg is applied directly to the image's grey-level function. This function is independent of any particular light source or reflectance function and reacts to smooth three-dimensional convex or concave patches on an object. Threshold values greatly influence the results obtained using the Darg operator. The choice of a suitable threshold is crucial. In addition, this method is not suitable for environments containing dark colors and concave backgrounds.



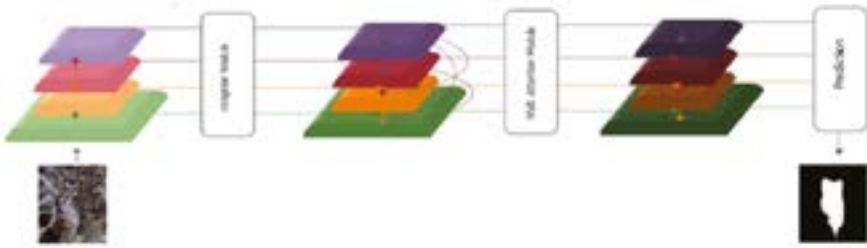
In the following years, most of the researchers studied the problems of finding camouflaged objects using texture features. (Galun et al., 2003) developed a technique for detecting camouflaged objects that captures their structural differences along with their responses to filters. It identifies texture elements based on their shape and then classes them according to their size, aspect ratio, orientation, brightness, etc. Different statistical measures of these properties then allow us to distinguish between different textures. As a consequence, if the object and background have the same texture, this technique may not work correctly. (Bhajantri & Nagabhushan, 2006) presented a technique for detecting camouflaged defects. Within a small region of the image, co-occurrence matrix-based texture features are computed. By clustering and segmenting watersheds, the defective portion is identified. This method's accuracy is dependent on the characteristics of its texture. It may not be effective for sequences with similar kinds of texture between objects and background. (Sengottuvelan et al., 2008) developed a method to detect objects that have camouflage and extract these objects from the surroundings in an image. Taking the given image and dividing it into smaller blocks makes using this technique time-consuming. Neither method works for images with shading effects and objects or backgrounds with similar textures. (Song & Geng, 2010) designed and evaluated camouflage textures based on the weighted structural similarity (WSSIM) method. A camouflage image is created hereby comparing structural similarity and original image features. Camouflage can be broken with it. Lately, (Rao et al., 2020) proposed a texture statistical characterization method combining linear equations and statistical features to detect camouflaged objects.

Because of strong similarities between the foreground and the background, low-level features are typically designed for maximum discrimination, but only work for a few simple and non-uniform backgrounds; as a result, their performance is not satisfactory in detecting camouflaged objects. Additionally, these techniques can only be applied to images with a uniform background when they are of relatively low resolution.

(Le et al., 2019) recently proposed a new approach to camouflaged object segmentation that takes advantage of deep features. A combination of segmentation and classification is used in this method. In addition

to the main branch for segmentation, the network has a second branch for classification that can predict whether or not there are camouflaged objects in an image, which is then fused into the main branch for classification so that segmentation accuracy can be improved.

### 3. Proposed Method



**Figure 3.** Our proposed MA-Net model architecture.

In Figure 3, we propose a Multi Attention Network (MA-Net) for segmenting camouflaged objects. Using the ResNet (He et al., 2016) backbone network, we first extract features from the input images. Following that, an inception module with multi-scale receptive fields is then added to enhance the features. In addition, we fuse top-down generated feature maps with multilevel semantic information. Our final step utilizes the Multi Attention Module (MAM) at each level and then we combine the results from all layers into one outcome.

#### 3.1. CNN Feature Extraction and Enhancement

Our method of extracting features from multiple levels relies on ResNet (He et al., 2016) due to its speed of convergence when compared to VGG (Simonyan & Zisserman, 2015). ResNet 101 consists of 101 convolutional layers, followed by an average pooling layer and a fully connected layer. We modified it to meet our needs for identifying camouflaged targets. In the first step, we remove the completely connected layers that are specifically designed for classification tasks. This also leads to a considerable reduction in parameters. The second reason is that the result of directly upsampling the original ResNet feature map will be

too coarse since its size is 32 times smaller than the input. We overcome this by utilizing dilated convolution in levels 4 and 5 (Chen et al., 2016) which holds the same receptive field without reducing the features map resolution or introducing any additional parameters. Consequently, the resultant feature map is 8 times smaller than the input.



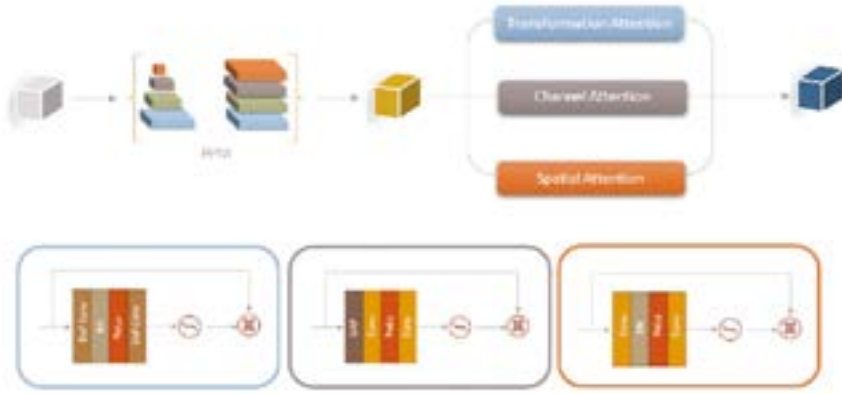
**Figure 4.** Our inception module.

The extracted features from diverse levels are then fed into an inception module to enhance feature representation by capturing multi-scale receptive field features. In Figure 4, the designed module consists of 4 branches with a  $1 \times 1$  convolution at the beginning to reduce the number of channels. The outputted features from three branches undergo a  $1 \times y$  dilated convolution, followed by a  $y \times 1$  dilated convolution at a rate of 3. Here,  $y=3, 5$ , and  $7$ . At the end of each branch, a deformable convolution (Dai et al., 2017) layer is added to localize small and irregular objects. We will concatenate all features from all branches and then proceed to  $1 \times 1$  convolution, with the residual connection to the input features for a faster optimization process.

In a top-down way, we densely connect the features to add more contextual information to low levels by reusing high-level feature maps multiple times.

### 3.2. Feature Attention and Prediction

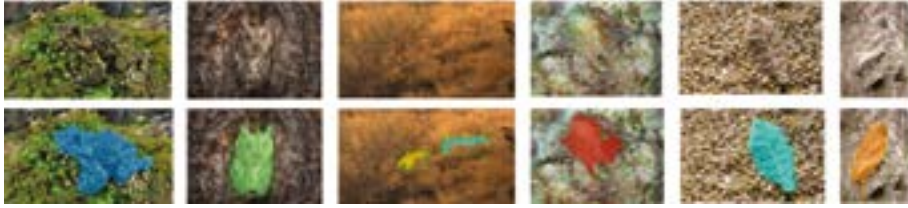
Animals use camouflage to avoid drawing attention to themselves, thus making it difficult to find them. The resulting multi-feature attention network was used to better detect the disguised target and to create finer features that would help to draw attention to the hidden target. Our multi-feature attention module focuses on the important features of an image while disregarding the less important ones.



**Figure 5.** Multi Attention Module.

As seen in Figure 5, a Pyramid Pooling Module (PPM) (Zhao et al., 2017) is initially applied to the input feature, and the output feature is used as an input feature for the multi-attention module. It comprises three attention blocks: Transformation, Channel, and Spatial. Using deformable convolution, the first block attempts to represent feature transformations (Dai et al., 2017). This can improve the network's attention to foreground areas. The feature map is processed by a  $3 \times 3$  deformable convolutional layer, followed by a normalization layer, ReLU, and a second  $3 \times 3$  deformed convolutional layer. By highlighting the camouflaged target, the channel attention block reduces the inaccuracies caused by duplicated channel features. Feature maps are re-allocated using two  $1 \times 1$  convolutions and global pooling. This global attention map specifically makes the positions of the hidden objects known on feature maps. The spatial attention block investigates were to focus on a feature map. To make a final attention map, the refined features of all the blocks are combined.

Following the refinement of the camouflaged map, the connected components are determined to identify each object in the image. Afterward, each connected component's bounding box is calculated. The final results of object detection are illustrated in Figure 6.



**Figure 6.** Some examples of camouflaged object detection results of our proposed approach.

## 4. Experiments

In the following section, we introduce the dataset. We then explain the evaluation metrics. Lastly, we present experimental results showing the effectiveness of the proposed model is compared to existing methods.

### 4.1. Dataset

The Camouflaged Object (CAMO) dataset (Le et al., 2019) contains 1250 images of varying sizes. Figure 7 illustrates a few examples along with their associated ground truth label annotations. This dataset corresponds to animals and humans in the real world, respectively. Various kinds of animals hide in various environments, including amphibians, birds, insects, mammals, reptiles, and underwater animals; these include animals that live on land, underwater, in deserts, forests, mountains, and on snow. Human body paint and camouflaged soldiers on the battlefields.

In this dataset, 80% of images are selected randomly for training and 20% for testing. Data augmentation is applied to selected training images. Mirror reflections and rotations were used. Using GPU Nvidia GTX 1080, we implemented our model based on the Caffe framework (Jia et al., 2014). The stochastic gradient descent optimization (SGD) algorithm was used for training.



**Figure 7.** Some examples of the dataset for Camouflaged Objects (CAMO) (Le et al., 2019).

#### 4.2. Evaluation Metrics

The following metrics are used to evaluate our experiments: Mean Absolute Error (MAE) (Perazzi et al., 2012), F-Measure (Achanta et al., 2009), E-measure (Fan et al., 2018), and Structure Measure (S-Measure) (Fan et al., 2017) as explained below.

**MAE:** A metric that calculates the average absolute error between prediction maps and ground-truth maps. Following is the formula:

$$MAE = \frac{1}{H \times W} \sum_{x=1}^W \sum_{y=1}^H |S(x, y) - G(x, y)| \quad (1)$$

where  $W$  and  $H$  are the width and height of the input image. A lower MAE generally indicates a better result.

**F-measure:** As such, this criterion is defined as the weighted harmonic average of recall and precision metrics and its non-negative weight. F-measure can be described as follows:

$$F_\beta = \frac{(1 + \beta^2) Precision \times Recall}{\beta^2 Precision + Recall} \quad (2)$$

where we set  $\beta^2$  to a fixed value of 0.3 as suggested in (Achanta et al., 2009), to emphasize the precision over recall. Note that unlike MAE, a higher  $F_\beta$  indicates a better performance.

**E-measure:** is a perceptual-inspired criterion and is defined as:

$$S_e = (1 - \alpha) S_o + \alpha S_r \quad (3)$$

in which  $\Phi_{FM}$  an enhanced alignment matrix. The greater the E Score, the better is the performance.

**S-measure:** It is a measure of how similar predicted maps are to the ground truth maps.

$$S_e = (1 - \alpha) S_o + \alpha S_r \quad (4)$$

in which  $S_r$  indicates the region-aware structural similarity and  $S_o$  denotes the object-aware structural similarity. As suggested in (Fan et al., 2017), we set  $\alpha = 0.5$ . An increased S-measure score indicates a better performing model.

### 4.3 Comparison

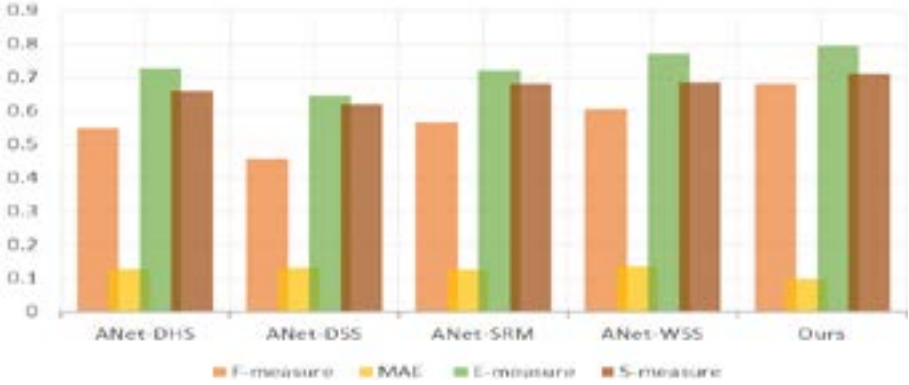
We compared our model with other state-of-the-art camouflaged object detection approaches (Le et al., 2019), including ANet- (DHS, DSS, SRM, and WSS).

**Table 1.** Quantitative results on CAMO dataset.

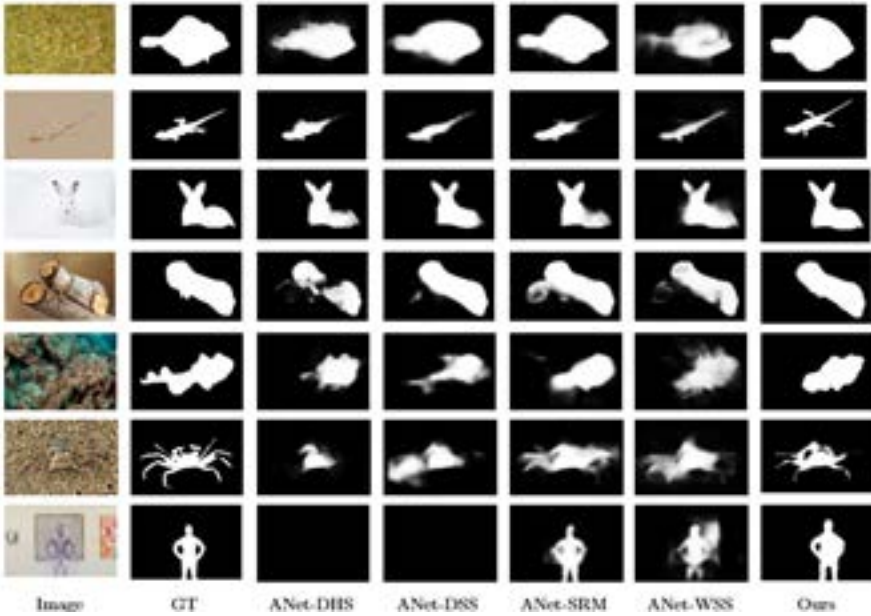
Model	Evaluation Metrics			
	MaxF $\uparrow$	MAE $\downarrow$	E $\phi$ $\uparrow$	S $\alpha$ $\uparrow$
ANet-DHS	0.549	0.130	0.730	0.663
ANet-DSS	0.459	0.132	0.648	0.623
ANet-SRM	0.566	0.126	0.722	0.682
ANet-WSS	0.608	0.138	0.773	0.686
Ours	0.683	0.098	0.798	0.711

Table 1 summarizes the quantitative results. Despite differences in evaluation metrics, our model outperforms competing approaches by far, demonstrating its superiority. By comparison with state-of-the-art methods, our method increases F-measure by 7.5%, E-measure by 2.5%, and S-measure by 2.5%, respectively. Furthermore, our model significantly lowers MAE scores by 2.8%. In other words, our mask maps are more accurate because our model is more convinced of the predicted target regions. In all cases, our proposed method is among the top contenders as illustrated in Figure 8.





**Figure 8.** Comparison of evaluation metrics scores across CAMO dataset.



**Figure 9.** Qualitative visual comparison of segmentation masks of our proposed model with the state-of-art methods.

The prediction results of our network with state-of-the-art methods in different scenarios are visualized to better illustrate the advantages of the proposed method. Based on Figure 9, we can observe that the proposed method has a greater degree of precision than other methods and highlights the hidden target completer. Our model excels at handling multiple challenging scenarios, object appearance (row 1, row 2, row 3,



and row 4), background clutter (row 5), shape complexity (row 6), and distraction (row 7). Compared to other methods, our proposed model produces more accurate and sharper segmentation maps. Consistent outperformance of our model is shown over the state-of-the-art methods. This may also illustrate how effective the proposed approach is.

## 5. Discussion

Even though there is a wide range of potential applications for the detection of camouflaged objects, the problem of detecting them has not been well studied. Because these applications have a common characteristic where the target objects and background have similar appearances, we uncover some uses for these applications. Accordingly, the studied problem should be considered important in the following areas:

**Ecosystem and biodiversity applications:** such as wildlife preservation and new species discovery. It is important to discover new species because this contributes to their protection. In addition, a new species may produce compounds that can lead to new medicines. The application of camouflaged object detection algorithms can assist in the detection of many different camouflaged species found in nature.



**Figure 10.** Examples of some new species discovered in 2020 (California Academy of Science, 2020).

**Defense and military applications:** allowing soldiers to be identified on the battlefields when they are camouflaged. It may be possible to develop a system that recognizes targets based on artificial intelligence. In complex environments, it can increase the accuracy of target detection and assist in making these systems more capable of locating camouflaged targets.

**Other applications:** It can also be used in surveillance systems and even in search-and rescue missions in the event of natural disasters, such as earthquakes, floods, or hurricanes.



**Figure 11.** Search and rescue system operations (Bejiga et al., 2016).

## 6. Conclusion

We present a new approach to detect camouflaged objects using multiple attention networks. By first modifying ResNet with dilated convolution, we can extract more features from images while retaining the spatial size of the feature map. Inception is then used to enhance the feature representation. Furthermore, a dense feature pyramid provides an effective way of fusing multilevel information, leading to an effective feature map with rich semantic information. For better-camouflaged target detection in small and ambiguous areas, a multi-attention module was proposed. We tested our method on the camouflaged object dataset (CAMO) and compared it extensively with state-of-the-art methods. Based on the experiment, it is clearly evident that our method performs better both visually and quantitatively than all the others. In the future, we plan to incorporate real-time detection and feature representation improvements for better model performance.

## REFERENCES

Achanta, R., Hemami, S., Estrada, F. & Susstrunk, S. (2009). Frequency-tuned salient region detection. *IEEE Conference on Computer Vision and Pattern Recognition*, Miami, FL, USA. DOI: 10.1109/CVPR.2009.5206596

Bejiga, M.B., Zeggada, A. & Melgani, F. (2016). Convolutional neural networks for near real-time object detection from UAV imagery in avalanche search and rescue operations. *IEEE International Geoscience and Remote Sensing Symposium*, Beijing, China.

Bhajantri, N.U. & Nagabhushan, P. (2006). Camouflage Defect Identification: A Novel Approach. *IEEE International Conference on Information Technology*, Bhubaneswar, India. DOI: 10.1109/ICIT.2006.34

California Academy of Science (2020). Academy scientists describe 213 new species in 2020. Retrieved from: <https://www.calacademy.org/press/releases/academy-scientists-describe-213-species-in-2020>

Chen, L., Papandreou, G., Kokkinos, I., Murphy, K. & Yuille, A.L. (2016). Deeplab: Semantic image segmentation with deep convolutional nets, atrous convolution, and fully connected CRFs. *Journal of IEEE Transactions on Pattern Analysis and Machine Intelligence*, 40 (4), 834 – 848.

Dai, J., Qi, H., Xiong Y., Li Y., Zhang, G., Hu, H. & Wei, Y. (2017). Deformable convolutional networks. *IEEE International Conference on Computer Vision*, Venice, Italy. DOI: 10.1109/ICCV.2017.89

Fan, D.-P., Gong, C., Cao, Y., Ren, B., Cheng, M.-M. & Borji, A. (2018). Enhanced-alignment measure for binary foreground map evaluation. *International Joint Conference on Artificial Intelligence*, 698–704.

Fan, D.P., Cheng, M.-M., Liu, Y., Li, T. & Borji, A. (2017). Structure-measure: a new way to evaluate foreground maps. *IEEE International Conference on Computer Vision*, Venice, Italy. DOI: 10.1109/ICCV.2017.487

Galun, M., Sharon, E., Basri, R. & Brandt A. (2003). Texture segmentation by multiscale aggregation of filter responses and shape elements. *IEEE International Conference on Computer Vision*, Nice, France. DOI: 10.1109/ICCV.2003.1238418

He, K., Zhang, X., Ren, S. & Sun, J. (2016). Deep residual learning for image recognition. *IEEE Conference on Computer Vision and Pattern Recognition*, Las Vegas, NV, USA. DOI :10.1109/ICCV.2003.1238418

Jia, Y., Shelhamer, E., Donahue, J., Karayev, S., Long, J., Girshick, R., Guadarrama, S. & Darrell, T. (2014). Caffe: Convolutional architecture for fast feature embedding. *ACM international conference on Multimedia*, 675–678.

Le, T., Nguyen, T.V, Nie, Z., Tran, M. & Sugimoto, A. (2019). Anabran network for camouflaged object segmentation. *Journal of Computer Vision and Image Understanding*, 184, 45–56.

Perazzi, F., Krähenbühl, P., Pritch, Y. & Hornung, A. (2012). Saliency filters: Contrast based filtering for salient region detection. *IEEE conference on computer vision and pattern recognition*, Providence, RI, USA. DOI: 10.1109/CVPR.2012.6247743

Rao, C., Reddy, A. & Rao, C. (2020). Camouflaged object detection for machine vision applications, *International Journal of Speech Technology*, 23, 327–335.

Sengottuvelan, P., Wahi, A., Shanmugam, A. (2008). Performance of de-camouflaging through exploratory image analysis. *IEEE International Conference on Emerging Trends in Engineering and Technology*, Nagpur, India.

Song, L. & Geng, W. (2010). A new camouflage texture evaluation method based on WSSIM and nature image features. *IEEE International Conference on Multimedia Technology*, Ningbo, China.

Tankus, A. & Yeshurun, Y. (2001). Convexity-Based Visual Camouflage Breaking. *Journal of Computer Vision and Image Understanding*, 82 (3), 208–237.

Zhao, H., Shi, J., Qi, X., Wang, X. & Jia, J. (2017). Pyramid scene parsing network. *IEEE Conference on Computer Vision and Pattern Recognition*, Honolulu, HI, USA. DOI: 10.1109/CVPR.2017.660



**SAĞLIK BİLİMLERİ ÇALIŞMALARI**  
*HEALTH SCIENCES STUDIES*



# EVALUATION OF ADVERSE DRUG REACTIONS IN PEDIATRIC PATIENTS AT A TERTIARY CARE HOSPITAL IN TURKEY: A RETROSPECTIVE APPROACH

*Zakir Khan<sup>1</sup>*

---

## Abstract

**Background:** Drug safety in pediatrics is a serious public health concern around the world. The pediatric population is more prone to adverse drug reactions (ADRs) than adults. Moreover, there is a scarcity of information about ADRs in pediatric. **Objectives:** This study was conducted to determine the frequency, causality, severity, preventability of pediatrics ADRs reported in a tertiary care hospital in Adana, Turkey. **Methods:** A retrospective study was conducted on all spontaneously reported ADRs between January 01, 2020, to July 30, 2021, in pediatrics. The ADRs reports were evaluated in terms of gender, age, ADR char-

---

1 PhD Student, Cukurova University, Faculty of Medicine, Department of Medical Pharmacology, ORCID: 0000-0003-1365-548X



acteristics, suspected drugs and reporting source. All included ADRs reports were characterized according to the Naranjo Algorithm/World Health Organization (WHO) causality scales, Hartwig/Siegel and Common Terminology Criteria for Adverse Events (CTCAE) severity scales, the modified Schoumcock and Thornton preventability scale and hospital pharmacovigilance center criteria for seriousness. Therapeutic groups were also coded using the WHO-Anatomical Therapeutic and Chemical (ATC) classification. **Results:** During the study period, 8912 pediatric patients who were admitted had 16 ADRs with 1.7 ADRs/1,000 admissions. The majority of ADRs were found in infants (31.2%) and children (56.2%) as compared to adolescents (12.5%). ADRs were observed more in females (81.2%) than males. Skin (62.5%) was the most affected organ due to the ADRs, and maculopapular rash and erythema multiforme were the most commonly reported symptoms. Most ADRs were probable/likely (93.7%), severe (50%), preventable or probably preventable (43.7%) and serious (37.5%). Antibiotics (87.5%) were found to be the most common cause of ADRs in pediatrics. The majority of ADRs were associated with vancomycin (68.7%). Most of the ADRs were reported by a medical doctor in this study. **Conclusion:** This feasibility study highlights significant problems of ADRs in pediatrics, mainly caused by antibiotics and with a majority of ADRs manifest as skin reactions. Furthermore, a high proportion of the identified ADRs were found to be preventable. More focused efforts are needed at the national level to avoid preventable ADRs in hospitals. Monitoring and management of ADRs and future studies would be beneficial for better patient care and safety.

**Keywords:** Adverse Drug Reactions, Children, Pediatrics, Antibiotics, Patient Safety, Turkey.

## 1. Introduction

Adverse drug reactions (ADRs) are a leading cause of illness and mortality worldwide (Giardina et al., 2018). Spontaneous reporting of ADRs is critical for effective post-marketing drug surveillance and patient safety (Noda et al., 2020). Drug safety is an important part of health care and understanding ADRs is crucial for avoiding harmful effects (Dittrich et al., 2020). The safety of drugs in pediatrics is a serious public health problem (Khan et al., 2020; Rosli et al., 2017). ADRs in pediatric have been shown to cause not only hospital admissions or lengthy hospitalization, but also chronic disability or even death (Le et al., 2006).

The medication mistakes in pediatric were found to be three times higher than in adults, mostly due to considerable variation in body mass, which necessitates individual dose measurements depending on patient age, weight, or body surface as well as the clinical situation (Khan et al., 2020). The development of renal functions and enzyme systems, pharmacokinetic and pharmacodynamic parameters in pediatric also alter throughout time (Rosli et al., 2017). Pediatric patients are provided a wide range of medications, with an elevated risk of ADRs linked with off-label prescribing (Bellis et al., 2014). Medication errors lead to mild to severe ADRs. (Venkatasubbaiah et al., 2018; Angamo et al., 2016). As a result, ADRs can cause significant morbidity in pediatric (Priyadharsini et al., 2011).

Pediatric are one of the most vulnerable populations to ADRs. It is reported that ADRs account for nearly 5% of all hospital admissions in pediatric (Angamo et al., 2016). A previous study revealed that ADRs affect around one out of every ten children in the hospital, with 12% of them were serious (Clavenna & Bonati, 2009). According to systematic reviews, the overall average incidence of ADRs in pediatric was 9.52% to 9.53% (Khan et al., 2020a; Impicciatore et al., 2001). ADRs also imposed a higher financial cost on patients. It is reported that the average cost of treating an ADR per patient was estimated to be United States dollars (USD) 9,491, with hospitalization or room expenditures accounting for 50% of the total cost (Ayani et al., 1999; Oshikoya et al., 2011). Another study calculated a total cost to a hospital of USD 27,358 for the hospitalization of patients with ADRs in an emergency room over six weeks (Patel et al., 2007).

Children rarely articulate their personal medication therapy experiences; they are more susceptible to ADRs. As a result, pediatrics' drugs have a significant chance of causing a variety of ADRs (Khan et al., 2020; Nasso et al., 2020). The pediatrics population includes as susceptible populations and are frequently underrepresented in randomized controlled trials (RCTs). Therefore, there is scarce data about detecting ADRs which provides limited safety information in pediatrics. (Nor-Aripin et al., 2012). During the development phase of a drug, only mild, moderate, or non-serious ADRs are often recorded. The serious and latent ones, on the other hand, may not be caught (Rosli et al., 2017). To compensate for the limitations of RCTs, spontaneous ADR reporting is an important source of medication safety data in pediatric populations that aren't often studied in RCTs (Gentili et al., 2018).

A statewide, volunteer pharmacovigilance (PV) system exists in Turkey, as in many other nations. Its primary goal is to alert the public about previously unknown risks associated with the use of medications in everyday life (TUFAM, 2005). Additional research is usually required to confirm these safety signals. All Health care professionals (HCPs; doctors, nurses, pharmacists, etc.), patients and pediatrics parents/caregivers are the primary source of voluntary ADRs reporting (Ergün et al., 2019; Haines et al., 2020; Khan et al., 2020b). Under-reporting of ADRs continues to be a widespread issue (Ergün et al., 2019; Güner & Ekmekci, 2019; Khan et al., 2020c). According to a recent report, Turkey submitted only 89 ADR reports per million population to the World Health Organization (WHO) Vigiflow database in 2020 (TPDMA, 2020a). However, the WHO recommended that ADR reports should be produced at a rate of 200 per million population per year (WHO, 2021a).

Underreporting is a well-known issue in voluntary ADRs reporting schemes (Khan et al., 2020b; Hazell & Shakir, 2006). Underreporting of ADRs in pediatric patients is also due to a lack of knowledge about adverse reactions to prescribed drugs (Dittrich et al., 2020; Khan et al., 2020b; Rosli et al., 2017). Periodic monitoring of ADRs is useful for improved pediatric care and safety (Dittrich et al., 2020). Moreover, there is a scarcity of information about ADRs in pediatric in our healthcare setting and as well as in Turkey. Therefore, this study aimed to determine the frequency, causality, severity, preventability of pediatrics ADRs recorded in a tertiary care hospital in Adana, Turkey.

## **2. Methods**

### **Study Design and Setting**

A retrospective study was conducted in a pharmacovigilance center of Balcalı Hospital in Adana, Turkey, to evaluate pediatric (patients from 0 to 17 years old) ADR reporting forms. Balcalı Hospital is a tertiary care teaching hospital with 1171 beds that provides both in-patient and out-patient care. It offers health care facilities to the rural and urban population of Adana, (Turkey's fifth-largest city). This research was carried out per the Helsinki Declaration's principles. Due to the retrospective nature of the study and examination of ADRs reporting forms, the hospital's institutional ethics committee waived ethical approval.

### **Inclusion Criteria**

All pediatrics ADRs reported to pharmacovigilance officer (PVO) by HCPs from January 1, 2020, to July 30, 2021, were included.

### **Exclusion Criteria**

ADR forms with missing information with unclear causality were omitted from the analysis.

### **Adrs Data Collection Procedure and Tools**

A clinical pharmacologist working at the pharmacovigilance center and researchers analyzed all individual recognized ADR reports. The ADRs reports were evaluated in terms of gender, age, ADR characteristics, suspected drugs, reporting source and outcomes were extracted. The Naranjo algorithm (the total scores range from -4 to 13, the reaction is considered Definite if score >8, probable 5–8, possible 1–4 and doubtful=0) and WHO-Uppsala Monitoring Centre (the suspected ADR is assessed as certain, probable, possible, unlikely and unclassified/unclassifiable) criteria were used to determine the causality of each suspected ADR (Naranjo et al., 1981; WHO & UMC, 2013). These validated tools have been used in several studies (Dittrich et al., 2020; Nasso et al., 2020; Trubiano et al., 2016). Hartwig's Severity Assessment Scale was used to evaluate the ADRs' severity. ADRs were classified as mild, moderate, or severe (Hartwig et al., 1992). The severity of the ADRs was also determined by using the Common Terminology Criteria for

Adverse Events (CTCAE) scale. For each ADR, the CTCAE displays grades 1 through 5 along with a specific clinical description of severity (CTCAE, 2017; Ditttrich et al., 2020). The modified Schoumlock and Thornton scale was used to assess preventability (ADRs are divided into three categories: definitely preventable, probably preventable and not preventable) (Al-Damen & Basheti, 2019; Schumock & Thornton, 1992). Hospital pharmacovigilance center criteria were used to determine the seriousness of ADR. Therapeutic groups and drugs were also coded using the WHO-Anatomical Therapeutic and Chemical (ATC) classification (WHO, 2020b).

### **Data Analysis**

SPSS Statistics version 25 (IBM Corp., SPSS Statistics) was used to perform a descriptive analysis of the data for frequency, mean, and percentage. All of the information is presented in tabular and graphical formats.

### **3. Results**

A total of 29 ADRs were submitted to the hospital pharmacovigilance center during 2020-2021. Of these 17 (58.6%) were related to pediatric patients. One ADR form was excluded due to the missing information. Finally, 16 eligible ADRs forms (9 reports during 2020 and 7 in 2021) were analyzed in this study. According to the hospital data, a total of 8912 (4701 in 2020 and 4211 in 2021) pediatric patients were admitted during the study period with 1.7 ADRs/1,000 admissions. The majority of ADRs were found in infants (31.2%) and children (56.2%) as compared to adolescents (12.5%). ADRs were observed more in females (81.2%) than males. The median age of the patients was 6.5 years (2 months -13.5 years).

According to the Naranjo algorithm/WHO-UMC scales, 15 of the ADRs were probable/likely (93.75%) and 1 was definite/certain (15.8%). Hartwig's Severity Assessment Scale shows that 3 of the ADRs were mild (18.75%), 5 were moderate (31.25%) and 8 were severe (50%) requiring an intensive medical intervention. The CTCAE criteria showed that five ADRs were grade 2, four ADRs were grade 3, and seven ADRs

were grade 4. According to the modified Schumock and Thornton scale, 7 ADRs were measured as preventable (43.5%) and among them, 4 were “definitely preventable” (25%) and 3 were “probably preventable” (18.75%). The remaining (n=9; 56.25%) were “non-preventable”. Moreover, according to the hospital pharmacovigilance center criteria, 9 (56.25%) of the ADRs caused hospitalization/prolonged hospitalization and 6 (37.5%) were life-threatening (Table 1).

Skin (62.5%) and renal system (25%) were the most affected organs due to the ADRs. The suspected medication was discontinued in 10 (62.5%) of the patients and replaced with another medication for the same indication. The dose of suspected medication was reduced in 2 (12.5%) patients to alleviate symptoms, while another drug was given to overcome adverse effects in 4 (25%) cases. The results of ADR management revealed that 87.5% had been recovered and 12.5% were in the process of recovering. No fatal case due to ADR was reported in the current study (Table 1).

**Table 1:** Characteristics and assessment of pediatrics ADR reports.

<b>Gender</b>	<b>n (%)</b>
Male	3 (18.75)
Female	13 (81.25)
<b>Age groups</b>	
Neonates (birth to 1 month)	0 (0)
Infants (>1 month to 2 years)	5 (31.25)
Children (>2 to 12 years)	9 (56.25)
Adolescents (> 12 years to 17 years)	2 (12.5)
<b>Year of reporting</b>	
2020	11 (68.75)
2021	5 (31.25)
<b>Causality</b>	
<b>Naranjo algorithm</b>	
Probable	15 (93.75)
Definite	1 (6.25)
<b>WHO/UMC</b>	
Likely	15 (93.75)

Certain	1 (6.25)
<b>Severity</b>	
<b>Modified Hartwig/Siegel scale</b>	
Level 2 (mild)	3 (18.75)
Level 4 (moderate)	5 (31.25)
Level 5 (severe)	8 (50)
<b>CTCAE scale</b>	
Grade 2 (moderate)	5 (31.25)
Grade 3 (severe)	4 (25)
Grade 4 (life-threatening)	7 (43.75)
<b>Preventability</b>	
Definitely preventable/ Probably preventable	7 (43.75)
Not preventable	9 (56.25)
<b>Seriousness criteria (Hospital criteria)</b>	
Death	0 (0)
Life-threatening	6 (37.5)
Caused hospitalization/prolonged hospitalization	9 (56.25)
Caused permanent disability	0 (0)
Other	1 (6.25)
<b>System organ class</b>	
Skin	<b>10 (62.5)</b>
Renal and urinary disorders	<b>4 (25)</b>
Circulatory system	<b>2 (12.5)</b>
<b>Management</b>	
The medication was stopped	9 (56.25)
Another medication was substituted	1 (6.25)
Dose was reduced	2 (12.5)
Another medication was added to combat adverse effect	4 (25)
<b>Outcomes</b>	
Recovered	14 (87.5)
Recovering	2 (12.5)
Fatal	0 (0)

**Abbreviation:** ADRs=Adverse drug reactions, n=frequency, %=percentage, WHO/UMC= World health organization - Uppsala monitoring centre, CTCAE=Common terminology criteria for adverse events.

In our study, ADRs were mostly associated with antibiotics (14; 87.5%) followed by antifungal (n=1; 6.25%) and antiviral (n=1, 6.25%) in our study. Vancomycin (n = 11, 68.75%) was associated with the highest number of ADRs. The most common reported ADRs with vancomycin use were maculopapular rash (n=5, 31.25%) and anaphylaxis (n=2, 12.5%). Antifungal drug (Amphotericin B) caused rashes and antiviral drug (aciclovir) associated with acute kidney failure. The most common drugs that cause ADRs, as well as associated reactions, are listed in Table 2.

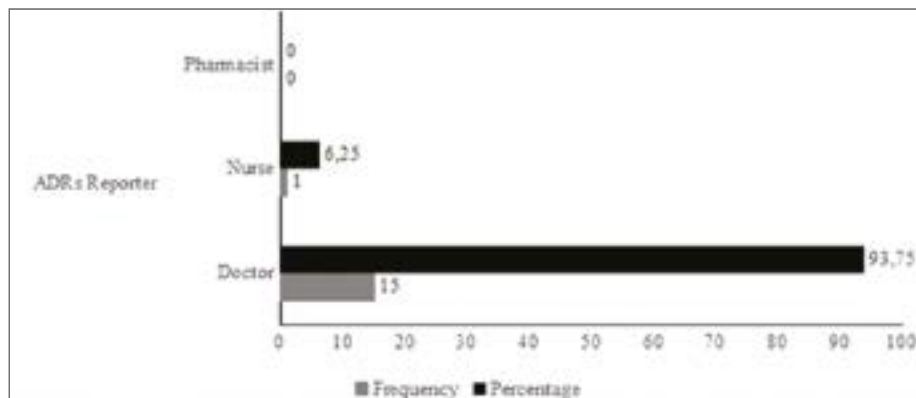
**Table 2:** Drugs associated with ADRs.

Drug Class	WHO/ATC Code	n (%)	Reaction details (no of patients)
<b>Antibiotic</b>			
Vancomycin	J01XA01	11 (68.75)	Maculopapular rash (5)
		-	Anaphylaxis (2)
		-	Erythema multiforme/Redness on the whole body (2)
		-	Acute kidney injury(1)
		-	Increase creatinine level (1)
Clindamycin	J01FF01	1 (6.25)	Maculopapular rash (1)
Colistin-Linezolid	J01XB01- J01XX08	1 (6.25)	Increase creatinine level (1)
Ceftriaxone	J01DD04	1 (6.25)	Rashes and urticaria (1)
<b>Antifungal</b>			
Amphotericin B	J02AA01	1 (6.25)	Maculopapular rash (1)
<b>Antiviral</b>			
Aciclovir	J05AB01	1 (6.25)	Acute kidney injury(1)

**Abbreviation:** ADRs=Adverse drug reactions, n=frequency, %=percentage, WHO/ATC=World health organization/ Anatomical therapeutic and chemical classification.

These ADRs were first time reported in the hospital pharmacovigilance center. All of the ADRs were reported by doctors (n=15, 93.75%) and nurses (n=1; 6.25%). We did not observe any ADR reported by a pharmacist and other paramedical staff in this study (Figure 1).





**Figure 1:** Reporting of ADRs by healthcare professionals.

#### 4. Discussion

ADRs are a significant public health issue in the pediatric population. Despite efforts to lower the incidence of medication-related adverse events, morbidity and death from drug-induced reactions, particularly in pediatrics, remain unacceptably high. Periodic evaluation of ADRs in the pediatric population is very important. This study explored the causality, preventability, severity of ADRs as well as therapeutic groups and reactions related to ADRs. The current study is the first attempt that has been conducted to analyze the pediatric ADRs in a selected healthcare setting as well as in Turkey. As a result, it could serve as a baseline for future study, as well as provide critical evidence for healthcare stakeholders and government decision-makers to take the necessary steps to reduce the burden of ADRs in pediatrics.

In our study, out of the total reported ADRs in hospital pharmacovigilance centers, 58.6% were related to the pediatric population. Similar studies conducted in the Netherlands (Dittrich et al., 2020) and Malaysia (Rosli et al., 2017) observed that 26% and 14% of admitted pediatric patients had ADRs, respectively. Moreover, the observed rate of ADR related to pediatrics was 1.7 ADRs per 1000 admissions. Nasso et al also reported similar findings (1.6 ADRs/1000 admissions) in pediatrics (Nasso et al., 2020). However, another study conducted by Lombardi et al., observed 2.2 ADRs per 1000 pediatric admissions, which was high-

er as compared to our study (Lombardi et al., 2018). These differences in ADR rates among studies may be due to variation in data collection methods, sample size, methodology, and healthcare setting.

One of the risk variables for acquiring ADRs in the current study was presumed to be the female gender. The supported result was also reported by a systematic review in pediatrics found that gender was a risk factor in ten of the 19 studies, with females being more likely to develop an ADR (Smyth et al., 2012). However, a study conducted in Malaysia presented a higher ADRs proportion in males (Rosli et al., 2017). Furthermore, a multicenter study among pediatric patients in hospitals from five countries found no significant differences in ADRs by gender (Rashed et al., 2012). An Italian study also did not observe any ADRs difference by gender (Nasso et al., 2020). It is reported that males and females respond to medications due to anatomical and physiological variations (Rosli et al., 2017; Smyth et al., 2012).

Causality analysis is necessary to understand the factors that contribute to the occurrence of ADRs (Venkatasubbaiah et al., 2018). In the current study, the Naranjo algorithm and WHO-UMC scales of causality assessment observed that most of the ADRs were probable/likely categories. Similar findings were also reported by Nasso et al., 2020; Al-Damen & Basheti, 2019; Saqib et al., 2018. Because of their simplicity, the Naranjo algorithm and WHO-UMC scales are also used to evaluate the causality score in pediatrics. These scales were developed for individual case safety reports to support PV system (Comfort et al., 2018; Vázquez-Alvarez et al., 2017)

In the current study, according to the severity assessment of ADRs using the Modified Hartwig and Siegel scale, the majority of ADRs fell into the severe followed by moderate and mild categories. However, these findings deviated from the studies conducted in Malaysia (Rosli et al., 2017) and India (Sundaran et al., 2018) which disclosed a higher ADRs proportion as mild and moderate while a small number were severe. In addition, CTCAE criteria showed that the majority of ADRs were grade 3 (severe) and 4 (life-threatening) categories in this study. Similar findings were also reported in the Netherlands study (Dittrich et al., 2020). The cause for the higher severity of ADRs in our study is due

to that most ADRs were responsible for prolonging hospitalization and were also life-threatening. The severity of ADRs must be assessed to take serious steps against the drug's continued use. Severe ADRs have been linked to a longer stay in the hospital and a higher financial cost due to the need for more intensive medical care (Fasipe et al., 2019; Walter et al., 2017).

In this study, preventability assessment using Modified Schumock and Thornton scale showed 43.7% of ADRs were definitely and probably preventable. Supported findings were also reported in the Jordan study and reported that 44.7% of ADRs were definitely and probably preventable (Al-Damen & Basheti, 2019). Another study conducted among pediatric observed that 20% of ADRs were preventable or probably preventable (Nasso et al., 2020). In the current study, a large proportion of the identified ADRs were found to be preventable. The most important factors associated with preventable ADRs were insufficient monitoring and incorrect dosing (Al-Damen & Basheti, 2019). The establishment of active ADR surveillance and raise awareness is important to encourage safer drug use. Periodic ADR reporting programs are required to educate and enhance awareness among all HCPs. More focused efforts are needed at the national level to avoid preventable ADRs in hospitals. Therefore, ADRs should be monitored carefully to avert hazardous effects.

The skin was the most affected organ by ADRs in this study. Similar findings were also reported by previously published studies (Nasso et al., 2020; Priyadharsini et al., 2011; Rosli et al., 2017). However, a study conducted by Dittrich and colleagues observed that gastrointestinal disorders were more frequently seen in pediatric (Dittrich et al., 2020). The reason for pediatrics' increased cutaneous involvement ADRs can be attributed to this age group's unique physiology; in fact, they have a partially matured epidermis that is not fully developed (Rashed et al., 2012; Rosli et al., 2017). As a result, the skin becomes more porous and vulnerable to chemical and microbial attacks (Stamatas et al., 2011).

In the present study, antibiotics were the most common drug class followed by antifungal and antiviral reported for ADRs in pediatrics. Similar results were detected by previously published studies (Rashed et al., 2012; Rosli et al., 2017). The most frequently involved antibiotics

associated with ADRs were Vancomycin followed by Ceftriaxone, Clindamycin and Colistin-Linezolid in our study. However, Penicillin and Erythromycin were the most frequent antibiotics associated with ADR in Malaysian pediatric patients (Rosli et al., 2017). Another study conducted among pediatrics reported Amoxicillin and beta-lactamase inhibitors as frequently contributed to ADRs (Nasso et al., 2020). A large number of antibiotics were prescribed in the general pediatric population, and a higher number of ADRs were reported for drugs in this treatment group (Gallo et al., 2012; Nasso et al., 2020; Priyadharsini et al., 2011). Due to the problem of antibiotic resistance, pediatric infections were frequently treated with a combination and broad-spectrum of antibiotics at high doses (Manan et al., 2016).

In this study, the majority of the antibiotics were linked to ADRs related to skin reactions, which is consistent with the findings of other studies (Priyadharsini et al., 2011; Rosli et al., 2017). Maculopapular rashes followed by anaphylaxis and redness on the whole body (erythema multiforme), acute kidney injury were the main ADRs of Vancomycin observed in our study. Al-Damen & Basheti were also reported acute kidney injury with Vancomycin use (Al-Damen & Basheti, 2019). In addition, erythema multiforme has been linked to a variety of antibiotics, including b-lactams, macrolides, aminoglycosides, glycopeptides, and others (Diaz & Ciurea, 2012). According to the previously published study, the main Vancomycin-related ADRs were skin rashes and elevated serum creatinine (An et al., 2011). Another study also reported anaphylaxis to intravenous Vancomycin in a pediatric patient (Xie et al., 2021). Close monitoring of laboratory testing, including complete blood counts with differential analysis, is recommended for the early and precise diagnosis of ADRs associated with Vancomycin use (An et al., 2011; Xie et al., 2021)

Antifungal drug (Amphotericin B) caused rashes in one pediatric case in this study. A study conducted in India observed renal failure and diarrhea as ADRs due to Amphotericin-B use (Sundaran et al., 2018). It is reported that prolonged Amphotericin-B treatment can be associated with maculopapular rash, eosinophilia and also systemic symptoms (Cesaro et al., 1999; Hagihara et al., 2015). Careful monitoring of the patient being treated for the first time is warranted in the case of Amphotericin B. Antiviral drug (Aciclovir) was responsible for Acute kidney injury relat-

ed ADR in our study. Acyclovir is an antiviral medicine that is commonly prescribed to pediatric, and it can cause acute kidney injury (Fleischer & Johnson, 2010). A recent study also reported that an acute renal injury occurred in 13% of parenteral Aciclovir treatment episodes (Ryan et al., 2018). Therefore, dosage adjustments for baseline renal function and optimal body weight are crucial to prevent ADRs (Yildiz et al., 2013).

Most of the ADRs were reported by a medical doctor in this study. Nurses reported only one ADR and reporting from the pharmacist was not observed. The accurate spontaneous ADRs reporting mechanisms used by prescribers, nurses, pharmacists, and other paramedical workers are critical for the detection of serious ADRs in hospitals (Giardina et al., 2018; Güner & Ekmekci, 2019). ADR underreporting is a global issue that has been documented in previous international studies (AlShammari & Almoslem, 2018; Alwhaibi & AlAloola, 2020). One of the Turkish government's major priorities is to monitor and report ADRs (TPMDA, 2014b). In 2005, Turkey established the "Turkish Pharmacovigilance Center (Turkish: Türkiye Farmakovijilans Merkezine)" to coordinate PV activities across the country. In Turkey, all HCPs are expected to be vigilant in identifying and reporting ADRs to the hospital pharmacovigilance center or directly to TUFAM (Ergün et al., 2019; Khan et al., 2020b). However, despite the potential hazards of ADRs and the implementation of WHO standard pharmacovigilance in Turkey, the under-reporting of ADRs continues to be a widespread issue (Ergün et al., 2019; Khan et al., 2020b; Güner & Ekmekci, 2019; TPDMA, 2020a). Previously published studies in Turkey as well as at a global level reported that HCPs have insufficient knowledge about pharmacovigilance systems and ADRs reporting (Alwhaibi & AlAloola, 2020; Ergün et al., 2019; Güner & Ekmekci, 2019; Nadeu et al., 2020). Lack of knowledge about adverse reactions to prescribed drugs in pediatric patients is also responsible for underreporting of ADRs (Dittrich et al., 2020; Khan et al., 2020b; Rosli et al., 2017). Therefore, the creation of a mandatory unified periodic education intervention on ADRs of drugs is crucial for better pediatric care. Turkish health policymakers should also emphasize the importance of adequate cooperation between international, local health authorities and manufacturers to stimulate and support regular joint training programs for all HCPs to increase ADR knowledge and reporting.

### **Limitations and strength**

Our research contains both limitations and strengths. This is a single-center study involving only pediatric patients; therefore, it cannot be generalized to other healthcare settings across the country. Moreover, a lower number of identified ADRs were evaluated due to a low reporting rate in hospital pharmacovigilance centers. Lack of training, inaccessibility to ADR reporting forms, poor skills, time restrictions, and a lack of incentives are all plausible reasons for HCPs underreporting (Venkatasubbaiah et al., 2018). On the other hand, our study highlights the importance of a pharmacovigilance monitoring system to improve quality reporting. Periodic monitoring of ADRs is useful for pediatric patient safety and also for additional literature data, which is currently rare. Moreover, this is the first study of ADRs among pediatrics in our hospital context as well as in Turkey. As a result, it could serve as a starting point for future research and give essential evidence for healthcare stakeholders and government decision-makers to take the required actions to lessen the burden of ADRs in pediatrics.

### **5. Conclusion**

ADRs in the pediatrics are a substantial public health problem. Antibiotics were the leading cause of ADRs, which may reflect the widespread use of antibiotics in this population. The majority of ADRs were related to skin reactions, and a considerable proportion was preventable types. More focused efforts are needed at the national level to avoid preventable ADRs in hospitals. Monitoring and management of ADRs and future studies would be valuable for improved patient care and safety. This study also strongly recommended the implementation of active pharmacovigilance activities to significantly minimize the health and financial burden on the pediatric population and also on the regional healthcare system.

#### **Conflict of Interest**

The authors declare no conflict of interest

#### **Funding**

No funding was received for this study from any private and government-based organization.

## REFERENCES

Al-Damen, L., & Basheti, I. (2019). Preventability analysis of adverse drug reactions in a Jordanian hospital: a prospective observational study. *International journal of clinical pharmacy*, 41(6), 1599–1610.

AlShammari, T. M., & Almoslem, M. J. (2018). Knowledge, attitudes & practices of healthcare professionals in hospitals towards the reporting of adverse drug reactions in Saudi Arabia: A multi-centre cross sectional study. *Saudi Pharmaceutical Journal*, 26, 925-931.

Alwhaibi, M., & Alaloola, N. A. (2020). Healthcare students' knowledge, attitude and perception of pharmacovigilance: A systematic review. *PLoS ONE*, 15, e0233393.

An, S. Y., Hwang, E. K., Kim, J. H., Kim, J. E., Jin, H. J., Jin, S. M., Kyun, J. O., Lee, Y. H., Park, H. S., Choi, Y. W., Lim, S. K., & Ye, Y. M. (2011). Vancomycin-associated spontaneous cutaneous adverse drug reactions. *Allergy, asthma & immunology research*, 3(3), 194–198.

Angamo, M.T., Chalmers, L., Curtain, C. M., Bereznicki, L. R. (2016). Adverse-drug reaction- related hospitalisations in developed and developing countries: A review of prevalence and contributing factors. *Drug Safety*, 39(9):847–857

Ayani, I., Aguirre, C., Gutiérrez, G., Madariaga, A., Rodríguez-Sasiáin, J. M., & Martínez-Bengochea, M. J. (1999). A cost-analysis of suspected adverse drug reactions in a hospital emergency ward. *Pharmacoepidemiology and drug safety*, 8(7), 529–534.

Bellis, J. R., Kirkham, J. J., Nunn, A. J., and Pirmohamed, M. (2014). Adverse drug reactions and off-label and unlicensed medicines in children: a prospective cohort study of unplanned admissions to a paediatric hospital. *British Journal of Clinical Pharmacology*, 77, 545–553.

Cesaro, S., Calore, E., Messina, C., & Zanesco, L. (1999). Allergic reaction to the liposomal component of liposomal amphotericin B. *Supportive care in cancer: official journal of the Multinational Association of Supportive Care in Cancer*, 7(4), 284–286.

Clavenna, A., & Bonati, M. (2009). Adverse drug reactions in childhood: a review of prospective studies and safety alerts. *Archives of Disease in Childhood*, 94, 724–728.

Comfort, S.; Dorrell, D.; Meireis, S.; Fine, J. (2018). Modified Naranjo causality scale for ICSRs (MONARCSI): A decision support tool for safety scientists. *Drug Safety*.

Common Terminology Criteria for Adverse Events (CTCAE). U.S. Department of health and human services.1-155. Retrieved from: [https://ctep.cancer.gov/protocoldevelopment/electronic\\_applications/docs/ctcae\\_v5\\_quick\\_reference\\_5x7.pdf](https://ctep.cancer.gov/protocoldevelopment/electronic_applications/docs/ctcae_v5_quick_reference_5x7.pdf)

Diaz, L., & Ciurea, A. M. (2012). Cutaneous and systemic adverse reactions to antibiotics. *Dermatologic Therapy*, 25, 12-22.

Dittrich, A., Draaisma, J., van Puijenbroek, E. P., & Loo, D. (2020). Analysis of reporting adverse drug reactions in paediatric patients in a university hospital in the Netherlands. *Paediatric drugs*, 22(4), 425-432.

Ergün, Y., Ergün, T. B, Toker, E, Ünal, E., & Akben, M. (2019). Knowledge attitude and practice of Turkish health professionals towards pharmacovigilance in a university hospital. *International Health*. 11, 177-184.

Fasipe, O. J., Akhiden, P. E., & Owhin OS. (2019). The observed effect of adverse drug reactions on the length of hospital stay among medical inpatients in a Nigerian University Teaching Hospital. *Toxicology Research and Application*, 3, 2397847319850451.

Fleischer, R., & Johnson, M. (2010). Acyclovir nephrotoxicity: a case report highlighting the importance of prevention, detection, and treatment of acyclovir-induced nephropathy. *Case reports in medicine*, 602783.

Gentili, M., Pozzi, M., Peeters, G., Radice, S., & Carnovale, C. (2018). Review of the methods to obtain paediatric drug safety information: Spontaneous reporting and healthcare databases, active surveillance programmes, systematic reviews and meta-analyses. *Current clinical pharmacology*, 13(1), 28-39.

Giardina, C., Cutroneo, P. M., Mocciaro, E., Russo, G. T., Mandraffino, G., Basile, G., Rapisarda, F., Ferrara, R., Spina, E., & Arcoraci, V. (2018). Adverse drug reactions in hospitalized patients: Results of the FORWARD (Facilitation of reporting in hospital ward) study. *Frontiers in pharmacology*, 9, 350.

Güner, M. D., & Ekmekci, P. E. (2019). Healthcare professionals' pharmacovigilance knowledge and adverse drug reaction reporting behavior and factors determining the reporting rates. *Journal of drug assessment*, 8, 13-20.



Hagihara, M., Yamagishi, Y., Hirai, J., Koizumi, Y., Kato, H., Hamada, Y., Matsuura, K., & Mikamo, H. (2015). Drug-induced hypersensitivity syndrome by liposomal amphotericin - B: a case report. *BMC research notes*, 8, 510.

Haines, H. M., Meyer, J. C., Summers, R. S., Godman, B. B. (2020). Knowledge, attitudes and practices of health care professionals towards adverse drug reaction reporting in public sector primary health care facilities in a South African district. *European Journal of Clinical Pharmacology*, 76, 991-1001.

Hartwig, S. C, Siegel, J, & Schneider, P. J. (1992). Preventability and severity assessment in reporting ADRs. *American Journal of Health-System Pharmacy*, 49, 2229-32.

Hazell, L., & Shakir, S. A. (2006). Under-reporting of adverse drug reactions: a systematic review. *Drug Safety*, 29(5), 385-96.

Impicciatore, P., Choonara, I., Clarkson, A., Provasi, D., Pandolfini, C., & Bonati, M. (2001). Incidence of adverse drug reactions in paediatric in/ out-patients: a systematic review and meta-analysis of prospective studies. *British journal of clinical pharmacology*, 52(1), 77-83.

Khan, Z., Muhammad, K., & Karatas, Y. (2020a). Pharmacovigilance and incidence of adverse drug reactions in hospitalized pediatric patients: a mini systematic review. *Egyptian Pediatric Association Gazette*, 68, 24.

Khan, Z., Karataş, Y., & Rahman, H. (2020b). Adverse drug reactions reporting in Turkey and barriers: an urgent need for pharmacovigilance education. *Therapeutic Advances in Drug Safety*. 11, 1-3.

Le, J., Nguyen, T., Law, A. V., & Hodding, J. (2006). Adverse drug reactions among children over a 10-year period. *Pediatrics*, 118(2), 555-562.

Lombardi, N., Crescioli, G., Bettiol, A., Marconi, E., Vitiello, A., Bonaiuti, R., Calvani, A. M., Masi, S., Lucenteforte, E., Mugelli, A., Giovannelli, L., & Vannacci, A. (2018). Characterization of serious adverse drug reactions as cause of emergency department visit in children: a 5-years active pharmacovigilance study. *BMC pharmacology & toxicology*, 19(1), 16.

Manan, M. M., Ibrahim, N. A., Aziz, N. A., Zulkifly, H. H., Al-Worafi, Y. M., & Long, C. M. (2016). Empirical use of antibiotic therapy in the prevention of early onset sepsis in neonates: a pilot study. *Archives of Medical Science*, 12, 603-613.

Nadew, S. S., Beyene, K. G., & Beza, S. W. (2020). Adverse drug reaction

reporting practice and associated factors among medical doctors in government hospitals in Addis Ababa, Ethiopia. *PLoS One*, 15, e0227712.

Naranjo, C. A., Busto, U., Sellers, E. M., Sandor, P., Ruiz, I., & Roberts, E. A. (1981). A method for estimating the probability of adverse drug reactions. *Clinical Pharmacology & Therapeutics*. 30, 239–245.

Nasso, C., Mecchio, A., Rottura, M., Valenzise M, Menniti-Ippolito F, Cutroneo PM, Squadrito V, Squadrito F, Pallio G, Irrera N., Arcoraci, V., & Altavilla, D. (2020). A 7-Years Active Pharmacovigilance Study of Adverse Drug Reactions Causing Children Admission to a Pediatric Emergency Department in Sicily. *Frontier in Pharmacology*. 11:1090.

Noda, A., Sakai, T., Obara, T., Miyazaki, M., Tsuchiya, M., Oyanagi, G., Murai, Y., & Mano, N. (2020). Characteristics of pediatric adverse drug reaction reports in the Japanese Adverse Drug Event Report Database. *BMC pharmacology & toxicology*, 21(1), 36.

Nor-Aripin, K. N., Choonara, I., and Sammons, H. M. (2012). Systematic review of safety in paediatric drug trials published in 2007. *European Journal of Clinical. Pharmacology*. 68, 189–194.

Oshikoya, K. A., Chukwura, H., Njokanma, O. F., Senbanjo, I. O., & Ojo, I. (2011). Incidence and cost estimate of treating pediatric adverse drug reactions in Lagos, Nigeria. *Sao Paulo medical journal = Revista paulista de medicina*, 129(3), 153–164.

Patel, K. J., Kedia, M. S., Bajpai, D., Mehta, S. S., Kshirsagar, N. A., & Gogtay, N. J. (2007). Evaluation of the prevalence and economic burden of adverse drug reactions presenting to the medical emergency department of a tertiary referral centre: a prospective study. *BMC clinical pharmacology*, 7, 8.

Priyadharsini, R., Surendiran, A., Adithan, C., Sreenivasan, S., & Sahoo, F. K. (2011). A study of adverse drug reactions in pediatric patients. *Journal of pharmacology & pharmacotherapeutics*, 2(4), 277–280.

Rashed, A. N., Wong, I. C. K., Cranswick, N., Tomlin, S., Rascher, W., and Neubert, A. (2012). Risk factors associated with adverse drug reactions in hospitalised children: International multicentre study. *Eurpian Journal of Clinical Pharmacology*. 68, 801–810.

Rosli, R., Dali, A. F., Aziz, N. A., Ming, L. C., & Manan, M. M. (2017). Reported adverse drug reactions in infants: A nationwide analysis in Malaysia. *Frontiers in pharmacology*, 8, 30.

Ryan, L., Heed, A., Foster, J., Valappil, M., Schmid, M. L., & Duncan, C. (2018). Acute kidney injury (AKI) associated with intravenous aciclovir in adults: Incidence and risk factors in clinical practice. *International journal of infectious diseases: IJID: official publication of the International Society for Infectious Diseases*, 74, 97-99.

Saqib, A., Sarwar, M. R., Sarfraz, M., & Iftikhar, S. (2018). Causality and preventability assessment of adverse drug events of antibiotics among inpatients having different lengths of hospital stay: a multicenter, cross-sectional study in Lahore, Pakistan. *BMC pharmacology & toxicology*, 19(1), 34.

Schumock, G. T., & Thornton, J. P. (1992). Focusing on the preventability of adverse drug reactions. *Hospital Pharmacy*, 27, 538-542.

Smyth, R. M., Gargon, E., Kirkham, J., Cresswell, L., Golder, S., & Smyth, R. (2012). Adverse drug reactions in children—a systematic review. *PLoS ONE*, 7, e24061.

Stamatas, G. N., Nikolovski, J., Mack, M. C., and Kollias, N. (2011). Infant skin physiology and development during the first years of life: a review of recent findings based on in vivo studies. *International Journal of Cosmetic Science*. 33, 17-24.

Sundaran, S., Udayan, A., Hareendranath, K., Eliyas, B., Ganesan, B., Hassan, A., Subash, R., Palakkal, V., & Salahudeen, M. S. (2018). Study on the classification, causality, preventability and severity of adverse drug reaction using spontaneous reporting system in hospitalized patients. *Pharmacy (Basel, Switzerland)*, 6(4), 108.

Turkey pharmacovigilance center (TÜFAM). (2005). Retrieved from <https://titck.gov.tr/PortalAdmin/Uploads/UnitPageAttachment/QSI4TS8m.pdf>.

Turkey Pharmaceuticals and Medical Devices Agency, (TPDMA). (2020a). Administration annual report, number of adverse reaction reports sent to WHO. Page 108. [Turkish: Türkiye İlaç ve Tıbbi Cihaz Kurumu. (2020a). İdare Faaliyet Raporu, DSÖ'ye gönderilen advers reaksiyon bildirimi sayısı. Sayfa 108]. Retrieved from <https://www.titck.gov.tr/kurumsal/faaliyetraporu>.

Turkey Pharmaceuticals and Medical Devices Agency (TPMDA). (2014b). Legislation on drug safety official gazette. no: 28973 [Turkish: Türkiye İlaç ve Tıbbi Cihaz Kurumu. (2014b). İlaçların Güvenliliği Hakkında Yönetmelik

Resmi Gazete. Sayı: 28973] Retrieved from <http://www.resmigazete.gov.tr/eskiler/2014/04/20140415-6.htm>.

Vázquez-Alvarez, A. O., Brennan-Bourdon, L. M., Rincón-Sánchez, A. R., Islas- Carbajal, M. C., & Huerta-Olvera, S. G. (2017). Improved drug safety through intensive pharmacovigilance in hospitalized pediatric patients. *BMC Pharmacology and Toxicology*, 18, 79.

Venkatasubbaiah, M., Reddy, P. D., & Satyanarayana, S. V (2018). Analysis and reporting of adverse drug reactions at a tertiary care teaching hospital. *Alexandria Medical Journal*, 54(4):597–603.

Walter, S. R., Day, R. O., & Gallego, B. (2017). The impact of serious adverse drug reactions: a population-based study of a decade of hospital admissions in New South Wales, Australia. *British journal of clinical pharmacology*, 83, 416-426.

World health organization (WHO). (2021a). WHO programme for international drug monitoring. Members of the who programme for international drug monitoring. Retrieved from: <https://www.who-umc.org/global-pharmacovigilance/who-programme-for-international-drug-monitoring/who-programme-members/>.

World Health organization (WHO). (2020b). Anatomical Therapeutic Chemical code (ATC) methodology. Retrieved from: [https://www.whocc.no/atc\\_ddd\\_index/](https://www.whocc.no/atc_ddd_index/).

World health organization and Uppsala Monitoring Centre (WH/UMC). (2013). The use of the WHO-UMC system for standardised case causality assessment. Retrieved from: <https://www.who.int/publications/m/item/WHO-causality-assessment>.

Xie, S. S., Soler, X., & Risma, K. A. (2021). Perioperative anaphylaxis to intravenous vancomycin in a pediatric patient with previous topical exposures. *Annals of allergy, asthma & immunology: official publication of the American College of Allergy, Asthma, & Immunology*, 127(2), 264–266.

Yildiz, C., Ozsurekci, Y., Gucer, S., Cengiz, A. B., & Topaloglu, R. (2013). Acute kidney injury due to acyclovir. *CEN case reports*, 2(1), 38–40.



# N-HEPTİL-D-GALAKTONAMİD İLE ÜÇ BOYUTLU OLARAK KÜLTÜRE EDİLEN HİPOKAMPAL HÜCRELERDE EPİDERMAL BÜYÜME FAKTÖRÜ'NÜN ÖNEMİ

*Aida Nurul Barokah<sup>1</sup>*

---

## Özet

Günümüzde nöronal hücrelerin büyümesi ve farklılaşabilmesi için üç boyutlu (3B) hücre kültürü tekniklerinin geliştirilmesi kapsamında yeni biyomateriyaller geliştirilmektedir. Araştırmacıların biyomateriyallerden en büyük beklentisi *in vivo* davranışları daha iyi taklit edebilmeleridir. Daha önce yapılan çalışmalar ile N-heptil-D-galaktonamid (GalC7) jelinin protein ve transkript düzeyinde hem glial hem de nöronal hücrelere farklılaşmayı desteklediği gösterilmiştir. Bu çalışmada E19,5 günlük fare embriyosunun hipokampusundan ve bu hipokampus bölgesinin Epidermal Büyüme Faktörü (EGF) varlığındaki koşullarda

---

<sup>1</sup> Master's Student, Ankara Yıldırım Beyazıt University, Faculty of Medicine, Translational Medicine, ORCID: 0000-0003-3102-7858

hem Poly (2-hydroxyethyl methacrylate) (pHEMA) hem de GalC7 jeli ile kültüre edildiği hücrelerinden TRIzol yardımıyla RNA izole edilerek qPCR tekniği ile *Doublecortin (Dcx)* ve *Nöronal farklılaşma faktörü 1 (Neurod1)* mRNA ifade düzeyleri ölçülmüştür. pHEMA'ya kıyasla GalC7 jelinde EGF varlığında, nörogenez belirtici olan *Dcx* ve *Neurod1* aşırı düzeyde ifade olmuştur. Buna ek olarak GalC7 jeli *Dcx* ve *Neurod1* ifade düzeyi açısından hipokampus dokusunun kendi doğasına en yakın sonuçları vermiştir. GalC7 jelinin hem glia hem de nöronal hücrelere farklılaşma açısından ideal olduğu tespitimize ek olarak nöronal kök hücrelerin çoğalmasına, göçüne ve nöronlara farklılaşmasına katkı sağlayan EGF'nin, GalC7 jeli ile yapılacak kültür çalışmalarına dahil edilmesi gerekmektedir.

**Anahtar Kelimeler:** Düşük Moleküler Ağırlıklı Hidrojel, EGF, GalC7, qPCR, *Dcx*, *Neurod1*.

## 1. Giriş

İnsan beynine dair şimdiye kadar edinilen bilgiler, etik sorunlar nedeniyle, çoğunlukla ölümü gerçekleştirmiş bireylerin beyin örneklerine dayanmaktadır. İnsan olmayan primatlar da dahil olmak üzere hayvan modellerinin, insan beynine kıyasla bazı farklılıklara sahip olması sebebiyle insan merkezi sinir sisteminin ve ilgili hastalıklarının araştırılabilmesi zorluk arz etmektedir (Adams et al., 2019; Shou et al., 2020). Kök hücre teknolojilerinin hızlı ilerleyişine ek olarak üç boyutlu (3B) organoidlerin ortaya çıkışı rejeneratif tıpta büyük ilgi görmüştür (Shou et al., 2020). Çünkü bu teknolojiler, insan beyninin gelişiminin araştırılabilmesi noktasında yeni kapılar açarken nörodejeneratif hastalıklarda tedavi protokollerinin geliştirilebilmesi için de umut vaadedici olmuştur.

Şimdiye kadar nörodejeneratif hastalıkları modellemek için bazı yapısal ve biyolojik sınırlamalara sahip iki boyutlu (2B) kültürler kullanılmıştır ancak bu platformların beyin karmaşık 3B yapısını, dokuya özgü hücrel organizasyonları, hücre-hücre ve hücre-ekstreselüler matriks etkileşimlerini yansıtmadığı gösterilmiştir (Anton et al., 2015; Cenini et al., 2021; Centeno et al., 2018). Buna ek olarak, 2B kültür ile kıyaslandığında 3B kültür sistemlerinin hücre büyümesi ve işlevi için fizyolojik olarak daha uygun bir ortam sağladığı düşünülmektedir (Chalard et al., 2018). Ayrıca, nöronal kültürlerin 3B olarak gerçekleştirilmesinin *in vivo* davranışa daha yakın sonuçlar verdiği de artık bilinen bir gerçektir. Örneğin, Alzheimer hastalığı durumunda, karakteristik amiloid plaklarının sadece 3B modellerde geliştiği görülmektedir.

Normal veya patolojik koşulları incelemek için daha sağlam *in vitro* modelleri temsil eden bu 3B kültür sistemleri ilaç çalışmaları için de kullanılabilirler (Chalard et al., 2018). İlaçlara hücrel yanıt söz konusu olduğunda da 2B ve 3B kültür koşulları arasında çok büyük farklılıkların olduğunu gösteren çalışmalar mevcuttur (Cenini et al., 2021). Bu nedenle, ilaçların etkinliğini daha iyi değerlendirmek veya daha gerçekçi fonksiyonel organlar geliştirmek için 3B kültür tekniğini geliştirmek zorunlu hale gelmiştir. Sinir sisteminde, bu 3B kültür sistemleri ile iki ana uygulama hedeflenmektedir. Birincisi, yaygın nörodejeneratif hastalıkları tedavi edebilecek veya yavaşlatabilecek yeni ilaçların araştırılması ile ilgilidir. İkincisi ise sinir sisteminin fiziksel yaralanmalarını hedeflemektedir.



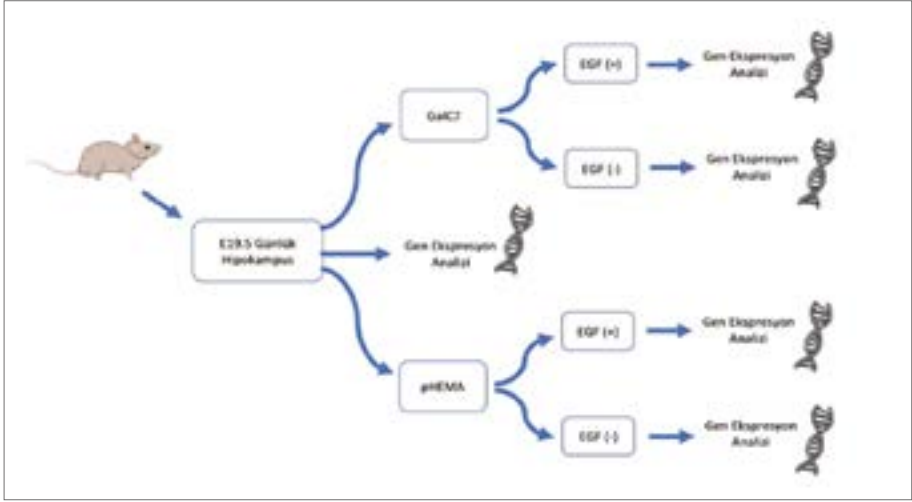
Şu anda, nöronal hücrelerin büyümesine ve farklılaşmasına izin vermek için 3B hücre kültürü teknikleri kapsamında yeni biyomalzemeler geliştirilmektedir. Araştırmacıların biyomalzeme için en büyük beklentisi, *in vivo* davranışı daha iyi taklit edebilmeleridir (Bruggeman et al., 2019; Centeno et al., 2018; George et al., 2020; Grasman et al., 2018). Beyin vücuttaki en yumuşak organlardan biridir dolayısıyla nöronlar ve glial hücrelerin gelişip farklılaşması için çok yumuşak iskelelere ihtiyaç vardır. Bu nedenle, nöronların tıpkı kendi doğasındaki gibi gelişimini sağlayan iskele hala oldukça azdır. Günümüzde nöronal hücrelerin *in vitro* 3B hücre kültürlerini ele almak için farklı türde birçok biyomateryal geliştirilmektedir. 3B hücre kültürünü yapılandırmak için sadece sferoidlere dayanan modellerin yanı sıra, fare sarkomundan ekstrakte edilen ve tümör kaynaklı hücre dışı bir matris olan matrigel (Kim et al., 2015; Palm et al., 2015), kolaj (Kaneko et al., 2015; Zychowicz et al., 2019), jelatin (Han et al., 2019) gibi doğal veya sentetik biyolojik moleküllere dayanan makromoleküller mevcuttur.

Sakaritlerden türetilmiş, gram ölçekte hazırlanabilen moleküler hidrojel kategorisindeki GalC7 hidrojelini sentezleyerek, erişkin insan nöral kök hücrelerinin kültüründe kullanılan Dr. Juliette Fitremann ve ekibi 2018 yılında bu jelin çok yoğun bir nöron ve glial hücre ağını oluşturduğunu göstermişlerdir (Chalard et al., 2018). Buna ek olarak, çok yoğun uzun nörit demetlerinin (en az 500 µm) heterojen jel liflerini takip ederek heterojen morfolojiler sergilediklerini de gözlemlemişlerdir (Chalard et al., 2018). Bu gözlem, aksonların ve dendritlerin büyümesinin sadece biyokimyasal değil, aynı zamanda mekanik sinyallere de tepki verdiğini gösteren diğer çalışmaları anımsatmaktadır. O halde, bir nöritin bir akson veya dendrite farklılaşabilmesi, biyomalzemenin sertliğine (Koser et al., 2016) ve biyomalzeme içinde nörit tarafından alınan yola bağlıdır (Franze et al., 2009). com/documents/?uuid=411aac74-a569-4ac9-a25b-2956f533129b”]]],”-mendeley”:{“formattedCitation”:(Franze et al., 2009.

Bayram ve ark. GalC7 jelini kullanarak fare hipokampus hücrelerinde 3B kültür yaptığı çalışma ile ülkemizde nörodejeneratif hastalıkların tedavisine yönelik yeni ve umut vadeci bir adım atmıştır (Bayram et al., 2021). Bu çalışma ile GalC7 jeli kullanılarak 3B kültüre edilen nöronal hücrelerden ilk kez RNA izole edilerek, nörojenezin bir belirteci olan

Doublecortin (*Dcx*) ve nöronal farklılaşmanın bir belirtici olan *Neurod1* mRNA ifade düzeylerinin hipokampus hücrelerinin kendi doğasına benzer profil sergilediğini göstermişlerdir

Bu noktada, hücre göçünü uyarması, hücre büyümesi, yaşaması, proliferasyonu ve farklılaşmasında önemli rol oynayan bir büyüme faktörü olan epidermal büyüme faktörü (EGF)'nin hem pHEMA hem de GalC7 jeli ile 3B olarak kültüre edilen hipokampal hücrelerdeki etkisi merak konusu olmuştur (Şekil 1).



**Şekil 1.** Çalışmanın Tasarımı: Embriyonik fare hipokampusunun qPCR tekniği ile 5 farklı koşuldaki mRNA ekspresyonu. E19,5. günde *in vivo* (1); 7 gün boyunca GalC7'de EGF (-) (2) ve EGF (+) (3) kültüre edildi; 12 gün boyunca pHEMA ile EGF (-) (4) ve EGF (+) (5) kültüre edildi.

Nöronal kök hücrelerin *in vitro* ve *in vivo* proliferasyonunu, göçlerini ve nöroglial hücre hattına doğru farklılaşmalarını indüklediği bilinen (Scalabrino, 2020) EGF'nin özellikle GalC7 jeli kullanılarak kültüre edilen nöron hücrelerinin büyümesi ve farklılaşabilmesine katkı sağlayacağını düşünmekteyiz.

GalC7 jeli ile kültüre edilen hipokampal hücrelere EGF ekleyerek sinir hücreleri için en uygun yöntemi geliştirmeyi ve böylece ülkemizde nörodejeneratif hastalıkların tedavisine yönelik umut vadeci bir adım daha atmayı amaçlamaktayız.

## 2. Yöntem

### 2.1. Hidrojelin Hazırlanışı:

Her bir örnek için 9 mg GalC7 tartılıp yaklaşık 5 kat hacimdeki kapaklı cam şişe içine dökülmüştür ve üzerine 2 mL iki kez distile edilmiş su eklenmiştir. Progralanabilir fırın 115 ° C'ye kadar ısıtılmıştır ve cam şişe kapağı hafif kapalı şekilde fırına yerleştirilmiştir. Toz halindeki GalC7 çözünene kadar ara ara kontrol edilerek fırında inkübe edilmiştir. Toz halindeki GalC7 çözününce fırının ısı 105 ° C'ye düşürülmüştür ve 24 well kültür plate de fırına alınmıştır. Dışarda sıcak zeminde metal kap (plate sığacak büyüklükte) içinde su kaynayana kadar bekletilmiştir. Sıcak su içine fırındaki plate yerleştirildikten sonra hafif şekilde ısıya maruz kalmış pipet yardımıyla çözünen GalC7 kuyucuklara 500 µL çok hızlı şekilde pipetlenmiştir.

Plate içindeki GalC7 jel haline gelmeden plate hızlıca fırına ve iki boş plate arasına sandviç gibi alınmıştır. Plate'lerin en üst kısmına çelik blok yerleştirilerek fırının 105 ° C'den yavaş yavaş oda ısısına düşmesi (min 90 dk) bekletilmiştir. Böylece termal şoktan korunularak yavaş yavaş soğuma ile jel elde edilmiştir. Jel oluşunca plate laminar kabin içine taşınmıştır ve burada kapağı açılarak kuyucuk içindeki su pipet yardımıyla uzaklaştırılmıştır. Jel üzerine çok yavaş şekilde, 300 µL hazır medium pipetlenip %5 CO<sub>2</sub> içeren etüvde 37 °C'de 5 saat inkübe edilmiştir. İnkübasyon sonrası eski medium pipet ile çekilip yerine tekrar 300 µL hazır medium eklenerek %5 CO<sub>2</sub> içeren etüvde 37 °C'de bir gece inkübe edilmiştir. İnkübasyon sonrası eski medium pipet yardımıyla çekilip atılmıştır ve yerine 300 µL hazır medium eklenerek tekrar %5 CO<sub>2</sub> içeren etüvde 37 °C'de 5 saat inkübe edilmiştir. Böylece jel içindeki su ile mediumun yer değiştirilmesi sağlanmıştır. Yedi günlük kültür boyunca medium değiştirilemediği için bu sayede, jelin mediumun her yerine ulaşması sağlanmıştır.

### 2.2. Çalışmada Kullanılan Fareler:

Balb/c ırkı, 8 haftalık fareler kullanılmıştır. Fareler, oda sıcaklığı 20-24 °C ve nisbi nem miktarı %45-70 şartlarında minimum kafes alanı 180 cm<sup>2</sup> ve minimum kafes yüksekliği 12 cm<sup>2</sup> olacak şekilde barındırılmıştır. Eşeyssel olgunluğa erişen fareler bir erkeğe iki dişi olacak şekilde çiftleşmeye atılmıştır. Sabah erken vakitte dişilerde çiftleşme belirteci olan vajinal tıkaç

kontrol edilmiştir. Vajinal tıkaçı olan fareler 0,5 günlük gebe kabul edilerek takip edilmişlerdir. Gebelik 19 günlük olduğunda (E19,5) anneler sakrifiye edilerek uteruslar Phosphate Buffered saline (PBS) içine alınmıştır.

### 2.3. Embriyonik Hipokampus Çıkarılması:

E19,5 günlük gebe farelerin uteruslarından embriyolar pens yardımıyla çıkarılmıştır. Her bir embriyonun total beyini çıkarıldıktan sonra kuyruktan bir parça alınarak cinsiyet tespiti için DNA izole edilmiştir. Embriyonun total beyini lam üzerine alınmıştır ve 2 dk -20 °C'de bekletilmiştir. Soğuk blok üzerinde ve binoküler mikroskop altında sağ/sol hipokampus pipet yardımıyla aspire edilmiştir. Aspire edilen hipokampus 1 mL Hanks' Balanced Salt (HBS) solüsyonu içine alınmıştır.

### 2.4. Embriyodan Cinsiyet Tayini:

#### *DNA İzolasyonu*

DNA izolasyonu yapılırken aşağıdaki prosedür takip edilmiştir:

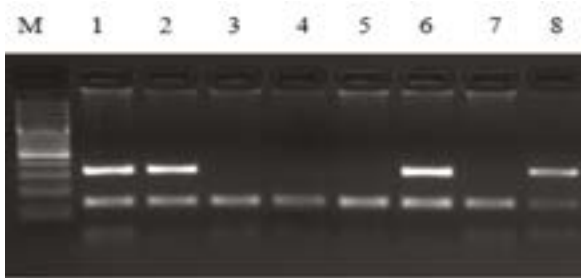
1. Embriyoların kuyruklarından doku parçası 300 µL lizis buffer (1M Tris, 0,5M EDTA, %4 Sodyum Dodesil Sülfat (SDS) , distile su (dH2O) ve proteinaz K içeren ependorf tüplere alınmıştır.
2. Örnekler 55°C'de bir gece inkübasyona bırakılmıştır. Inkübasyondan sonra 100 µL Amonyum asetat eklenerek ve iyice karıştırılmıştır.
3. Örnekler 4000 rpm'de 20 dk santifüj edilmiştir. Süpernatant temiz bir ependorfa alınarak 500 µL izopropanol eklenmiştir ve 5dk oda ısısında inkübe edilmiştir.
4. Inkübasyon sonrası 4000 rpm'de 10 dk santifüj yapılmıştır ve süpernatant atılarak oluşan pellete 1000 µL %70 etanol eklenmiştir.
5. Örnekler 4000 rpm'de 10 dk santifüj edilmiştir ve süpernatant atılmıştır.
6. Oluşan pelletten alkolü uzaklaştırmak için ependorf tüp kapağı açık şekilde 10 dk oda ısısında inkübe edilmiştir.
7. Pellet kuruduktan sonra 100 µL Nuclease-Free Water (NFW) (Qiagen, Almanya) ile çözülmüştür.
8. Biospec Nano (Shimadzu) kullanılarak DNA konsantrasyon ölçümü yapılmıştır.

### Polimeraz Zincir Reaksiyonu (PCR)

Cinsiyet tayini için embriyonun kuyruk dokusundan DNA izolasyonu yapıldıktan sonra Sry geni forward 5' TGCACAATTGTCTAGAGAGC3', reverse 5' ACTGCAGAAGGTTGTACAGT3' ve Pax6 geni forward 5' CTTTCTCCAGAGCCTCAAT3', reverse 5' GCAACAGGAAGGAGGGGGAGA3' primerleri kullanılarak (Tablo 1) PCR ile çoğaltma işlemi yapılmıştır. PCR işlemi için 5 µL DNA (10 pg-1 µg), 5 µL 10X Taq Buffer, 4 µL 25mM MgCl<sub>2</sub>, 4 µL dNTP mix (2.5 mM each), her bir primerden 0.5 µL 10µM Sry F, Sry R, Pax6 F, Pax6 R 0.5 µL 1,25U Taq DNA Polimeraz (Thermo Fisher, Amerika), son hacmi 50 µL'ye tamamlayacak şekilde Nuclease Free Water kullanılmıştır. 95 °C'de 5 dk ön denatürasyon, 30 döngü boyunca 94 °C'de 1 dk denatürasyon, 57 °C'de 45 saniye annealing, 72 °C'de 1 dk uzama ve son olarak 72 °C'de 10 dk olacak şekilde Thermal Cycler PCR Cihazı (SensoQuest) çalıştırılmıştır. PCR ürünleri, etidyum bromid içeren %2'lik agaroz jelde koşurulmuştur. Jel görüntüleme sistemi (Bio-Rad) ve Image Lab analiz programı kullanılarak jel görüntülenmiştir (Şekil 2).

**Tablo 1.** Cinsiyet tayini için gerekli primer dizileri.

Targeted Genes	Primer Sequences (5'-3')	Product Size (bp)	Primer (mM)	Concentration
Sry	F: TGCACAATTGTCTAGAGAGC	329	0,01 mM	
	R: ACTGCAGAAGGTTGTACAGT		0,01 mM	
Pax6	F: CTTTCTCCAGAGCCTCAAT	150	0,01 mM	
	R: GCAACAGGAAGGAGGGGGAGA		0,01 mM	



**Şekil 2.** Cinsiyet tayini jel görüntüsü: M: Markır (100bç-3000bç), 1.,2. ve 6. embriyoların cinsiyeti erkek iken 3.,4. ve 5. embriyoların cinsiyeti dişidir. 7. örnek kontrol dişi, 8. örnek kontrol erkektir.

## 2.5. Hücre Kültürü

### *Poly-Hema ile Primer Hücre Kültürü:*

Hipokampusten primer hücre kültürü yapılırken aşağıdaki prosedürler takip edilmiştir:

1. pHEMA (Sigma, Almanya) kültüre başlamadan bir gün önceden hazırlanmıştır. 300mg pHEMA 10ml %95 Etanol ile su banyosunda (65 °C) ara ara vorkteks yapılarak çözündürülmüştür.

2. Laminar hava kabini içinde 24 well-plate'in her bir kuyucuğuna 200 µL pHEMA pipetlenmiştir. Plate kapağı açık şekilde alkolün uçması için bir gece kabinde bırakılmıştır.

3. Ertesi gün E19,5 günlük gebe farelerin embriyolarından aspire edilen sağ ve sol hipokampus 1mL Hanks' Balanced Salt (HBS) solüsyonu içine alınmıştır.

4. Dokular resüspanse edilip 1000 rpm'de 2 dk oda ısısında santrifüj edilmiştir.

5. Hücrelerin ekimi için Dulbecco's Modified Eagle Medium: Nutrient Mixture F-12 (DMEM/F12) (Sigma, Almanya) medium kullanılmıştır. DMEM/F12 mediuma; %10 oranında Fetal Bovine Serum (FBS) (Sigma, Almanya), %1 oranında Penicillin-Streptomycin (Pen Strep) (Gibco, Life Technologies) ve L-Glutamine (200 mM) (Gibco, Life Technologies) eklenerek kullanıma hazır medium elde edilmiştir.

6. Santrifüj sonrası supernatant atılıp hücreler 1mL hazır medium ile resüspanse edilerek her örnek ikişer pHEMA kaplı well plate'e (her bir well'e 500 µL) ekilmiştir. %5 CO<sub>2</sub> içeren etüvde 37 °C'de inkübe edilmiştir.

7. Kültürün 3.gününde her well'e 1X Insulin-Transferrin-Selenium-A (ITS), 1X B27 Supplement eklenmiştir. Çift ekilen örneklerden birine 20 ng/mL Epidermal Büyüme Faktörü (EGF) eklenirken diğerine aynı hacimde hazır medium eklenmiştir.

8. Kültürün 7.gününde 7.basamaktaki işlem tekrarlanmıştır.

9. Kültürün 12. gününde kültür sonlandırılıp RNA izolasyonu yapılmıştır.

***GalC7 Jeli ile Primer Hücre Kültürü:***

Aspire edilen embriyonik hipokampus HBS ile yıkandıktan sonra 1000 rpm'de 2 dk oda ısısında santrifüj edilmiştir ve pellet 250 µL hazır medium ile resüspanse edilmiştir. Örneğe 1X B27 Supplement, 1X ITS eklenip naif şekilde alt-üst edilmiştir. Çift ekilecek örneklerden birine 20 ng/mL Epidermal Büyüme Faktörü (EGF) eklenirken diğerine aynı hacimde hazır medium eklenmiştir. Resüspanse edilen örnek GalC7 jeli bulunan kuyucuğa jele zarar vermeyecek şekilde dikkatle pipetlenmiştir. Plate %5 CO<sub>2</sub> içeren etüvde 37 °C'de inkübe edilmiştir. Yedi gün sonra kültür sonlandırılıp RNA izolasyonu yapılmıştır.

**2.6. RNA İzolasyonu*****Poly-Hema ile Yapılan Primer Hücre Kültüründen RNA İzolasyonu:***

Kültür 12 günlük olduğunda pHEMA kaplı plate pastör pipeti yardımıyla epandorf tüpe taşınmıştır. Kültürün sonlanması sonrası RNA izolasyonu için aşağıdaki prosedürler takip edilmiştir.

1. Tüpler 1000 rpm'de 2 dk oda ısısında santrifüj edildikten sonra 1 mL TriPure Isolation Reagent (Roche, Almanya) ve 1 µL (20ng/mL) Glikojen eklenmiştir ve iyice vorteks yapılmıştır.
2. Tüplere, 200 µL Kloroform eklenmiştir ve 15 sn vorteks yapılmıştır.
3. Tüpler 12000 g'de 20 dk 4 °C'de santrifüj edilmiştir. Santrifüjden sonra aköz faz yeni ependorf tüpe alınmıştır.
4. Aköz fazın taşındığı tüpe 500 µL İzopropanol eklenip iyice vortekslenmiştir ve -20 °C dolapta bir gece bekletilmiştir.
5. İnkübasyon sonrası tüpler, 12000 g'de 10 dk 4 °C'de santrifüj edilmiştir ve süpernant atılmıştır.
6. Yıkama işlemi için pellete 1 mL %75 Etanol eklenip alt-üst edilmiştir ve 7500 g'de 5 dk 4°C'de santrifüj edilmiştir ve süpernant atılmıştır.
7. Yıkama işlemi tekrar edilmiştir ve santrifü sonrası süpernant atılmıştır.
8. Pellet 30 µL Nükleaz içermeyen su (Qiagen, Almanya) ile çözülür ve Biospec Nano (Shimadzu) kullanılarak absorbans ölçümü yapılmıştır.

***GalC7 Jeli ile Yapılan Primer Hücre Kültüründen RNA İzolasyonu***

Kültür 7 günlük olduğunda jele zarar vermeyecek şekilde medium çekilip atılmıştır. Jele zarar vermeyecek şekilde 200 µL PBS jel üzerine pipetlenip geri çekilerek jele tutunmamış hücreler uzaklaştırılmıştır. Akabinde, RNA izolasyonu için aşağıdaki prosedürler takip edilmiştir.

1. GalC7 jeli bulunan kuyucuğa 1 mL TriPure Isolation Reagent (Roche, Almanya) eklenmiştir bu evrede pipetaj yapılarak jelin çözünmesi sağlanmıştır. Pipet yardımıyla trizol ve hücre karışımı kuyucuktan ependorf tüpe taşınmıştır.

2. Ependorf tüpe 1 µL (20ng/mL) Glikojen eklenerek iyice vorteks yapıldıktan sonra 200 µL Kloroform eklenmiştir ve 15 sn vorteks yapılmıştır.

3. Tüpler 12000 g'de 20 dk 4 °C'de santrifüj edilmiştir. Santrifüjden sonra aköz faz yeni ependorf tüpe alınmıştır.

4. Aköz fazın taşındığı tüpe 500 µL İzopropanol eklenip iyice vortekslenmiştir ve -20 °C dolapta bir gece bekletilmiştir.

5. İnkübasyon sonrası tüpler, 12000 g'de 10 dk 4 °C'de santrifüj edilmiştir ve süpernant atılmıştır.

6. Yıkama işlemi için pellete 1 ml %75 Etanol eklenip alt-üst edilmiştir ve 7500 g'de 5 dk 4 °C'de santrifüj edilmiştir ve süpernant atılmıştır.

7. Yıkama işlemi tekrar edilmiştir ve santrifü sonrası süpernant atılmıştır.

8. Pellet 30 µL NFW (Qiagen, Almanya) ile çözölmüştür ve Biospec Nano (Shimadzu) kullanılarak absorbands ölçümü yapılmıştır.

**2.7. cDNA Sentezi**

RNA örneklerinden cDNA sentezlenirken EvoScript cDNA Kiti (Roche, Almanya) kiti kullanılmıştır; 4 µL Reaction Buffer (5X), 14 µL Template RNA (2,5 µg / 20 µL) karışımı 5 dk buz üzerinde bekletilmiştir. Bu süre sonunda her bir örnek üzerine 2 µL Enzim karışımı eklenerek Thermal Cycler (SensoQuest) cihazında 42 °C'de 15 dk, 85°C'de 5 dk ve 65°C'de 15 dk inkübe edilmiştir. İnkübasyon sonrası elde edilen cDNA örnekleri Pre-Amplifikasyon işlemi için kullanılmıştır.



### 2.8. Pre-Amplifikasyon Yöntemi (Ön Çoğaltma)

mRNA ekspresyon seviyesi araştırılacak primer/probe (Integrated DNA Technologies, Belçika) %10 seyreltilerek ön çoğaltma işlemi için Pre-AMP Master Kit (Roche, Almanya) ile birlikte kullanılmıştır; 5 µL cDNA 10 µL Pre-amp master mix, 1,4 µL %10 seyreltilmiş primer/probe ve son hacimi 25 µL'ye tamamlayacak şekilde NFW eklenmiştir (Tablo 2). Thermal Cycler (SensoQuest) cihazında ön denatasyon için 95 °C'de 1 dk, 13 döngü boyunca 95°C'de 15 sn, 60°C'de 4dk inkübe edilmiştir.

**Tablo 2.** Pre-Amplifikasyon işlemi için gerekli malzemeler ve miktarları.

Materials		Volumes
Primerler	%10 <i>Dcx</i>	1.4 µL
	%10 <i>Neurod1</i>	1.4 µL
Pre-Amp Master Mix		10 µL
NFW		1.6 µL
cDNA		5 µL

### 2.9. PCR ile mRNA Ekspresyon Çalışması

mRNA ekspresyon seviyesinin ölçümü için 10 µL 2X Probe Master Mix, 1 µL Primer/Probe, 4 µL NFW ve 5 µL pre-amp cDNA (1/40 oranında seyreltilmiş) karışımı 96 well plate (Roche, Almanya) üzerine pipetlenmiştir. 96 well plate, seal ile kapatılarak LightCycler 480 II (Roche, Almanya) Real-Time PCR cihazında ön denatasyon için 95 °C'de 10 dk, 50 döngü boyunca 95°C'de 10 sn, 60°C'de 30 sn, 72°C'de 1sn ve cooling için 40°C'de 30 sn inkübe edilmiştir. House-keeping gen olarak actin, beta kullanılmıştır ve her bir örnek çift çalışılmıştır. Veriler delta delta ct metodu kullanılarak normalize edilmiştir.

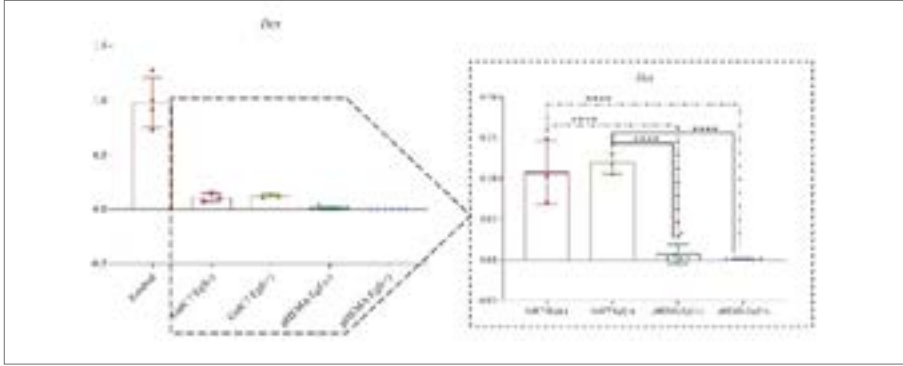
### 3. Tartışma

EGF'nin hipokampal nöronal 3B hücre kültürleri üzerindeki etkisini göstermek için planladığımız bu çalışma ile E19,5 günlük hipokampal hücreleri hem pHEMA hem de GalC7 jeli kullanarak kültüre ederek bu primer hücre kültürlerinde bir nöroenez belirteci olan *Dcx* ve

bir nöronal farklılaşma belirteci olan *Neurod1* mRNA ifade düzeylerini qPCR tekniği ile araştırdık ve sonuçlarımızı aşağıda olduğu şekilde yorumladık.

*Dcx*, insanlarda normal hipokampal gelişim için gerekli olan mikrotübüle bağlı bir proteindir. *Dcx*'in protein düzeyinde ekspresyonuna engel olan bir mutasyon taşıyan farelerin hipokampusunun CA3 bölgesinde çok şiddetli bozulmuş tabakalaşma tespit edilmiştir. Özetle, hipokampusun yapısal gelişimi için *Dcx* gereklidir (Corbo et al., 2002) whereas heterozygous females show a mosaic phenotype with a normal cortex as well as a second band of misplaced (heterotopic. 2019 yılında Nature dergisinde yayınlanan bir makalede *Dcx* proteinini bolca ifade eden olgunlaşmamış nöronların bolluğunu tespit eden araştırmacılar, bu hücrelerin insanlarda yetişkin hipokampal nörogenezi boyunca önemli olduğu çıkarımını yapmışlardır (Moreno-Jiménez et al., 2019). Bayram ve ark. 2021 yılında yaptıkları çalışmada hipokampal hücreleri hem pHEMA hem de GalC7 jeli kullanarak kültüre etmişlerdir. pHEMA kullanarak elde ettikleri nörosferlerde *Dcx* mRNA ifade düzeyini yok denecek kadar az tespit ederken GalC7 jeline ekilen hipokampal hücrelerde aşırı *Dcx* ekspresyonu tespit ederek GalC7 jelinin nöron hücre kültürü için ideal olduğu çıkarımını yapmışlardır. (Bayram et al., 2021). Bu çalışmada ise pHEMA kullanarak elde edilen nörosferlere kıyasla GalC7 jeline *Dcx* ifade düzeyinin hem EGF varken hem de yokken anlamlı olarak arttığı tespit edilmiştir ( $p < 0,0001$ ) (Şekil 3). Garcez ve ark. bıldırcın embriyoları ile yaptıkları çalışmada EGF'in nörogenezi desteklediğini tespit etmişlerdir (Garcez et al., 2009) we further investigate the effect of microenvironmental factors on quail trunk NC development. We show for the first time that EGF induces differentiation of NC to the neuronal and melanocytic phenotypes, while fibroblast growth factor 2 (FGF2. Nitekim biz de çalışmamızda EGF (+) GalC7 jeline bir nörogenez biyobelirteci olan *Dcx*'in mRNA ifade düzeyinin daha yüksek olduğunu tespit ettik (Şekil 3).

Nöronal farklılaşma faktörü olarak bilinen *Neurod1*, periferik ve merkezi sinir sistemlerinin nöronlarının gelişimi sırasında yüksek oranda ifade olmaktadır (Chae et al., 2004). Fare ve insan hipokampusunda yetişkinlik dönemi boyunca *Neurod1* mRNA ekspresyonu çok

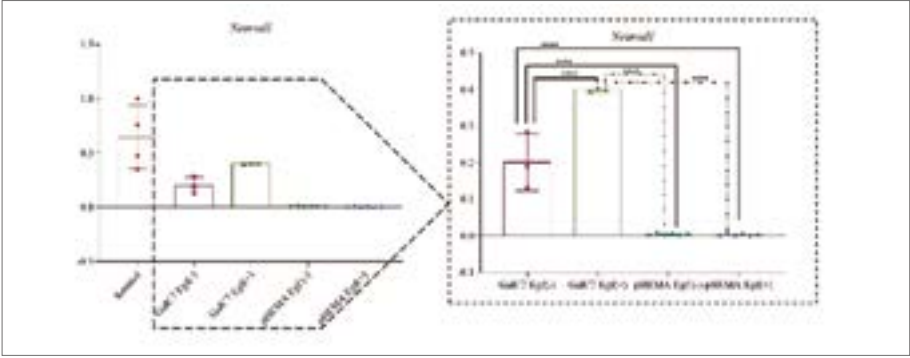


**Şekil 3.** Gruplar arasında *Dcx* mRNA ekspresyonunun kıyaslanması.

yüksek seviyede kalarak dokunun bakım ve onarım görevini üstlenmektedir (Lee et al., 2000; *Molecular Cloning of a Human NeuroD from a Neuroblastoma Cell Line Specifically Expressed in the Fetal Brain and Adult Cerebellum*. - PubMed - NCBI, n.d.). *Neurod1* geninin homozigot yokluğunda hipokampusda nörogenezin gerçekleştiği bölge olarak bilinen dentat girusun, dramatik bir şekilde küçüldüğü gösterilmiştir (Miyata et al., n.d.; Schwab et al., n.d.). Bu sayede, *Neurod1*'in yenidoğan nöronlarının göçü, olgunlaşması ve hayatta kalmasının yanı sıra nörogenez için de gerekli olduğu gösterilmiştir (Apréa et al., 2014). Bayram ve ark. 2021 yılında yaptıkları çalışmada hipokampal hücreleri hem pHEMA hem de GalC7 jeli kullanarak kültüre etmişlerdir. pHEMA kullanılarak elde edilen nörosferlere kıyasla GalC7 jeline ekilen hipokampal hücrelerde *Neurod1* mRNA ekspresyonunun aşırı derecede yüksek olduğunu tespit ederek GalC7 jelinin nöron kültürü için ideal olduğu çıkarımını yapmışlardır (Bayram et al., 2021). Bu çalışmada ise pHEMA kullanarak elde edilen nörosferlere kıyasla GalC7 jeline EGF varlığında *Neurod1* mRNA ifade düzeyinin anlamlı olarak arttığı tespit edilmiştir ( $p<0,0001$ ) (Şekil 4). Bu bulgular ağ organizasyonu gerçekten hücre dışı matris mimarisini taklit ediyor gibi görünen GalC7 jelinin (Chalard et al., 2018) nöron kültürü için ideal olduğunun bir kez daha göstergesidir. Buna ek olarak Angénieux ve ark. fare retinal göz kök hücreleri ile yaptıkları çalışmada (Angénieux et al., 2006), Casper ve ark. rat embriyonik nöron hücreleri ile yaptıkları çalışmada (D et al., 1991) EGF'in nöronların hayatta kalmasını sağladığını tespit etmişlerdir. Ayrıca Garcez ve ark. bıldırcın embriyoları ile yaptıkları çalışmada EGF'in nörogenezi desteklediğinin yanı sıra EGF'in nöronal kök hücrelerin nörona doğru farklılaşmaya teşvik ettiğini göstermişlerdir (Garcez et al., 2009). Nitekim biz de çalışmamız-

da EGF(+) GalC7 jelinde kültüre edilen hipokampal hücrelerin bir nöronal farklılaşma biyobelirteci olan *Neurod1* mRNA ifade seviyesinin arttığını tespit ettik ( $p<0,0001$ ) (Şekil 4).

Özetle, nöronal kök hücrelerin *in vitro* ve *in vivo* çoğalmasını, göçünü ve nöroglial hücrelere doğru farklılaşmasını indükleyen EGF'nin (Scalabrino, 2020), GalC7 jeli ile yapılacak nöronal kültür çalışmalarında protokole eklenmesi gerektiğini tespit ettik (Şekil 3 ve Şekil 4). Nöronal progenitör hücreler açısından zengin olduğu düşünülen pHEMA kullanılarak elde edilen nörosferlerin hem kendi başına hem de EGF varlığında GalC7 ile yarışamayacak kadar geride olduğu moleküler düzeyde bir kez daha gösterilmiş olmuştur ( $p<0,0001$ ) (Şekil 3 ve Şekil 4).



Şekil 4. Gruplar arasında *Neurod1* mRNA ifade seviyesinin kıyaslanması.

## Sonuç

Birçok nörodejeneratif hastalığa tanı konulabilmesi ve özellikle tedavi edilebilmesi için nöronların uygun şekilde çoğalabileceği biyomalzemelere olan gereksinim böyle bir çalışma yapmamız için ilham vermiştir. Tam bir iç içe geçmiş nöronal ağın gelişmesine izin veren ve nöral doku rejenerasyonunu destekleme potansiyeli protein düzeyinde (Chalard et al., 2018) ve mRNA düzeyinde (Bayram et al., 2021) ortaya koyulmuş olan GalC7 jelinin hem glia hem de nöronal hücrelere farklılaşma açısından ideal olduğu tespitimize ek olarak nöronal kök hücrelerin çoğalmasına, göçüne ve nöronlara farklılaşmasına katkı sağlayan EGF'nin, GalC7 jeli ile yapılacak kültür çalışmalarına protokole eklenmesi kanaatindeyiz.

## KAYNAKÇA

Adams, J. W., Cugola, F. R., & Muotri, A. R. (2019). Brain organoids as tools for modeling human neurodevelopmental disorders. *Physiology*, 34(5), 365-375. <https://doi.org/10.1152/physiol.00005.2019>

Angénioux, B., Schorderet, D. F., & Arsenijevic, Y. (2006). Epidermal Growth Factor Is a Neuronal Differentiation Factor for Retinal Stem Cells In Vitro. *STEM CELLS*, 24(3), 696-706. <https://doi.org/10.1634/STEMCELLS.2005-0190>

Anton, D., Burckel, H., Josset, E., & Noel, G. (2015). Three-dimensional cell culture: A breakthrough in vivo. *International Journal of Molecular Sciences*, 16(3), 5517-5527. doi: <https://doi.org/10.3390/ijms16035517>

Apréa, J., Nonaka-Kinoshita, M., & Calegari, F. (2014). Generation and characterization of Neurod1-CreER<sup>T2</sup> mouse lines for the study of embryonic and adult neurogenesis. *Genesis*, 52(10), 870-878. doi: <https://doi.org/10.1002/dvg.22797>

Bayram, K. K., Fitremann, J., Bayram, A., Yilmaz, Z., Mehmetbeyoğlu, E., Özkul, Y., & Rassoulzadegan, M. (2021). Gene expression of mouse hippocampal stem cells grown in a galactose-derived molecular gel compared to in vivo and neurospheres. *Processes*, 9(4). doi: <https://doi.org/10.3390/pr9040716>

Bruggeman, K. F., Moriarty, N., Dowd, E., Nisbet, D. R., & Parish, C. L. (2019). Harnessing stem cells and biomaterials to promote neural repair. *British Journal of Pharmacology*, 176(3), 355-368. doi: <https://doi.org/10.1111/bph.14545>

Cenini, G., Hebisch, M., Iefremova, V., Flitsch, L. J., Breitkreuz, Y., Tanzi, R. E., Kim, D. Y., Peitz, M., & Brüstle, O. (2021). Dissecting Alzheimer's disease pathogenesis in human 2D and 3D models. *Molecular and Cellular Neuroscience*, 110, 103568. doi: <https://doi.org/10.1016/j.mcn.2020.103568>

Centeno, E. G. Z., Cimarosti, H., & Bithell, A. (2018). 2D versus 3D human induced pluripotent stem cell-derived cultures for neurodegenerative disease modelling. *Molecular Neurodegeneration*, 13(1), 1-15. doi: <https://doi.org/10.1186/s13024-018-0258-4>

Chae, J. H., Stein, G. H., & Lee, J. E. (2004). NeuroD: The predicted and the suprising. *Molecules and Cells*, 18(3), 271-288.

Chalard, A., Vaysse, L., Joseph, P., Malaquin, L., Souleille, S., Lonetti, B., Sol, J. C., Loubinoux, I., & Fitremann, J. (2018). Simple Synthetic Molecular Hydrogels from Self-Assembling Alkylgalactonamides as Scaffold for 3D Neuronal Cell Growth. *ACS Applied Materials and Interfaces*, 10(20), 17004–17017. doi: <https://doi.org/10.1021/acsami.8b01365>

Corbo, J. C., Deuel, T. A., Long, J. M., LaPorte, P., Tsai, E., Wynshaw-Boris, A., & Walsh, C. A. (2002). Doublecortin is required in mice for lamination of the hippocampus but not the neocortex. *Journal of Neuroscience*, 22(17), 7548–7557. doi: <https://doi.org/10.1523/jneurosci.22-17-07548.2002>

D, C., C, M., & M, B. (1991). EGF enhances the survival of dopamine neurons in rat embryonic mesencephalon primary cell culture. *Journal of Neuroscience Research*, 30(2), 372–381. doi: <https://doi.org/10.1002/JNR.490300213>

Franze, K., Gerdemann, J., Weick, M., Betz, T., Pawlizak, S., Lakadamyali, M., Bayer, J., Rillich, K., Gögler, M., Lu, Y. B., Reichenbach, A., Janmey, P., & Käs, J. (2009). Neurite branch retraction is caused by a threshold-dependent mechanical impact. *Biophysical Journal*, 97(7), 1883–1890. doi: <https://doi.org/10.1016/j.bpj.2009.07.033>

Garcez, R. C., Teixeira, B. L., dos Santos Schmitt, S., Alvarez-Silva, M., & Trentin, A. G. (2009). Epidermal Growth Factor (EGF) Promotes the In Vitro Differentiation of Neural Crest Cells to Neurons and Melanocytes. *Cellular and Molecular Neurobiology* 29:8, 29(8), 1087–1091. doi: <https://doi.org/10.1007/S10571-009-9406-2>

George, J., Hsu, C. C., Nguyen, L. T. B., Ye, H., & Cui, Z. (2020). Neural tissue engineering with structured hydrogels in CNS models and therapies. *Biotechnology Advances*, 42. doi: <https://doi.org/10.1016/j.biotechadv.2019.03.009>

Grasman, J. M., Ferreira, J. A., & Kaplan, D. L. (2018). Tissue Models for Neurogenesis and Repair in 3D. *Advanced Functional Materials*, 28(48), 1–10. doi: <https://doi.org/10.1002/adfm.201803822>

Han, H. W., Hou, Y. Te, & Hsu, S. hui. (2019). Angiogenic potential of co-spheroids of neural stem cells and endothelial cells in injectable gelatin-based hydrogel. *Materials Science and Engineering C*, 99, 140–149. doi: <https://doi.org/10.1016/j.msec.2019.01.089>

Kaneko, A., Matsushita, A., & Sankai, Y. (2015). A 3D nanofibrous hydrogel and collagen sponge scaffold promotes locomotor functional recovery, spinal repair, and neuronal regeneration after complete transection of the spinal cord in adult rats. *Biomedical Materials (Bristol)*, 10(1), 15008. doi: <https://doi.org/10.1088/1748-6041/10/1/015008>

Kim, Y. H., Choi, S. H., D'Avanzo, C., Hebisch, M., Sliwinski, C., Bylkbashi, E., Washicosky, K. J., Klee, J. B., Brüstle, O., Tanzi, R. E., & Kim, D. Y. (2015). A 3D human neural cell culture system for modeling Alzheimer's disease. *Nature Protocols*, 10(7), 985-1006. doi: <https://doi.org/10.1038/nprot.2015.065>

Koser, D. E., Thompson, A. J., Foster, S. K., Dwivedy, A., Pillai, E. K., Sheridan, G. K., Svoboda, H., Viana, M., Costa, L. D. F., Guck, J., Holt, C. E., & Franze, K. (2016). Mechanosensing is critical for axon growth in the developing brain. *Nature Neuroscience*, 19(12), 1592-1598. doi: <https://doi.org/10.1038/nn.4394>

Lee, J.-K., Cho, J.-H., Hwang, W.-S., Lee, Y.-D., Reu, D.-S., & Suh-Kim, H. (2000). Expression of neuroD/BETA2 in mitotic and postmitotic neuronal cells during the development of nervous system. *Developmental Dynamics*, 217(4), 361-367. doi: [https://doi.org/10.1002/\(SICI\)1097-0177\(200004\)217:4<361::AID-DVDY3>3.0.CO;2-8](https://doi.org/10.1002/(SICI)1097-0177(200004)217:4<361::AID-DVDY3>3.0.CO;2-8)

Miyata, T., Maeda, T., development, J. L.-G. & 1999, undefined. (n.d.). NeuroD is required for differentiation of the granule cells in the cerebellum and hippocampus. *Genesdev.Cshlp.Org*.

*Molecular cloning of a human neuroD from a neuroblastoma cell line specifically expressed in the fetal brain and adult cerebellum.* - PubMed - NCBI. (n.d.).

Moreno-Jiménez, E. P., Flor-García, M., Terreros-Roncal, J., Rábano, A., Cafini, F., Pallas-Bazarra, N., Ávila, J., & Llorens-Martín, M. (2019). Adult hippocampal neurogenesis is abundant in neurologically healthy subjects and drops sharply in patients with Alzheimer's disease. *Nature Medicine*, 25(4), 554-560. doi: <https://doi.org/10.1038/s41591-019-0375-9>

Palm, T., Bolognin, S., Meiser, J., Nickels, S., Träger, C., Meilenbrock, R. L., Brockhaus, J., Schreitmüller, M., Missler, M., & Schwamborn, J. C. (2015). Rapid and robust generation of long-term self-renewing human neural stem cells with the ability to generate mature astroglia. *Scientific Reports*, 5(November), 1-16. doi: <https://doi.org/10.1038/srep16321>

Scalabrino, G. (2020). Epidermal Growth Factor in the CNS: A Beguiling Journey from Integrated Cell Biology to Multiple Sclerosis. An Extensive Translational Overview. *Cellular and Molecular Neurobiology*, 0123456789. doi: <https://doi.org/10.1007/s10571-020-00989-x>

Schwab, M., Bartholomae, A., B. & H.-J.(2000). Neuronal basic helix-loop-helix proteins (NEX and BETA2/Neuro D) regulate terminal granule cell differentiation in the hippocampus. *Soc Neuroscience*.

Shou, Y., Liang, F., Xu, S., & Li, X. (2020). The Application of Brain Organoids: From Neuronal Development to Neurological Diseases. *Frontiers in Cell and Developmental Biology*, 8(October), 1-10. doi: <https://doi.org/10.3389/fcell.2020.579659>

Zychowicz, M., Pietrucha, K., Podobinska, M., Kowalska-Wlodarczyk, M., Lenart, J., Augustyniak, J., & Buzanska, L. (2019). The collagen scaffold supports hiPSC-derived NSC growth and restricts hiPSC. *Frontiers in Bioscience - Scholar*, 11(1), 105-121. doi: <https://doi.org/10.2741/S529>





# MEDICAL SIGNIFICANCE OF CAMEL URINE: A REVIEW

*Wasiu Ayodele Abibu<sup>1</sup>, Sherifdeen Bamidele Onigbinde<sup>2</sup>  
Dahiru Salihu Abubakar<sup>3</sup>, Abdullahi Tunde Aborode<sup>4</sup>*

---

## Abstract

The quest for an alternative form of medicine aside from the orthodox one is ever increasing. Herbal medicine and others with history dated to more than a decade century are now being reintegrated into modern medicine. For more than 14 centuries, the Arabian Peninsula have used mammary secretions and urine of camels in the treatment of chronic infections. *Camellus* (Camel) is the most common animal whose milk and urine are used in traditional medicine. In the last decade, various articles and researches have documented its potential as an antimicrobial, anti-inflammatory, anticancer and antioxidant property, which can be used against animal and human pathogens. The major challenges

---

1 PhD Student, Dokuz Eylul University, The Graduate School of Natural and Applied Sciences, Biotechnology, ORCID: 0000-0002-1156-3779 (Corresponding Author)

2 Texas Tech University Department of Chemistry and Biochemistry

3 Federal University Kashere Department of Chemical Sciences

4 Research and Development Healthy Africans Platform

in camel urine research are low public awareness, accessibility, availability, religious beliefs and non-authorization by health regulatory agencies. However, Chemical synthesis, clinical trials and elucidation via advanced research of bioactive elements of camel urine are potential possibilities where camel urine researches can be channelled.

**Keywords:** Camel, Urine, Milk, Pathogens.

## 1. Introduction

Camel is a one-of-a-kind animal that lives and reproduces in harsh climatic environments, which are unsuitable for most domestic animals. The camel remains an important source of food and transportation for desert dwellers in Asia and Africa. Camel milk and urine have long been used to cure a host of diseases due to their healing properties. Camel urine and milk contain bioactive compounds with anti-inflammatory, antimicrobial, anticancer, and antioxidant properties, which can be used to treat a variety of diseases. Camel urine and milk may have acquired healing properties as a result of the camel's intake of active-substance-rich desert shrubs. Camel milk has antiviral and antibacterial effects, making it helpful in killing bacteria and protecting the body against a variety of diseases, including curing cancer in some cases (Gabry & Wadi, 2003). Furthermore, camel urine has anticancer effects, which are due to the inclusion of nanomaterials in urine, which can effectively attack cancer cells while preserving healthy cells in a cancer patient (Wadi, 2012).

Many chemical constituents contained in camel urine have been shown to have biological activities, including antibacterial, antifungal, antiviral, and anticancer properties (Alhaider et al., 2011; Al-Yussef et al., 2012; Romli et al., 2017). The medicinal efficacy of camel urine has been studied in Asian countries, for example, in the treatment of diabetic neuropathy (Agarwal et al., 2009). Profiling of urinary acids and metabolites by NMR and GCMS is becoming increasingly important in clinical studies (Ahamad et al., 2017). While there aren't enough scientific trials, camel milk and urine have long been thought to be a high-quality alternative treatment for a variety of ailments particularly chronic imbalance of the liver (Soliman et al., 2016; Zuberu et al., 2017). Al-Harbi et al. (1996) conducted several *in vivo* experiments on albino mice to determine whether using camel urine and milk to treat liver and stomach had any side effects (Al-Harbi et al., 1996). The results have shown that the biological activity of either camel milk or urine, or its combination mixtures, is a healthy alternative medicine.

Numerous studies have recently been conducted on these alleged therapeutic effects, and there is now a growing body of scientific evidence describing the components of camel products, as well as their

medicinal constituents. These findings provide empirical evidence to back up the current trend of using camel milk and urine for medicinal purposes. Some factors, however, can limit the use of raw camel urine and milk. This review will explore the plausibility of using Camel urine and milk as a therapeutic intervention, as well as challenges and potential possibilities.

## 2. Microbiological Importance of Camel Urine

**Antimicrobial effect:** The adverse effect of pathogens on human and animal health cannot be over-emphasized. The majority of human and animal infections are attributed to pathogens of bacterial, fungal and viral origin (Leeds et al., 2006). Antimicrobial agents involved in the control of pathogens had been classified into natural and synthetic antimicrobial. Natural and synthetic antimicrobial drugs can be obtained from plants, animals and microorganisms. Ye et al (2020) classified natural antibacterial drugs into; daptomycin, fidaxomicin, tigecycline, natural antifungal drugs into; caspofungin acetate and micafungin sodium as approved by the Food and Drug Administration (FDA) (Leeds et al., 2006). Van Vuuren et al (2017) on the other hand classified natural antimicrobials into medicinal plants, essential oils and compounds (Van Vuuren et al., 2017). Common examples are found in marine products (such as peptides, alkaloids, polypeptides and many more), camel milk and camel urine. In the last two (2) decades, the efficacy of some natural and synthetic antimicrobial agents became questionable due to increasing reports of antimicrobial resistance by pathogens. However, no literature or scientific research exists to date on the antimicrobial resistance of camel urine and camel milk by pathogens. Shinashal (2015) reported the efficacy of camel urine against pathogenic bacteria when compared with established antibiotics against pathogens (Shinashal, 2015). Camel urine exhibits a complete bactericidal effect on clinical bacterial pathogens with the disappearance of signs and symptoms within a limited time than that achievable with standard antibiotics of such pathogens. In the antibacterial efficacy of camel urine study as reported by Sumia (2016) and co-authors, the disc diffusion test and agar well diffusion tests were the anti-microbial susceptibility tests commonly employed to study

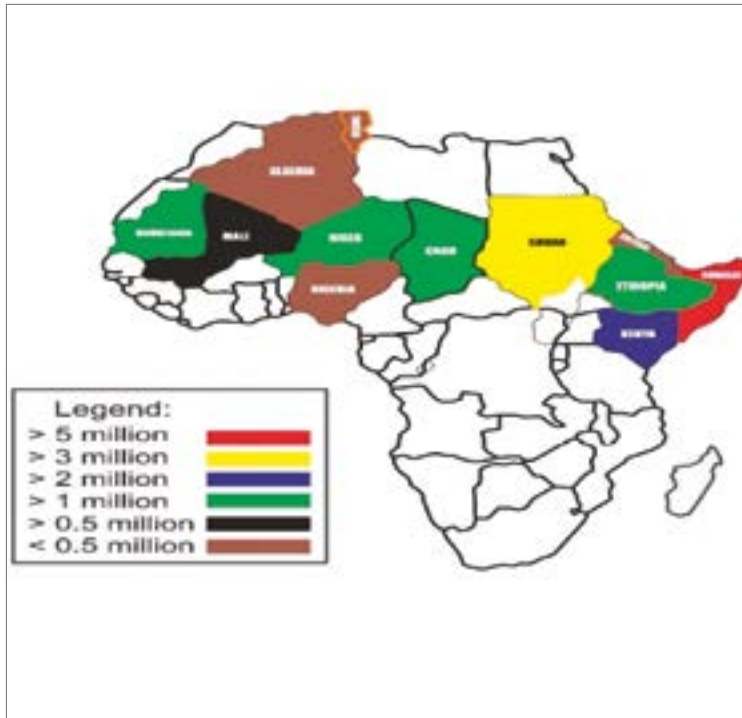
the effects of camel urine against pathogens. Sumia (2016) and co-authors thought that concentrated camel urine is best in treating pathogens (Sumia et al., 2016). In addition, Kabbashi and Omer (2016) proved the anti-fungal activity of camel urine against dermatomycosis causing fungal genera like *Trichophyton*, *Microsporum* and *Epidermophyton*. From the results, camel urine proved its worth as an antifungal and anti-dermatophytes agent by inhibiting the growth of the fungal genera tested (Kabbashi & Omer, 2016).

Numerous reports exist on the antimicrobial and anticancer potential of camel urine. Khalifa (2005) and co-authors are of the view that the mode of action of camel urine on microbial and cancer cells were the same with no histopathological effects in the experimental studies conducted (Khalifa et al., 2005). Furthermore, Shoeib and Ba-hathea (2008) are of the view that "camel urine acts by antagonizing microbial cells and plasmids, thus defeating killer cells via rapid growth disruption in microorganisms and eventual cell death (Shoeib & Ba-Hathea, 2008). On the contrary, Mostafa and Dwedar (2016) credited the camel's antimicrobial to the high salt and alkaline presence amongst its constituents in addition to the natural bioactive compounds it possessed (Mostafa & Dwedar, 2016).

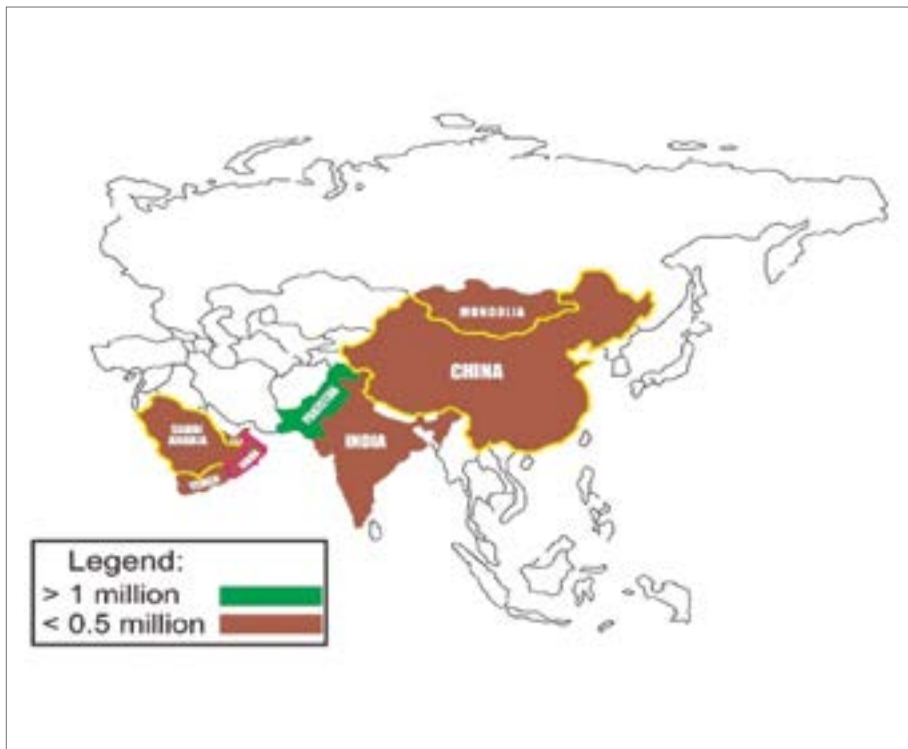
***Antagonistic effect on plant pathogens:*** The devastating effects of pathogens on plants and crops led to the introduction of biotechnologically improved seedlings in agriculture. However, research is still ongoing on finding ways to ameliorate the harmful effects of pathogens in plants. Current techniques in combating plant pathogens can be classified into "inducible and constitutive or chemical, structural and morphological" as described by Zaynab et al (2019) (Zaynab et al., 2019). Besides, primary metabolites (such as carbohydrates, proteins, lipids, enzymes, hormones) and secondary metabolites (alkaloids, flavonoids and phenolics) confer immunity against plant pathogens (Zaynab et al., 2018; Zaynab et al., 2019). Similarly, The urine of ruminant animal had been reported to possess antimicrobial effects (Anami et al., 2012). However, no literature exists on the efficacy of animal urine against plant pathogens except the study of Nafie (2004). Nafie (2014) proved the potential of camel urine as an antagonist to plant pathogens. From the study, foliar application of

camel urine on tomato seedlings acted as a primary defence mechanism employed by tomato plants against the notorious tomato pathogen *Fusarium oxysporum*. This study is an eye-opener to botanists regarding natural ways of combating plant pathogens which often require huge expenditure to combat (Nafie, 2014). It is worthy of note that camels are the most enduring beast of burden and the only animal capable of adapting to changing weather and climatic conditions as reported by Hoffman (2010). However, camel and camel products research is still challenged despite their numerous benefits. Only few countries are known to have Camel research institutes (Abri & Faye, 2019). Camels' products of high value with global demand include its meat, milk, wool, and its natural value as an ultimate beast of burden (Kadim et al., 2013).

**Tables 1.** shows a Comparison of the Antimicrobial effectiveness of Camel Urine with known antimicrobial agents. In addition, Figures 1 and 2 are maps showing Camel population in Africa and Asia respectively.



**Figure 1:** Camel population in Africa (Ali et al., 2019).



**Figure 2:** Camel population in Asia (Ali et al., 2019).



**Table 1.** Comparison of Antimicrobial effectiveness of Camel Urine with known antimicrobial agents

Isolate types	Antimicrobial used as control	Pathogen tested against	Camel urine dosage (ml/kg)	Antibiotics dosage (ml/kg)	Duration of antimicrobial effect in camel urine (hrs)	Duration of anti-microbial effect of antibiotics used as control (hrs)	References
Clinical pathogens	Gentamicin and Diclloxacin	<i>E. coli</i> , <i>Staphylococcus aureus</i>	3 ml/kg	1 ml/kg	48	72	Shinashal (2015) [14]
		<i>Salmonella</i> SP, <i>Pseudomonas aeruginosa</i>	1 ml/kg		24-48		Sumia <i>et al</i> (2016) [15]
		<i>E. cloacae</i>					
		<i>Escherichia coli</i>					
		<i>Staphylococcus</i> , Group A & B haemolytic streptococci, Enterics, <i>Candida albicans</i> and <i>Aspergillus niger</i>	25-100%		72		Al Bashan (2011) [28]
	Erythromycin, Clindamycin, Cephalosporine, Aminoglycoside, Tetracycline and Chloramphenicol	<i>Staphylococcus aureus</i> MRSA and Lactic acid bacteria <i>E.coli</i>	4-20%		72		Al-Zahrani and Al-Harbi (2011) [29]

					S. aureus, E. coli; <i>Proteus mirabilis</i> , <i>Klebsiella pneumoniae</i>	25-100%	48	Nazar Abdalazeem Osman, et al. (2013) [30]
Multidrug-Resistant Clinical Bacterial and Fungal Isolates					Methicillin-resistant <i>Staphylococcus aureus</i> (MRSA) coagulase-negative staphylococci (CoNS) ESBL-producing Gram-negative bacilli carbapenemase-producing Gram-negative bacilli, multi-drug resistant <i>Enterococcus</i> spp. <i>Candida albicans</i>	2.5- 10 %		Marwa and Reham (2016) [31]

Fungal isolates		<i>Rhizoctonia solani</i> , <i>Fusarium moliniform</i> , <i>Pythium aphanidermatum</i> , <i>Aschocayta sp.</i> , <i>Sclerotinia sclerotiorum</i> , <i>Aspergillus flavus</i> and <i>A. niger</i>	25-50%		48	Al-Abdalall (2010) [32]
Dermatocosis causing fungal	Ketoconazole and Flucanazole	<i>Trichophyton</i> , <i>Microsporium</i> and <i>Epidermophyton</i>	200ml/kg	0.062- 2mg /ml (fluconazole) 0.007-0.25 mg/ ml (ketoconazole)	168	Noor and Alenini (2017) [33]
Gut pathogens		Lactobacilli, Bifidobacterium, Streptococci and Coliforms	1.8ml/200g		336	

### 3. Chemical Composition of Camel Urine/Milk and Possible Active Agents

The chemical composition of camel urine has been reported by Read (1925) to contain organic nitrogen, ammonia, urea, creatinine, creatine, hippuric acid and chloride (Read, 1925). Recently, more details about camel urine composition using liquid chromatography-mass spectrometry have been reported by Antakly (2012) (Antakly, 2012). This information showed many metabolites in camel urine. Benzoic acid (BEN), urea, creatinine, phenylacetate, citric acid and hippuric acid have been reported as the major constituents in camel urine. The concentration of these materials was matched with the amounts found in different camels, elephant and rat urine. The amount of benzoate salt was greatest in camel urine. To date, the fully characterized chemical composition of camel urine, not yet reported.

In a neutron activation analysis carried out by Al-Attas (2009), it was discovered that the milk and urine of camels have large amounts of Na and K, which can help reverse the electrolyte imbalance in patients with diarrhoea (Al-Attas, 2009). A large amount of Zn was also identified in the sample; Zinc acts as a cure for diarrhoeal infections. A recent study by Al-Yousef et al., (2012) stated that camel urine contains very slight traces of urea and ammonia, and these molecules are known to be responsible for the bad smell and toxicity of urine. Also, it has mentioned that camel urine contains approximately 10 folds more mineral salts than human urine.

Camel urine is rich in many organic and inorganic compounds. Palm Mid Fraction (PMF) and PM701 of camel urine possess different nanoparticles, crystals and nano-rods with varying shapes and sizes. PMF crystals contain various compounds such as calcium oxalate, cystine, tyrosine, uric acid crystals, ammonium urate, calcium phosphate, hippuric and benzoic acids as reported by Ahmed et al., (2015a) and Ahmed et al., (2015b). El-Shahawy et al., (2010) detected the presence of glycine, alanine, and arginine in PMF. It also contains several ions, but Cs, Rb, K, Ca, Cd, Y, Eu, Th and Zn are present in relatively high concentration. Zinc is present in the form of ZnO and Ca, Cd & Y are in the form of sulfates.

#### **4. Pharmacological and Physiological Basis of the Camel Urine Therapy**

Alhaidar et al., (2011) stated that camel urine is used for therapeutic purposes most widely in Asia and Africa since these locations are the largest camel habitats. The religious aspect of using camel urine stems from the fact that there has been convincing evidence that Prophet Mohammed advised its use in the treatment of a wide range of diseases. The traditional therapeutic benefits of camel urine can be collectively considered as the treatment of cancer and certain infectious and cardiovascular abnormalities. Alkhamees and Alsanad (2017) reported that camel urine acquired these therapeutic activities via the camel's consumption of desert plants possessing various active substances. Certain different desert plants have been shown to have strong antibacterial and antifungal activity (Alkhamees & Alsanad, 2017). Alkhamees and Alsanad (2017) stated that camel urine treating disease have been tested in several different trials conducted over the years. According to Muyldermans et al., (2009), many scientists believe that the therapeutic effect of camel urine can be attributed to the gamma globulins and other immune components, such as immunoglobulins, which are found in the urine. The single antigen-binding domains (VHH) of these heavy-chain antibodies, also known as nanobodies, could be used in the diagnosis and treatment of cancer, as well as in the development of biosensors.

According to Abdel Galil and Abdulqader (2016), camel milk and urine have been used as medicines in certain parts of the world since ancient times, but only recently have scientists shown interest in exploring the claimed therapeutic benefits of camel products. Significant evidence, drawn from laboratory and limited clinical studies, has shown that camel milk on its own and occasionally mixed with camel urine is effective in the management of diverse clinical conditions such as diabetes mellitus, cancer, food allergy, autism, viral hepatitis and a host of other viral, bacterial and parasitic infections. In addition, several potential benefits of camel milk and urine on the cardiovascular system, particularly their antiplatelet and fibrinolytic actions, have been demonstrated.

Abdel Galil and Abdulqader (2016) stated that recent studies from the laboratory have shown that camel milk and urine possess potent cardiovascular actions. In separate in vitro experiments, it was shown that camel

urine has potent platelet blocking properties similar to the actions of the widely used anti-platelet drugs, aspirin and clopidogrel. An earlier study has shown that lactoferrin isolated from sheep and human lactoferrin inhibits thrombin-induced aggregation; however, we could not confirm this observation using human lactoferrin. Our ongoing efforts are approaching the identification of the probable dual-platelet inhibitor in camel urine.

Yagil and Berlyne (1976) stated that the pH of fresh camel urine range from 8.2 to 9.2. This basic pH might be due to a high concentration of potassium salts. Amazingly, it was very difficult to filter the fresh camel urine through 0.22 or 0.45 $\mu$  nylon filters. In addition, camel urine was found not miscible with acetonitrile, even after shaking or sonication. The liquid-liquid extraction gave low and fluctuated percentage recoveries of targeted materials. The glucuronides metabolites were enzymatically hydrolyzed before the extraction. Antakly (2012) reported that the major polar compounds were identified by liquid chromatography-mass spectrometry (LC-MS) and GC-MS.

Al-Abdalall (2010) stated that camel urine has been proved to have a potent antiplatelet activity against adenosine diphosphate induced and arachidonic acid-induced platelet aggregation; neither human nor bovine urine exhibited such properties as ascertained by Alhaidar et al., (2011) (Al-Abdalall, 2010; Alhaidar et al., 2011).

Camel urine is a rich source of natural by-products with no harmful health effect on human. Compounds, such as ammonia and urea are known to offer a bad smell and toxicity of urine in human and all other animals are lacking or minimal in camel urine. Other distinguishing features of camel urine include; about ten folds more mineral salts than human urine as explained by Alebie et al., (2017).

The action of urine on the morphological properties of some human pathogenic bacteria was evaluated through electron microscopic studies by Shoeib and Ba-hatheq (2008). Their results showed that the chemical and organic constituents of urine have repression characteristics against the development of bacteria and fungi. In 2007, Shoeib and Ba-hatheq observed that there were no effects on deadly *E. coli* and *P. aeruginosa* bacterial cells when treated with fresh urine using two steps (Shoeib & Ba-hatheq, 2008).

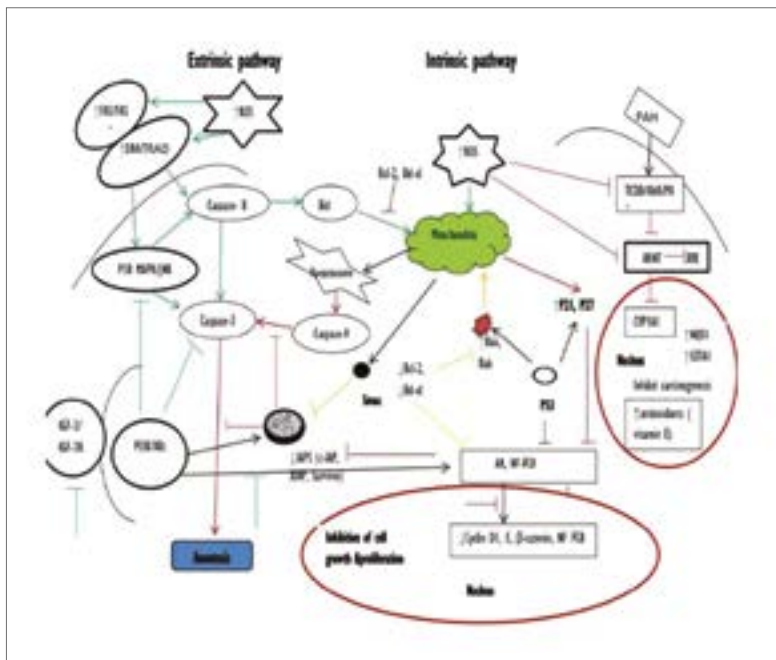
Camel urine has been found to have in vitro antibacterial effects concerning clinically important multidrug-resistant bacteria, as well as strong antifungal effects against *C. albicans* and *non-albicans Candida* according to recent research by Mostafa and Dwedar (2016).

Camel urine, despite being a waste product, is mostly used as a source for many therapeutic agents. Drinking camel urine is shown to be effective in treating numerous cancers in human as reported by Alhaidar et al., (2011).

A study conducted by Alebie et al., (2017) has shown that camel products could exert cytotoxic activity against cancer cells through different mechanisms while inhibition of carcinogen-activating genes signalling pathways is well understood in this regards.

Camel's milk and urine are recognized to significantly inhibit the induction of a cancer-activating gene (Cyp1a1) and to induce cancer protecting genes (Nqo1 and Gsta1) in several lines of cancer cells at the mRNA, protein and activity levels. These products mediate CYP1A1 inhibition at the experimental transcriptional level through AhR-dependent transcriptional control as shown in Figure 3 below.

**Source:** Alebie et al., (2017).



**Figure 3:** Anticancer effect of camel's milk and urine

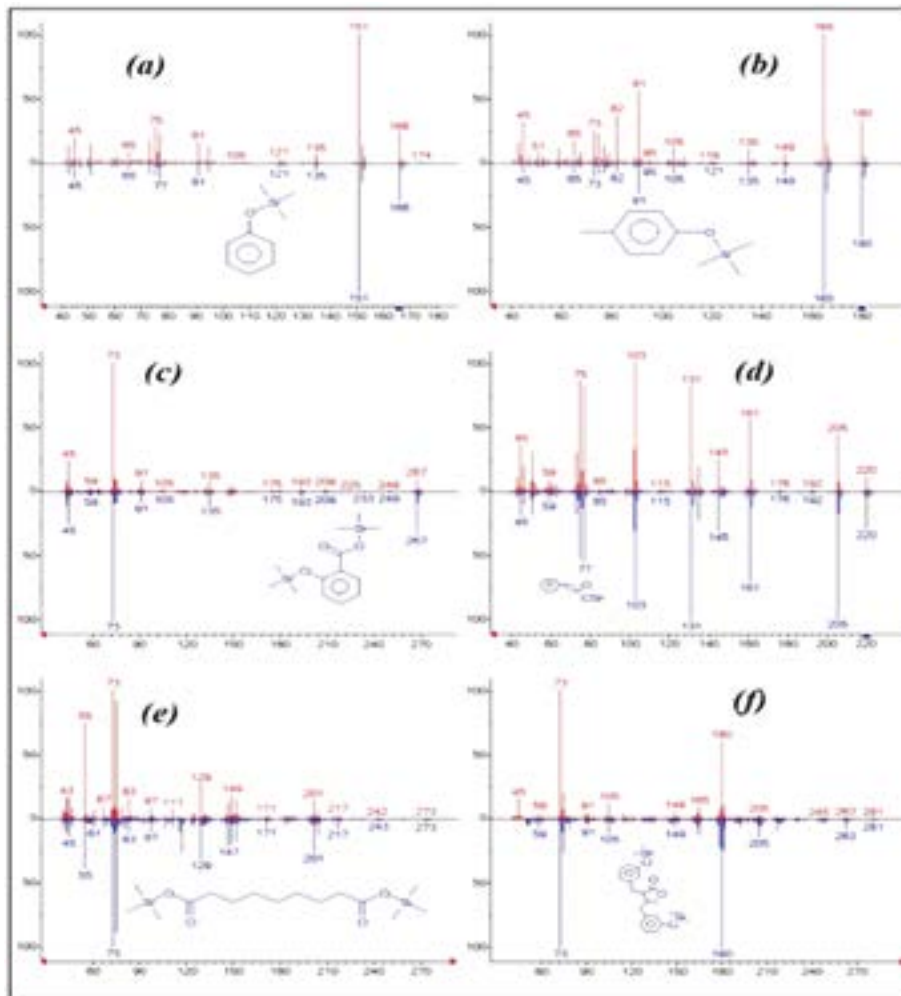
Anticancer effect of camel's milk and urine (CM & CU). CM & CU induce apoptosis in various cancer cells through the extrinsic pathway by enhancing DR4 expression and ROS production, causing activation of JNK and caspases and intrinsic pathways mainly by enhancing ROS production that leads to activation of caspases. Inhibit carcinogenesis by down-regulating the induction of Cyp1a1, cancer activating gene, and inducing Nqo1 and Gsta1, cancer-protecting genes. Inhibit cell cycle progression, proliferation and survival of cancer cells by interfering with the binding of insulin-like growth factor receptor, a known regulator of the phosphatidylinositol 3-kinase pathway as well as activation of caspases, causing an increase in cyclin-dependent kinase (CDK) inhibitor p21 and p27 protein levels. Activation by CM (green), CU (yellow), CM & CU (red); inhibition by CM (green), CU (yellow), CM & CU (red); ↑ increase, ↓ decrease.

Langmead and Rampton (2001) found that the information relating to the possible effects of alternative and complementary medicine is historical. Although there are very few controlled trials proving the beneficial effects of such practice in any disease, over 30% of the Western population now use some form of complementary and alternative medicine. The single most commonly used modality in most Western surveys is herbal therapy.

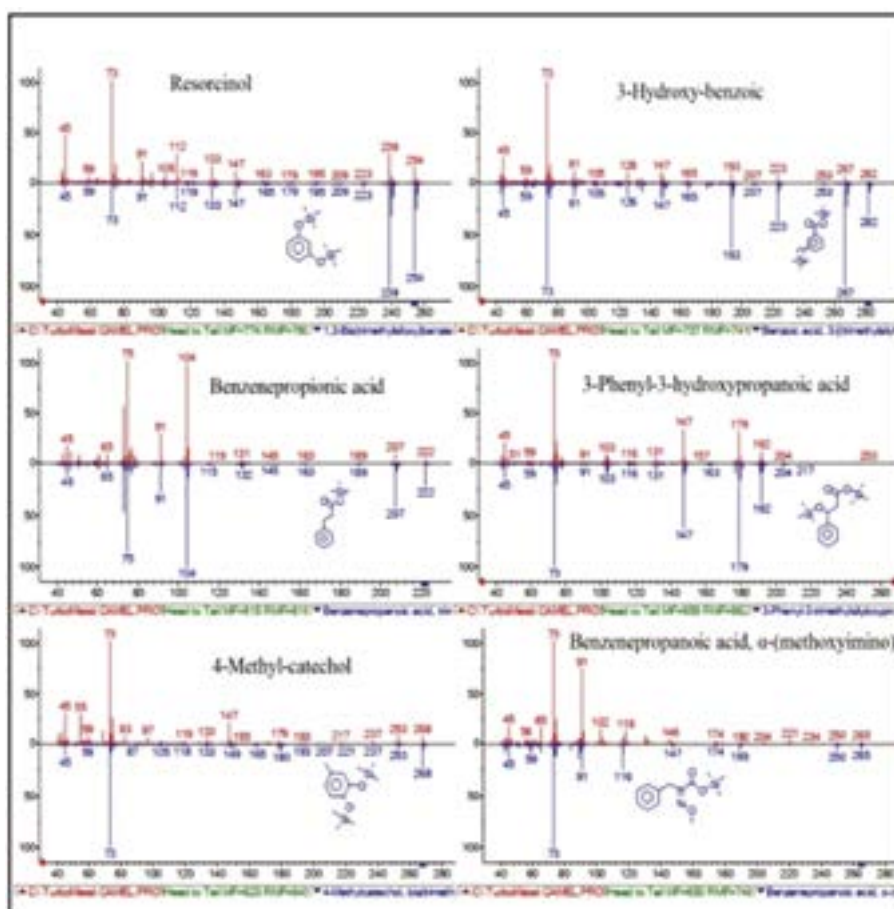
Accordingly, numerous camel urine compounds have been also used for such applications. Notably, multifunctional zinc oxide (ZnO) is used in various forms such as NPs or nanorods for biomedical applications including biosensing, imaging, drug delivery, and clinical implants (De Berardis et al., 2010, Huang et al., 2010 and Hanley et al., 2008). The additive or synergistic effects of ZnO NPs with anti-cancer compounds (or drugs) was found to upregulate induction of apoptosis in cancer cells (Yuan et al., 2014). Hippuric acid nanocomposite (HAN) (a preparation from hippuric acid (HA) and ZnO) combination with doxorubicin and/or with oxaliplatin induce suppression of cell proliferation and exhibit supreme cytotoxicity in several cancer cell lines as compared to individual effects. Importantly, the nanocomposite entails the drugs reaching the tumour cell membrane without early decomposition and the intercalation reaction enhances the permeability of the



drug into the target cell without any noticeable side effects (Hussein et al., 2013 and Choy et al., 2004). Figures 4 and 5 show EI-MS spectra of characterized compounds found in the extract of enzymatically hydrolyzed Camel urine and: EI-MS spectra of minor acidic and phenolic compounds found in the extract of enzymatically hydrolyzed Camel urine respectively.



**Figure 4:** EI-MS spectra of characterized compounds found in the extract of enzymatically hydrolyzed Camel urine including; phenol (a), p-cresol (b), salicylic acid (c), cinnamic acid (d), azelaic acid (e) and enterolactone (f) (Adapted from Khorshid and Faten, 2016).



**Figure 5:** EI-MS spectra of minor acidic and phenolic compounds found in the extract of enzymatically hydrolyzed Camel urine (Adapted from Khedr & Khorshid, 2016).

## 5. The Possible Therapeutic Candidates in Camel Milk

Camel milk is rich in vitamin C and protective proteins such as lactoferrin, lactoperoxidase, immunoglobulins and lysozyme. Camel milk lacks  $\beta$ -lactoglobulin and used as an option for individuals intolerant to lactose in cow's milk. Therefore, camel milk is extraordinary in terms of antioxidative agents, antibacterial, antiviral, antifungal, anti-hepatitis, anti-arthritis, treatment for paratuberculosis, preventing ageing, remedy for autoimmune diseases and cosmetics.

**Lactoferrin:** Lactoferrin-rich camel milk has potent antimicrobial and anti-inflammatory properties, including bacterial inhibition, antiviral effects, antifungal effects, immune supportive and immunomodulatory functions, lymphocyte (antioxidant and anti-inflammatory) maturation and function, and anti-cancer actions (Kanwar et al., 2015). To the best of our knowledge, the structure of camel lactoferrin has not been fully elucidated and deposited on any database.

**Globulins:** Gamma globulins and other immune components, including immunoglobulins, present in the two products could also be related to the medicinal properties of both camel milk and urine. (Alhaider et al., 2013). Half of camel blood's circulating antibodies comprise only two heavy chains and no light chains. (Hamers-Casterman et al., 1993). These antibodies can quickly pass into the milk of the lactating camel because of their decreased size, one-tenth the size of human antibodies can pass the blood-brain barrier can be diluted in urine, and are readily absorbed from the gut into the general circulation of camel milk and/or urine consumers. Moreover, in cancer diagnosis and therapy and biosensor development, the single antigen-binding domains of these heavy-chain antibodies, also known as nanobodies, may have applications (Muyldermans et al., 2009).

## 6. Anti-Diabetic Action of Camel Milk

Diabetes mellitus (DM) is characterized by abnormally high blood glucose levels, resulting from low insulin secretion and/or increased insulin resistance (Ferrannini, 1998). Because of their strong association with the risk of cerebrovascular and cardiovascular disorders, which have been recorded in 68 per cent of diabetes-related deaths among patients aged 65 years or older, DM and its complications have become a key subject of concern for researchers worldwide (Eriksson et al., 2012). Currently, the management of DM remains a great challenge for physicians to contend with. In addition to the traditional diet, insulin, oral hypoglycemic medications, and exercise diabetes treatment methods, diabetes has also gained attention because of the current broad interest in alternative treatments for chronic incurable diseases. There is growing evidence in this regard that the intake of camel milk (CM) is effective in regulating DM in both humans (Agrawal et al., 2011) and laboratory animals (Sboui et al., 2010). Overwhelming

support for this idea comes from camel breeders in India who regularly consume CM and have zero occurrences of DM compared to 5.5% in other societies where CM is not consumed (Agrawal et al., 2007). Additional support comes from the more recent finding that Type I diabetic patients' intake of CM resulted in an (Alhaider et al., 2014) per cent reduction in daily insulin requirements, with substantial reductions in both blood glucose and micro-albuminuria levels (Agrawal et al., 2011). The peculiar composition of CM, which is rich in insulin, insulin-like proteins (Malik et al., 2012), minerals, immunoglobulins (Alhaider et al., 2013) and trace elements with anti-inflammatory properties, can be attributed to these advantages in part. Moreover, CM includes antioxidants and free radical scavengers (Korish et al., 2015). In addition, camel insulin has distinctive features that differentiate it from human and other animal insulin and, when administered orally, make it more effective. Unlike insulin found in other animal and human kinds of milk, camel insulin is stored within micelles and is thus protected in the upper gastrointestinal tract from digestion and proteolysis; camel insulin has also been suggested to be enveloped in nanoparticles that facilitate its absorption and easy passage to the bloodstream (Malik et al., 2012). It is also possible that CM's antioxidant activity prevents metabolic syndrome symptoms, including hyperglycaemia, hyperlipidaemia, and insulin resistance. In essence, this will prevent the pathophysiological mechanisms that underlie DM's microvascular complications, including retinopathy, nephropathy, or cardiovascular complications that increase the disease's mortality and morbidity (Agrawal et al., 2011). The above results give strong support to the beneficial role of CM in DM management as a dietary supplement and therapeutic adjuvant.

## **7. Challenges in the Use of Camel Urine as Alternative Medicine**

Undoubtedly, the medical benefits embedded in the use of camel urine cannot be overemphasized despite its low level of awareness in many parts of the world and the lack of authorization for its usage by governmental and non-governmental health regulatory authorities both locally and internationally. Challenges in camel urine research are numerous. To be recognized as a potent medical concern, a long list of medical, psychological and religious hurdles need to be crossed. The authors of this review came up

with the following as challenges militating the recognition and acceptance of camel urine by health authorities.

**i. Safety and Clinical Trials:** The authorization of a drug translates into a successful clinical trial. The authors of this review had explained the numerous medicinal benefits of camel urine. It is worthy of note that all researches mentioned were an independent study conducted by researchers in academia. Unfortunately, the detection of MERS (Middle East Respiratory Syndrome) in camels in the Middle East shifted global attention towards the adverse effect of camel urine and milk. According to WHO, MERS that threatens humans can also be found in camels, hence, urging people to stay away from camel milk and urine (WHO, 2015). This truncated the work of intending researchers on the medicinal potential of camel urine coupled with embargo placed by nations on camel products to arrest any possibility of an epidemic from a zoonotic route.

The efficacy of camel urine has been reported by patients worldwide who believed in its medicinal benefits. The patients took camel urine without prescription by a certified medical practitioner and attested to its miraculous healing ability. The issue of safety and side effects are unknown since clinical trials are majorly concerned with efficacy, safety and presence or absence of side effects. Furthermore, there is no medical dosage approved for camel urine. This challenge will pose a danger to the physiological role of the camel urine when consumed. There is a need for an acceptable dosage to validate its efficacy.

**ii. Availability:** Camel population are found in a certain region of the world (most especially desert areas) unlike other domesticated animals. From the statistics in Fig. 1 and 2 above, it is clear that camels are very much available in two continents of the world, unlike others. This acts as an impediment towards the all-year-round availability in non-camel populated areas of the world. Camel urine is frequently transported into neighbouring countries making it available to consumers. However, the effects of changing weather condition from a desert to a non-desert area on the physical and chemical potency of camel urine are unknown. No researches have been conducted on this issue to date. In addition, more studies need to be conducted on the effect of changing weather on the preservation of camel urine.

**iii. Hypersensitivity:** The consumption of raw camel urine is a herculean task considering the warm piss taste and disgusting smell. It is even worse when mixed with raw camel milk as it is the traditional practice. There is difficulty in getting rid of the musk after taste that overtakes the mouth of the consumer. This is a mitigating factor that prevents many people from consuming camel urine.

Camel urine is characterized by a choky smell and a burning sensation when taken for the first time or on an empty stomach. Some individuals with an allergy to choky materials may find it difficult to consume. In the same vein, individuals with digestive allergy may feel irritated due to the burning sensation associated with its consumption.

**iv. Religious Belief:** Camel urine consumption is common amongst Muslims. The Holy Prophet of Islam, Muhammad (Peace be on Him) in his reported sayings emphasized the medical significance of camel urine and ordered its consumption for internal medical related problems. This had been an age-long tradition amongst the Arabs and Non-Arabs inhabitants of the Middle East region of the world with success stories. Presently, a camel research institute exists in the Kingdom of Saudi Arabia. It is worth mentioning that individual religious inclination may affect the public acceptance and certification of its consumption by individuals and health regulatory authorities respectively.

### **Conclusion and Potential Possibilities**

Interestingly, urine therapy has found to a commonplace in traditional medicine. Camel milk as well may similarly serve not only as a source of nutrients but also as a source of biologically active compounds with medicinal potentials. The latest scientific evidence for the therapeutic activity of camel milk and urine continues to unfold and attempts are ongoing to classify the medicinal constituents more accurately. As preventive and curative agents in humans, camel milk and urine warrant further studies. These are required, despite the reported results, to investigate the precise mechanisms of the therapeutic effects of camel milk and urine, as well as the active compounds responsible for a particular therapeutic action. Urokinase, for example, is a thrombolytic agent that can be isolated from (hu-

man) urine. Premarin, a hormone therapy drug, contains estrogens derived from the urine of pregnant mares (Brügger, 2019). Purified camel milk lactoferrin has also been shown to have an important inhibitory effect on HCV (genotype4) entry via direct interaction with viral molecules (Redwan and Tabll, 2007). Similarly, the bioactive elements of camel urine and milk that are responsible for the well-known medicinal effects can be chemically synthesized and tested in clinical trials. Thus, we encourage scientists worldwide to help elucidate the bioactive components of camel milk and urine through advanced research and then develop affordable, safe, and potent drugs against actual diseases from this source that has proven to be a treasure trove for researchers.

#### **Conflict of Interest**

No conflict of interest exists among the authors of this review.

## REFERENCES

- Abdel Galil, M., Abdel, G. & Abdulqader, A. A. (2016). The unique medicinal properties of camel products: A review of the scientific evidence. *Elsevier Article Review*, 2(1), 1-3. Doi: <https://doi.org/10.1016/j.jtumed.2015.12.007>
- Abri, M. A. A. & Faye, B. (2019). Genetic Improvement in Dromedary Camels: Challenges and Opportunities. *Frontiers in Genetics*, 10, 167.
- Agarwal, R. P., Dogra, R., Mohta, N., Tiwari, R., Singharl, S. & Sultania, S. (2009). Beneficial effect of camel milk in diabetic nephropathy. *Acta Biomed*, 80, 131-134.
- Agrawal, R. P., Budania, S., Sharma, P., Gupta, R., Kochar, D. K. *et al.* (2007). Zero prevalence of diabetes in camel milk consuming Raica community of north-west Rajasthan, India. *Diab Res Clin Pract*, 76, 290-296. Doi: [10.1016/j.diabres.2006.09.036](https://doi.org/10.1016/j.diabres.2006.09.036).
- Agrawal, R. P., Jain, S., Shah, S., Chopra, A. & Agarwal, V. (2011). Effect of camel milk on glycemic control and insulin requirement in patients with type 1 diabetes: 2-years randomized controlled trial. *Eur J Clin Nutr*, 65(9), 1048-1052. Doi: [10.1038/ejcn.2011.98](https://doi.org/10.1038/ejcn.2011.98).
- Ahamad, S. R., Alhaider, A. Q., Raish, M. & Shakeel, F. (2017). Metabolomic and elemental analysis of camel and bovine urine by GC-MS and ICP-MS. *Saudi J Biol Sci*, 24, 23-29. doi: [10.1016/j.sjbs.2015.09.001](https://doi.org/10.1016/j.sjbs.2015.09.001)
- Ahmed, G. A. R., Khorshid, F. A., Khedr, A., El-Hamidy, S. M. & Sallah, N. A. (2015). The Mechanism of PMF Nanoparticles in Invading A549 cells, A New Selective Drug Delivery for Cancer Therapy. *New Developments in Biology, Biomedical & Chemical Engineering and Materials Science*.
- Ahmed, G. A. R., Khorshid, F. A., Khedr, A., El-Hamidy, S. M. & Sallah, N. A. (2015). The effect of PMF Camel Urine Nanoparticles on A549 Cells: The Mechanism of Action and Drug Delivery. *Life Sci J*, 12.
- Al Bashan, M. M. (2011). In vitro assessment of antimicrobial activity and biochemical properties of camel urine against some human pathogenic microbes. *Middle East journal of scientific research*, 7(6), 947-958.
- Al-Abdalall, A. H. A. (2010). The inhibitory effect of camel's urine on mycotoxins and fungal growth. *Afr J Agric Res*, 5, 1331-1337. Doi: [10.5897/AJAR09.686](https://doi.org/10.5897/AJAR09.686)
- Al-Attas, A. (2009). Determination of essential elements in milk and urine of camel and *Nigella sativa* seeds. *Arab J Nucl Sci Appl*, 42, 59-67. Doi: [10.21010/ajtcam.v14i6.12](https://doi.org/10.21010/ajtcam.v14i6.12)



Alebie, G., Yohannes, S. & Worku, A. (2017). Therapeutic Applications of Camel's Milk and Urine against Cancer: Current Development Efforts and Future Perspectives. *J Cancer Sci Ther*, 9, 468-478. Doi: 10.4172/1948-5956.1000461

Alhaidar, A., Abdel Gader, A. G. & Mousa, S. A. (2011). The antiplatelet activity of camel urine. *J Altern Complement Med*, 17, 803-808. Doi: 10.1089/acm.2010.0473

Alhaider A. A., El Gendy M. A., Korashy H. M. & El-Kadi, A. O. (2011). Camel urine inhibits the cytochrome P450 1a1 gene expression through an AhR- dependent mechanism in Hep1c1c7 cell line. *J Ethnopharmacol*, 133, 184-190. Doi: <https://doi.org/10.1016/j.jep.2010.09.012>

Alhaider, A. A., Abdel Gader, A. M. & Saraswati, S. (2014). Camel milk inhibits inflammatory angiogenesis in mice, downregulating proangiogenic and proinflammatory cytokines. *APMIS*, 122, 599-607. Doi: 10.1111/apm.12199.

Alhaider, A., Murray, K., Abdelgader, A. M., Kiemele, L., Hansen, K., Shan, B., Ma, B., Hunsucker, S. W. & Duncan, M. W. (2013). Identification of the peptides & proteins in the milk of the one-humped camel (*Camelus dromedarius*) by mass spectrometry. *J Mass Spectros*, 48(7), 779-794. Doi: 10.1002/jms.3213.

Al-Harbi, M. M., Qureshi, S., Ahmed, M. M., Raza, M., Baig, M. Z. & Shah, A. H. (1996). Effect of camel urine on the cytological and biochemical changes induced by cyclophosphamide in mice. *J Ethnopharmacol*, 52, 129-137. Doi: 10.1016/0378-8741(96)01399-2.

Ali, A., Baby, B. & Vijayan, R. (2019). From Desert to Medicine: A Review of Camel Genomics and Therapeutic Products. *Frontiers in Genetics*, 10. Doi:10.3389/fgene.2019.00017

Alkhamees, O. & Alsanad, S. A. (2017). Review of the Therapeutic Characteristics of Camel Urine. *African Journal of Traditional, Complementary and Alternative medicines*, 14(6), 120-126. Doi: 10.21010/ajtcam.v14i6.12

Al-Yousef, N., Gaafar, A., Al-Otaibi, B., Al-Jammaz, I., Al-Hussein, K. A. & Boussekhra, A. (2012). Camel urine components display anti-cancer properties in vitro. *J Ethnopharmacol*, 143, 819-825. Doi: <https://doi.org/10.21010/ajtcam.v14i6.12>

Al-Yussef, N., Gaafar, A., Al-Otaibi, B., Al-Jammaz, I., Al-Hussein, K. & Aboussekhra, A. (2012). Camel urine components display anti-cancer properties in vitro. *J. Ethnopharmacol*, 143, 819-825. Doi: <https://doi.org/10.1016/j.jep.2012.07.042>

Al-Zahrani, S. & Al-Harbi, A. (2011). Antimicrobial Activity of Camel's Urine on Methicillin-Resistant *Staphylococcus Aureus* Isolated from Clinical Specimens.

*King Abdulaziz University Journal Science*, 23, 251-268. Doi: <https://doi.org/10.4197/sci.23-1.16>

Anami, A., Pushpander, K., Ankit, V. & Ranjeet, S. T. (2012). Antimicrobial Activities of Cow Urine against Various Bacterial Strains. *International Journal of Recent Advances in Pharmaceutical Research*, 2(2), 84-87.

Antakly, T. (2012). Bioactive compounds in camel urine and milk. WO Patents, WO2012019295A1.

Brügger, D. (2019). Hormone aus Stutenharn, pharma-kritik, Nr. 5/6/1997.

Choy, J. H., Jung, J. S. & Oh, J. M. (2004). Layered double hydroxide as an efficient drug reservoir for folate derivatives. *Biomaterials*, 25, 3059-3064. Doi: <https://doi.org/10.1016/j.biomaterials.2003.09.083>

De Berardis, B., Civitelli, G., Condello, M., Lista, P., Pozzi, R., et al. (2010). Exposure to ZnO nanoparticles induce oxidative stress and cytotoxicity in human colon carcinoma cells. *Toxicol Appl Pharmacol*, 246, 116-127. Doi: <https://doi.org/10.1016/j.taap.2010.04.012>

El-Shahawy, A., El-Sawi, N., Backer, W. S., Khorshid, F. A. & Geweely, N. S. (2010). Spectral Analysis, Molecular Orbital Calculations and Antimicrobial Activity of PMF-G Fraction. *Int J Pharm Biosci*, 1, 119-21.

Eriksson, M., Carlberg, B. & Eliasson, M. (2012). The disparity in long-term survival after the first stroke in patients with and without diabetes persists: the Northern Sweden MONICA Study. *Cerebrovasc D*, 34(2), 153-160. Doi: 10.1159/000339763

Ferrannini, E. (1998). Insulin resistance versus insulin deficiency in noninsulin-dependent diabetes mellitus: problems and prospects. *Endocr Rev*, 19(4), 477-490. Doi: 10.1210/edrv.19.4.0336.

Gabry G. H. & Wadi, F. M. (2003). Nanoparticles in Camel's Urine. *Vet Med J Giza*, 51, 5.

Hamers-Casterman, C., Atarhouch, T., Muyldermans, S., Robinson, G., Hamers, C., Songa, E. B., Bendahman, N. & Hamers, R. (1993). Naturally occurring antibodies devoid of light chains. *Nature*, 363(6428), 446-448. Doi: 10.1038/363446a0.

Hanley, C., Layne, J., Punnoose, A., Reddy, K., Coombs, I., et al. (2008). Preferential killing of cancer cells and activated human T cells using ZnO nanoparticles. *Nanotechnology*, 19, 295-103. Doi:10.1088/0957-4484/19/29/295103

Hoffmann, I. (2010). Climate change and the characterization, breeding and conservation of animal genetic resources. *Anim Genet*, 41(1), 32-46.

Huan, C. C., Aronstam, R. S., Chen, D. R. & Huang, Y. Y. (2010). Oxidative stress, calcium homeostasis, and altered gene expression in human lung epithelial

cells exposed to ZnO nanoparticles. *Toxicol in Vitro*, 24, 45-55. Doi: <https://doi.org/10.1016/j.tiv.2009.09.007>

Hussein, A. A. S. H., Al-Qubaisi, M., Hussein, M. Z., Ismail, M. & Bullo, S. (2013). Hippuric acid nanocomposite enhances doxorubicin and oxaliplatin-induced cytotoxicity in MDA-MB231, MCF-7 and Caco2 cell lines. *Drug Design Dev Ther*, 7, 25-31. Doi: 10.2147/DDDT.S37070

Kabbashi, M. A. & Omer, A. A. (2016). *In vitro* Antifungal Activity of Camel's Urine against Dermatophytes. *American Journal of Research Communication*, 4(4), 183-191.

Kadim, I., Mahgoub, O., Faye, B. & Farouk, M. (2013). *Camel Meat and Meat Products*. CABI, Oxfordshire, Boston.

Kanwar, J. R., Roy, K., Patel, Y., Zhou, S. F., Singh, M. R., Singh, D., Nasir, M., Sehgal, R., Sehgal, A., Singh, R. S., Garg, S. & Kanwar, R. K. (2015). Multifunctional iron-bound lactoferrin and nanomedical approaches to enhance its bioactive functions. *Molecules*, 20(6), 9703-9731. Doi: 10.3390/molecules20069703.

Khalifa, S., Al-Elyani, R. & Al-Alwani, A. (2005). Histological, Cytological and Histochemical Studies on the Effect of Camel's Urine on Liver of Rabbits Infected. *Escherichia coli*. *SJBS*, 2, 66-80.

Khedr, A. & Khorshid, F. (2016). Characterization and Determination of Major Bioactive Acids in Camel Urine Using Gas Chromatography-Mass spectrometry. *The Indian journal of pharmac*, 78. Doi: 10.4172/pharmaceutical-sciences.1000168

Korish, A. A., Abdel Gader, A. M., Al-Drees, A., Alhaider, A. A., Arafah, M. M. & Korashy, H. M. (2015). Camel milk attenuates the biochemical and morphological features of diabetic nephropathy in streptozotocin-induced diabetes. *Chem Biol Interact*, 229, 100-108. Doi: 10.1016/j.cbi.2015.01.013.

Langmead, L. & Rampton, D. S. (2001). Review article: herbal treatment in gastrointestinal and liver disease benefits and dangers. *Aliment Pharmacol Therap*, 15(9), 1239-1252. Doi: 10.1046/j.1365-2036.2001.01053.x.

Leeds, J. A., Schmitt, E. K. & Krastel, P. (2006). Recent developments in antibacterial drug discovery: Microbe-derived natural products-from collection to the clinic. *Expert Opinion on Investigational Drugs*, 15, 211-226. Doi: <https://doi.org/10.1517/13543784.15.3.211>

Malik, A., Al-Senaidy, A., Skrzypczak-jankun, E. & Jankun, J. (2012). A study of the anti-diabetic agents of camel milk. *Intern J Mol Med*, 30, 585-592. Doi: 10.3892/ijmm.2012.1051.

Marwa, S. M. & Reham, A. D. (2016). Antimicrobial Activity of Camel's Urine

and Its Effect on Multidrug-Resistant Clinical Bacterial and Fungal Isolates. *British Journal of Pharmaceutical Research*, 13(4), 1-6. Doi: 10.9734/BJPR/2016/29342

Mostafa, M. S. & Dwedar, R. A. (2016). Antimicrobial Activity of Camel's Urine and Its Effect on Multidrug-Resistant Clinical Bacterial and Fungal Isolates. *BJPR*, 14(1). Doi: 10.9734/BJPR/2016/29342

Muyldermans, S., Baral, T. N., Retamozzo, V. C., De Baetselier, P., De Genst, E., Kinne, J., Leonhardt, H., Magez, S., Nguyen, V. K., Revets, H., Rothbauer, U., Stijlemans, B., Tillib, S., Wernery, U., Wyns, L., Hassanzadeh-Ghassabeh, G. & Saerens, D. (2009). Camelid immunoglobulins and nanobody technology. *Vet Immunol Immunopathol*, 128, 178-183. Doi: 10.1016/j.vetimm.2008.10.299

Nafie, E. (2014). Camel Urine, a potent tool for plant protection. *African Journal of Plant Science*, 8(4), 167-177. Doi: 10.5897/AJPS2012.0720.

Nazar, A. O. *et al.* (2013). Antimicrobial Effect of Camel Urine in Some Human Pathogenic Bacteria. *Sebha Medical Journal*, 12(2).

Noor, S. O. & Alenini, M. S. (2017). Effects of Oral Administration of Camel Milk and Urine on Gut Microbiota: Biochemical and Microbiological Profiling in Rats. *American Journal of Molecular Biology*, 1, 1-12. Doi: <https://doi.org/10.4236/ajmb.2018.81001>.

Read, B. E. (1925). Chemical constituents of camel's urine. *J Biol Chem*, 64, 615-7. Doi: [https://doi.org/10.1016/S0021-9258\(18\)84901-8](https://doi.org/10.1016/S0021-9258(18)84901-8)

Redwan, E. M. & Tabll, A. (2007). Camel Lactoferrin Markedly Inhibits Hepatitis C Virus Genotype 4 Infection of Human Peripheral Blood Leukocytes. *Journal of Immunoassay and Immunochemistry*, 28(3), 267-277. Doi:10.1080/153218107014548

Romli, F., Abu, N., Khorshid, F. A., Syed Najmuddin, S. U. F. & Keong, Y. S. (2017). The growth inhibitory potential and antimetastatic effect of camel urine on breast cancer cells in vitro and in vivo. *Integr Cancer Ther*, 16, 540-555. Doi: 10.1177/1534735416656051.

Sboui, A., Khorchani, T., Djegham, M., Agrebi, A., Elhatmi, H. & Belhadj, O. (2010). Anti-diabetic effect of camel milk in alloxan-induced diabetic dogs: a dose-response experiment. *J Anim Physiol Anim Nutr Berl*, 94(4), 540-646. Doi: 10.1111/j.1439-0396.2009.00941.x.

Shinashal, R. Z. (2015). The capability of Camels urine in the treatment of infection caused by Escherichia coli and Staphylococcus aureus. *J College Edu Pure Sci.*, 4(1), 335-341. Doi: 10.1155/2018/7656752.

Shoeib, A. & Ba-Hatheq, A. (2008). Electromicroscopic Study of Camel Urine Effect on the Morphology of Some Human Pathogenic Bacteria. Comparison with

the Antibiotic Cefuroxime. *Saudi J of Biol Sci*, 15, 119-125.

Soliman, M. M., Hassan, M. Y., Mostafa, S. A., Ali, H. A. & Saleh, O. M. (2006). Protective effects of camel milk against pathogenicity induced by *Escherichia coli* and *Staphylococcus aureus* in Wistar rats. *Mol Med Rep*, 1, 8306-8312. Doi: <https://doi.org/10.3892/mmr.2015.4486>

Sumia, A. D., Ali, A. M. & Muna, E. A. (2016). Antimicrobial activity of Camels (*Camelus dromedarius*) and Sheep urine on some pathogenic bacteria. *IOSR Journal of Agriculture and Veterinary Science*, 9(10), 65-71.

Van Vuuren, S. & Holl, D. (2017). Antimicrobial natural product research: A review from a South African perspective for the years 2009-2016. *J Ethnopharmacol*, 208, 236-252. Doi: <http://dx.doi.org/10.1016/j.jep.2017.07.011>

Wadi FM. Nano-particles in Camels' Urine May Help Treat Cancer. 2012. Retrieved from: <http://www.saudigazette.com.sa/index.cfm?method=home.reg-con&contentID=2009071143333>.

World Health Organisation. 2015. Stop drinking Camel Urine, World Health Organization Says. Retrieved from: <https://www.usnews.com/news/articles/2015/06/10/stop-drinking-camel-urine-world-health-organization-says>.

Yagil, R. & Berlyne, G. M. (1976). Sodium and potassium metabolism in the dehydrated and rehydrated bedouin camel. *J Appl Physiol*, 41, 457-61. Doi: [10.1152/jappl.1976.41.4.457](https://doi.org/10.1152/jappl.1976.41.4.457)

Ye, L., Zhang, J., Xiao, W. & Liu, S. (2020). Efficacy and mechanism of actions of natural antimicrobial drugs. *Pharmacology & Therapeutics*, 216, 107671. Doi: <https://doi.org/10.1016/j.pharmthera.2020.107671>

Yuan, L., Wang, Y., Wang, J., Xiao, H. & Liu, X. (2014). Additive effect of zinc oxide nanoparticles and isoorientin on apoptosis in human hepatoma cell line. *Toxicol Lett*, 225, 294-304. Doi: <https://doi.org/10.1016/j.toxlet.2013.12.015>

Zaynab, M., Fatima, M., Abbas, S., Sharif, Y., Ali, M., Zafar, M. H. & Khan, K. H. (2019). Role of Primary metabolites in plant defence against pathogens, *Microbial Pathogenesis*, 137, 103728. Doi: <https://doi.org/10.1016/j.micpath.2019.103728>

Zaynab, M., Fatima, M., Abbas, S., Sharif, Y., Umair, M., Zafar, M. H. & Bahadar, K. (2018). Role of secondary metabolites in plant defence against pathogens. *Microbial Pathogenesis*. Doi: [10.1016/j.micpath.2018.08.034](https://doi.org/10.1016/j.micpath.2018.08.034).

Zuberu, J., Saleh, M. I. A., Alhassan, A. W., Adamu, B. Y., Aliyu, M. & Iliya, B. T. (2017). Hepatoprotective effect of camel milk on poloxamer 407 induced hyperlipidaemic Wistar rats. *Open Access Maced. J Med Sci*, 30, 852-858. Doi: [10.3889/oamjms.2017.158](https://doi.org/10.3889/oamjms.2017.158)